THE CRYSTAL CHEMISTRY OF THE CLINO-AMPHIBOLES

By

Frank C. Hawthorne, B.Sc., A.R.S.M.

A Thesis

Submitted to the School of Graduate Studies

in Partial Fulfilment of the Requirements

for the Degree

Doctor of Philosophy

McMaster University

August, 1973

DOCTOR OF PHILOSOPHY
(Geology)

McMaster University,
Hamilton, Ontario.

TITLE: The Crystal Chemistry of the Clino-Amphiboles

AUTHOR: Frank C. Hawthorne, B.Sc. (Imperial College, London)
A.R.S.M. (Royal School of Mines, London)

SUPERVISOR: Dr. H. Douglas Grundy

NUMBER OF PAGES: xvi, 332.

SCOPE AND CONTENTS: The crystal structures and site-populations of six clino-amphiboles have been refined using x-ray and neutron diffraction data. In addition, the Mössbauer spectra have been used to determine Fe^{2+} site-populations, and the results of both methods are compared. All available crystal structure data on the clino-amphiboles has been used in a crystal-chemical analysis of bonding and structural distortion in these minerals. Some geological applications of this analysis to cation ordering and thermal stability are discussed.

ACKNOWLEDGEMENTS

I would like to express my sincere thanks to my supervisor, Dr. H.D. Grundy for teaching me crystallography, enduring my obstinacy and curbing my wilder excursions into the realm of fantasy. I would also like to thank Dr. C. Calvo, Dr. I.D. Brown and Dr. R. Shannon for introducing me to crystal chemistry, although no blame should be attached to them for the result. Dr. T. Birchall was most generous in making available his Mössbauer spectrometer and Mr. R. Faggiani gave invaluable assistance with his Syntex. Mr. Jacobus L. Griep is to be thanked for our numerous and venomous arguments on amphiboles and metamorphism, and I am indebted to Mrs. Joyce Allen and Mrs. Lynn Falkiner for typing this thesis.

Finally, I would like to thank my wife, Robin, for her patience, understanding and many other things far too numerous to mention, but most of all for staying married to me for the past three years.

TABLE OF CONTENTS

LIST OF TABLES

LIST OF FIGURES

CHAPTER I

INTRODUCTION

The amphiboles are important rock-forming minerals in igneous and metamorphic rocks and consequently they have been the object of an immense amount of work in the past hundred years (Deer, Howie & Zussman, 1963). Despite the large amount of physical and chemical information available, major uncertainties exist concerning the chemistry and paragenesis of these minerals. Their complexity may be seen as arising from the general topology of the amphibole structure. Seven crystallographically unique cation sites occur, which may accommodate cations of formal charge +1 to +4 and ionic radius 0.25 to 1.4Å. Inspection of proposed average compositions of the crust (Holmes, 1965; Ringwood, 1969) shows that all major cations fall within this range. While the resulting complexity hinders present understanding of the geological significance of amphiboles, it is potentially of great significance to mineralogists and petrologists (Ernst, 1968). The complex inter-relationship between mineral composition, structural state and ambient chemical environment should be very responsive to differences in physical

and chemical conditions of crystallization and equilibration. However, before these factors can be of practical value, much more information is required concerning the chemical controls imposed by the amphibole structure. Recent work (Papike, Ross and Clarke, 1969; Robinson, Ross and Jaffe, 1971; Stout, 1972) has indicated much more structural control on chemical substitutions than was hitherto realized, and before the effect of physico-chemical environment may be assessed, these structural effects must be evaluated.

The present study was undertaken in an attempt to characterize some of these structural controls by an examination of structural distortions as a function of chemical composition in the clino-amphibole group. To extend the available data over a wider range of chemistry, six x-ray crystal structures and one neutron crystal structure were refined, with complementary work on the Mössbauer spectra of the iron-bearing species. These results, together with recent work reported in the literature were used to implement this study.

CHEMICAL COMPOSITION

The compositional variation in the amphiboles may be represented by the general formula (Deer, Howie & Zussman, 1963)

$$A_{0-1}X_2Y_5Z_8O_{22}W_2$$

where A = Na, K

X = Ca, Na, Mn, Fe^{2+}, Mg, Li ≡ M(4)

Y = Mg, Fe^{2+}, Fe^{3+}, Mn, Al, Ti, Zn ≡ M(1), M(2), M(3)

Z = Si, Al, Fe^{3+} ≡ T(1), T(2)

W = OH, F, Cl, O^{2-} ≡ O(3)

The large number of possible 'end member' species has given rise to a surfeit of terminology and great debate as to the mineralogical significance of 'ideal' amphiboles. Many schemes of classification have been derived (Sundius, 1946; Winchell and Winchell, 1951; Phillips and Layton, 1964; Phillips, 1966; Whittaker, 1968, 1971; Perry, 1967, 1968a,b) but none is satisfactory for every purpose. A detailed discussion of the classification problems encountered in this group is given by the I.M.A. Commission on amphibole nomenclature (to be published).

STRUCTURE

The crystal structure of an amphibole was first determined by Warren (1929) who solved the structure of tremolite by analogy with that of diopside. Subsequent work (Warren, 1930) showed that grunerite, actinolite and hornblende were isostructural with tremolite. Subsequent structure refinements are listed in Table 1.1 in chronological order.

TABLE 1.1

Crystal structure refinements of amphiboles; space group and type of data are given.

Crocidolite	C2/m	2-D	Whittaker (1949)
Actinolite	C2/m	2-D	Zussman (1955)
Karinthine	C2/m	2-D	Heritsch, Paulitsch & Walitzi (1957)
Barroisite	C2/m	2-D	Heritsch, Paulitsch & Walitzi (1957)
Tremolite	C2/m	2-D	Zussman (1959)
Grunerite	C2/m	3-D	Ghose & Hellner (1959)
Basaltic Hornblende	C2/m	2-D	Heritsch, Bertoldi & Walitzi (1960) Heritsch & Riechert (1960)
Karinthine	C2/m	2-D	Heritsch & Kahler (1960)
Proto-amphibole	Pbnm	3-D	Gibbs (1962, 1964, 1969) Gibbs, Bloss & Shell (1960)
Cummingtonite	C2/m	3-D	Ghose (1961), Fischer (1966) Mitchell, Bloss & Gibbs (1971)
Arfvedsonite	C2/m	2-D	Kawahara (1963)
$Na_2H_2Mg_5Si_8O_{22}F_2$	C2/m	3-D	Prewitt (1963), Gibbs & Prewitt (1968)*
$Na_2H_2Co_5Si_8O_{22}(OH)_2$	C2/m	3-D	Prewitt (1963), Gibbs & Prewitt (1968)*
Riebeckite	C2/m	3-D	Colville & Gibbs (1964)*
Anthophyllite	Pnma	2-D	Lindemann (1964)*
Grunerite	C2/m	3-D	Finger (1967, 1969a); Finger & Zoltai (1967)
Anthophyllite	Pnma	3-D	Finger (1967, 1970)

Kakanui Hornblende	C2/m	3-D	Papike & Clarke (1967); Robinson (1971); Papike, Ross & Clarke (1969)
Glaucophane	C2/m	3-D	Papike & Clarke (1968) Papike, Ross & Clarke (1969)
C-Mn Cummingtonite	C2/m	3-D	Papike, Ross & Clarke (1969)
P-Cummingtonite	$P2_1/m$	3-D	Papike, Ross & Clarke (1968, 1969)
Holmquistite	Pnma	2-D	Whittaker (1969)
K-Richterite	C2/m	3-D	Papike, Ross & Clarke (1969) Cameron (1970)
Tremolite	C2/m	3-D	Papike, Ross & Clarke (1969)
Gedrite 001	Pnma	3-D	Papike & Ross (1970)
Gedrite 002	Pnma	3-D	Papike & Ross (1970)
Syn Richterite 1	C2/m	3-D	Cameron (1970)
Syn Richterite 2	C2/m	3-D	Cameron (1970)
Fluor-Tremolite	C2/m	3-D	Cameron (1970)
Actinolite	C2/m	3-D	Mitchell, Bloss & Gibbs (1970, 1971)
Pargasite	C2/m	3-D	Robinson (1971)
Ti-Pargasite	C2/m	3-D	Robinson (1971)
Kaersutite	C2/m	3-D	Kitamura & Tokonami (1971)
High Cummingtonite	C2/m	3-D	Sueno, Papike, Prewitt & Brown (1972)†
Kôzulite	C2/m	3-D	Kitamura & Morimoto (1973)*

Cummingtonite	C2/m	3-D	Sueno, Cameron, Papike & Prewitt (1973)*†
Tremolite	C2/m	3-D	Sueno, Cameron, Papike & Prewitt (1973)*†
K-Fluor Richterite	C2/m	3-D	Cameron, Sueno, Prewitt & Papike (1973)*†

*Abstract only, complete structural data not available

† High temperature structure

Some investigators have used the space group I2/m instead of the more conventional C2/m; the relationship between the I-cell (subscript i) and the C-cell (subscript c) is given below:

$$\bar{a}_i = \bar{a}_c + \bar{c}_c$$

$$\bar{b}_i = \bar{b}_c$$

$$\bar{c}_i = \bar{c}_c$$

$$a_i \sin \beta_i = a_c \sin \beta_c$$

Figure 1.1 illustrates the basic clino-amphibole structure, which is formed from two basic elements, the octahedral strip and the tetrahedral double-chain, both of which extend infinitely in the c direction. These two elements link together in the b direction to form infinite sheets which stack along a*; the stacking sequence controls the space group of the resulting structure (Papike and Ross, 1970). At the junction of the two basic elements, the M(4) site is formed, linking the octahedral sheet to the chain-bridging anions. Sandwiched between two double chains is the A-site, a large cavity coordinated by eight-twelve anions. The resulting configuration is one of great structural compliance and accounts for the chemical complexity of the amphiboles.

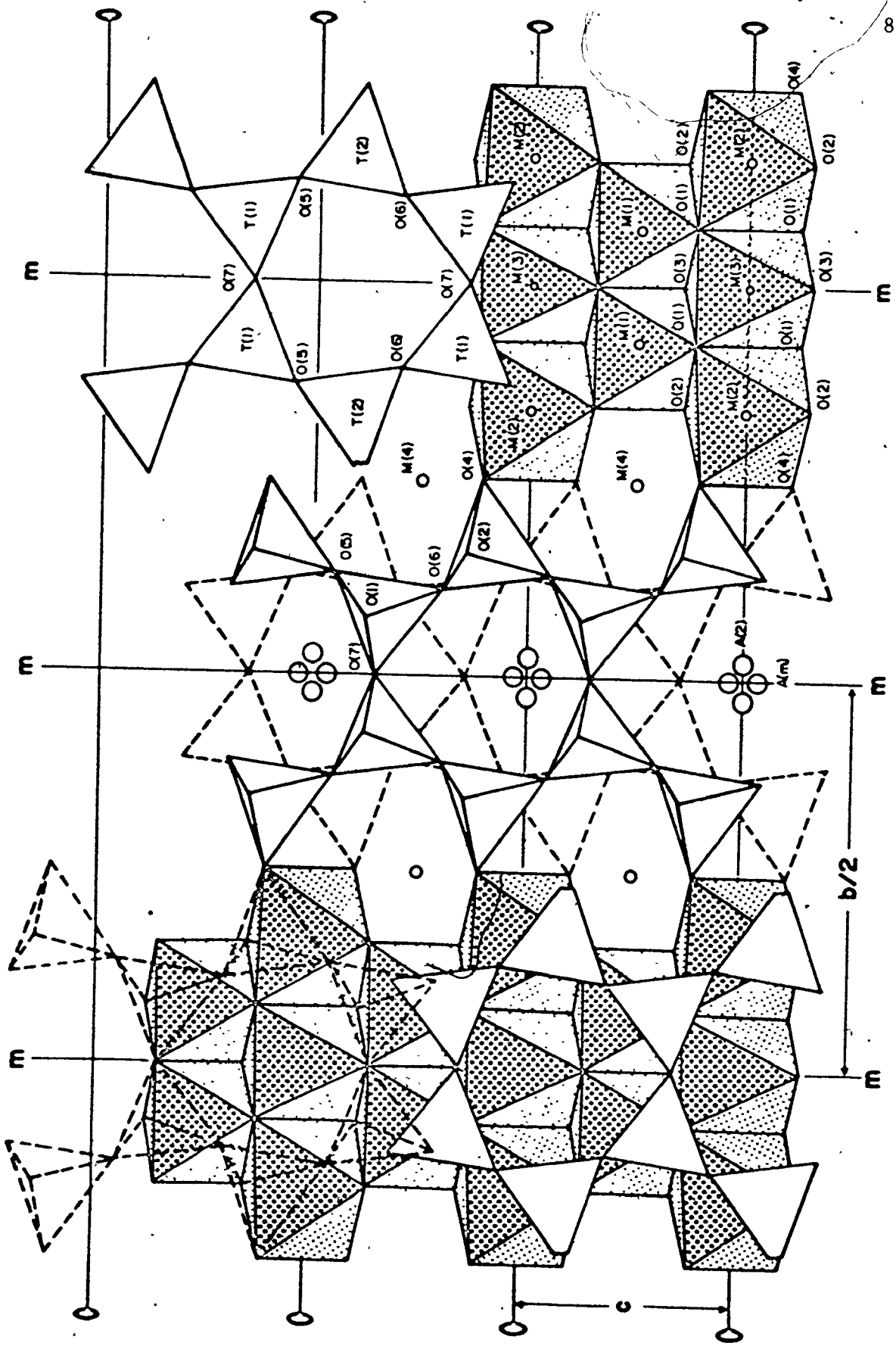

Figure 1.1 The Clino-amphibole Structure Projected Down a*

CHAPTER II

EXPERIMENTAL METHODS AND RESULTS

SAMPLE DESCRIPTION

In this section, the sample origin and environment (if known) are outlined, together with details of the chemical analyses and sample preparation methods. All new chemical analyses are presented in Table 2.1, and the unit formulae are given in Table 2.2.

Cell contents were calculated on the basis of 23 oxygens (excluding H_2O) except for Oxykaersutite and Tremolite, which were calculated on the basis of 24(O, OH, F, Cl). Water analysis in minerals is notoriously difficult and a poor analysis can introduce considerable error into the calculation of mineral formulae (Hey, 1954). Consequently, except where experimental evidence confirmed deviations from 2(OH, F) per unit formula, all calculations were made assuming 2(OH, F) per unit formula. For tremolite, the neutron refinement is compatible with the H occupancy indicated by the chemical analysis and a 24(OH, F, Cl) calculation. For oxykaersutite, the absorption band corresponding to the principal OH stretch in the infra-red spectrum is extremely weak relative to those of the other amphiboles, indicating that it is OH deficient.

TABLE 2.1: NEW CHEMICAL ANALYSES†

	FETSCH	FEHAST	OXYKER	TREMOL
SiO_2	40.12	39.51	39.90	56.67
TiO_2	0.87	2.44	4.65	0.08
Al_2O_3	18.67	10.08	14.35	2.11
Fe_2O_3	2.64	10.25	9.60	0.01
FeO	16.75	17.21	0.04	0.19
MgO	5.48	4.12	14.52	24.21
MnO	0.27	1.00	0.08	0.034
CaO	11.65	7.61	12.14	12.30
Na_2O	0.80	4.32	1.90	1.51
K_2O	0.75	2.20	2.31	0.68
H_2O+	1.61	n.d.	0.48	1.12
H_2O-	0.01	n.d.	0.02	0.09
F	0.07	n.d.	0.12	1.52
Cl	n.d.	n.d.	n.d.	0.05

† Analyses by John Muysson, Dept. of Geology, McMaster University.

TABLE 2.2: UNIT CELL CONTENTS (Z = 4)

	FETSCH	FEHAST	OXYKER	ALHAST	ZNCUMM	TREMOL
Si	6.00	6.17	5.88	5.27	7.87	7.75
Al^{IV}	2.00	1.83	2.12	2.73	0.09	0.25
Fe^{IV}	-	-	-	-	0.04	-
Al^{VI}	1.30	0.03	0.37	0.58	-	0.09
Fe^{3+}	0.30	1.21	1.06	0.79	0.03	0.00
Ti	0.10	0.29	0.52	0.39	Zn 0.75	0.03
Mg	1.22	0.96	3.19	1.17	3.70	4.94
Fe^{2+}	2.10	2.25	0.00	2.17	0.42	0.02
Mn	0.02	0.13	0.01	0.04	1.60	0.00
Ca	1.86	1.27	1.92	1.74	0.26	1.80
Na	0.23	1.31	0.54	0.95	0.21	0.40
K	0.14	0.44	0.43	0.30	0.02	0.12

Ferrotschermakite

Ore grade rock was obtained from Frood Mine, Sudbury, courtesy of the International Nickel Company of Canada. A blue-green amphibole coexists with quartz, alkali feldspar, biotite, magnetite, pyrite and pyrrhotite. Crystals were separated by a combination of magnetic susceptibility and heavy liquid techniques, and finally handpicked.

Ferrohastingsite

Crystals were obtained through the courtesy of Mr. M. L. Moyd, curator of the National Museum Collection, N.M.C., Ottawa. Optical absorption spectra and an electron probe analysis of this amphibole have been published (Faye and Nickel, 1970). Since the total of the reported analysis was low, major oxides were re-determined by atomic absorption.

Oxy-kaersutite

This amphibole is from Kangerdluarsuq, S. Greenland, and was taken from the McMaster University mineral collection. Large brown crystals up to one cm. across occur in a very fine-grained dull red matrix of volcanic dust. Crystals were picked from the rock with a needle, polished to remove any surface coating of matrix material, and crushed. Subsequent optical examination confirmed the purity of the separate.

Tremolite

The crystal used in this study was from the Gouveneur district, New York State; and was taken from the McMaster University mineral collection. It was a large crystal measuring 4"x1-1/2"x3/4" and showing a well-developed morphological habit. Thin slabs were sawn through the middle of the crystal, and polished; no evidence of zoning or inclusions was apparent under the optical microscope, except at the extreme edges of the crystal. The material used for experimental work was taken from the centre of the crystal; no impurities were observed in the powder used for chemical analysis.

Zinc Cummingtonite

The author is extremely grateful to Dr. Jun Ito of Harvard University for supplying a separate of this mineral. Details of the chemical analysis and paragenesis are given in Klein and Ito (1968).

Aluminous Hastingsite

A separate of this extremely unusual amphibole was very kindly supplied by Dr. E.C. Appleyard of Waterloo University. Details of the chemical analysis and paragenesis are given in Appleyard (1969, 1973) and Leake (1968).

SPACE GROUP AND CELL DIMENSIONS

Selection of crystals for intensity measurement was made on the basis of three criteria:

1. Optical clarity and uniform extinction

2. Sharpness and circular shape of spots on precession photographs.

3. Well-developed crystal form; this criterion was used in order to facilitate absorption corrections.

All crystals used for the collection of intensities were examined by single-crystal precession methods, and all showed diffraction symmetry 2/mC-/- consistent with space groups C2, Cm and C2/m; statistical tests made on the data indicated a centre of symmetry was present in each case, and the space group C2/m was assigned to all crystals. Preliminary short exposure precession photographs of oxy-kaersutite and arfvedsonite showed the systematic extinction hOl, l = 2n+1 noted by Kawahara (1963); formally, this denotes the presence of a c-glide. However, this symmetry element is incompatible with a double-chain structure, and long exposure photographs showed that the reflections were present but very weak, a rather nice example of the Templeton effect (Templeton, 1956).

Cell dimensions and orientation matrices were determined on a single-crystal diffractometer; these are given in Table 2.3, together with other miscellaneous information concerning data collection and refine-

TABLE 2.3: UNIT CELL PARAMETERS

	FETSCH	FEHAST	OXYKER	ALHAST	ZNCUMM	TREMOL
a (Å)	9.8179(7)	9.9226(8)	9.8920(11)	9.8659(4)	9.6063(4)	9.8635(2)
b (Å)	18.106(2)	18.134(2)	18.064(2)	18.0139(8)	18.1262(5)	18.0500(4)
c (Å)	5.3314(5)	5.3517(5)	5.3116(7)	5.3545(2)	5.3168(2)	5.2852(1)
β (°)	105.00(1)	104.836(4)	105.388(5)	105.082(1)	102.632(1)	104.801(1)
V ($Å^3$)	915.4(3)	930.9(2)	915.1(4)	918.9(1)	903.37(4)	909.72(3)
Sp. Gr.	C2/m	C2/m	C2/m	C2/m	C2/m	C2/m

ment. The first four crystals in Table 2.3 were mounted on a GE-XRD6 semi-automatic, four-circle diffractometer equipped with a 1/4 circle. The machine and the crystals were alligned manually (Hawthorne, 1972) and then, in each case, 31 strong reflections uniformly distributed over reciprocal space were manually aligned. The cell parameters and orientation matrix were calculated by a least-squares method, with an over-determination factor of four. The remaining crystals were mounted on a Syntex $P\bar{1}$ automatic four-circle diffractometer and automatically aligned using the software package provided. Cell parameters and orientation matrix were calculated as before.

INTENSITY COLLECTION AND DATA REDUCTION[†]

(i) X-Ray

The first four crystals in Table 2.3 were mounted on the GE-XRD6, and the intensities were collected using Zr filtered Mo radiation (λ = 0.71069Å), a scintillation counter and a pulse-height analyzer

---

[†] Where not stated, all programs for data processing and refinement were from X-Ray 67 and X-Ray 71, Program System for X-Ray Crystallography, by J.M. Stewart, University of Maryland, adapted by H.D. Grundy for the CDC6400.

set to pass 90% of the energy distribution. The θ-2θ scan method was employed, with a scan rate of 2 degrees/minute. The scan range was computed using the formula $1.8+\tan\theta$ (Alexander & Smith, 1964) and a 20 second fixed background count was made at the beginning and end of each scan. Six standard reflections were measured every fifty reflections, and the data output was examined each day to check for electronic fluctuations and constancy of crystal alignment.

The remaining crystals were mounted on the Syntex $P\bar{1}$ and the intensities were collected with graphite-monochromated Mo radiation and a scintillation counter. A θ-2θ scan method was used in a variable scan-rate mode with a minimum range of 2°/minute and a maximum range of 24°/minute. Reflections were gathered up to $65^{\circ}2\theta$ and two standard reflections were measured every fifty reflections to check for constancy of crystal alignment.

All data were corrected for absorption using an eight-point gaussian quadrature integration procedure (program from Cornell University) for polyhedral crystal shape. Subsequently the data were averaged, corrected for background, Lorentz and polarization effects. The criteria used for classification of a reflection as 'observed' is given in Table 2.4 together with the total number of reflections collected and the final number of F_{OBS}.

TABLE 2.4: DATA COLLECTION INFORMATION FOR AMPHIBOLES

	Diffractometer	Rad.*	Axis	Crystal Size (mm)	$\mu(cm^{-1})$	No. Inten.	No. $F_{OBS} > 0$	R(%)	R_W(%)
FETSCH	G.E.X.R.D.6	Mo/Zr	(10$\bar{1}$)*	.07x.10x.14	32.5	4887	1217	4.5	4.9
FEHAST	G.E.X.R.D.6	Mo/Zr	(10$\bar{1}$)*	.14x.14x.23	39.7	3362	1421	3.8	4.1
OXYKER	C.E.X.R.D.6	Mo/Zr	(10$\bar{1}$)*	.04x.10x.23	24.5	1984	1041	4.0	4.7
ALHAST	SYNTEX P$\bar{1}$	Mo-Gr	-	.08x.09x.18	37.8	1826	1263	4.1	4.4
ZNCUMM	SYNTEX P$\bar{1}$	Mo-Gr	-	.10x.20x.22	34.5	1761	1383	3.7	4.5
TREMOL	SYNTEX P$\bar{1}$	Mo-Gr	-	.05x.15x.26	14.3	3191	1376	3.5	3.8
NEUTRON	M.A. Mk 1	N-Al	(10$\bar{1}$)*	5.0x7.0x8.0	.004	731	709	2.2	2.8

(ii) Neutron

An equi-dimensional crystal of volume 0.28 cm^3 was cut from the larger crystal, and the preliminary alignment was done on a precession camera. At this stage, the crystal was transferred to a semi-automatic four-circle diffractometer† in the McMaster University Nuclear Reactor. The incident neutron beam was obtained from the (220) face of a single crystal of aluminium in the transmission geometry. Because of the mosaic spread of the aluminium crystal, the wavelength of the incident beam was variable across its width. Consequently, the wavelength was measured at the crystal and found to be 1.05926Å; this would indicate that the amount of secondary contamination is very small. The crystal was aligned manually and several peak profiles were examined to ensure that the mosaic spread was not excessive. Diffracted intensities were measured with a helium 3 counter using the w-scan method operating in the step-scan mode. The scan range was a step-function of two-theta and was wide enough to include several background counts on either side of the peak. To negate the effect of flux variations, counting time was controlled by a fixed count monitor on the incident beam. Diffractometer settings were calculated with the program MACDIF†† and reflections were

† built by Martin Anderson of the Physics Department, McMaster University.

†† written by Martin Anderson and modified by Frank Hawthorne.

collected up to 100° $2\theta(\sin\theta/\lambda = 0.723)$ in one asymmetric unit. Due to the low intensity of the incident beam, the rate of data collection was slow (about 10 reflections per day); to avoid collecting many "less thans", approximate neutron intensities were calculated from the atomic parameters of a preliminary x-ray refinement (R = 6%), and the neutron reflections were collected in sets of approximately equal intensity. As the intensity of the reflections decreased, the monitor count interval was increased in order to maintain good counting statistics. A standard reflection was examined manually each day to ensure constancy of crystal alignment.

The peak profile of each reflection was examined and those showing any irregularity were re-collected; in this way, a total of 731 unique reflections were collected. The data were corrected for background and the Lorentz effect using the program DIFDAT†. The resulting F_{OBS} were classed as unobserved if their magnitude fell below that of four times the standard deviation based on counting statistics, this resulted in 709 unique observed reflections. Because of the extremely small absorption coefficient for neutrons ($\mu = 0.004\ cm^{-1}$), no absorption corrections were made.

---

† written by Martin Anderson and modified by Frank Hawthorne.

MÖSSBAUER RESONANCE

Mössbauer spectra were recorded with an Austin Science Associates drive system used in conjunction with a Victoreen PIP400A multichannel analyser. The velocity wave form was an asymmetric triangle with the source velocity varying between limits that were adjusted for each amphibole to obtain the maximum amount of resolution while retaining sufficient background either side of the resonant absorption peaks to delineate the spectrum baseline. The source velocity limits used are given below:

Zinc Cummingtonite	± 0.55 cm/sec.
Oxy-kaersutite	± 0.25 cm/sec.
Rest	± 0.45 cm/sec.

The source was ^{57}Co in a palladium matrix and the velocity scale was calibrated against the spectrum of iron foil. In order to reduce asymmetry effects in the spectrum due to sample orientation (Pollak, de Coster and Amelinckx, 1962), the samples were ground with sugar before mounting (R.G. Burns, pers. comm.). In order to avoid saturation effects, absorber thicknesses were low, of the order of 4 mgs./cm^2 except in the case of zinc cummingtonite where not much sample was available, and the absorber thickness corresponded to 0.3 mgs/cm^2. Counts in excess of 2×10^6 per channel were accumulated for each spectrum.

REFINEMENT

(i) X-Ray Refinement

Scattering curves† were taken from Doyle and Turner (1968), Cromer and Mann (1968) and Tokonami (1965). Initial parameters for least-squares refinement were the final parameters of the structure closest in chemical composition, taken either from this study or from the literature. Where not specified, all R-factors are of the form

$$R = \frac{\Sigma \left| |F_{OBS}| - |F_{CALC}| \right|}{\Sigma |F_{OBS}|}$$

and all Rw-factors are of the form

$$Rw = \frac{\Sigma w(|F_{OBS}| - |F_{CALC}|)^2}{\Sigma w |F_{OBS}|^2}$$

with w = 1 (unit weights).

The refinement procedure was fairly similar in all cases. One cycle of refinement varying atomic positions was followed by one cycle varying site-occupancies ('multiplicity'). A third cycle was run varying isotropic temperature factors. Subsequently, several cycles of refinement were performed, gradually increasing the number of variable parameters until convergence of the isotropic thermal model was attained. R-factors at this stage are given in Table 2.5.

† see Appendix 1.

TABLE 2.5: A-SITE REFINEMENT INFORMATION

	FETSCH	FEHAST	OXYKER	ALHAST
Isotropic B for A-site ($Å^2$)	5.4	6.1	5.8	5.3
R-factor before splitting(%)	6.0	7.2	7.3	7.7
R_w-factor before splitting (%)	6.3	6.8	7.6	7.7
R-factor after splitting(%)	6.0	6.2	6.1	6.9
R_w-factor after splitting(%)	6.2	6.0	6.4	7.0
R-factor after refinement (%)	5.9	5.4	5.6	6.3
R_w-factor after refinement (%)	6.1	5.2	5.6	6.4
Final R-factor (%)	4.5	3.8	4.0	4.1
Final R_w-factor (%)	4.8	4.1	4.3	4.4

	TREMOL*	TREMOL^N
Isotropic B for A-site($Å^2$)	8.3	18.8
R-factor before refinement(%)	6.1	3.8
R_w-factor before refinement(%)	5.9	4.4
R-factor after refinement(%)	5.7	3.0
R_w-factor after refinement(%)	5.6	3.5
Final R-factor(%)	3.5	2.2
Final R_w-factor(%)	3.8	2.8

For those amphiboles containing significant A-site cations, the isotropic temperature factors of the cations at this site were unreasonably large (see Table 2.5) when compared with temperature factors of Na^+ and K^+ in other well-refined silicates (e.g. Clarke, Appleman & Papike, 1969; Brown & Gibbs, 1969a; Beger, 1969). In each case, the occupancy of the site was allowed to vary but, except in the case of tremolite which will be discussed later, there was little change in the occupancy and no significant improvement in the temperature factors. Figure 2.1 shows a series of Fourier sections parallel to {100} in the vicinity of the A-site for ferrotschermakite. Electron density maxima appear in the mirror plane and along the 2-fold axis, displaced from the special position at 0, 1/2, 0. Corresponding difference Fourier maps showed high residual density both in the mirror plane and along the two-fold axis. These features were common to all four amphiboles with significant A-site occupancy. They could be masked by artificially raising the temperature factors; in this case, the electron density maxima became smeared and in extreme cases resulted in a high residual on the special position.

These results were interpreted as two non-equivalent cation positions, one along the 2-fold axis and one confined to the mirror plane. The coordinates of the A-site maxima, were taken from the Fourier maps and used as input parameters to a structure factor calculation for a

Figure 2.1 Fourier Sections in the Vicinity of the A-site

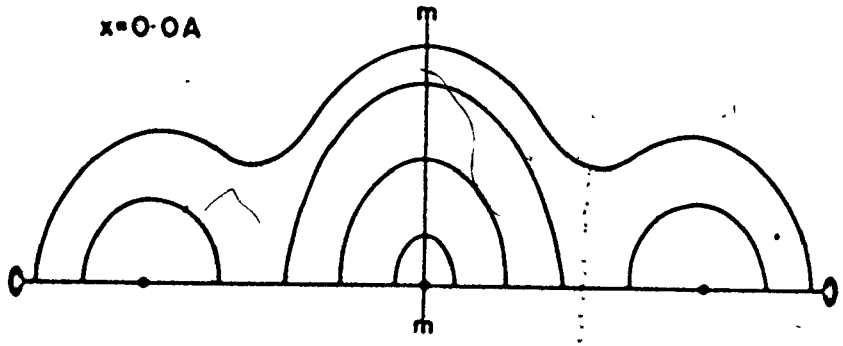

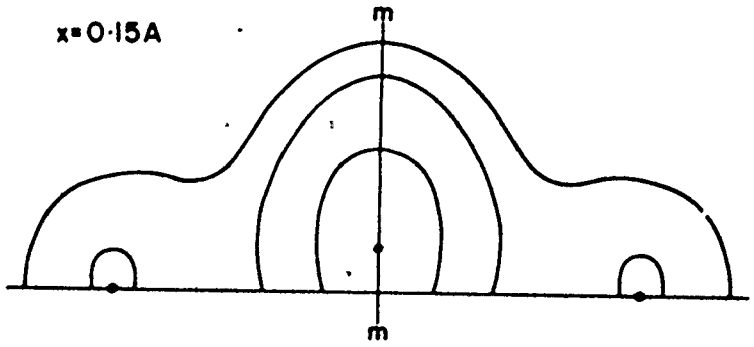

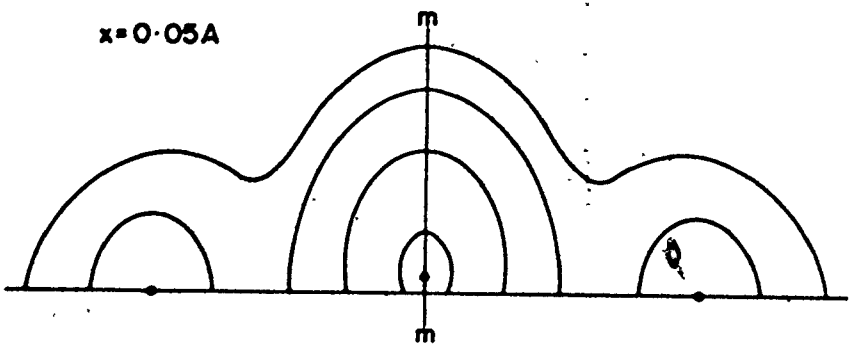

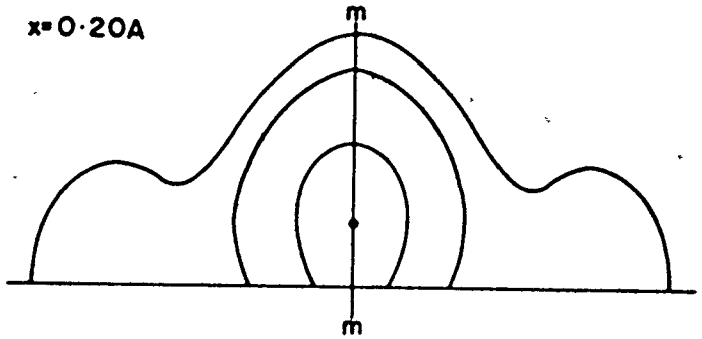

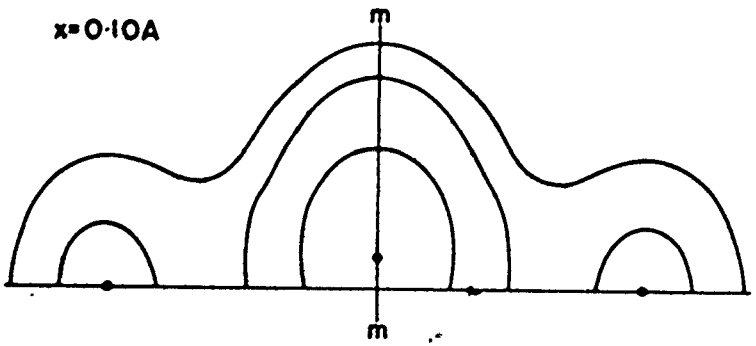

Fourier sections are parallel to the crystallographic yz plane.

Contours of electron density are at equal intervals, the outer one has equal value in all sections.

x spacing along the crystallograpic x direction, section x=0·0 Angstroms is through the A site.

m mirror plane

0 diad

• Location of a maxima in the electron density.

positionally disordered model. An immediate reduction in R-factor was apparent which was marginally significant for ferrotschermakite but highly significant for the remaining crystals at the 0.005 level using Hamilton's test (Hamilton, 1965). These differences in significance reflect the higher partial occupancy of the A-site in the latter cases. With the isotropic temperature factors set at 1.5$\AA^2$, one cycle of least-squares varying the positions and partial occupancies produced a reduction in R-factor that was highly significant for all four structures (see Table 2.5). In view of the double nature of the A-site disorder, the following site nomenclature is proposed:

A or A(2/m)	0, 1/2, 0
A(m)	x, 1/2, z
A(2)	0, y, 0

For the tremolite, refinement of the A-site occupancy produced a significant lowering of the occupancy and a reduction in the isotropic temperature factor. In addition, Fourier sections in the vicinity of the A-site indicated that the electron density maxima were confined to the mirror plane. Refinement of the neutron data confirmed that the A-site cations were overestimated by the chemical analysis, and thus the occupancy of the A(m) site was refined without constraints.

At this stage, the temperature factors* were converted to anisotropic of the form

$$\exp\left[-\sum_{i=1}^{3}\sum_{j=1}^{3} h_i h_j \beta_{ij}\right]$$

and one cycle of refinement was performed varying the coefficients. Further cycles were run gradually increasing the number of variables until convergence of the full matrix refinement.

Because of the problem of correlation in site-population refinement (discussed at length elsewhere), the final steps of refinement were performed using the program RFINE†, a least-squares program incorporating an extremely flexible set of linear constraints which were used to constrain the sum of the site chemistries to equal the bulk chemistry of the crystals as determined by chemical analysis. Because of the complexity of the chemistry of most of the crystals, not all site-populations of all species may be refined; some chemical species were assigned to sites on the basis of crystal-chemical criteria. The derivation of site-populations is not a trivial problem and each crystal will be discussed in detail. All bond lengths used in cation assignment were calculated from the input parameters to RFINE which differed little from the final refined parameters.

---

* see Appendix 1

† written by L. W. Finger (Finger, 1967, 1969a, b)

(a) Ferrotschermakite

The $\langle M(2)\text{-}O \rangle$ distance was significantly smaller than those of the other octahedra, consistent with an essentially ordered octahedral Al content; thus all available octahedral aluminium was assigned to M(2). All available Ti and Fe^{3+} was also assigned to M(2) in accord with the work on infra-red spectra (Bancroft and Burns, 1969) which indicated that the majority of Fe^{3+} ions occupy M(2) positions in alkali amphiboles; this is also in accord with ionic size criteria since the effective radius of octahedrally coordinated high spin Fe^{3+} is less than those of the other remaining octahedral cations (Shannon and Prewitt, 1969, 1970). This ordering of trivalent cations into the M(2) site is also expected on charge balance criteria since the O(4) anion shows a formal charge deficiency in the amphibole structure.

The $\langle M(4)\text{-}O \rangle$ distance is significantly larger than M(1) and M(3) distances, and consistent with previous work (Papike et al., 1969; Robinson et al., 1969; Robinson, 1971) all Ca was assigned to this site together with excess octahedral cations and sufficient Na for complete occupancy.

The disordered A-site chemistry was constrained to the total A-site chemistry by combining Na and K and treating the vacancies as a separate species with zero scattering power. The distribution of $Mg\text{-}Fe^{2+}$ over the four M-sites was refined using bulk chemical constraints.

(b) Ferrohastingsite

The structural formula was slightly low in octahedral cations and was normalized to full octahedral occupancy. The $\langle M(2)\text{-}O \rangle$ distance was significantly smaller than $\langle M(1)\text{-}O \rangle$ and $\langle M(3)\text{-}O \rangle$ at the end of the unconstrained refinement and, as with ferrotschermakite, all octahedral Al and Ti were assigned to M(2). All Ca was assigned to M(4) together with enough Na to fill the site. Initial tetrahedral Al occupancies were assigned on mean bond length criteria using Method 2 of Papike et al. (1969). As before, the A-site chemistry was refined using only a total scattering power constraint. The species Fe^{2+}, Fe^{3+} and Mn were combined (= Fe*) and expressed as Fe^{2+}. The distribution of Fe*-Mg was refined over the three octahedral sites, and the distribution of tetrahedral Al-Si was refined over T(1) and T(2). After convergence, mean bond length considerations indicated that Fe^{3+} was ordered into M(2).

(c) Oxy-kaersutite

As before, all Ca and Mn was assigned to the M(4) site, and all Ti and Al^{3+} was assigned to the M(2) site. Because of the oxidized nature of this amphibole, it seemed likely that most of the iron was in the ferrous state on formation of the crystal, and therefore would probably be located in the M(1) and M(3) sites. Consequently, the distribution of $Mg\text{-}Fe^{3+}$ was refined over the four M sites.

(d) Tremolite

All Ca was assigned to M(4) and the deficiency was filled with Na. As indicated previously, no constraints were applied to the A-site occupancy refinement since the analysis appeared to be in error with respect to the alkalis. The distribution of Mg-Fe^{2+} was refined over the octahedral sites.

(e) Al-hastingsite

As before all Ca^{2+} was assigned to the M(4) site and all Ti and Al^{oct} was assigned to M(2). Initial tetrahedral Al occupancies were assigned by method 2 of Papike, Ross & Clarke (1969). The species Fe^{2+} and Fe^{3+} were combined and expressed as neutral Fe; the distribution of Mg-Fe was refined over all four M sites and the distribution of Al-Si was refined over the T sites, using bulk chemical constraints from the chemical analysis.

Full-matrix refinement with the program RFINE resulted in convergence at the R-factors given in Table 2.5. The final positional parameters and equivalent isotropic temperature factors are presented in Table 2.6 and observed and calculated structure factors are given in Appendix 2. Site-occupancies are presented in Table 2.7. Interatomic distances and angles were calculated using the program ERRORS (Finger,

TABLE 2.6: FINAL ATOMIC POSITIONS AND EQUIVALENT ISOTROPIC TEMPERATURE FACTORS FOR AMPHIBOLES

Atom		FETSCH	FEHAST	OXYKER	ALHAST	ZNCUMM	TREMOL*	TREMOL^N
O(1)	x	0.1046(4)	0.1064(2)	0.1058(4)	0.1035(3)	0.1138(3)	0.1115(2)	0.1115(1)
	y	0.0936(2)	0.0912(1)	0.0870(2)	0.0935(1)	0.0864(1)	0.0858(1)	0.0857(1)
	z	0.2099(7)	0.2135(4)	0.2196(7)	0.2109(5)	0.2116(5)	0.2182(5)	0.2182(3)
	β	1.01(5)	0.90(3)	0.76(5)	0.77(4)	0.64(3)	0.53(3)	0.45(2)
O(2)	x	0.1198(4)	0.1210(2)	0.1184(4)	0.1180(3)	0.1224(3)	0.1191(2)	0.1187(1)
	y	0.1766(2)	0.1745(1)	0.1713(2)	0.1766(1)	0.1723(1)	0.1707(1)	0.1707(1)
	z	0.7419(7)	0.7354(4)	0.7291(7)	0.7455(6)	0.7198(5)	0.7245(5)	0.7251(3)
	β	0.80(5)	0.87(3)	0.75(5)	0.79(4)	0.74(3)	0.54(3)	0.46(2)
O(3)	x	0.1136(6)	0.1103(3)	0.1065(5)	0.1111(4)	0.1105(4)	0.1078(4)	0.1082(2)
	y	0	0	0	0	0	0	0
	z	0.7126(10)	0.7097(6)	0.7160(10)	0.7097(8)	0.7104(7)	0.7153(6)	0.7153(4)
	β	0.99(7)	0.93(4)	0.94(7)	0.91(6)	0.72(5)	0.76(5)	0.60(3)
O(4)	x	0.3713(4)	0.3662(2)	0.3651(4)	0.3717(3)	0.3751(3)	0.3646(3)	0.3642(2)
	y	0.2511(2)	0.2498(1)	0.2514(2)	0.2518(1)	0.2469(1)	0.2480(1)	0.2482(1)
	x	0.7951(7)	0.7938(4)	0.7891(8)	0.7946(5)	0.7767(5)	0.7931(5)	0.7927(3)
	β	0.89(5)	0.98(3)	0.86(5)	0.79(4)	0.98(4)	0.71(3)	0.61(2)

TABLE 2.6 continued

Atom		FETSCH	FEHAST	OXYKER	ALHAST	ZNCUMM	TREMOL*	TREMOL^N
O(5)	x	0.3516(4)	0.3495(2)	0.3504(4)	0.3526(3)	0.3501(3)	0.3462(3)	0.3466(1)
	y	0.1401(2)	0.1365(1)	0.1402(2)	0.1401(1)	0.1307(2)	0.1341(1)	0.1339(1)
	z	0.1093(7)	0.1007(4)	0.1107(7)	0.1155(6)	0.0673(5)	0.1005(5)	0.0996(3)
	β	0.99(5)	1.13(5)	1.01(5)	0.88(4)	1.00(4)	0.78(3)	0.64(2)
O(6)	x	0.3418(4)	0.3425(2)	0.3469(4)	0.3418(3)	0.3492(3)	0.3435(3)	0.3437(1)
	y	0.1206(2)	0.1189(1)	0.1181(2)	0.1181(1)	0.1204(2)	0.1183(1)	0.1180(1)
	z	0.6021(7)	0.6016(4)	0.6094(8)	0.6105(6)	0.5616(5)	0.5914(5)	0.5910(3)
	β	1.01(5)	1.10(3)	1.02(5)	0.98(4)	1.10(4)	0.70(3)	0.62(2)
O(7)	x	0.3323(6)	0.3353(3)	0.3414(6)	0.3328(4)	0.3439(4)	0.3381(4)	0.3380(2)
	y	0	0	0	0	0	0	0
	z	0.2861(12)	0.2885(7)	0.2859(12)	0.2807(9)	0.2787(8)	0.2915(7)	0.2920(4)
	β	1.39(5)	1.34(5)	1.27(8)	1.29(7)	1.11(6)	0.80(5)	0.74(3)
T(1)	x	0.2799(1)	0.2797(1)	0.2823(1)	0.2789(1)	0.2864(1)	0.2801(1)	0.2799(2)
	y	0.0864(1)	0.08621(4)	0.08560(7)	0.0869(5)	0.08426(5)	0.08420(4)	0.08424(9)
	z	0.3012(3)	0.3005(1)	0.3045(3)	0.3042(2)	0.2784(2)	0.2978(2)	0.2974(4)
	β	0.59(2)	0.60(1)	0.47(2)	0.46(4)	0.58(2)	0.41(1)	0.33(2)

TABLE 2.6 continued

Atom		FETSCH	FEHAST	OXYKER	ALHAST	ZNCUMM	TREMOL*	TREMOL^N
T(2)	x	0.2926(1)	0.2908(1)	0.2908(1)	0.2920(1)	0.2955(1)	0.2881(1)	0.2883(2)
	y	0.1736(1)	0.17242(4)	0.17304(7)	0.17394(6)	0.16977(5)	0.17135(4)	0.17132(9)
	z	0.8161(2)	0.8106(1)	0.8118(3)	0.8188(2)	0.7853(2)	0.8049(2)	0.8056(4)
	β	0.59(2)	0.54(1)	0.48(2)	0.43(4)	0.60(2)	0.39(1)	0.38(3)
M(1)	x	0	0	0	0	0	0	0
	y	0.0902(1)	0.08945(4)	0.0817(1)	0.09076(6)	0.08711(6)	0.0882(1)	0.0883(1)
	z	1/2	1/2	1/2	1/2	1/2	1/	1/2
	β	0.65(2)	0.73(2)	0.63(4)	0.66(3)	0.70(2)	0.56(4)	0.39(3)
M(2)	x	0	0	0	0	0	0	0
	y	0.1782(1)	0.17994(3)	0.1767(1)	0.17904(6)	0.17744(7)	0.1767(1)	0.1770(1)
	z	0	0	0	0	0	0	0
	β	0.55(2)	0.57(2)	0.63(4)	0.62(3)	0.71(2)	0.59(4)	0.31(3)
M(3)	x	0	0	0	0	0	0	0
	y	0	0	0	0	0	0	0
	z	0	0	0	0	0	0	0
	β	0.60(2)	0.64(2)	0.64(6)	0.64(3)	0.73(4)	0.57(5)	0.37(4)

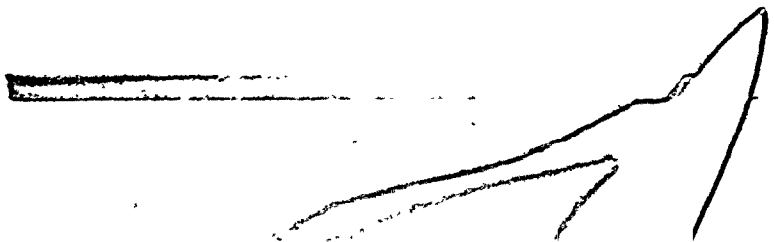

TABLE 2.6 continued

Atom		FETSCH	FEHAST	OXYKER	ALHAST	ZNCUMM	TREMOL*	TREMOL^N
M(4)	x	0	0	0	0	0	0	0
	y	0.2806(1)	0.28034(5)	0.27890(8)	0.28193(7)	0.26251(5)	0.27798(5)	0.27784(13)
	z	1/2	1/2	1/2	1/2	1/2	1/2	1/2
	β	0.85(2)	0.98(2)	0.84(3)	0.81(2)	0.92(2)	0.72(2)	0.89(3)
A(2)	x	0	0	0	0	-	-	-
	y	0.4784(17)	0.4878(4)	0.4917(8)	0.4848(5)	-	-	-
	z	0	0	0	0	-	-	-
	β	1.30(5)	1.95(5)	1.15(5)	1.93(12)	-	-	-
A(m)	x	0.0272(34)	0.0444(7)	0.0467(11)	0.0391(24)	-	0.0259(16)	0.0304(39)
	y	1/2	1/2	1/2	1/2	-	1/2	1/2
	z	0.0621(63)	0.0928(14)	0.0901(22)	0.0908(50)	-	0.0592(29)	0.0753(76)
	β	1.74(7)	1.90(4)	1.76(7)	1.82(11)	-	1.7(2)	1.3(4)
H	x	0.202(14)	0.196(8)	-	-	-	-	0.2090(6)
	y	0	0	-	-	-	-	0
	z	0.784(26)	0.758(14)	-	-	-	-	0.7634(15)
	β	0.5	0.5	-	-	-	-	1.51(9)

* X-ray refinement
N Neutron refinement

TABLE 2.7: SITE-POPULATIONS FOR AMPHIBOLES

	FETSCH	FEHAST	OXYKER
T(1)	$0.46(3)Al+0.54(3)Si$	$0.42(6)Al+0.58(6)Si$	$0.47(4)Al+0.53(4)Si$
T(2)	$0.04(3)Al+0.96(3)Si$	$0.04(6)Al+0.96(6)Si$	$0.06(4)Al+0.94(4)Si$
M(1)	$0.610(5)Fe^{2+}+0.390(5)Mg$	$0.693(5)Fe^{*}+0.307(5)Mg$	$0.343(9)Fe^{3+}+0.657(9)Mg$
M(2)	$0.15Fe^{3+}+0.05Ti+0.65Al$ $+0.100(5)Mg+0.050(5)Fe^{2+}$	$0.160Ti+0.020Al$ $+0.118(5)Mg+0.702(5)Fe^{*}$	$0.185Al+0.257Ti$ $+0.502(9)Mg+).056(9)Fe^{3+}$
M(3)	$0.780(7)Fe^{2+}+0.220(7)Mg$	$0.817(5)Fe^{*}+0.183(5)Mg$	$0.235(14)Fe^{3+}+0.765(14)Mg$
M(4)	$0.01Mn^{2+}+0.05Na+0.93Ca$ $+0.010(6)Mg+0.000(6)Fe^{2+}$	$0.635Ca+0.365Na$	$0.009Mn^{2+}+0.958Ca$ $+0.025(15)Mg+0.010(15)Fe^{3+}$
A(m)	Na_x+K_y $x+1.8y=0.080(9)$	Na_x+K_y $x+1.8y=0.378(6)$	Na_x+K_y $x+1.8y=0.802(10)$
A(2)	$Na_{0.13-x}+K_{0.14-y}$	$Na_{0.56-x}+K_{0.44-y}$	$Na_{0.543-x}+K_{0.434-y}$

TABLE 2.7: continued

	ALHAST	ZN-CUMM	TREMOL*	TREMOL^N
T(1)	0.49(11)Al+0.51(11)Si	0.022Al+ 0.978Si	0.06(8)Al+0.94(8)Si	0.062(9)Al+0.938(9)Si
T(2)	0.19(11)Al+0.81(11)Si	0.01Fe^{3+}+0.99Si	0.00(8)Al+1.00(8)Si	0.00(1)Al+1.00(1)Si
M(1)	0.691(8)Fe*+0.309(8)Mg	0.252(42)Zn+0.708(80)Mg+ 0.039(65)Mn^{2+}	0.996(7)Mg+0.004(7)Fe*	1.00(2)Mg+0.00(2)Fe*
M(2)	0.195Ti+0.290Al+ 0.214(8)Mg+0.301(8)Fe*	0.165Fe^{2+}+0.020Fe^{3+} +0.034(53)Zn+0.781(53)Mg	0.046Al+0.935(7)Mg+ 0.019(7)Fe*	0.046Al+0.924(30)Mg+ 0.030(30)Fe*
M(3)	0.839(12)Fe*+0.161(12)Mg	0.177(83)Zn+0.722(98)Mg+ 0.101(91)Mn	0.994(10)Mg±0.006(10)Fe*	1.00(3)Mg+0.00(3)Fe*
M(4)	0.870Ca+0.060Na+ 0.070(15)Fe*+0.000(15)Mg	0.710Mn^{2+}+0.045Fe^{2+} +0.140Ca+0.105Na	0.902Ca+0.054Na +0.039(11)Mg+0.005(11)Fe*	0.902Ca+0.054Na +0.044(30)Mg+0.000(30
A(m)	Na_x+K_y x+1.8y=0.193(13)	-	0.154(7)Na	0.10(1)Na
A(2)	$Na_{0.70=x}+K_{0.30-y}$	-	-	-

TABLE 2.8: INTERATOMIC DISTANCES FOR AMPHIBOLES

BOND	FETSCH-	FEHAST	OXYKER	ALHAST	ZNCUMM	TREMOL*	TREMOL^N
T(1)-O(1)	1.668(4)	1.665(3)	1.684(4)	1.675(3)	1.618(3)	1.609(3)	1.606(3)
T(1)-O(5)	1.692(4)	1.683(3)	1.689(4)	1.688(3)	1.628(3)	1.634(3)	1.637(3)
T(1)-O(6)	1.679(4)	1.680(3)	1.682(5)	1.692(4)	1.632(4)	1.638(4)	1.636(3)
T(1)-O(7)	1.656(2)	1.665(1)	1.665(2)	1.669(2)	1.624(2)	1.627(2)	1.628(2)
⟨T(1)-O⟩	1.674	1.673	1.680	1.681	1.625	1.627	1.627
T(2)-O(2)	1.640(4)	1.630(3)	1.644(4)	1.660(3)	1.623(3)	1.611(3)	1.617(3)
T(2)-O(4)	1.620(4)	1.603(2)	1.615(4)	1.630(3)	1.600(3)	1.585(3)	1.586(2)
T(2)-O(5)	1.636(4)	1.647(3)	1.651(5)	1.661(4)	1.637(3)	1.663(3)	1.657(3)
T(2)-O(6)	1.656(4)	1.658(3)	1.663(4)	1.668(3)	1.658(3)	1.675(3)	1.681(3)
⟨T(2)-O⟩	1.638	1.634	1.643	1.655	1.630	1.634	1.635

TABLE 2.8 continued

BOND	FETSCH	FEHAST	OXYKER	ALHAST	ZNCUMM	TREMOL*	TREMOL^N
M(1)-O(1)	2.067(5)	2.073(4)	2.037(5)	2.065(4)	2.069(4)	2.065(4)	2.065(4)
M(1)-O(2)	2.170(5)	2.153(4)	2.173(5)	2.163(4)	2.129(4)	2.072(4)	2.071(3)
M(1)-O(3)	2.131(4)	2.112(3)	1.988(5)	2.120(3)	2.096(4)	2.084(4)	2.086(3)
⟨M(1)-O⟩	2.123	2.113	2.066	2.116	2.098	2.074	2.074
M(2)-O(1)	2.014(4)	2.096(3)	2.106(5)	2.023(4)	2.155(4)	2.142(4)	2.146(3)
M(2)-O(2)	2.029(5)	2.080(4)	2.085(5)	2.010(4)	2.092(4)	2.094(4)	2.089(4)
M(2)-O(4)	1.928(5)	1.964(4)	1.981(5)	1.907(4)	2.026(4)	2.020(4)	2.017(4)
⟨M(2)-O⟩	1.990	2.047	2.057	1.980	2.091	2.085	2.084
M(3)-O(1)	2.141(4)	2.130(3)	2.070(4)	2.135(3)	2.092(3)	2.071(3)	2.070(3)
M(3)-O(3)	2.115(6)	2.117(4)	2.060(6)	2.122(5)	2.069(5)	2.052(5)	2.055(4)
⟨M(3)-O⟩	2.132	2.126	2.067	2.131	2.084	2.065	2.065

TABLE 2.8 continued

BOND	FETSCH	FEHAST	OXYKER	ALHAST	ZNCUMM	TREMOL*	TREMOL^N
M(4)-O(2)	2.410(4)	2.437(4)	2.424(5)	2.425(4)	2.195(4)	2.414(4)	2.413(3)
M(4)-O(4)	2.330(5)	2.367(4)	2.351(5)	2.345(4)	2.099(4)	2.337(4)	2.338(4)
M(4)-O(5)	2.636(6)	2.728(5)	2.642(6)	2.602(6)	3.109(5)	2.765(5)	2.769(5)
M(4)-O(6)	2.519(4)	2.551(3)	2.560(4)	2.551(3)	2.630(3)	2.550(3)	2.553(2)
$\langle M(4)\text{-}O\rangle^8$	2.474	2.521	2.494	2.481	2.508	2.517	2.518
$\langle M(4)\text{-}O\rangle^6$	2.420	2.452	2.445	2.440	2.308	2.434	2.434
A-O(5)	3.056(4)	3.010(4)	3.068(9)	3.055(4)	2.835(4)	2.975(2)	2.970(2)
A-O(6)	3.159(3)	3.152(4)	3.079(5)	3.101(4)	3.289(4)	3.148(2)	3.147(2)
A-O(7)	2.518(4)	2.519(5)	2.456(7)	2.504(5)	2.327(5)	2.485(3)	2.490(2)
A-O(7)	3.735(4)	3.739(6)	3.700(7)	3.775(6)	3.800(5)	3.680(4)	3.676(3)
$\langle A\text{-}O\rangle^{12}$	3.114	3.097	3.075	3.099	3.062	3.069	3.067

TABLE 2.8 continued

BOND	FETSCH	FEHAST	OXYKER	ALHAST	ZNCUMM	TREMOL*	TREMOL^{N}
A(m)-O(5)	3.042(4)	2.977(5)	3.026(6)	3.057(9)	-	2.95(1)	2.96(2)
A(m)-O(5)	3.114(4)	3.148(5)	3.210(7)	3.146(11)	-	3.04(1)	3.04(2)
A(m)-O(6)	2.905(5)	2.765(6)	2.705(8)	2.737(19)	-	2.90(1)	2.84(3)
A(m)-O(6)	3.433(6)	3.589(9)	3.507(11)	3.510(24)	-	3.42(1)	3.47(3)
A(m)-O(7)	2.504(7)	2.552(8)	2.515(11)	2.501(15)	-	2.47(2)	2.45(4)
A(m)-O(7)	2.584(7)	2.614(8)	2.527(11)	2.620(17)	-	2.55(2)	2.60(4)
A(m)-O(7)	3.391(8)	3.219(8)	3.204(12)	3.273(29)	-	3.35(2)	3.26(4)
A(m)-O(7)	4.084(10)	4.273(12)	4.104(12)	4.285(29)	-	4.01(2)	4.09(4)
$\langle A\text{-}O \rangle^{12}$	3.129	3.134	3.104	3.132	-	3.08	3.09
$\langle A\text{-}O \rangle^{8}$	2.901	2.868	2.866	2.875	-	2.85	2.84

TABLE 2.8 continued

BOND	FETSCH	FEHAST	OXYKER	ALHAST	ZNCUMM	TREMOL*	TREMOL^N
A(2)-O(5)	2.739(27)	2.831(7)	2.945(11)	2.834(8)	-	-	-
A(2)-O(5)	3.388(30)	3.194(7)	3.192(12)	3.285(8)	-	-	-
A(2)-O(6)	2.901(22)	3.005(7)	2.978(11)	2.921(8)	-	-	-
A(2)-O(6)	3.441(27)	3.307(7)	3.185(12)	3.295(8)	-	-	-
A(2)-O(7)	2.548(9)	2.529(5)	2.490(7)	2.519(6)	-	-	-
A(2)-O(7)	3.756(9)	3.746(8)	3.703(9)	3.785(8)	-	-	-
$\langle A\text{-}O \rangle^{12}$	3.129	3.102	3.078	3.106	-	-	-
$\langle A\text{-}O \rangle^{8}$	2.894	2.890	2.893	2.889	-	-	-
T(1)-T(2) through O(6)	3.140(2)	3.123(1)	3.106(2)	3.143(1)	3.094(1)	3.092(1)	3.097(4)
T(1)-T(2) through O(5)	3.060(2)	3.079(1)	3.077(2)	3.066(1)	3.063(1)	3.061(1)	3.055(4)
T(1)-T(1) through O(7)	3.130(3)	3.127(1)	3.091(3)	3.132(2)	3.055(2)	3.039(2)	3.040(4)

TABLE 2.8 continued

BOND	FETSCH	FEHAST	OXYKER	ALHAST	ZNCUMM	TREMOL*	TREMOL^N
M(1)-M(1)	3.266(2)	3.244(2)	2.950(4)	3.270(2)	3.158(2)	3.184(3)	3.186(4)
M(1)-M(2)	3.106(1)	3.139(1)	3.163(1)	3.114(1)	3.122(1)	3.088(1)	3.090(2)
M(1)-M(3)	3.126(1)	3.129(1)	3.038(1)	3.137(1)	3.092(1)	3.085(1)	3.086(1)
M(1)-M(4)	3.448(2)	3.462(1)	3.563(3)	3.444(1)	3.179(1)	3.426(2)	3.422(3)
M(2)-M(3)	3.226(2)	3.263(1)	3.192(2)	3.225(1)	3.216(1)	3.190(2)	3.195(2)
M(2)-M(4)	3.247(1)	3.236(1)	3.234(1)	3.256(1)	3.073(1)	3.213(1)	3.209(2)
A(m)-T(1)	3.228(13)	3.435(7)	3.395(9)	3.446(13)	-	3.37(1)	3.36(4)
A(m)-T(2)	3.413(28)	3.504(3)	3.490(5)	3.523(11)	-	3.57(1)	3.55(2)
A(2)-T(1)	3.402(4)	3.311(5)	3.324(7)	3.306(6)	-	-	-
A(2)-T(2)	3.583(2)	3.564(7)	3.611(7)	3.506(8)	-	-	-
A(m)-A(m')	0.735(2)	1.147(15)	1.140(11)	1.07(6)	-	0.699(28)	0.90(11)
A(2)-A(2')	0.784(7)	0.442(15)	0.299(29)	0.55(2)	-	-	-
A(m)-A(2)	0.537(7)	0.615(6)	0.589(11)	0.60(2)	-	-	-
O(3)-H	0.85(12)	0.86(8)	-	-	-	-	0.961(6)

TABLE 2.9: POLYHEDRAL EDGE LENGTHS FOR AMPHIBOLES

ATOMS	FETSCH	FEHAST	OXYKER	ALHAST	ZNCUMM	TREMOL*	TREMOL^N
O(1)-O(5)	2.748(5)	2.757(4)	2.803(5)	2.766(4)	2.673(4)	2.691(4)	2.697(3)
O(1)-O(6)	2.741(9)	2.750(8)	2.770(9)	2.772(8)	2.667(8)	2.677(8)	2.677(7)
O(1)-O(7)	2.750(6)	2.755(4)	2.755(6)	2.767(4)	2.668(4)	2.664(4)	2.663(2)
O(5)-O(6)	2.677(5)	2.718(3)	2.688(6)	2.710(4)	2.637(4)	2.617(3)	2.621(3)
O(5)-O(7)	2.730(4)	2.688(3)	2.707(4)	2.698(3)	2.629(3)	2.631(3)	2.632(2)
O(6)-O(7)	2.745(5)	2.720(3)	2.731(5)	2.752(4)	2.645(4)	2.652(3)	2.645(2)
⟨O-O⟩ T(1)	2.732	2.731	2.742	2.744	2.653	2.655	2.656
O(2)-O(4)	2.763(5)	2.736(3)	2.782(5)	2.798(4)	2.737(4)	2.738(4)	2.740(2)
O(2)-O(5)	2.673(8)	2.677(7)	2.688(9)	2.707(8)	2.646(7)	2.670(8)	2.672(7)
O(2)-O(6)	2.679(5)	2.677(4)	2.683(5)	2.709(4)	2.672(5)	2.662(4)	2.671(3)
O(4)-O(5)	2.655(5)	2.662(3)	2.667(5)	2.685(4)	2.655(4)	2.656(3)	2.657(2)
O(4)-O(6)	2.563(5)	2.573(3)	2.579(5)	2.590(4)	2.551(4)	2.559(3)	2.566(2)
O(5)-O(6)	2.704(5)	2.673(3)	2.684(6)	2.707(4)	2.693(4)	2.699(4)	2.696(3)
⟨O-O⟩ T(2)	2.673	2.666	2.680	2.699	2.659	2.664	2.667

TABLE 2.9: continued

ATOMS	FETSCH	FEHAST	OXYKER	ALHAST	ZNCUMM	TREMOL*	TREMOL^{N}
$O(1^{u})$-$O(2^{d})$	2.733(5)	2.787(3)	2.764(5)	2.709(4)	2.840(4)	2.822(3)	2.818(2)
$O(1^{u})$-$O(2^{u})$	3.178(5)	3.146(3)	3.079(6)	3.200(4)	3.104(4)	3.068(3)	3.072(2)
$O(1^{u})$-$O(3^{d})$	2.844(5)	2.825(4)	2.718(5)	2.823(4)	2.788(4)	2.755(4)	2.757(2)
$O(1^{u})$-$O(3^{u})$	3.153(6)	3.171(4)	3.064(6)	3.143(4)	3.081(4)	3.058(4)	3.056(3)
O(2)-O(2)	3.007(11)	3.003(9)	2.896(10)	3.024(10)	2.930(9)	2.882(9)	2.881(9)
O(2)-O(3)	3.201(3)	3.168(2)	3.097(4)	3.188(3)	3.125(3)	3.083(2)	3.083(1)
O(3)-O(3)	2.738(11)	2.705(9)	2.666(13)	2.699(11)	2.756(9)	2.689(10)	2.693(9)
$\langle O\text{-}O \rangle_{M(1)}$	2.998	2.992	2.917	2.987	2.964	2.929	2.929

TABLE 2.9: continued

ATOMS	FETSCH	FEHAST	OXYKER	ALHAST	ZNCUMM	TREMOL*	TREMOL^N
O(1)-O(1)	2.617(10)	2.685(9)	2.689(10)	2.622(9)	2.774(9)	2.751(9)	2.751(8)
$O(1^u)$-$O(2^d)$	2.733(5)	2.787(3)	2.764(5)	2.709(4)	2.840(4)	2.822(3)	2.818(2)
$O(1^u)$-$O(2^u)$	2.949(5)	3.007(3)	3.049(6)	2.942(4)	3.060(4)	3.043(3)	3.041(2)
O(1)-O(4)	2.822(5)	2.898(3)	2.935(5)	2.797(4)	3.022(4)	3.011(3)	3.010(2)
$O(2^u)$-$O(4^d)$	2.847(5)	2.963(3)	2.958(5)	2.822(4)	2.862(4)	3.009(4)	3.005(2)
$O(2^u)$-$O(4^u)$	2.776(5)	2.844(3)	2.881(5)	2.757(4)	3.046(4)	2.910(3)	2.907(2)
O(4)-O(4)	2.882(11)	2.987(9)	2.994(11)	2.890(9)	2.984(9)	2.989(9)	2.996(9)
⟨O-O⟩M(2)	2.813	2.889	2.905	2.797	2.952	2.944	2.942
$O(1^u)$-$O(1^d)$	2.617(10)	2.685(9)	2.689(10)	2.622(9)	2.774(9)	2.751(9)	2.751(8)
$O(1^u)$-$O(1^u)$	3.390(7)	3.307(4)	3.142(7)	3.370(5)	3.133(5)	3.096(5)	3.094(2)
$O(1^u)$-$O(3^d)$	2.844(5)	2.825(4)	2.718(5)	2.823(4)	2.788(4)	2.755(4)	2.757(2)
$O(1^u)$-$O(3^u)$	3.167(6)	3.171(4)	3.107(6)	3.186(4)	3.090(4)	3.068(4)	3.068(3)
⟨O-O⟩M(3)	3.004	2.997	2.914	3.002	2.944	2.916	2.916

TABLE 2.9: continued

ATOMS	FETSCH	FEHAST	OXYKER	ALHAST	ZNCUMM	TREMOL*	TREMOL^N
O(2)-O(2)	3.007(11)	3.003(9)	2.896(10)	3.024(10)	2.930(9)	2.882(9)	2.881(9)
$O(2^u)$-$O(4^u)$	3.170(5)	3.179(3)	3.128(5)	3.191(4)	3.023(4)	3.145(3)	3.146(2)
$O(2^u)$-$O(4^d)$	2.847(5)	2.963(3)	2.958(5)	2.822(4)	2.862(4)	3.009(4)	3.005(3)
$O(2^u)$-$O(5^u)$	3.407(5)	3.532(3)	3.504(5)	3.380(4)	3.737(4)	3.638(4)	3.641(2)
$O(4^u)$-$O(5^d)$	3.314(5)	3.418(4)	3.383(6)	3.317(4)	3.337(5)	3.445(4)	3.447(3)
$O(4^u)$-$O(6^u)$	2.563(5)	2.573(3)	2.579(5)	2.590(4)	2.551(4)	2.559(3)	2.566(2)
$O(5^u)$-$O(6^u)$	2.677(5)	2.718(3)	2.668(6)	2.710(4)	2.637(4)	2.617(3)	2.621(3)
$O(5^u)$-$O(6^d)$	3.026(8)	3.080(7)	2.994(8)	3.017(7)	3.128(9)	3.091(8)	3.087(7)
O(6)-O(6)	3.547(8)	3.562(6)	3.519(8)	3.615(7)	3.107(6)	3.462(6)	3.457(5)
$\langle$O-O$\rangle$M(4)	3.035	3.093	3.055	3.043	3.037	3.085	3.085

TABLE 2.10: INTERATOMIC ANGLES FOR AMPHIBOLES

ATOMS	FETSCH	FEHAST	OXYKER	ALHAST	ZNCUMM	TREMOL*	TREMOL^N
O(1)-T(1)-O(5)	109.8(2)	110.9(2)	112.4(2)	110.7(2)	111.0(2)	112.2(2)	112.5(2)
O(1)-T(1)-O(6)	109.9(3)	110.6(2)	110.8(3)	110.8(3)	110.3(2)	111.1(2)	111.3(3)
O(1)-T(1)-O(7)	111.2(3)	111.7(1)	110.7(2)	111.7(2)	110.8(2)	110.9(2)	110.9(1)
O(5)-T(1)-O(6)	105.2(2)	107.8(1)	105.8(2)	106.6(2)	108.1(2)	106.2(1)	106.3(1)
O(5)-T(1)-O(7)	109.6(3)	106.9(2)	107.6(3)	107.0(2)	108.0(2)	107.6(2)	107.4(2)
O(6)-T(1)-O(7)	111.0(3)	108.9(2)	109.4(3)	109.9(2)	108.7(2)	108.6(2)	108.2(2)
⟨O-T(1)-O⟩	109.4	109.5	109.5	109.5	109.5	109.5	109.5
O(2)-T(2)-O(4)	115.9(2)	115.7(1)	117.2(2)	116.5(1)	116.3(2)	117.8(1)	117.6(1)
O(2)-T(2)-O(5)	109.6(2)	109.6(2)	109.3(3)	109.7(2)	108.5(2)	109.3(2)	109.4(3)
O(2)-T(2)-O(6)	108.6(2)	109.0(2)	108.5(2)	109.0(2)	109.0(2)	108.2(2)	108.1(2)
O(4)-T(2)-O(5)	109.1(2)	110.0(2)	109.5(2)	109.3(2)	110.2(2)	109.7(2)	110.0(2)
O(4)-T(2)-O(6)	103.0(2)	104.2(2)	103.8(2)	103.5(2)	103.0(2)	103.4(2)	103.5(2)
O(5)-T(2)-O(6)	110.5(2)	108.0(1)	108.2(2)	108.9(1)	109.6(2)	107.9(1)	107.7(1)
⟨O-T(2)-O⟩	109.5	109.4	109.4	109.4	109.4	109.4	109.4

TABLE 2.10: continued

ATOMS	FETSCH	FEHAST	OXYKER	ALHAST	ZNCUMM	TREMOL*	TREMOL^N
$O(1^u)$-M(1)-$O(2^d)$	80.3(1)	82.5(1)	82.0(1)	79.6(1)	85.2(1)	95.7(1)	95.9(1)
$O(1^u)$-M(1)-$O(2^u)$	97.2(1)	96.2(1)	94.0(1)	98.4(1)	95.4(1)	86.0(1)	85.9(1)
$O(1^u)$-M(1)-$O(3^d)$	85.3(2)	84.9(1)	84.9(2)	84.8(1)	84.0(1)	94.9(1)	94.8(1)
$O(1^u)$-M(1)-$O(3^u)$	97.4(2)	96.4(1)	99.1(2)	97.3(1)	95.4(1)	83.2(1)	83.2(1)
O(2)-M(1)-O(2)	87.7(2)	88.5(2)	83.6(2)	88.7(2)	87.0(2)	88.1(2)	88.2(2)
O(2)-M(1)-O(3)	96.2(2)	96.0(2)	96.1(2)	96.2(2)	95.4(2)	95.8(2)	95.7(2)
O(3)-M(1)-O(3)	79.9(3)	79.6(2)	84.2(3)	79.1(2)	82.2(2)	80.4(2)	80.4(2)
⟨O-M(1)-O⟩	90.0	90.0	90.0	90.0	90.0	90.0	90.0

TABLE 2.10: continued

ATOMS	FETSCH	FEHAST	OXYKER	ALHAST	ZNCUMM	TREMOL*	TREMOL^N
O(1)-M(2)-O(1)	81.0(3)	79.7(2)	79.4(3)	80.8(2)	80.1(2)	79.9(2)	79.7(2)
$O(1^u)$-M(2)-$O(2^d)$	85.1(1)	83.7(1)	82.5(1)	84.4(1)	83.9(1)	91.9(1)	91.8(1)
$O(1^u)$M(2)-$O(2^u)$	93.7(1)	92.1(1)	93.4(1)	93.7(1)	92.2(1)	83.6(1)	83.4(1)
O(1)-M(2)-O(4)	91.4(2)	91.1(2)	91.7(2)	90.7(2)	92.5(1)	92.7(2)	92.5(2)
$O(2^u)$-M(2)-$O(4^d)$	92.0(1)	94.2(1)	93.3(2)	92.1(1)	88.0(1)	90.0(1)	90.1(1)
$O(2^u)$-M(2)-$O(4^u)$	89.1(1)	89.3(1)	90.2(1)	89.5(1)	95.4(1)	94.0(1)	94.1(1)
O(4)-M(2)-O(4)	96.8(3)	99.1(2)	98.2(3)	98.5(2)	94.9(2)	95.5(2)	95.9(2)
⟨O-M(2)-O⟩	90.0	90.0	90.0	90.0	89.9	90.0	90.0
$O(1^u)$-M(3)-$O(1^d)$	75.3(2)	78.1(2)	81.1(3)	75.8(2)	83.0(2)	96.8(2)	96.7(2)
$O(1^u)$-M(3)-$O(1^u)$	104.7(2)	101.9(2)	98.9(3)	104.2(2)	97.0(2)	83.2(2)	83.3(2)
$O(1^u)$-M(3)-$O(3^d)$	83.9(1)	83.4(1)	82.3(1)	83.1(1)	84.1(1)	96.2(1)	96.1(1)
$O(1^u)$-M(3)-$O(3^u)$	96.2(1)	96.6(1)	97.7(1)	96.9(1)	95.9(1)	83.8(1)	83.9(1)
⟨O-M(3)-O⟩	90.0	90.0	90.0	90.0	90.0	90.0	90.0

TABLE 2.10: continued

ATOMS	FETSCH	FEHAST	OXYKER	ALHAST	ZNCUMM	TREMOL*	TREMOL^N
O(2)-M(4)-O(2)	77.2(2)	76.1(2)	73.4(2)	77.1(2)	83.8(2)	73.3(2)	73.3(2)
$O(2^u)$-M(4)-$O(4^d)$	73.8(1)	76.2(1)	76.6(1)	72.5(1)	83.6(1)	78.6(1)	78.5(1)
$O(2^u)$-M(4)-$O(4^u)$	83.9(1)	82.9(1)	81.9(2)	84.0(1)	89.5(1)	82.9(1)	83.0(1)
$O(2^u)$-M(4)-$O(5^u)$	84.8(2)	86.1(2)	87.4(1)	84.4(2)	87.8(2)	89.0(2)	89.0(2)
$O(4^u)$-M(4)-$O(5^d)$	83.5(1)	84.0(1)	85.1(1)	84.1(1)	77.0(1)	84.5(1)	84.5(1)
$O(4^u)$-M(4)-$O(6^u)$	63.7(1)	63.0(1)	63.2(1)	63.7(1)	64.1(1)	63.0(1)	63.1(1)
$O(5^u)$-M(4)-$O(6^d)$	71.8(2)	71.3(1)	70.3(2)	71.7(1)	65.4(1)	71.0(1)	70.9(1)
$O(5^u)$-M(4)-$O(6^u)$	62.5(1)	61.9(1)	62.2(1)	63.4(1)	53.9(1)	58.8(1)	58.8(1)
O(6)-M(4)-O(6)	89.5(2)	88.5(1)	86.8(2)	90.2(1)	72.4(1)	85.5(1)	85.2(1)
⟨O-M(4)-O⟩	75.9	76.0	75.9	75.9	74.9	75.9	75.9

TABLE 2.10: continued

ATOMS	FETSCH	FEHAST	OXYKER	ALHAST	ZNCUMM	TREMOL*	TREMOL^N
O(7)-O(7)-O(7)	65.8(1)	65.7(1)	64.5(1)	64.9(1)	59.9(1)	65.8(1)	65.9(1)
Δ +	0.269	0.270	0.283	0.279	0.334	0.269	0.268
T(1)-O(5)-T(2)	133.7(2)	135.3(2)	134.3(3)	132.6(2)	139.7(2)	136.4(2)	136.2(1)
T(1)-O(6)-T(2)	140.7(2)	138.7(2)	136.4(2)	138.7(2)	140.2(2)	137.9(2)	137.8(1)
T(1)-O(7)-T(1)	141.9(4)	139.8(2)	136.4(3)	139.5(3)	140.3(2)	138.2(2)	138.2(2)
O(5)-O(6)-O(5)	164.4(2)	166.1(1)	162.9(2)	162.6(2)	172.0(2)	167.7(2)	167.6(1)
O(5)-O(7)-O(6)	163.1(3)	164.7(1)	161.8(2)	160.2(2)	171.0(2)	166.4(2)	166.6(1)
O(3')-O(3)-H	100(9)	95(7)	-	-	-	-	90.4(2)

+ $\Delta = (90^\circ - [O(7)\text{-}O(7)\text{-}O(7)]) / 90^\circ$

TABLE 2.11: ANISOTROPIC TEMPERATURE FACTOR COEFFICIENTS FOR AMPHIBOLES

ATOM	i j*	FETSCH	FEHAST	OXYKER	ALHAST	ZNCUMM	TREMOL*	TREMOL^N
O(1)	11	0.00287(33)	0.00249(19)	0.00222(34)	0.00175(21)	0.00182(22)	0.00166(20)	0.00111(11)
	22	0.00037(9)	0.00072(5)	0.00058(9)	0.00079(6)	0.00034(6)	0.00033(5)	0.00034(3)
	33	0.00312(113)	0.00763(68)	0.00719(126)	0.00567(77)	0.00749(74)	0.00532(73)	0.00450(46)
	12	-0.00014(15)	-0.00013(8)	-0.00014(14)	-0.00012(9)	-0.00012(9)	0.00004(9)	-0.0004(5)
	13	0.00126(49)	0.00109(29)	0.00138(52)	0.00042(32)	0.00050(32)	0.00089(30)	0.00035(18)
	23	-0.00015(27)	-0.0005(16)	-0.00020(27)	-0.00003(18)	-0.00001(17)	-0.00003(16)	-0.00009(9)
O(2)	11	0.00222(31)	0.00187(18)	0.00191(30)	0.00217(21)	0.00201(23)	0.00144(20)	0.00098(11)
	22	0.00060(8)	0.00079(5)	0.00061(9)	0.00055(6)	0.00050(6)	0.00049(6)	0.00044(3)
	33	0.00733(103)	0.00799(67)	0.00784(117)	0.00747(76)	0.00779(73)	0.00519(72)	0.00441(47)
	12	-0.00002(13)	-0.00003(8)	0.0013(14)	0.00013(9)	0.00002(10)	-0.00005(9)	-0.00006(4)
	13	0.00077(45)	0.00063(27)	0.00153(47)	0.00047(31)	0.00074(32)	0.00099(29)	0.00070(18)
	23	-0.00009(24)	0.00000(15)	0.00013(14)	0.00000(18)	-0.00001(18)	-0.00009(6)	-0.00018(9)

TABLE 2.11: continued

ATOM	i j*	FETSCH	FEHAST	OXYKER	ALHAST	ZNCUMM	TREMOL*	TREMOL^N
O(3)	11	0.00419(54)	0.00219(21)	0.00282(52)	0.00300(35)	0.00263(34)	0.00287(31)	0.00168(17)
	22	0.00059(12)	0.00066(6)	0.00060(13)	0.00076(9)	0.00037(8)	0.00043(8)	0.00046(4)
	33	0.00781(69)	0.00793(80)	0.00944(81)	0.00634(115)	0.00735(107)	0.00681(106)	0.00578(70)
	12	0	0	0	0	0	0	0
	13	0.00285(77)	0.00104(33)	0.00153(80)	0.00135(51)	0.00145(48)	0.00147(45)	0.00093(29)
	23	0	0	0	0	0	0	0
O(4)	11	0.00357(33)	0.00385(21)	0.00333(36)	0.00269(22)	0.00327(26)	0.00275(22)	0.00212(11)
	22	0.00033(8)	0.00054(5)	0.00043(9)	0.00058(6)	0.00042(6)	0.00042(6)	0.00035(3)
	33	0.01034(120)	0.00389(72)	0.00332(135)	0.00704(79)	0.01102(85)	0.00627(77)	0.00642(56)
	12	-0.00029(13)	-0.00045(9)	-0.00015(15)	-0.00015(9)	-0.00056(10)	-0.00046(9)	-0.00030(5)
	13	0.00297(51)	0.00287(30)	0.00211(57)	0.00213(33)	0.00078(38)	0.00177(32)	0.00166(19)
	23	0.00016(24)	-0.00025(16)	0.00014(29)	0.00008(17)	0.00026(18)	-0.00022(17)	-0.00013(9)

TABLE 2.11: continued

ATOM	i j*	FETSCH	FEHAST	OXYKER	ALHAST	ZNCUMM	TREMOL*	TREMOL^N
O(5)	11	0.00261(32)	0.00249(19)	0.00303(36)	0.00198(21)	0.00255(25)	0.00221(22)	0.00159(11)
	22	0.00035(9)	0.00107(6)	0.00035(9)	0.00081(6)	0.0086(7)	0.00072(6)	0.00065(3)
	33	0.00311(110)	0.00971(74)	0.00784(121)	0.00312(78)	0.00905(81)	0.00585(78)	0.00467(45)
	12	-0.00009(14)	0.00000(9)	-0.00003(15)	-0.00004(10)	0.00006(11)	-0.00003(9)	-0.00008(5)
	13	0.00071(47)	0.00109(30)	0.00124(53)	0.00101(32)	0.00112(35)	0.00103(33)	0.00076(18)
	23	-0.00034(26)	0.00130(17)	0.00103(30)	0.00065(18)	0.00151(19)	0.00076(18)	0.00073(10)
O(6)	11	0.00306(34)	0.00275(19)	0.00282(36)	0.00209(22)	0.00237(25)	0.00219(22)	0.00157(11)
	22	0.00068(8)	0.00090(6)	0.00077(9)	0.00074(6)	0.00109(7)	0.00059(6)	0.00055(3)
	33	0.00996(115)	0.01053(74)	0.01104(135)	0.01094(81)	0.00893(81)	0.00565(75)	0.00553(44)
	12	-0.00013(14)	-0.00003(8)	0.00008(15)	0.00006(10)	0.00016(11)	-0.00004(9)	0.00002(5)
	13	0.00153(51)	0.00158(30)	0.00244(56)	0.00089(34)	0.00024(35)	0.00144(32)	0.00094(17)
	23	-0.00099(26)	-0.00120(17)	-0.00110(31)	-0.00121(19)	-0.00128(20)	-0.00065(17)	-0.00061(10)

TABLE 2.11: continued

ATOM	i j*	FETSCH	FEHAST	OXYKER	ALHAST	ZNCUMM	TREMOL*	TREMOL^N
	11	0.00414(56)	0.00344(31)	0.00268(54)	0.00378(35)	0.00294(39)	0.00257(33)	0.00205(16)
	22	0.00071(13)	0.00083(8)	0.00063(14)	0.00074(10)	0.00025(9)	0.00027(8)	0.00029(4)
	33	0.01722(204)	0.01498(120)	0.01804(227)	0.01269(141)	0.01839(146)	0.01054(122)	0.01030(79)
O(7)	12	0	0	0	0	0	0	0
	13	0.00304(87)	0.00140(49)	0.00010(90)	0.00024(56)	0.00200(60)	0.00140(50)	0.00101(29)
	23	0	0	0	0	0	0	0
	11	0.00189(12)	0.00187(7)	0.00166(13)	0.00116(8)	0.00194(8)	0.00146(8)	0.00099(15)
	22	0.00036(3)	0.00042(2)	0.00029(3)	0.00032(2)	0.00032(2)	0.00027(2)	0.00025(4)
	33	0.00544(41)	0.00539(24)	0.00433(44)	0.00440(27)	0.00557(27)	0.00361(27)	0.00292(55)
T(1)	12	-0.00013(5)	-0.00009(3)	-0.00011(5)	-0.00002(3)	-0.00003(3)	-0.00004(3)	-.0.00002(6)
	13	0.00073(18)	0.00099(10)	0.00080(19)	0.00005(11)	0.00041(12)	0.00092(11)	0.00054(23)
	23	0.00001(9)	-0.00008(6)	-0.00007(9)	0.00002(6)	-0.00003(6)	-0.00009(6)	-0.00012(11)

TABLE 2, 11: continued

ATOM	i j*	FETSCH	FEHAST	OXYKER	ALHAST	ZNCUMM	TREMOL*	TREMOL^N
T(2)	11	0. 00203(12)	0. 00163(7)	0. 00143(12)	0. 00147(8)	0. 00212(9)	0. 00131(8)	0. 00104(15)
	22	0. 00034(3)	0. 00041(2)	0. 00032(3)	0. 00032(2)	0. 00034(2)	0. 00029(2)	0. 00027(4)
	33	0. 00503(38)	0. 00489(24)	0. 00480(42)	0. 00343(26)	0. 00546(27)	0. 00332(26)	0. 00396(58)
	12	0. 00001(4)	-0. 00007(3)	-0. 00005(5)	-0. 00006(3)	-0. 00014(4)	-0. 00003(3)	-0. 00006(6)
	13	0. 00097(17)	0. 00102(9)	0. 00057(18)	0. 00070(11)	0. 00051(12)	0. 00078(11)	0. 00048(25)
	23	0. 00007(9)	0. 00007(5)	0. 00005(9)	-0. 00006(6)	0. 00001(6)	-0. 00007(6)	-0. 00012(11)
M(1)	11	0. 00278(12)	0. 00230(7)	0. 00211(18)	0. 00200(9)	0. 00274(12)	0. 00209(17)	0. 00129(16)
	22	0. 00038(3)	0. 00069(2)	0. 00035(6)	0. 00047(2)	0. 00035(3)	0. 00041(5)	0. 00024(4)
	33	0. 00523(38)	0. 00482(25)	0. 00697(66)	0. 00641(30)	0. 00654(37)	0. 00399(58)	0. 00374(64)
	12	0	0	0	0	0	0	0
	13	0. 00181(17)	0. 00154(9)	0. 000169(25)	0. 00123(11)	0. 00117(15)	0. 00105(22)	0. 00060(27)
	23	0	0	0	0	0	0	0

TABLE 2.11: continued

ATOM	i j*	FETSCH	FEHAST	OXYKER	ALHAST	ZNCUMM	TREMOL*	TREMOL^N
	11	0.00201(15)	0.00173(6)	0.00194(19)	0.00155(10)	0.00257(7)	0.00219(17)	0.00093(16)
	22	0.00029(3)	0.00040(2)	0.00038(5)	0.00051(3)	0.00037(3)	0.00038(5)	0.00028(5)
	33	0.00495(49)	0.00557(23)	0.00727(69)	0.00616(34)	0.00700(43)	0.00478(57)	0.00238(67)
M(2)	12	0	0	0	0	0	0	0
	13	0.00064(21)	0.00121(8)	0.00159(26)	0.00089(13)	0.00096(17)	0.00093(22)	0.00045(27)
	23	0	0	0	0	0	0	0
	11	0.00252(15)	0.00244(9)	0.00234(29)	0.00221(11)	0.00279(19)	0.00233(25)	0.00138(23)
	22	0.00021(3)	0.00034(3)	0.00027(7)	0.00036(3)	0.00037(5)	0.00032(7)	0.00019(6)
	33	0.00548(50)	0.00513(33)	0.00619(102)	0.00577(37)	0.00667(58)	0.00438(85)	0.00356(88)
M(3)	12	0	0	0	0	0	0	0
	13	0.00059(22)	0.00082(12)	0.00057(39)	0.00064(14)	0.00090(23)	0.00057(32)	0.00074(38)
	23	0	0	0	0	0	0	0

TABLE 2.11: continued

ATOM	i j*	FETSCH	FEHAST	OXYKER	ALHAST	ZNCUMM	TREMOL*	TREMOL^N
M(4)	11	0.00316(14)	0.00343(10)	0.00309(15)	0.00258(10)	0.00285(9)	0.00274(10)	0.00292(20)
	22	0.00051(3)	0.00060(3)	0.00055(4)	0.00059(3)	0.00086(2)	0.00042(3)	0.00060(6)
	33	0.00302(44)	0.01045(35)	0.00896(55)	0.00759(33)	0.00694(26)	0.00769(35)	0.01015(83)
	12	0	0	0	0	0	0	0
	13	0.00233(19)	0.00368(15)	0.00362(22)	0.00201(13)	0.00226(12)	0.00293(13)	0.00359(33)
	23	0	0	0	0	0	0	0
H	11	-	-	-	-	-	-	0.0085(52)
	22	-	-	-	-	-	-	0.00166(18)
	33	-	-	-	-	-	-	0.01799(237)
	12	-	-	-	-	-	-	0
	13	-	-	-	-	-	-	-0.00018(91)
	23	-	-	-	-	-	-	0

* i j of βij

TABLE 2.12: MAGNITUDES AND ORIENTATIONS OF THE PRINCIPAL AXES OF THE THERMAL ELLIPSOIDS

ATOM	*	FETSCH	FEHAST	OXYKER	ALHAST	ZNCUMM	TREMOL*	TREMOL^N
	R.M.S.	0.104(7)	0.101(4)	0.093(8)	0.084(7)	0.073(7)	0.073(6)	0.069(4)
	a	92(36)	84(74)	81(242)	55(25)	71(14)	103(20)	46(19)
	b	80(24)	78(61)	39(147)	83(10)	20(15)	15(26)	62(20)
	c	16(39)	24(94)	56(277)	50(26)	90(9)	79(28)	70(14)
	R.M.S.	0.112(7)	0.104(4)	0.094(8)	0.095(7)	0.091(6)	0.083(6)	0.076(3)
	a	152(26)	140(24)	39(75)	37(25)	146(18)	64(46)	121(28)
O(1)	b	118(27)	127(31)	73(252)	79(14)	71(15)	77(28)	32(25)
	c	74(40)	66(95)	138(255)	140(26)	105(19)	162(40)	86(34)
	R.M.S.	0.123(6)	0.114(4)	0.107(8)	0.115(5)	0.104(5)	0.088(5)	0.080(4)
	a	62(26)	50(18)	52(26)	103(12)	117(18)	30(44)	119(26)
	b	105(24)	140(17)	124(24)	13(13)	85(10)	84(22)	106(31)
	c	87(17)	94(16)	68(26)	86(12)	15(19)	75(47)	20(15)

TABLE 2.12: continued

ATOM	*	FETSCH	FEHAST	OXYKER	ALHAST	ZNCUMM	TREMOL*	TREMOL^N
	R.M.S.	0.097(7)	0.092(4)	0.088(8)	0.090(6)	0.091(6)	0.076(6)	0.065(4)
	a	67(90)	29(13)	18(20)	56(17)	103(66)	147(30)	9(14)
	b	113(40)	87(9)	98(49)	136(33)	13(68)	91(22)	86(10)
	c	45(37)	76(13)	122(43)	75(25)	89(20)	42(30)	111(20)
	R.M.S.	0.099(7)	0.107(4)	0.094(8)	0.098(6)	0.095(5)	0.084(6)	0.074(4)
	a	121(80)	62(13)	94(59)	107(30)	159(46)	118(33)	94(21)
O(2)	b	147(112)	86(26)	39(23)	129(34)	103(69)	118(35)	115(10)
	c	91(110)	166(14)	126(42)	129(23)	95(25)	127(33)	149(16)
	R.M.S.	0.105(7)	0.115(4)	0.110(7)	0.111(6)	0.104(5)	0.091(6)	0.088(3)
	a	140(45)	95(14)	72(15)	142(15)	107(25)	74(23)	84(6)
	b	68(46)	5(22)	52(19)	106(17)	92(20)	152(35)	155(10)
	c	45(37)	87(25)	52(18)	42(20)	5(25)	72(26)	68(10)

TABLE 2.12: continued

ATOM	*	FETSCH	FEHAST	OXYKER	ALHAST	ZNCUMM	TREMOL*	TREMOL^N
	R.M.S.	0.091(12)	0.106(6)	0.099(10)	0.091(10)	0.079(9)	0.85(8)	0.087(4)
	a	116(9)	118(44)	90	103(15)	90	90	90
	b	90	90	0	90	0	0	0
	c	11(9)	14(44)	90	2(15)	90	90	90
	R.M.S.	0.099(10)	0.111(6)	0.112(10)	0.112(8)	0.095(8)	0.093(7)	0.085(6)
	a	90	152(44)	23(136)	90	56(22)	72(13)	139(53)
	b	0	90	90	0	90	90	90
O(3)	c	90	103(44)	130(136)	90	159(22)	177(13)	34(53)
	R.M.S.	0.140(9)	0.113(6)	0.115(10)	0.117(8)	0.110(7)	0.115(6)	0.089(5)
	a	26(9)	90	65(136)	13(15)	34(22)	18(13)	49(53)
	b	90	0	90	90	90	90	90
	c	79(9)	90	40(136)	92(15)	69(22)	87(13)	56(53)

TABLE 2.12: continued

ATOM	*	FETSCH	FEHAST	OXYKER	ALHAST	ZNCUMM	TREMOL*	TREMOL^N
	R.M.S.	0.065(10)	0.035(5)	0.031(9)	0.082(7)	0.067(7)	0.069(7)	0.065(4)
	a	71(7)	62(7)	105(10)	127(8)	64(4)	60(7)	58(4)
	b	23(9)	31(12)	158(18)	113(17)	26(4)	30(9)	34(6)
	c	107(8)	108(16)	70(19)	35(15)	98(5)	101(17)	106(7)
	R.M.S.	0.106(7)	0.099(5)	0.101(9)	0.099(6)	0.119(5)	0.086(6)	0.085(4)
	a	54(10)	70(9)	69(15)	86(16)	115(11)	74(10)	66(7)
O(4)	b	112(9)	113(15)	111(19)	153(17)	81(7)	104(15)	113(7)
	c	149(10)	156(13)	158(18)	117(17)	141(12)	166(14)	154(7)
	R.M.S.	0.135(6)	0.142(4)	0.126(7)	0.116(5)	0.136(5)	0.122(5)	0.108(3)
	a	42(9)	36(4)	27(13)	38(8)	143(9)	35(5)	42(4)
	b	97(6)	109(3)	97(9)	103(15)	66(4)	116(5)	113(4)
	c	64(10)	75(4)	80(14)	70(10)	52(12)	86(6)	70(6)

TABLE 2.12: continued

ATOM	*	FETSCH	FEHAST	OXYKER	ALHAST	ZNCUMM	TREMOL*	TREMOL^N
	R.M.S.	0.091(8)	0.094(5)	0.082(9)	0.092(7)	0.077(7)	0.074(7)	0.063(4)
	a	92(18)	98(14)	102(9)	132(67)	98(9)	104(9)	109(7)
	b	125(9)	125(3)	126(7)	121(23)	131(3)	120(5)	119(3)
	c	36(7)	37(4)	36(7)	46(50)	41(4)	30(6)	30(3)
	R.M.S.	0.103(7)	0.103(4)	0.117(7)	0.097(6)	0.106(5)	0.101(5)	0.085(3)
	a	157(12)	168(10)	154(17)	136(67)	171(8)	162(11)	157(7)
O(5)	b	103(15)	93(9)	102(16)	74(37)	88(7)	93(12)	92(5)
	c	90(7)	87(12)	98(13)	115(54)	87(8)	93(10)	98(7)
	R.M.S.	0.133(6)	0.150(4)	0.134(7)	0.125(5)	0.144(5)	0.119(5)	0.114(3)
	a	113(12)	99(4)	113(18)	100(9)	95(6)	101(12)	103(4)
	b	40(8)	36(3)	39(8)	35(8)	41(3)	30(5)	29(3)
	c	54(7)	54(3)	55(7)	55(8)	49(3)	60(5)	62(3)

TABLE 2.12: continued

ATOM	*	FETSCH	FEHAST	OXYKER	ALHAST	ZNCUMM	TREMOL*	TREMOL^N
	R.M.S.	0.036(8)	0.090(5)	0.077(10)	0.036(7)	0.091(6)	0.069(7)	0.069(4)
	a	92(11)	113(8)	116(9)	104(24)	82(22)	110(8)	114(10)
	b	39(7)	48(4)	46(7)	38(5)	60(9)	59(7)	56(4)
	c	52(7)	44(4)	48(6)	53(6)	36(8)	32(6)	37(4)
	R.M.S.	0.117(7)	0.114(4)	0.120(7)	0.098(6)	0.102(5)	0.099(5)	0.036(3)
	a	176(19)	155(8)	154(9)	159(18)	161(10)	155(14)	155(10)
O(6)	b	94(16)	98(7)	112(14)	92(20)	71(13)	114(18)	98(8)
	c	74(18)	99(8)	88(15)	96(16)	80(19)	84(13)	98(9)
	R.M.S.	0.131(6)	0.143(4)	0.136(7)	0.142(5)	0.152(5)	0.110(5)	0.106(3)
	a	86(22)	100(6)	86(17)	105(6)	107(4)	75(20)	97(6)
	b	129(7)	137(4)	128(10)	127(5)	144(4)	139(14)	144(4)
	c	43(11)	47(4)	42(6)	38(5)	56(4)	59(7)	54(4)

TABLE 2.12: continued

ATOM	*	FETECH	FEHAST	OXYKER	ALHAST	ZNCUMM	TREMOL*	TREMOL^N
	R.M.S.	0.109(10)	0.117(6)	0.102(11)	0.110(9)	0.065(11)	0.067(10)	0.070(5)
	a	90	90	90	90	90	90	90
	b	0	0	0	0	0	0	0
	c	90	90	90	90	90	90	90
	R.M.S.	0.131(10)	0.126(6)	0.111(11)	0.119(8)	0.113(8)	0.103(7)	0.097(4)
	a	165(19)	158(14)	160(9)	127(12)	177(7)	177(32)	166(9)
O(7)	b	90	90	90	90	90	90	90
	c	60(19)	97(14)	94(9)	128(12)	80(7)	78(32)	89(9)
	R.M.S.	0.153(9)	0.145(6)	0.160(10)	0.150(8)	0.158(6)	0.118(7)	0.118(5)
	a	75(19)	112(14)	110(9)	143(12)	93(7)	93(32)	104(9)
	b	90	90	90	90	90	90	90
	c	30(19)	7(4)	4(9)	38(12)	10(7)	12(32)	1(9)

TABLE 2.12: continued

ATOM	*	FETSCH	FEHAST	OXYKER	ALHAST	ZNCUMM	TREMOL*	TREMOL^N
	R.M.S.	0.074(3)	0.031(2)	0.067(4)	0.067(5)	0.072(3)	0.063(3)	0.058(6)
	a	70(7)	72(18)	75(9)	46(7)	85(5)	107(12)	104(30)
	b	20(7)	22(9)	17(8)	83(26)	7(8)	53(26)	56(29)
	c ⌒	96(13)	82(37)	87(21)	60(8)	86(7)	38(25)	34(28)
	R.M.S.	0.035(3)	0.034(2)	0.075(4)	0.073(4)	0.036(2)	0.068(3)	0.066(5)
	a	93(13)	64(15)	74(12)	89(19)	111(9)	66(11)	138(63)
T(1)	b	163(13)	86(35)	87(20)	171(21)	83(8)	39(26)	129(53)
	c	73(13)	163(26)	177(21)	81(16)	146(9)	125(25)	66(40)
	R.M.S.	0.096(3)	0.095(2)	0.039(4)	0.037(4)	0.096(2)	0.033(2)	0.069(5)
	a	20(7)	32(7)	22(9)	136(7)	22(8)	30(6)	51(63)
	b	110(7)	112(6)	107(7)	84(9)	93(4)	100(6)	123(53)
	c	107(13)	81(7)	91(11)	32(7)	124(9)	77(6)	67(35)

TABLE 2.12: continued

ATOM	*	FETSCH	FEHAST	OXYKER	ALHAST	ZNCUMM	TREMOL*	TREMOL^N
	R.M.S.	0.075(3)	0.075(2)	0.071(4)	0.067(5)	0.073(3)	0.063(3)	0.063(5)
	a	93(7)	126(6)	72(15)	102(13)	74(4)	114(8)	63(27)
	b	163(13)	119(9)	19(12)	78(30)	16(4)	77(17)	37(22)
	c	73(13)	38(9)	161(19)	12(32)	92(8)	16(13)	74(21)
	R.M.S.	0.036(3)	0.034(2)	0.079(4)	0.071(4)	0.036(2)	0.070(3)	0.071(5)
	a	75(12)	91(13)	116(28)	110(12)	98(6)	107(13)	152(30)
T(2)	b	107(13)	143(12)	88(23)	159(20)	87(8)	162(15)	70(47)
	c	163(13)	125(10)	138(28)	78(32)	159(6)	79(17)	58(69)
	R.M.S.	0.097(3)	0.089(2)	0.084(3)	0.083(4)	0.101(2)	0.078(2)	0.074(5)
	a	15(12)	36(6)	147(25)	23(10)	18(4)	30(9)	84(66)
	b	88(7)	111(13)	71(12)	107(10)	105(4)	102(12)	120(34)
	c	90(12)	77(10)	50(28)	89(8)	110(6)	78(7)	37(66)

ABLE 2.12: continued

TOM	*	FETSCH	FEHAST	OXYKER	ALHAST	ZNCUMM	TREMOL*	TREMOL^N
	R.M.S.	0.076(3)	0.073(2)	0.076(6)	0.038(3)	0.076(3)	0.070(5)	0.070(6)
	a	115(3)	117(2)	90	90	90	106(6)	77(36)
	b	90	90	0	0	0	90	90
	c	10(3)	12(2)	90	90	90	2(6)	178(36)
	R.M.S.	0.079(3)	0.105(2)	0.095(4)	0.089(3)	0.093(3)	0.083(5)	0.063(6)
DC(1)	a	90	153(2)	43(15)	47(11)	74(6)	90	90
	b	0	90	90	90	90	0	0
	c	90	102(2)	148(15)	152(11)	176(6)	90	90
	R.M.S.	0.114(2)	0.107(2)	0.107(3)	0.098(2)	0.110(2)	0.098(4)	0.077(5)
	a	25(3)	90	47(15)	43(11)	16(6)	16(6)	13(36)
	b	90	0	90	90	90	90	90
	c	80(3)	90	58(15)	62(11)	86(6)	88(6)	92(36)

TABLE 2.12: continued

ATOM	*	FETSCH	FEHAST	OXYKER	ALHAST	ZNCUMM	TREMOL*	TREMOL^N
	R.M.S.	0.070(4)	0.030(2)	0.079(5)	0.034(3)	0.079(4)	0.079(5)	0.055(9)
	a	90	136(5)	90	2(16)	90	101(8)	106(32)
	b	0	90	0	90	0	90	90
	c	90	31(5)	90	107(16)	90	4(8)	1(32)
	R.M.S.	0.032(4)	0.032(2)	0.035(5)	0.091(3)	0.097(3)	0.079(5)	0.068(6)
	a	93(11)	90	31(11)	90	81(12)	90	90
(2)	b	90	0	90	0	90	0	0
	c	162(11)	90	136(11)	90	176(12)	90	90
	R.M.S.	0.097(4)	0.093(2)	0.103(5)	0.091(3)	0.107(3)	0.100(4)	0.065(6)
	a	3(11)	46(5)	59(11)	88(16)	9(12)	11(8)	165(32)
	b	90	90	90	90	90	90	90
	c	103(11)	59(5)	46(11)	17(16)	94(12)	94(8)	91(32)

TABLE 2.12: continued

ATOM	*	FETESCH	FEHAST	OXYKER	ALHAST	ZNCUMM	TREMOL*	TREMOL^N
	R.M.S.	0.059(5)	0.076(3)	0.067(9)	0.077(4)	0.079(5)	0.072(8)	0.056(9)
	a	90	90	90	90	90	90	90
	b	0	0	0	0	0	0	0
	c	90	90	90	90	90	90	90
	R.M.S.	0.036(4)	0.033(3)	0.090(8)	0.038(4)	0.095(4)	0.076(7)	0.067(9)
	a	96(6)	84(4)	103(14)	99(9)	86(9)	91(9)	69(27)
M(3)	b	90	90	90	90	90	90	90
	c	159(6)	169(4)	151(14)	156(9)	171(9)	164(9)	84(27)
	R.M.S.	0.110(3)	0.107(2)	0.103(6)	0.103(3)	0.112(4)	0.103(6)	0.030(7)
	a	6(6)	4(4)	13(14)	9(9)	4(9)	1(9)	21(27)
	b	90	90	90	90	90	90	90
	c	111(6)	102(4)	119(14)	114(9)	99(9)	106(9)	84(27)

ABLE 2.12: continued

TOM	*	FETSCH	FEHAST	OXYKER	ALHAST	ZNCUMM	TREMOL*	TREMOL^N
	R.M.S.	0.092(3)	0.C88(2)	0.074(4)	0.090(3)	0.082(2)	0.074(3)	0.078(6)
	a	90	138(2)	136(2)	133(4)	128(2)	135(2)	142(4)
	b	0	90	90	90	90	90	90
	c	90	33(2)	31(2)	28(4)	25(2)	30(2)	37(4)
	R.M.S.	0.093(3)	0.1CC(2)	0.094(3)	0.099(3)	0.118(2)	0.082(3)	0.099(5)
	a	55(4)	90	90	90	142(2)	90	90
1C(4)	b	90	0	0	0	90	0	0
	c	160(4)	90	90	90	115(2)	90	90
	R.M.S.	0.123(3)	0.139(2)	0.132(3)	0.114(2)	0.120(2)	0.123(2)	0.133(4)
	a	35(4)	48(2)	47(2)	43(4)	90	45(2)	52(4)
	b	90	90	90	90	0	90	90
	c	70(4)	57(2)	58(2)	63(4)	90	60(2)	52(4)

TABLE 2.12: continued

ATOM	*	FETISCH	FEHAST	OXYKER	ALHAST	ZNCUMM	TREMOL*	TREMOL^N
	R.M.S.	-	-	-	-	-	-	0.062(19)
	a	-	-	-	-	-	-	19(6)
	b	-	-	-	-	-	-	90
	c	-	-	-	-	-	-	86(6)
	R.M.S.	-	-	-	-	-	-	0.161(10)
	a	-	-	-	-	-	-	71(6)
H	b	-	-	-	-	-	-	90
	c	-	-	-	-	-	-	176(6)
	R.M.S.	-	-	-	-	-	-	0.067(9)
	a	-	-	-	-	-	-	90
	b	-	-	-	-	-	-	0
	c	-	-	-	-	-	-	90

1969a and personal communication) in which the associated standard deviations are those obtained from the full matrices of errors both in atomic positions and cell parameters. These are presented in Tables 2.8, 2.9 and 2.10 respectively. Final anisotropic temperature factor coefficients are given in Table 2.11. The magnitudes and orientations of the principal axes of the thermal ellipsoids were calculated using the program ERRORS (Finger, personal communication) and are presented in Table 2.12.

(ii) Neutron Refinement

Atomic coordinates and isotropic temperature factors from the x-ray refinement of tremolite (Papike et al., 1969) were used as input parameters to the least-squares program RFINE. Coherent neutron scattering amplitudes were taken from the compilation by the Neutron Diffraction Commission (1969).

One cycle of refinement varying the atomic positions resulted in an R-factor of 11.4%; varying the isotropic temperature factors resulted in an R-factor of 4.1% and a further cycle varying atomic positions and isotropic temperature factors gave an R-factor of 3.8%. At this stage, it was noted that the temperature factor for the A-site was extremely large at 18.8$\AA^2$. Reducing this value to a typical single A-site value of 6.0$\AA^2$ (Hawthorne & Grundy, 1972) resulted in a drastic increase in the R-factor. This would indicate that the scattering power at the A-site

is much less than that assigned by the chemical analysis. Consequently, the A-site temperature factor was set at 6.0$\AA^2$ and the site-occupancy was refined; this led to a substantial reduction in the amount of alkalis on the A-site and an R-factor of 3.7%. The same procedure for the x-ray data gave a similar result.

At this stage, the temperature factors were converted to anisotropic and refined, giving an R-factor of 3.1%. Fourier and difference fourier sections in the vicinity of the A-site indicated a splitting of the A-site in the mirror plane only for both x-ray and neutron data. Since the correlations between temperature factor and site-occupancy are high in unconstrained refinement, the isotropic temperature factors of the split A-sites were set at a typical value of 1.6$\AA^2$ and the positions and occupancy were refined, giving an R-factor of 3.0%. Refining the occupancies of the octahedral and tetrahedral sites with chemical constraints together with all other parameters except the temperature factors of the A(m) sites gave an R-factor of 2.9%. At this stage, a parameter for isotropic extinction was introduced into the refinement (Zachariasen, 1963). Several cycles of refinement gradually increasing the number of variables resulted in convergence at an R-factor of 2.2%. Slight negative occupancies were observed at the M(3) and T(2) sites, but these were well within the standard deviation, and setting them to zero did not produce any significant change in the R-factor or the structural parameters. Unconstrained

refinement of the A(m)-site parameters resulted in high correlations between parameters but the results were statistically the same as those obtained from the above procedure. This together with the parallel result of the x-ray refinement, indicates that the chemical analysis is in error with respect to the alkalis.

Final positional parameters and equivalent isotropic temperature factors are presented in Table 2.6 and observed and calculated structure factors are given in Appendix 2. Site-occupancies are given in Table 2.7. Interatomic distances and angles were calculated with the program ERRORS and are presented in Tables 2.8, 2.9 and 2.10. Final anisotropic temperature factors are given in Table 2.11. The magnitudes and orientations of the principal axes of the thermal ellipsoids were calculated using the program ERRORS, and are presented in Table 2.12.

(iii) Mössbauer Refinement

Ferrotschermakite

The experimental spectrum showed one resolved ferrous iron doublet and a small satellite peak on the upper velocity side of the lower velocity component peak. This satellite peak was attributed to ferric iron with a quadrupole split component at lower velocity. In addition, the upper velocity peak has a slight shoulder, indicating that it contains more than one peak. Preliminary fitting of six peaks indicated

that the Fe^{3+}/Fe^{2+} ratio derived from the chemical analysis was slightly low. The X-ray site populations for ferrotschermakite indicated a small amount of ferrous iron in M(2); if this iron is considered as Fe^{3+}, the Mössbauer Fe^{3+}/Fe^{2+} ratio agrees with the chemical analysis, i.e.,

$$\left(\frac{Fe^{3+}}{Fe^{2+}}\right)_{MOSS} = \left(\frac{2Fe^{M(2)}}{2Fe^{M(1)}+Fe^{M(3)}}\right)_{X\text{-}RAY}$$

This suggests that all the iron in the M(2) site of the ferrotschermakite is Fe^{3+}. The preliminary fitting also showed that the intensity of the upper velocity doublets was slightly less than the lower velocity doublets, indicating that a slight amount of sample orientation was still present. Because of this, the components of the Fe^{2+} quadrupole split doublets were not constrained to be equal during the refinement. Least squares fitting of two ferrous doublets and one ferric doublet with all half widths constrained to be equal and the area ratios constrained to the x-ray site-populations gave a statistically acceptable χ^2 value of 423. Thus the experimental results of the Mössbauer spectrum are completely compatible with the X-ray site-populations. The resolved spectrum is shown in figure 2.2. The half-width constraint was then released and a constraint of equal half-widths for each doublet was applied; refinement converged at a χ^2 value of 412. The half-widths are all virtually identical and essentially equal to the half-widths of the previous refinement.

Figure 2.2 The resolved Mössbauer Spectrum for Ferrotschermakite

All half-widths are equal and the peak area ratios have been constrained to be equal to the x-ray derived site-populations. Experimental points are represented by the vertical 'dashes' which cover 1 standard deviation either side of the measured point.

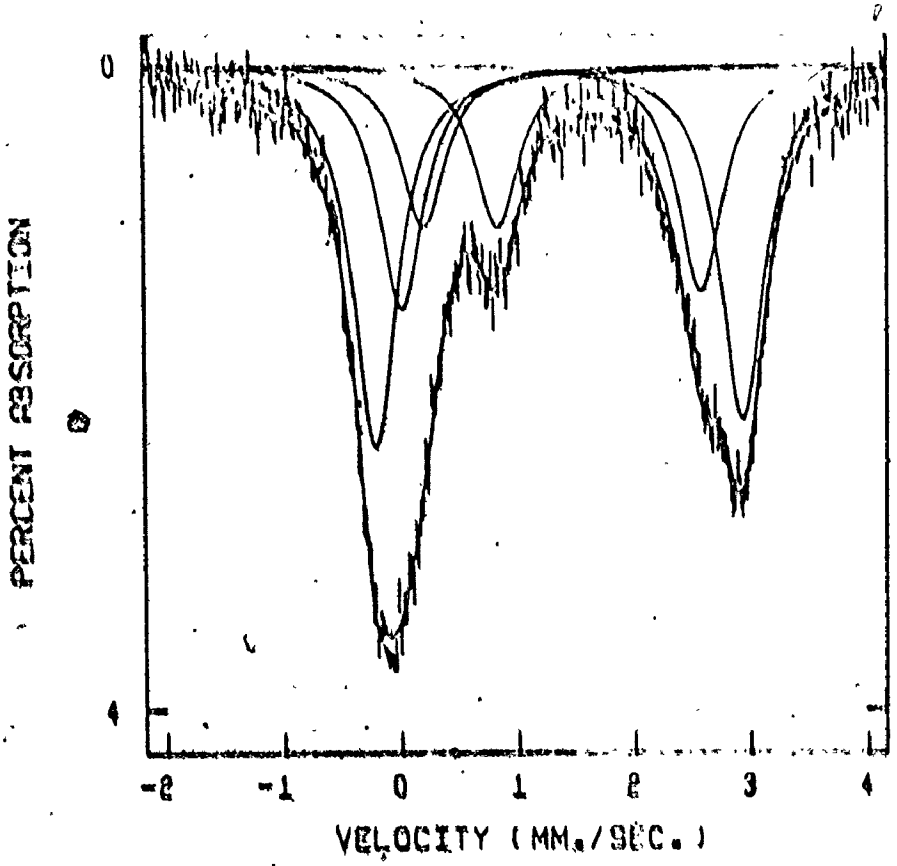

At this stage, the area constraints derived from the x-ray refinement were removed. In most work on complex spectra, the areas of doublet components are constrained to be equal to prevent excessive variable correlation. However, the presence of asymmetry due to sample orientation invalidates this constraint. This difficulty was overcome by constraining the area ratios of quadrupole-split peaks to be equal to the asymmetry factor (= 1.078 for this spectrum). With this constraint plus the constraint of equal half-widths for all peaks, the least-squares refinement converged at a χ^2-value of 419.

Releasing the constraint of equal half-widths for all peaks and imposing the constraint of equal half-width for doublet components, refinement converged at a χ^2-value of 407. Removing all area constraints and imposing the constraint of equal half-widths for all peaks, refinement converged at a χ^2-value of 417. Releasing the constraint of equal half-widths for all peaks and imposing the contraint of equal half-widths for doublet components, refinement converged at a χ^2-value of 401.

Attempts to refine the spectrum with no imposed constraints were unsuccessful and resulted in divergence. Final parameters for each refinement are given in Table 2.12a together with the χ^2-value and the 1% and 99% points of the chi-squared distribution.

TABLE 2.12a: MOSSBAUER PARAMETERS FOR FERROTSCHERMAKITE

I.S. = Isomer shift H.W. = Half-width

Q.S. = Quadrupole splitting A.R. = Intensity ratio, normalized to $I_{M(1)} = 1.$

	CONSTRAINTS	$Fe^{2+}_{M(1)}$	$Fe^{2+}_{M(3)}$	$Fe^{3+}_{M(2)}$	X^2	1%	99%
I.S.		1.220	1.161	0.444			
Q.S.	X-ray area constraints	2.884	2.354	0.577	423	312	440
H.W.	All half-widths equal	0.420	0.420	0.420			
A.R.		1.00	0.639	0.328			
I.S.		1.219	1.161	0.433			
Q.S.	X-ray area constraints	2.874	2.335	0.599	412	311	439
H.W.	Doublet half-widths equal	0.419	0.461	0.441			
A.R.		1.0	0.639	0.328			
I.S.		1.219	1.158	0.442			
Q.S.	'Equal' areas	2.870	2.332	0.583	419	311	439
H.W.	All half-widths equal	0.427	0.427	0.427			
A.R.		1.0	0.565	0.313			
I.S.		1.222	1.172	0.427			
Q.S.	'Equal' areas	2.897	2.377	0.613	407	309	436
H.W.	Doublet half-widths equal	0.391	0.513	0.438			
A.R.		1.0	0.957	0.348			

TABLE 2.12a: continued

CONSTRAINTS	$Fe^{2+}_{M(1)}$	$Fe^{2+}_{M(3)}$	$Fe^{3+}_{M(2)}$	X^2	1%	99%
I.S.	1.210	1.135	0.436			
Q.S. No area constraints	2.887	2.374	0.593			
H.W. All half widths equal	0.422	0.422	0.422	417	308	435
A.R. L.V.	1.0	.740	.452			
A.R. U.V.	1.097	.614	.370			
I.S.	1.212	1.152	0.438			
Q.S. No area constraints	2.924	2.418	0.594			
H.W. Doublet half-widths equal	0.369	0.505	0.427	401	308	435
A.R. L.V.	1.0	1.769	0.514			
A.R. U.V.	1.240	1.256	0.527			

L.V. signifies lower velocity component

U.V. signifies upper velocity component

Ferrohastingsite

The experimental spectrum showed one resolved ferrous iron doublet and a fairly intense single peak at ~0.8 mm/sec. on the velocity scale (see figure 2.3). The position of the single peak is compatible with it being the higher velocity component of a ferric iron doublet, the lower velocity component of which overlaps with the low velocity ferrous peak(s). The upper velocity ferrous peak shows two slight shoulders, indicating that it is made up of three closely overlapping peaks; the presence of three ferrous doublets is also indicated by the x-ray site-population refinement. Thus the lower velocity peak consists of three ferrous and one ferric peak, closely overlapped.

Preliminary fitting confirmed that the Fe^{3+}/Fe^{2+} ratio determined by chemical analysis was correct and that orientation effects were negligible. As before, the area ratios were constrained to be equal to the site-population ratios determined by x-ray refinement. However, Mn^{2+} occurs in the octahedral sites in this particular amphibole, and thus the x-ray site-populations were refined as Fe*, where $Fe^{*}=Fe^{2+}+Fe^{3+}+Mn$. Using the regression equations for $\langle M\text{-}O \rangle$ distance as a function of ionic radius (developed in a later section), site-populations may be derived. Assuming all the Fe^{3+} is in the M(2) site, a $\langle M(2)O \rangle$ distance of 2.045Å is forecast and is statistically equal to the observed value of 2.047(2)Å.

A similar procedure for M(1) and M(3) gives the Mn site-occupances of M(1) = 0.03Mn and M(3) = 0.08Mn with the observed and calculated mean bond lengths given below:

⟨M(1)-O⟩	OBSERVED = 2.113(2)	CALCULATED = 2.111
⟨M(3)-O⟩	OBSERVED = 2.126(2)	CALCULATED = 2.123

The confidence in the Fe^{3+} result is high but the results for Mn must be treated with caution as the correlations for M(1) and M(3) are not as well developed as that for M(2). Least-squares fitting of three ferrous and one ferric doublet with all half-widths constrained to be equal and the area ratios constrained to the x-ray results (with the Mn correction) resulted in convergence at a statistically acceptable χ^2 value of 439. The resolved spectrum is shown in figure 2.3. Imposing the constraint of equal half-widths on quadrupole split doublets, refinement converged at a χ^2 value of 432 with negligible change in the refined parameters. The asymmetry factor for the ferrous iron doublets was 1.050.

Removing the x-ray site-population constraints and imposing the constraint of equal areas (corrected for the asymmetry factor) for component doublet peaks and equal half-widths for all peaks, the least-squares refinement converged to a χ^2-value of 419. Changing the half-width constraints to equal half-widths for component doublets, convergence

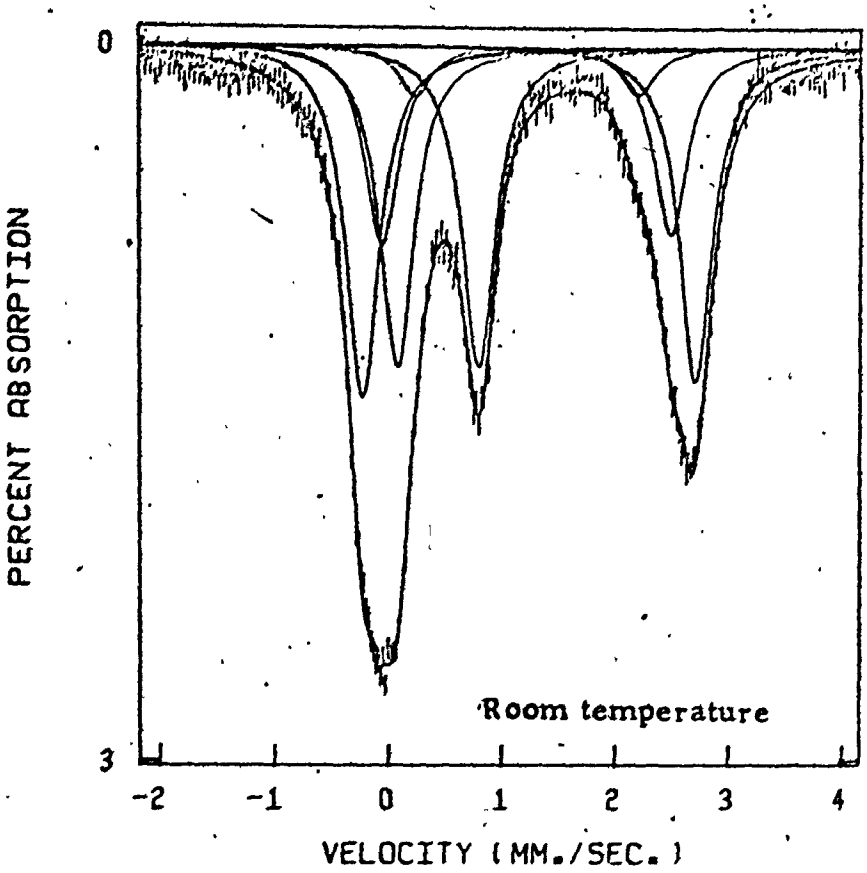
PERCENT ABSORPTION
0
3
Room temperature
-2
-1
0
1
2
3
4
VELOCITY (MM./SEC.)

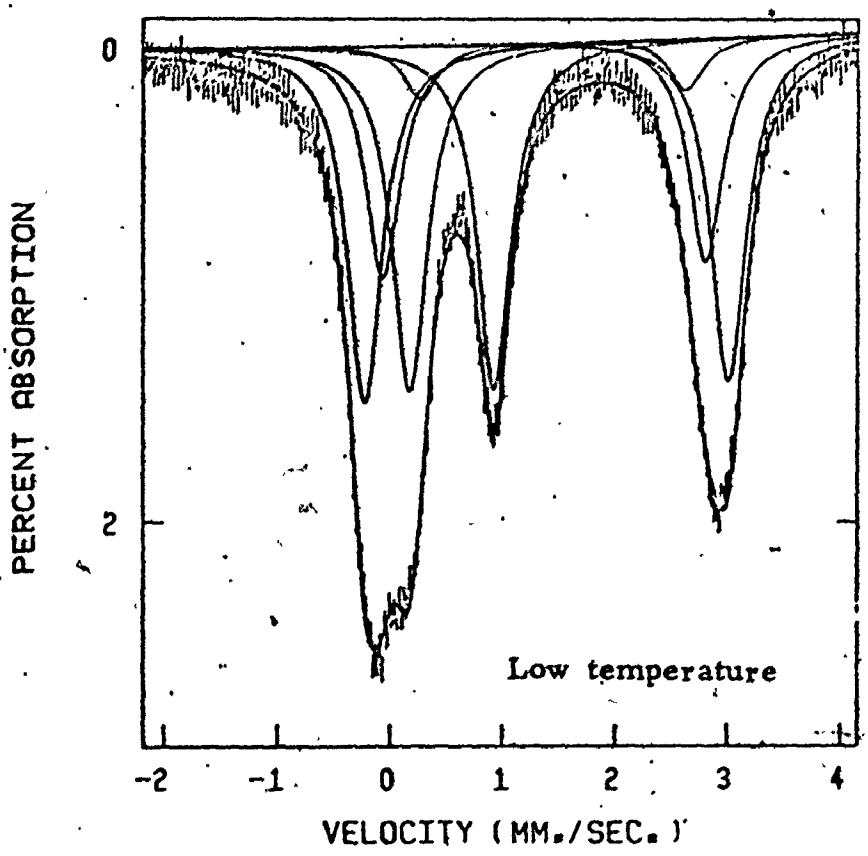
PERCENT ABSORPTION
0
2
Low temperature
-2
-1
0
1
2
3
4
VELOCITY (MM./SEC.)

TABLE 2.14: MOSSBAUER PARAMETERS FOR FERROHASTINGSITE

Legend as in Table 2.12a

(i) Room Temperature Spectrum

CONSTRAINTS		$Fe^{2+}_{M(1)}$	$Fe^{2+}_{M(2)}$	$Fe^{2+}_{M(3)}$	$Fe^{3+}_{M(2)}$	X^2	1%	99%
I.S.		1.113	1.091	1.089	0.374			
Q.S.	X-ray area constraints	2.688	1.798	2.326	0.649	439	302	441
H.W.	All half-widths equal	0.324	0.324	0.324	0.324			
A.R.		1.0	0.146	0.563	0.913			
I.S.		1.113	1.095	1.089	0.373			
Q.S.	X-ray area constraints	2.693	1.794	2.341	0.650	432	304	439
H.W.	Doublet half-widths equal	0.330	0.276	0.312	0.317			
A.R.		1.0	0.146	0.563	0.913			
I.S.		1.114	1.102	1.094	0.370			
Q.S.	'Equal' area constraints	2.718	1.844	2.386	0.656	419	307	434
H.W.	All half-widths equal	0.315	0.315	0.315	0.315			
A.R.		1.0	0.238	0.747	1.063			

TABLE 2.14: continued

CONSTRAINTS	$Fe^{2+}_{M(1)}$	$Fe^{2+}_{M(2)}$	$Fe^{2+}_{M(3)}$	$Fe^{3+}_{M(2)}$	X^2	1%	99%
I.S.	1.115	1.105	1.100	0.368			
Q.S. 'Equal' area constraints	2.749	1.893	2.425	0.661	414	305	431
H.W. Doublet half-widths equal	0.287	0.343	0.320	0.320			
A.R.	1.0	0.370	1.111	1.348			

TABLE 2.14: continued

(ii) Low Temperature Spectrum

	CONSTRAINTS	$Fe^{2+}_{M(1)}$	$Fe^{2+}_{M(2)}$	$Fe_{M(3)}$	$Fe^{3+}_{M(2)}$	X^2	1%	99%
I.S.		1.251	1.302	1.231	0.474			
Q.S.	X-ray area constraints	2.973	2.168	2.638	0.688	434	302	441
H.W.	All half-widths equal	0.339	0.339	0.339	0.339			
A.R.		1.0	0.146	0.563	0.913			
I.S.		1.250	1.307	1.236	0.470			
Q.S.	X-ray area constraints	2.993	2.130	2.660	0.693	427	304	439
H.W.	Doublet half-widths equal	0.345	0.225	0.295	0.329			
A.R.		1.0	0.146	0.563	0.913			
I.S.		1.254	1.303	1.238	0.472			
Q.S.	'Equal' Areas	3.027	2.141	2.692	0.691	401	307	434
H.W.	All half-widths equal	0.325	0.325	0.325	0.325			
A.R.		1.0	0.234	1.076	1.204			

resulted at a χ^2-value of 414 after a large number (29) of iterations. Attempts to remove further constraints during refinement were unsuccessful.

In an attempt to improve the resolution of the peaks, spectra were recorded at liquid nitrogen temperatures. Examination of the experimental data (figure 2.3) shows that the resolution of the lower velocity component peaks is improved but that of the higher velocity component peaks is decreased. The same refinement procedure was employed as for the room temperature spectrum and the results are similar. With the x-ray site-populations used as area constraints, χ^2-values of 434 and 427 respectively were produced while release of further constraints produced lower χ^2-values.

Final parameters and χ^2-values for the room- and low-temperature fitted spectra are given in Table 2.14.

Oxy-Kaersutite

Preliminary spectra run at 6 mm/sec. confirmed the chemical analysis result that no ferrous iron was present, and subsequent spectra were run at 2.5 mm/sec. in an attempt to achieve better resolution of the overlapping peaks. The experimental spectrum shows one ferric doublet with only the slightest asymmetry in the peak shapes; however, a single doublet fit to the spectrum is completely

unsatisfactory. Least-squares refinement of a single doublet with the constraints of equal areas and equal half-widths converged to a χ^2-value of 912. Subsequent refinement with the constraints removed converged to a χ^2-value of 874; the fitted spectrum is shown in Figure 2.4. The single doublet fits are completely unsatisfactory and as the structure refinement indicated that Fe^{3+} occupied all three octahedral sites, a three doublet fit was attempted. The peak areas were constrained to be equal to the x-ray site-population refinement results and all half-widths were constrained to be equal; least-squares refinement resulted in convergence at a χ^2-value of 404. However, a large number of cycles had to be performed before convergence was attained as the correlations between parameters were extremely high and the variables tended to oscillate. All attempts to remove any of the constraints were unsuccessful and resulted in divergence. Final parameters are given in Table 2.15 and the resolved spectrum is shown in figure 2.4.

Zn-Cummingtonite

Mössbauer investigations into the ferromagnesian amphiboles have been quite extensive (Bancroft, Burns and Maddock, 1967; Hafner & Ghose, 1971; Buckley & Wilkins, 1971) and the spectra are well characterized. Consequently, the Mössbauer results for Zn-Cummingtonite were used in conjunction with the x-ray results in an attempt to assign complete site-occupancies.

Figure 2.4 Mössbauer spectrum of Oxy-kaersutite

(a) 2-Peak Fit

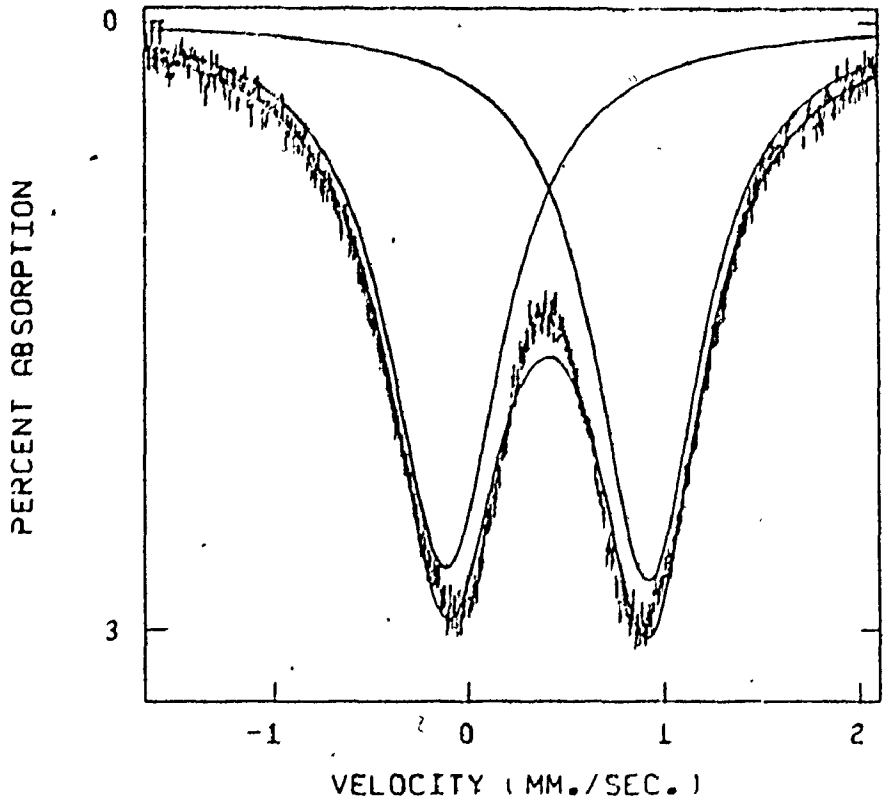

(b) 6-Peak Fit

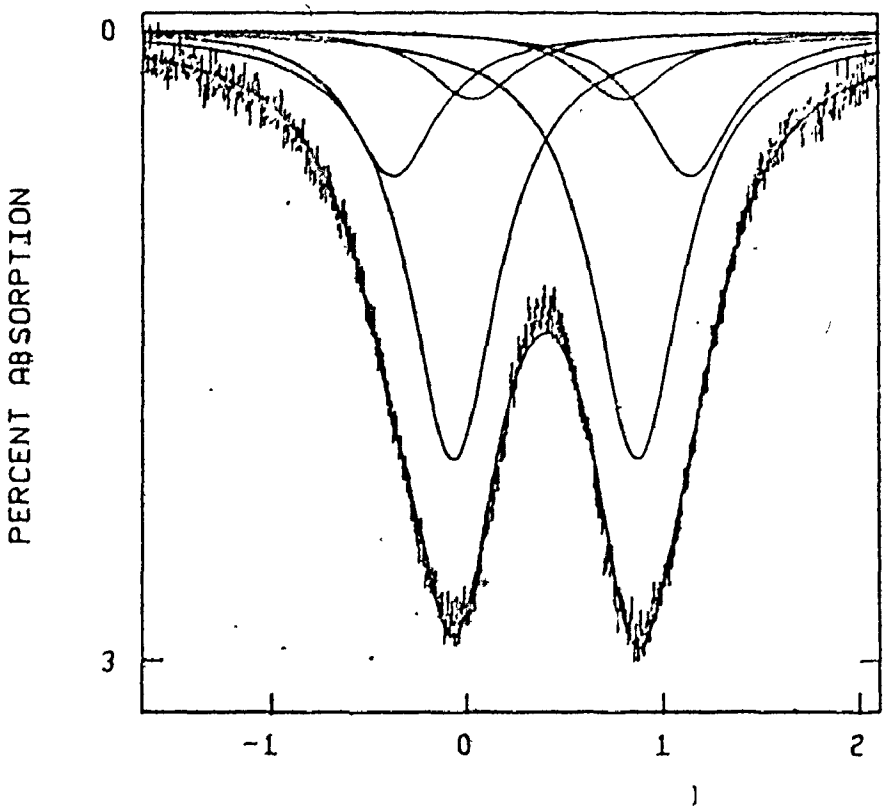

TABLE 2.15: MOSSBAUER PARAMETERS FOR OXYKAERSUTITE

Legend as in Table 2.12a

(i) Two Peak Fit

CONSTRAINTS	Fe^{3+}	X^2	1%	99%
I.S.	.388			
Q.S.	1.033			
None		874	311	442
H.W.	.682			
A.R.	-			

(ii) Six Peak Fit

CONSTRAINTS	$Fe^{3+}_{M(1)}$	$Fe^{3+}_{M(2)}$	$Fe^{3+}_{M(3)}$	X^2	1%	99%
I.S.	.389	.393	.368			
Q.S. X-ray area constraints	.956	.589	1.533			
				404	313	440
H.W. All half-widths equal	.514	.514	.514			
A.R.	1.0	2.092	.343			

The experimental spectrum shows two quadrupole-split ferrous doublets (see figure 2.5); by analogy with the previous work on ferromagnesian amphiboles, the inner doublet was assigned to Fe^{2+} in M(4) while the outer doublet was assigned to Fe^{2+} in M(1), M(2) and M(3). This outer doublet could consist of three overlapping doublets; however, the small half-width indicates that either this overlap is nearly perfect or the octahedral Fe^{2+} is ordered into one site.

In addition to these two doublets, an inflexion is present on the upper velocity site of the lower velocity component of the M(4) ferrous doublet. The chemical analysis indicates the presence of Fe^{3+} in both octahedral and tetrahedral coordination, and this inflexion can be assigned to the high velocity component of an octahedrally coordinated Fe^{3+} doublet. Even allowing for the hidden Fe^{3+}_{IV} component, the lower velocity absorption is much greater than the higher velocity absorption; however, the method of sample preparation precludes significant asymmetry effects due to preferred orientation. This suggests the presence of another ferric iron doublet in the low velocity part of the spectrum as is indicated by the chemical analysis, and an attempt was made to fit four doublets to the spectrum.

Starting parameters were estimated visually from the experimental spectrum. The position of the lower velocity component of the octahedral Fe^{3+} doublet was estimated from isomer shift and quadrupole splitting values of similar doublets in other amphiboles examined in this study. The [illegible] and intensities of the hidden Fe^{3+} doublet

Figure 2.5 The resolved Mössbauer Spectra of Zn-Cummingtonite

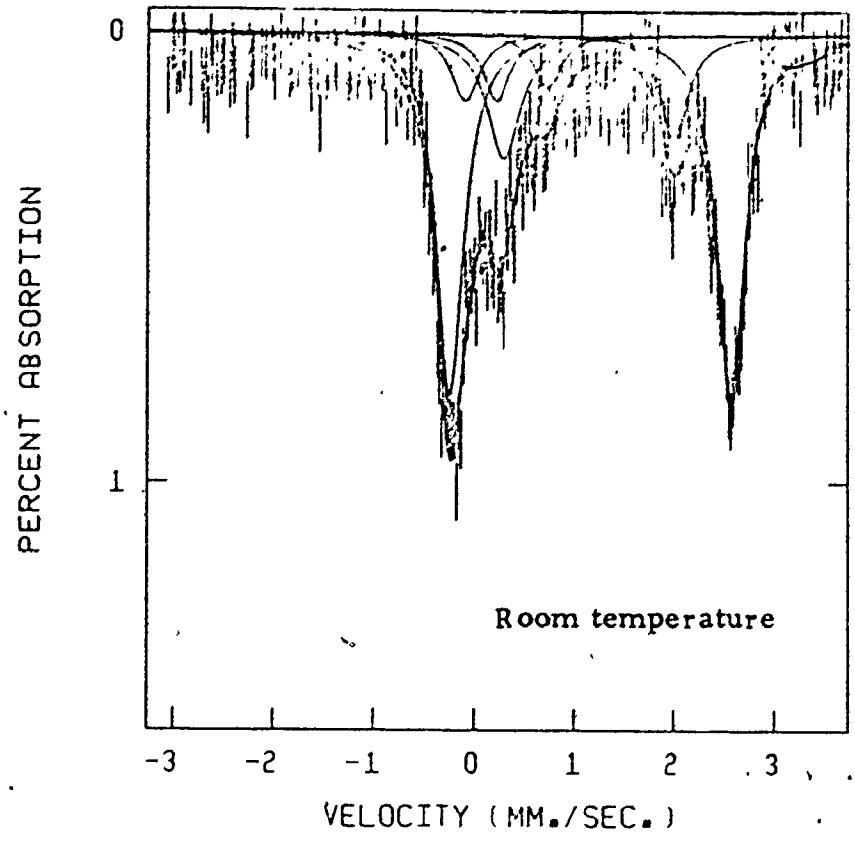

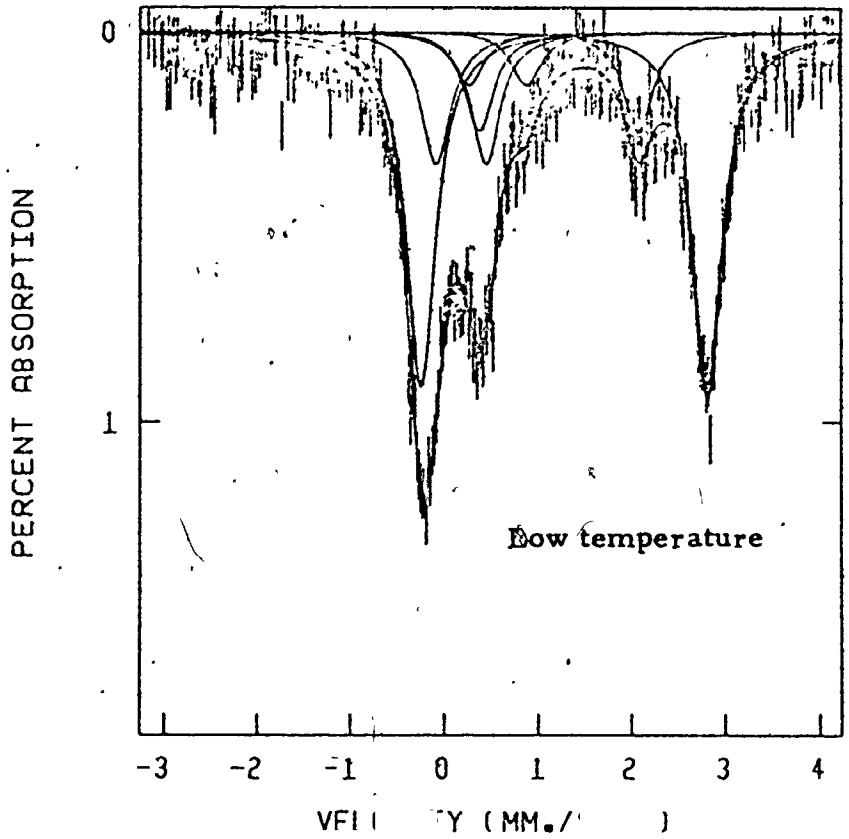

components were estimated by examining the residuals obtained by subtracting the high velocity ferrous peaks and the octahedral Fe^{3+} doublet from thelow velocity ferrous peaks. During the initial refinement cycles, area ratios and all other parameters were kept constant.

Attempts to vary all the positions with the constraints of equal half-widths for all peaks and equal area for doublet components resulted in divergence. Examination of the iterations prior to divergence showed that the positions of two peaks (initially assigned as the low velocity component of the M(4) Fe^{2+} doublet and the low velocity component of the octahedral Fe^{3+} doublet) were converging on the same value, and when they became equal to within one standard deviation, extreme divergence immediately occurred indicating an imminent singularity in the matrix. This was taken as indicative of nearly perfect overlap of these two peaks, and thus they were combined with the intensity of the joint peak constrained to be equal to the sum of the intensities of their high velocity counterparts. In addition, all half-widths except that of the 'double' peak were constrained to be equal, and refinement resulted in convergence at a χ^2-value of 415. The half-width of the 'double' peak was only slightly larger than those of the single peaks (see Table 2.16), thus justifying the assumption of complete overlap of these two peaks.

TABLE 2.16: MOSSBAUER PARAMETERS FOR ZN - CUMMINGTONITE

Legend as in Table 2.12a

(i) Room Temperature Spectrum

	CONSTRAINTS	$Fe^{2+}_{M(4)}$	$Fe^{2+}_{M(1,2,3)}$	$Fe^{3+}_{M(2)}$	$Fe^{3+}_{T(2)}$	X^2	1%	99%
I.S.		1.078	1.130	0.447	0.111			
Q.S.	Equal area constraints	1.775	2.808	0.514	0.494	423	308	435
H.W.	All half-widths equal	0.329	0.329	0.329	0.329			
A.R.		1.0	3.614	0.569	0.618			

(ii) Low Temperature Spectrum

	CONSTRAINTS	$Fe^{2+}_{M(4)}$	$Fe^{2+}_{M(1,2,3)}$	$Fe^{3+}_{M(2)}$	$Fe^{3+}_{T(2)}$	X^2	1%	99%
I.S.		1.147	1.232	0.454	0.118			
Q.S.	Equal area constraints	1.743	3.076	0.637	0.519	421	307	434
H.W.	All half-widths equal	0.357	0.357	0.357	0.357			
A.R.		1.0	3.642	0.547	1.620			

TABLE 2:16: continued

(iii) Site-Occupancies

$Fe^{2+}_{M(4)}$	$Fe^{2+}_{M(1,2,3)}$	$Fe^{3+}_{M(2)}$	$Fe^{3+}_{T(2)}$
0.045	0.165	0.020	0.01

To check the validity of this result, the low temperature (liquid nitrogen) spectrum was recorded. The refinement converged to a χ^2-value of 421 for 8 peaks with the constraint of equal half-widths for all peaks. All attempts to remove this half-width constraint resulted in divergence, and examination of the correlation matrix derived from the least-squares procedure showed that there was extreme correlation between variables of strongly overlapping peaks (see discussion in Chapter 3).

Final parameters for both spectra are given in Table 2.16 and the fitted spectra are shown in figure 2.5. The Mössbauer parameters for the octahedral Fe^{3+} doublet indicate that the Fe^{3+} is ordered into M(2) {c.f. Oxy-kaersutite, Table 2.15}. The remaining doublet is a little more problematical; initially it was tentatively assigned to Fe^{3+} in tetrahedral coordination and the x-ray refinement results are marginally improved by inclusion of the amount of tetrahedral Fe^{3+} indicated by the chemical analysis. In addition, the isomer shift values are in good agreement with values obtained for a doublet in the spectra of titanium-zirconium garnets (Dowty, 1971) which was assigned to tetrahedral Fe^{3+}. However, these values are low when compared with the isomer shifts of Fe^{3+} in R.E. iron garnets ($\langle$ I.S. $\rangle$ = 0.30 mm/sec., Nicholson & Burns, 1964), spinel-type cubic ferrites ($\langle$ I.S. $\rangle$ = 0.25 mm/sec., Mizoguchi & Tanaka, 1963) and Fe^{3+} bearing orthoclase ($\langle$ I.S. $\rangle$ = 0.46 mm/sec., Brown & Pritchard, 1969). Dowty's fitting of the garnet

spectra has been critized by Burns (1972) on two counts: firstly that the garnet structure has only one octahedral site and thus cannot give rise to more than one octahedral Fe^{3+} doublet, and secondly that the isomer shift of the tetrahedral Fe^{3} doublet is lower than that of tetrahedral Fe^{3+} in sulphides, inferring that the Fe^{3+}-O bond is more covalent than the Fe^{3+}-S bond. The first criticism is not relevant to this study but the second criticism is pertinent and must be considered with reference to the Zn-cummingtonite spectra.

Examination of the Zn-cummingtonite spectra shows that the intensity of the disputed doublet is proportionally much greater at low temperature than at high temperature, indicating that the recoil-free fraction of this component is much more temperature dependent than the recoil-free fractions of the octahedral sites. This indicates that the bonding is much stronger for the doublet assigned to tetrahedral Fe^{3+} than for octahedral Fe^{3+} as would be expected if the assignment is correct.

The magnitude of the isomer shift is a function of the s-electron density at the nucleus, and the extremely low values of the I.S. for this particular doublet indicates a high s-electron density at the nucleus. Changes in s-electron density at the nucleus are mainly the result of variations in the shielding properties of the 3d-electrons.

Increase in oxidation state, increased covalent bonding and/or high spin → low spin transitions will decrease I.S. values. Tetrahedral low spin Fe^{3+} has never been recorded and it is extremely unlikely that the crystal field stabilization energy could be adequate to compensate for the spin-pairing energy. Increase in oxidation state would result (in this case) in Fe^{4+} in tetrahedral coordination. Fe^{4+} ions do occur in oxygen-ligated compounds (e.g. $SrFeO_3$) with I.S. values of 0.05-0.10 mm/sec. which is fairly conformable with the parameters for Ti-garnet and Zn-cummingtonite, suggesting that this doublet could be due to Fe^{4+} ions in tetrahedral coordination. Although a substitution of this type is favourable from a bond-strength viewpoint, the occurrence of unusual cation valence states in natural minerals is rare and this possibility is considered unlikely.

Comparison with I.S. values for tetrahedral Fe^{3+} in R.E. iron garnets and other silicates would indicate that the increased covalent bonding expected in tetrahedral coordination is not, in general, sufficient to produce I.S. values as low as those observed here. However, recent work on synthetic ferri-diopsides (Hafner & Huckenholz, 1971), natural ferri-augites (Virgo, 1972) and synthetic ferri-phlogopite (Annersten, Devanarayanan, Häggström & Wäppling, 1971) has shown peaks with parameters compatible with those obtained in the present study. In particular, the ferri-phlogopite spectrum shows a single Fe^{3+} doublet with an I.S. of 0.17 mm/sec. (with no possibility that the doublet could be generated

by the fitting process since no other doublet is present). Thus an oxygen environment can produce I.S. values smaller than those generally encountered in sulphides. The reason for this becomes apparent from the crystallography of these minerals. The x-ray results indicate that the Fe^{3+} occurs in the T(2) tetrahedron in zinc-cummingtonite which is analogous to the tetrahedron in the clinopyroxenes. The most apparent feature of these tetrahedra is their extremely short T-O(nbr) bonds. Brown & Shannon (1973) have suggested that the covalency of a bond is related to its length (see discussion in Chapter 4); accordingly, the T(2)-O(4) and T(2)-O(2) bonds in the amphiboles and the T-O(2) and T-O(1) bonds in the pyroxenes will be extremely covalent, and the small amounts of Fe^{3+} occurring in these tetrahedra will show very low isomer shifts.

Combining the peak intensities with the chemical analysis gives the site-populations given in Table 2.16. The peak area of the tetrahedral Fe^{3+} peak was not used in the site-population calculation because of the expected difference in the recoil-free fractions between octahedral and tetrahedral bonding environments. Fe^{3+} was assigned to the tetrahedral sites $\{T(2)\}$ to fill them up and the remaining populations were assigned from the Mössbauer and chemical analysis results.

CHAPTER III

SITE-POPULATIONS BY LEAST-SQUARES FITTING OF X-RAY AND/OR MÖSSBAUER DATA

Site-populations from X-Ray Data

The elucidation of cation ordering in crystals is a problem of great current interest in mineralogical crystallography. Where sufficient difference in scattering power occurs between cation species, site-populations may be derived during structural refinement. Early attempts involved the manual adjustment of site-populations at non-equivalent sites until the isotropic temperature factors were equal (Ghose & Hellner, 1959). Subsequent methods involved the least-squares refinement of binary site-populations (Fischer, 1966) or total site scattering powers (Dollase, 1969). In general it was found that the summation of the resulting site-populations did not agree with the bulk chemistry of the crystal (e.g. Finger, 1967, 1969a; Burnham, Okashi, Virgo and Hafner, 1971); this is probably due to high variable correlation during refinement. This problem was overcome for the refinement of two species distributed over more than one site by the use of linear constraints in the least-squares process. A

least-squares program (RFINE, Finger, 1969a) is currently available which incorporates linear constraints of the form

$$\sum_{i=1}^{m} a_i b + c = 0 \qquad 3.1$$

where a_i is any variable, and b and c are constants.

The use of linear constraints in site-population refinement was first treated by Finger (1969b) who gave the necessary constraints as

$$\sum_{j=1}^{n} a_{ij} = 1 \qquad (i = 1, m) \qquad 3.2$$

$$\sum_{i=1}^{m} b_i a_{ij} = c_j \qquad (j = 1, n) \qquad 3.3$$

where a_{ij} is the fractional occupancy of the i^{th} site by the j^{th} atom

b_i is the multiplicity of the i^{th} site

c_j is the total number of atoms of species j per unit cell

Although this approach has only been used for cation disorder involving two species, equations 3.2 and 3.3 are completely general and apply to any number of cation species distributed over any number of non-equivalent sites. Thus, there is no a priori reason why the preceding equations cannot be applied to more complex situations. Inspection of the existing least-squares programs show that direct application of these

equations in more complicated cases would involve extensive re-writing of parts of these programs. This may be circumvented by using the following simple algebraic procedure.

Let m = total number of non-equivalent cation sites of interest in the unit cell

n = total number of cation species distributed over these sites.

Each site may be split up into (n-1) 'subsites', each of which is occupied by two species with site-occupancies a_{kj} and a_{kn}, where the first subscript denotes the 'subsite' and takes the values (k=1, n-1), the second subscript denotes the cation species and j takes the value (j=1, n-1), and the following relation holds

$$\sum_{k=1}^{n-1} (a_{kj} + a_{kn}) = 1 \qquad 3.4$$

A set of (n-1) complete occupancy constraints modified from equation 3.2 may be written for these 'subsites'

$$a_{kj} + a_{kn} = K_k \quad (k=1, n-1) \qquad 3.5$$

where K_k are a group of constants which may be set by the user.

There are m sets of equations of type 3.5 corresponding to the m unique cation sites of interest in the unit cell, and (n-1) non-redundant bulk chemical constraints of the form of equation 3.3 may be written.

The initial situation of n species distributed over m sites involves mn population variables. However, division of each site into (n-1) 'subsites' produces 2m(n-1) variables. Equation 3.3 provides (n-1) constraints and equation 3.5 provides m(n-1) constraints, leaving (m-1)(n-1) variables to be determined by refinement.

During refinement, the positional and thermal parameters of all 'subsites' in a set are constrained to be equal by simple application of equation 3.1 to each parameter in turn. Least-squares refinement determines the occupancy parameters a_{ij} where i=1,m and j=1,(n-1), and the occupancies of the dependent species may thus be determined using

$$a_{in} = \sum_{k=1}^{n-1} a_{kn} \qquad (i=1,m) \qquad 3.7$$

It should be stressed that this is an algebraic way of obtaining a solution, provided a solution does exist; it does not insure that a unique solution does occur. The conditions for this are developed now.

Let A_i (i=1, m) be the scattering power at each site and x_j(j=1, n) be the scattering power of the j^{th} atom. The following set of equations define A_i in terms of a_{ij} (occupancy factor) and x_j

$$\sum_{j=1}^{n} a_{ij} x_j = A_i \qquad (i=1, m) \qquad 3.8$$

The condition for complete occupancy of the sites may be written as

$$\sum_{j=1}^{n} a_{ij} = 1 \qquad (i=1, m) \qquad 3.9$$

There are also (n-1) non-redundant bulk chemical constraints of the form

$$\sum_{i=1}^{m} a_{ij} b_i = c_j \qquad (j=1, n-1) \qquad 3.10$$

where b_i and c_j are as defined previously.

Thus, there are mn variables a_{ij} and (2m+n-1) equations; solutions only exist for

$$mn \leqslant 2m+n-1 \qquad 3.11$$

This condition holds for

(a) $m = 1 \rightarrow \infty$, $n = 2$ 3.12

(b) $m = 2$, $n = 3$

Condition (a) corresponds to the normal constrained refinement of binary site-populations, while condition (b) applies to refinement of three species over two sites (e.g. olivines, pyroxenes). For all other values of m and n, there is no unique solution to the site-distribution equations, and hence any attempt to apply the previous algebraic procedures will rely on the relative proportional fall-off of scattering factor with $\sin \theta/\lambda$. Since this is a marginal effect, it is only just within the resolution of modern x-ray data and every attempt must be made to remove systematic error in the data as this could easily obscure this effect.

The presence of high correlations is due to an ill-conditioned design matrix where two or more of the normal equations are sub-parallel. Formally, a limiting condition occurs where the rank of the matrix is greater than that necessary to span the manifold of the variables, when the matrix becomes singular upon inversion. Consider the distribution of 2 species of scattering powers A_1 and A_2 distributed over 2 sites 1 and 2. The contribution of these two sites to the structure factors may be written as

$$(a_{11}A_1 + a_{12}A_2)\, e^{h_k r_{1k} - t_1} + (a_{21}A_1 + a_{22}A_2)\, e^{h_k r_{2k} - t_2} \qquad 3.14$$

where $h_k r_{ik} = 2\pi(hx_i + ky_i + lz_i)$

$$t_i = B(\sin\theta/\lambda)^2$$

If the minimization function is given by

$$R = \sum(|F_o| - |F_c|)^2 = \sum\Delta^2 \qquad 3.15$$

assuming unit weights for simplicity, the form of the normal equations is given by

$$\sum_{i=1}^{n} e_i \left\{ \sum_{hkl} \frac{\partial|F_c|}{\partial u_j} \frac{\partial|F_c|}{\partial u_i} \right\} = \sum_{hkl} \Delta \frac{\partial|F_c|}{\partial u_j} \quad (j=1, n) \qquad 3.16$$

Assuming that the sites 1 and 2 are completely occupied, the following constraints may be written

$$a_{11} + a_{12} = 1 \qquad a_{21} + a_{22} = 1 \qquad 3.17$$

Rearranging the first derivative of these equations with respect to $|F_c|$ gives

$$\frac{\partial|F_c|}{\partial a_{12}} = -\frac{\partial|F_c|}{\partial a_{11}} \qquad \frac{\partial|F_c|}{\partial a_{22}} = -\frac{\partial|F_c|}{\partial a_{21}} \qquad 3.18$$

A similar situation occurs with the variables a_{11} and a_{21}. A bulk compositional constraint may be written as

$$a_{11} + a_{21} = \text{constant} \qquad 3.19$$

$$\frac{\partial a_{21}}{\partial a_{11}} = -1 \qquad 3.20$$

with the derivative with respect to a_{11} as shown. The derivatives of $|F_c|$ with respect to a_{11} and a_{21} may be written as

$$\frac{\partial |F_c|}{\partial a_{11}} = (A_1 - A_2)e^{h_k r_{1k} - t_1} + \frac{\partial a_{21}}{\partial a_{11}} (A_1 - A_2)e^{h_k r_{2k} - t_2} \qquad 3.21a$$

$$\frac{\partial |F_c|}{\partial a_{21}} = \frac{\partial a_{11}}{\partial a_{21}} (A_1 - A_2)e^{h_k r_{1k} - t_1} + (A_1 - A_2)e^{h_k r_{2k} - t_2} \qquad 3.21b$$

Substitution of 3.20 into 3.21 shows that the magnitude of the two derivatives are equal and thus the normal equations for a_{11} and a_{21} will be parallel. However, if the constraint of 3.19 is <u>not</u> applied, the derivatives $\partial a_{21}/\partial a_{11}$ and $\partial a_{11}/\partial a_{21}$ are ignored, and the normal

equations for a_{11} and a_{21} are consequently not parallel. The equations for the shifts are then

$$e_{a_{11}} \sum_{hkl} \left(\frac{\partial|F_c|}{\partial a_{11}}\right)^2 + e_{a_{21}} \sum_{hkl} \left(\frac{\partial|F_c|}{\partial a_{11}} \frac{\partial|F_c|}{\partial a_{21}}\right) + e_i \sum_{i=3}^{n} \left(\sum_{hkl} \frac{\partial|F_c|}{\partial a_{11}} \frac{\partial|F_c|}{\partial u_i}\right)$$

$$= \sum_{hkl} \Delta \frac{\partial|F_c|}{\partial a_{11}} \qquad 3.22a$$

$$e_{a_{11}} \sum_{hkl} \left(\frac{\partial|F_c|}{\partial a_{21}} \frac{\partial|F_c|}{\partial a_{11}}\right) + e_{a_{21}} \sum_{hkl} \left(\frac{\partial F_c}{\partial a_{21}}\right)^2 + e_i \sum_{i=3}^{n} \left(\sum_{hkl} \frac{\partial|F_c|}{\partial a_{21}} \frac{\partial|F_c|}{\partial u_i}\right)$$

$$= \sum_{hkl} \Delta \frac{\partial|F_c|}{\partial a_{21}} \qquad 3.22b$$

with the derivatives of F_c with respect to a_{11} and a_{22} being given by

$$\frac{\partial|F_c|}{\partial a_{11}} = (A_1 - A_2)\, e^{h_k r_{1k} - t_1} \qquad 3.23a$$

$$\frac{\partial|F_c|}{\partial a_{21}} = (A_1 - A_2)\, e^{h_k r_{2k} - t_2} \qquad 3.23b$$

These derivatives are incorrect because the derivative $\partial a_{11}/\partial a_{21}$ has been wrongly set equal to zero, and consequently the normal equations obtained from 3.22a and 3.22b are poor. This has a drastic

effect on the least-squares refinement using this procedure. It is apparent from equations 3.21, 3.20a and 3.20b that the correct derivatives $\frac{\partial|F_c|}{\partial a_{11}}$ and $\frac{\partial|F_c|}{\partial a_{21}}$ have the opposite sign and hence the shifts will exhibit a negative correlation (obviously -1 in this case). However, the derivatives given by 3.23a and 3.23b can even have the same sign depending upon the relative positions of the two sites, and hence the shifts can exhibit a positive correlation. Thus the bulk chemistry as indicated by the occupancy parameters cannot stay on composition during refinement. This will produce an overall increase or decrease (depending on the sign of the shift) in the magnitude of all the $|F_c|$'s which will be compensated by an opposite shift in the scale factor; hence a negative correlation coefficient will be exhibited between one or both occupancy parameters and the scale factor. In addition, sympathetic variation of the temperature factors with the occupancy parameters will also help to compensate for the variation in total scattering power, and hence a positive correlation will occur between occupancies and temperature factors.

This type of behaviour has been observed in refinements performed in this manner (Burnham et al., 1971), refinement of all variables resulted in convergence at a composition markedly different from that indicated by the chemical analysis. The correlation coefficients quoted by Burnham et al. (1971) ξ -0.7 between scale and occupancies, +0.5

between occupancies and up to +0.4 between anisotropic temperature factor coefficients and occupancies} conform to the above analysis and the correct solution was arrived at by a complicated procedure of cyclic refinement of various combinations of the variables in turn. Using the linear constraint of equation 3.21 (see Finger, 1969a,b), rapid convergence with low correlations were obtained. However, as shown above, the movement off-composition is not the result of high correlations as suggested by both Finger (1969a) and Burnham et al. (1971) but both the movement off-composition and the high correlations are due to ill-conditioned normal equations stemming from the incorrect expressions for the derivatives concerned.

The case of two species distributed over more than two sites is very similar. In the unconstrained refinement, the matrix is ill-conditioned because the proper derivatives are not calculated; hence the spurious correlations arise in this case too. However, when the form of the derivatives is properly modified (Finger, 1969b) as indicated previously, the correlations between occupancy parameters and scale and temperature factors decreases markedly. When more than two chemical variables are refined simultaneously using the procedure described previously, extremely high correlations between occupancy parameters are encountered. However, the correlation between the occupancy parameters

and scale and temperature factors is negligible. Using this procedure, the derivatives are properly modified and the total site-population chemistry is constrained; the matrix is ill-conditioned not because the normal equations are a poor approximation but because the solution is defined by an extremely marginal effect. This is illustrated by the zinc cummingtonite refinement where refinement of all the population parameters lead to extremely rapid convergence rather than the slow convergence that is encountered in unconstrained refinement.

Although the presence of high correlations does not invalidate the use of the least-squares procedure, the possibility does arise that the refinement may converge upon a local minimum rather than the true minimum, and additional information is needed to substantiate the final result. As indicated previously, the measured bulk chemistry may be used for this purpose in an unconstrained refinement involving two chemical species. However, with more than two species, the known bulk chemistry is already applied as constraints and it is necessary to look elsewhere for confirmation of true minimum convergence.

If convergence at a true minimum can be demonstrated, the least-squares results are perfectly valid despite the large correlations, provided that the standard deviations are extracted from the full variance-covariance matrix. This stipulation is extremely important as the use of a partitioned matrix at this stage can give rise to erroneously low standard deviations. Particular attention was paid to this point in the refinement

of zinc cummingtonite where two separate methods of refinement were used:

(i) simultaneous site-population refinement of all three chemical species;

(ii) successive cycles of refinement of site-populations of chemical species taken in pairs.

After convergence was attained in case (i), examination of the correlation matrix showed extremely high correlation coefficients between the various site-populations ($\gtrsim \pm 0.994$) but negligible correlation coefficients between site-populations and scale and temperature factors. The magnitude of the correlation coefficients between the site-populations is reflected in the magnitude of the standard deviations assigned to the final calculated site-populations by the least-squares routine (see Table 3.1). The ionic radii of the cations in each site were used to calculate the expected mean bond lengths for the octahedral sites using the regression equations developed in Chapter 4. The close correspondence between these values and those calculated from the final atomic coordinates appears to indicate (see Table 2.8) that the refinement has converged on the true minimum.

In case (ii) of the refinement procedure, the final structure of case (i) was used as input to each cycle of refinement in turn. There was no change in the parameters but examination of the correlation matrix after each cycle showed greatly reduced correlations between the two

TABLE 3.1: STANDARD DEVIATIONS FOR THE SITE-POPULATIONS in Zn-CUMMINGTONITE, CALCULATED USING THE FULL NORMAL EQUATIONS MATRIX AND USING A PARTITIONED NORMAL EQUATIONS MATRIX

(a) Full Normal Equations Matrix

M(1)	(0.042) Zn, (0.080) Mg, (0.065) Mn
M(2)	(0.053) Zn, (0.053) Mg
M(3)	(0.083) Zn, (0.098) Mg, (0.091) Mn

(b) Partitioned Normal Equations Matrix

M(1)	(0.004) Zn, (0.004) Mg, (0.004) Mn
M(2)	(0.004) Zn, (0.004) Mg
M(3)	(0.007) Zn, (0.007) Mg, (0.008) Mn

species refined ($\gtrsim \pm 0.4$) and increased correlation between site-populations and temperature factors ($\gtrsim 0.1$-0.4). This is reflected in the much lower standard deviations (see Table 3.1) assigned to the site-populations during this procedure. This factor of 10 difference between the magnitude of the assigned standard deviations has a great effect on the significance of the final result. According to method (ii), the presence of Zn in the M(2) site in zinc cummingtonite is highly significant whereas utilization of the full matrix as in case (i) indicates that the presence of Zn in M(2) is not significant, i.e. zero to within 1 standard deviation. This would tend to indicate that site-populations derived by method 2 (e.g. Cameron, 1970; Robinson, 1971; Robinson, Gibbs & Ribbe, 1973) have erroneous standard deviations, and the significance of site-populations can only be assessed from a full-matrix refinement.

Site Populations from Mössbauer Data

Mössbauer line shapes for the conditions of this experiment have been shown to be essentially Lorentzian (Bancroft, Williams & Essene, 1969); thus the intensity of the transmitted gamma beam y(x) as a function of its energy x has the form

$$y(x) = b - \frac{y(z)}{H\left(\frac{x-x(z)}{a/2}\right)^2}$$

where y(z) is the intensity at the resonance velocity x(z), a is the line width at half-peak height and b is the baseline intensity. The observed spectrum in an experiment performed with a multi-site phase consists of the resultant envelope of all the single absorption doublets corresponding to each site and species in the phase. Thus for i lines, the equation of the envelope is given by

$$y(x) = b - \sum_i \frac{y(z)_i}{1+\left(\frac{x-x(z)_i}{a_i/2}\right)^2}$$

In addition, slight sinusoidal and linear deviations occur in the baseline due to source movement and instrumental drift; thus b is modified in the above equation to account for these features. The parameters y(z), x(z) and a for each component peak, and b together with the correction terms, are determined by least-squares refinement; the function R_o is minimized where

$$R_o = \sum_{m=1}^{n} W_m (y(x|q) - y_m^{OBS})^2$$

W_m is the weight of each observation (determined by counting statistics), y_m^{OBS} is the observed count in channel m, $y(x)_m$ is the value of the count in channel m calculated from the previous equation, n is the total number of channels in the spectrum and q is the vector of the fitted parameters.

The fitting process is not trivial for complex structures such as the amphiboles, and several aspects of this process warrant further consideration.

If there is no systematic error in the data or the model, the residual R_o will be due entirely to random error in the counting (provided no other random error such as a dropped channel count is encountered). The resulting parameters determined by the least-squares will be correct and the residual is defined as

$$R_o' = \sum_{m=1}^{n} W_m (y(x|q') - y_m^{OBS})^2$$

where q' is the vector of the resultant parameters. R_o' follows the chi-squared distribution; if a set of parameters q is a valid approximation for q', then R_o is a value from this distribution. To test the hypothesis that q is a valid approximation for q', the percentage points of the chi-squared distribution are used to assess the probability that R_o' will exceed the value R_o (Law, 1973). In most Mössbauer work, an R_o value below the 1% point of the chi-squared distribution is considered as acceptable. However, below the 1% point, statistical tests cannot discriminate; there are no statistical grounds for preferring one R_o value over another if both lie below the 1% point since there is quite a high probability that R_o' will exceed the lower R_o value in this case.

The previous discussion relates purely to random error; the present study indicates that considerable systematic error occurs in the fitting procedure for complex overlapping spectra. In all the amphiboles examined, application of area constraints derived from the x-ray site-populations together with equal half-width constraints for all lines led to statistically acceptable χ^2 values for the fitting procedure. Thus the Mössbauer data is competely compatible with the x-ray refinement results. Relaxation of the half-width constraints to equal half-widths for components of a doublet resulted in a reduction in χ^2 which, as indicated above, is not statistically significant; results from both procedures were not significantly different. However, removal of the x-ray derived area constraints produced considerable changes in the refined areas. With the constraint of equal half-widths for all lines and equal areas for doublet components, considerable reductions in χ^2 were produced; these reductions are not significant. However, in some cases the area ratios changed drastically. Relaxation of the half-width constraints to equal half-widths for doublet components produced further reductions in χ^2 and further change in the area ratios which, in some cases, bore not the slightest resemblance to the x-ray results. In addition, the half-widths of the doublets changed markedly to become significantly different from each other. Removal of the equal area constraints resulted either in spectra that would not converge, or in spectra with completely

asymmetric doublets. Subsequent removal of half-width constraints generally resulted in divergence of the least-squares process.

The good agreement between the x-ray site-population results and the Mössbauer data indicates that the unconstrained (no x-ray derived area constraints) least-squares fitting procedure is giving spurious results. Examination of the correlation matrix after each refinement revealed large inter-parameter correlations. Even when the x-ray area constraints were applied, correlations of the order of $\sim|0.4|$ are common; relaxation of the x-ray area constraints produced increased coefficients in the correlation matrix. Obviously the design matrix is extremely ill-conditioned, the normal equations being far from orthogonal. One of the effects apparent was the increase in the number of iterations necessary before convergence as the constraints were relaxed. In extreme cases where the refinements failed, convergence could not be attained; the trial parameters were continually modified by a series of large, apparently random shifts that showed no systematic behaviour as the number of cycles increased. Further relaxation of constraints resulted in divergence where the matrix becomes singular. As the inter-parameter correlation increases, the minimum of the function becomes less well-defined until in extreme cases, it 'disappears'; in effect, the minimum becomes so broad that it approaches

a hyper-plane where convergence is impossible. As the matrix approaches this condition, the difference between the true minimum and the surrounding surface becomes statistically insignificant and "convergence" may occurr in any small random flexure in this surface.

This problem is similar to that encountered in the refinement of x-ray site-populations; in that case, however, small numbers of variables were involved and the problem was to some extent, susceptible to correction. For example, where two normal equations are parallel, the minimum becomes infinite in one dimension; similarly, where one normal equation can be expressed as a linear combination of other normal equations, the same situation occurs. This may be corrected by application of a suitable linear constraint. However, in the case of the spectrum fitting process, a large number of variables are not orthogonal and thus combine together to produce a hyper-surface with a very small radius of curvature.

The effect of releasing the constraints in a spectrum is shown in Table 3.2 where the correlation matrices for the room temperature ferrohastingsite spectrum are shown. Clearly, the presence of correlation coefficients of $\sim|0.8|$ in the unconstrained fit are affecting the refined parameters. Further examples of correlation matrices for the refinements of the various spectra are given in Appendix 3.

TABLE 3.2: THE CORRELATION MATRICES FOR THE ROOM TEMPERATURE MOSSBAUER SPECTRUM OF FERROHASTINGSITE, WITH ALL HALF WIDTHS CONSTRAINED TO BE EQUAL

```
 .03 -.09  .04 1.00
-.02  .04  .05 1.00

-.26  .40  .37  .19 1.00
-.29  .47  .32  .38 1.00

-.45  .69  .43 -.06  .72 1.00
-.13  .21  .16  .76  .45 1.00

-.02  .01  .02 -.25 -.07 -.01 1.00
-.01 -.01  .07  .54  .17  .77 1.00

.... .... .... .... .... .... .... ....
-.01 -.01  .04 -.64 -.12 -.77 -.52 1.00

 .00 -.02 -.03  .20 -.19 -.07 -.45 .... 1.00
 .03 -.06  .02  .23 -.02  .18  .23  .22 1.00

.... .... .... .... .... .... .... .... .... 1.00
-.40  .65  .26  .09  .64  .25 -.06 -.08 -.08 1.00

-.04  .03 -.03 -.09 -.38 -.06  .33 .... -.17 .... 1.00
 .01 -.07  .02  .01 -.33  .07  .32  .07  .15 -.16 1.00

.... .... .... .... .... .... .... .... .... .... .... 1.00
-.03  .01  .03 -.35 -.17 -.42 -.54 -.05 -.70 -.11 -.29 1.00

-.09  .11  .10  .02  .07  .17  .07 .....  .03 .....  .17 .....  1.00
-.08  .09  .12  .03  .08  .05  .05  .02  .03  .09  .13  .01 1.00

 .16 -.17 -.19  .05 -.02 -.14 -.01 ..... -.01 ..... -.05 ..... -.02 1.00
 .09 -.12 -.08 -.15 -.06 -.27 -.36 -.11 -.47 -.02 -.28  .57 -.03 1.00

 .10 -.08 -.10  .09  .20  .02 -.03 ..... -.05 ..... -.13 ..... -.01  .37 1.00
 .06 -.09 -.04 -.60 -.16 -.80 -.74 -.51 -.42 -.08 -.26  .66 -.02  .50 1.00

 .07 -.13  .04 -.01 -.13 -.10  .01 .....  .03 .....  .05 .....  .00  .13  .03 1.00
 .11 -.19 -.05 -.66 -.40 -.82 -.59  .74 -.05 -.27  .04  .30 -.01  .20  .63 1.00
```

The upper row refers to the fit with x-ray area constraints, the lower row to the fit without x-ray area constraints. The first three rows are not shown here; they are similar for all spectra and other examples are shown in Appendix 3.

The unconstrained fit for the ferrotschermakite spectrum (all half-widths equal) agrees reasonably with the x-ray results. Inspection of the correlation matrix (see Appendix 3) shows that its elements are not (in general) as large as those of the ferrohastingsite spectra. The amount of correlation appears to depend on the complexity of the spectrum and the amount of overlap of its constituent peaks.

These results indicate that the site-populations derived from Mössbauer spectra of complex structures such as the amphiboles, must be treated with extreme caution. This is further indicated by the fact that the errors usually attached to the derived site-populations are not derived from the full dispersion matrix, but solely from its diagonal elements. The presence of large off-diagonal elements in this matrix will greatly increase the size of the standard deviations of the derivative information. Thus discrepancies between x-ray and Mössbauer site-populations (e.g. see Burns & Greaves, 1971) could be the result of a poor error analysis for the spectral site-populations, provided the x-ray site-populations have been calculated using the correct constraints to reduce correlation. Conversely, the Mössbauer refinement could have converged at a false minimum.

There appears to be no way to improve the least-squares fitting process for Mössbauer spectra. In the case of the x-ray method, chemical constraints are usually applied to reduce this problem to manageable pro-

portions. However, no recourse can be made to this procedure in the case of Mössbauer spectra. If the values of the isomer shift and quadrupole splitting were known, this could provide sufficient information to reduce correlation significantly, but no way exists as yet of accurately predicting these parameters. Possibly an empirical correlation of these parameters with chemical composition could be made from data on a suite of well-characterized minerals, but again, these parameters may be sensitive to ordering (a factor that may not be apparent when examining a single suite of minerals) and small errors could make a significant difference to the fitting process since the area ratios and half-width parameters appear to be far more sensitive than the peak positions in the fitting process.

In summary, two possible situations exist in the fitting procedure with respect to the disagreement between x-ray and Mössbauer techniques noted in the literature:

(i) The spectrum fitting process may have converged on the correct solution but the calculated standard deviations are woefully underestimated.

(ii) The spectrum fitting process may have converged on a false minimum.

Before any weight can be given to Mössbauer site-populations for complex structures, confirmatory evidence is needed from an additional source such as the constrained site-population refinement of single-crystal x-ray data.

CHAPTER IV

CRYSTAL CHEMISTRY

THE IDEAL AMPHIBOLE STRUCTURE

The clino-amphibole structure may be conveniently considered as a sheet structure composed of alternating octahedral and tetrahedral layers parallel to the b-c plane. The ideal repeat element for each layer is shown in figure 4.1. The octahedral unit consists of a strip of edge-sharing holosymmetric octahedra extending infinitely in the c direction; the tetrahedral unit consists of a straight double chain of corner-sharing holosymmetric tetrahedra extending infinitely in the c-direction. These two elements are linked in the a and b directions (see Thompson, 1970; Papike & Ross, 1970) to produce an ideal amphibole structure with the M(4) and A sites generated by the joining of adjacent elements. Atomic coordinates may be derived from this ideal structure; it is convenient to work in an orthogonal system and the axes used to derive the coordinates in Table 4.1 were a*, b and c. Comparison of these coordinates with those of the refined amphiboles (transformed to the same axial system) shows that grunerite (see Table 4.1) is the least distorted from the ideal configuration, closely followed by the Mn-cummingtonites.

Figure 4.1 The ideal repeat units of the clino-amphibole structure

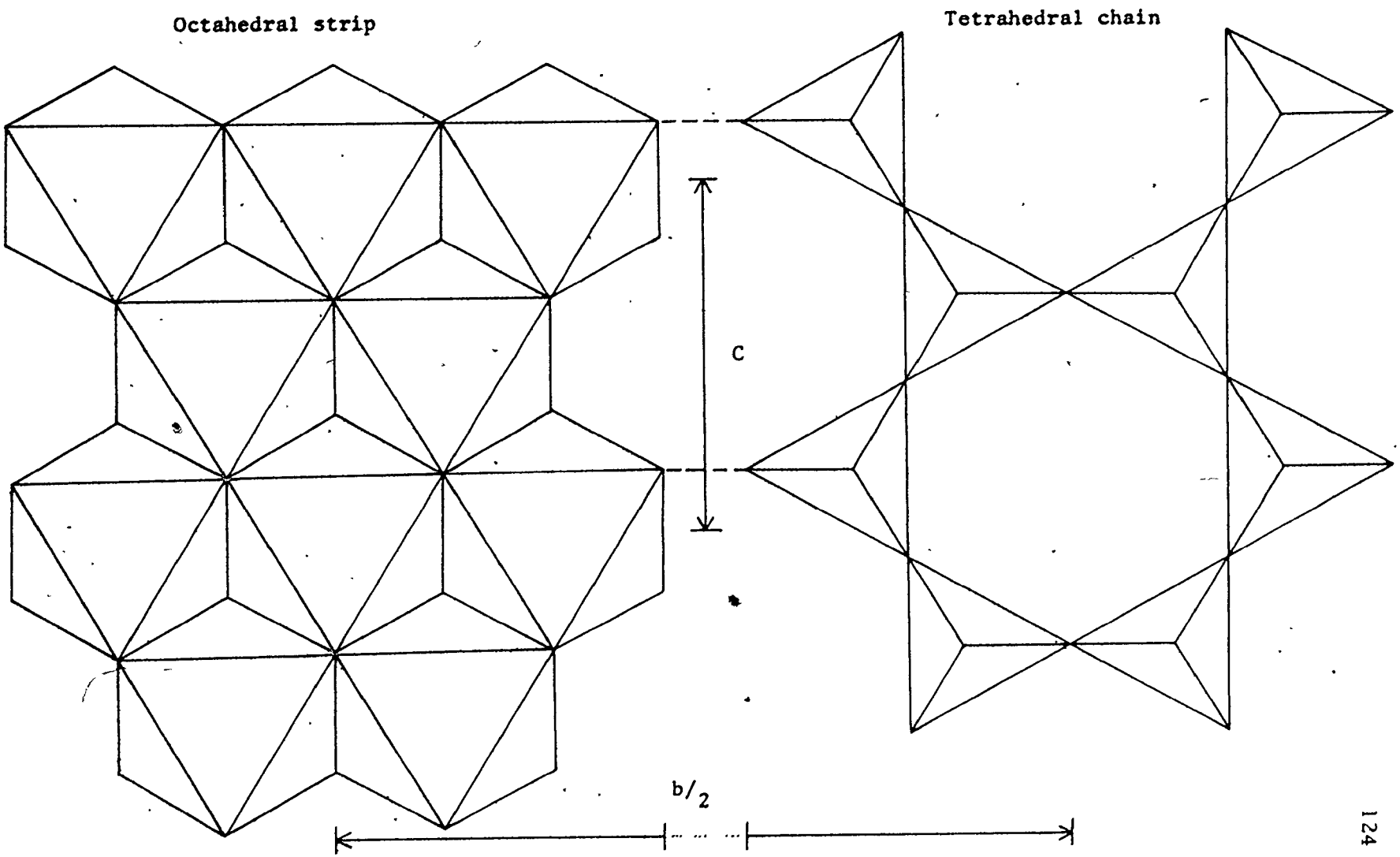

TABLE 4.1: METRIC COORDINATES OF THE IDEAL AMPHIBOLE STRUCTURE (UPPER SET) COMPARED WITH THE METRIC COORDINATES OF GRUNERITE

Atom	x	y	z
O(1)	0.1340	0.0833	0.1667
	0.1120	0.0882	0.1631
O(2)	0.1340	0.1667	0.6667
	0.1253	0.1735	0.6679
O(3)	0.1340	0	0.6667
	0.1147	0	0.6612
O(4)	0.3660	0.2500	0.6667
	0.3839	0.2416	0.6272
O(5)	0.3660	0.1250	-0.0833
	0.3483	0.1275	-0.0767
O(6)	0.3660	0.1250	0.4167
	0.3478	0.1182	0.4246
O(7)	0.3660	0	0.1667
	0.3376	0	0.1454
T(1)	0.3080	0.0833	0.1667
	0.2867	0.0836	0.1649
T(2)	0.3080	0.1667	0.6667
	0.2993	0.1667	0.6675
M(1)	0	0.0833	0.5
	0	0.0878	0.5
M(2)	0	0.1667	0
	0	0.1794	0
M(3)	0	0	0
	0	0	0
M(4)	0	0.2500	0.5
	0	0.2574	0.5

It is profitable to examine the deviations from ideality imposed by the articulation requirements of elements of variable dimensions. If the edge length of the octahedra is 2ℓ and the edge length of the tetrahedra is $2d$, cross linkage in the a and b directions requires that

$$\ell = 2d/\sqrt{3} \qquad 4.1$$

when no deviation from ideality occurs (i.e. the double chain is straight and T-O(br)-T = 141°). This results in an ideal octahedral:tetrahedral bond length ratio of 4:3. Using the ionic radii values of Shannon & Prewitt (1969, 1970a), the Si-O bond length may be calculated: a value of 1.62Å was derived which is fairly close to the tetrahedral bond length observed in non-aluminous amphiboles. Calculating the mean octahedral bond length from the above ratio and subtracting the mean anion radius gives 0.78Å as the ideal cation size necessary for no deviation from the ideal structure. This value corresponds to [6]-coordinated Fe^{2+} and correlates well with the fact that the grunerite structure shows the best agreement of all the amphiboles with the ideal structure represented by the coordinates of Table 4.1.

Substitution of larger cations into the tetrahedral positions and/or smaller cations in the octahedral positions causes the tetrahedral unit to be oversized with respect to the octahedral unit. Since the elements are linked by the geminal anions O(1) and O(2), the separation of these anions

(when considered as part of the chain) must be decreased as to coincide with their separation on the octahedral strip. This may be done by ditrigonal distortion of the double-chain element (while maintaining individual polyhedron holosymmetry). If θ is the angle of rotation, simple geometrical arguments show that the condition

$$(M\text{-}O) = \frac{4}{3} (T\text{-}O) \cos \theta \qquad 4.2$$

is required for complete articulation. This is the only way that the structure may adjust while still retaining the holosymmetry of the individual polyhedra. Any changes in the T-O(br)-T angles destroy the holosymmetry of the individual octahedra and/or tetrahedra. By the same token, the ideal structure cannot incorporate larger octahedral cations or smaller tetrahedral cations while retaining individual holosymmetry.

When the constraint of holosymmetry is removed, the misfit between the octahedral and tetrahedral units may be accommodated both by ditrigonal rotation and by variation of the T-O(br)-T angles (see next section). In addition, certain distortions occur that are due to crystal-chemical factors and these also influence the linkage requirements. Cation-cation repulsion in the octahedral strip shortens shared edges with the concommitant extension of unshared edges; thus all octahedral edges involved in inter-element linkage are increased which will tend to compensate for the substitution of larger tetrahedral cations and/or smaller octahedral cations. Conversely, T-O(br) bonds tend to be longer than

T-O(nbr) bonds (see next section) which extends the dimensions of the chain in the directions of polymerization, offsetting the cation-cation repulsion effect in the octahedral strip. Assuming that the individual T-O bond lengths are a function of other stereochemical variations in the tetrahedra, the most regular tetrahedra should show the least difference between $\langle$T-O(br)$\rangle$ and $\langle$T-O(nbr)$\rangle$ and between the observed $\langle$T-O(br)-T$\rangle$ angle and its ideal value of 141°. This is the case for grunerite; both tetrahedra show the least distortion for the Si clino-amphiboles, $\langle$T-O(br)-T$\rangle$ is close to the ideal value and $\langle$T-O(br)$\rangle$ - $\langle$T-O(nbr)$\rangle$; here the lengthening of the unshared octahedral edges has been compensated by ditrigonal rotation without any great distortion of the individual tetrahedra.

Obviously these linkage constraints may be described completely rigorously by developing the complex trigonometric conditions required. It is of more use, however, to relate changes in topology to chemical variation in an attempt to account for the types of chemical substitution and bulk chemical limitations encountered in the clino-amphiboles. Figure 4.2 shows the variation in $\cos\{180^{\circ}$-(O(5)-O(6)-O(5))$\}$ with 3/4 $\langle$M-O$\rangle$/$\langle$T-O$\rangle$; this is derived from equation 4.2 and exhibits a marked linear correlation with glaucophane deviating significantly from the trend. As $\langle$M-O$\rangle$ and $\langle$T-O$\rangle$ are a function of the chemistry, the variation of O(5)-O(6)-O(5) is seen to be the result of chemical variation. The effect of tetrahedral Al is to decrease the O(5)-O(6)-O(5) angle

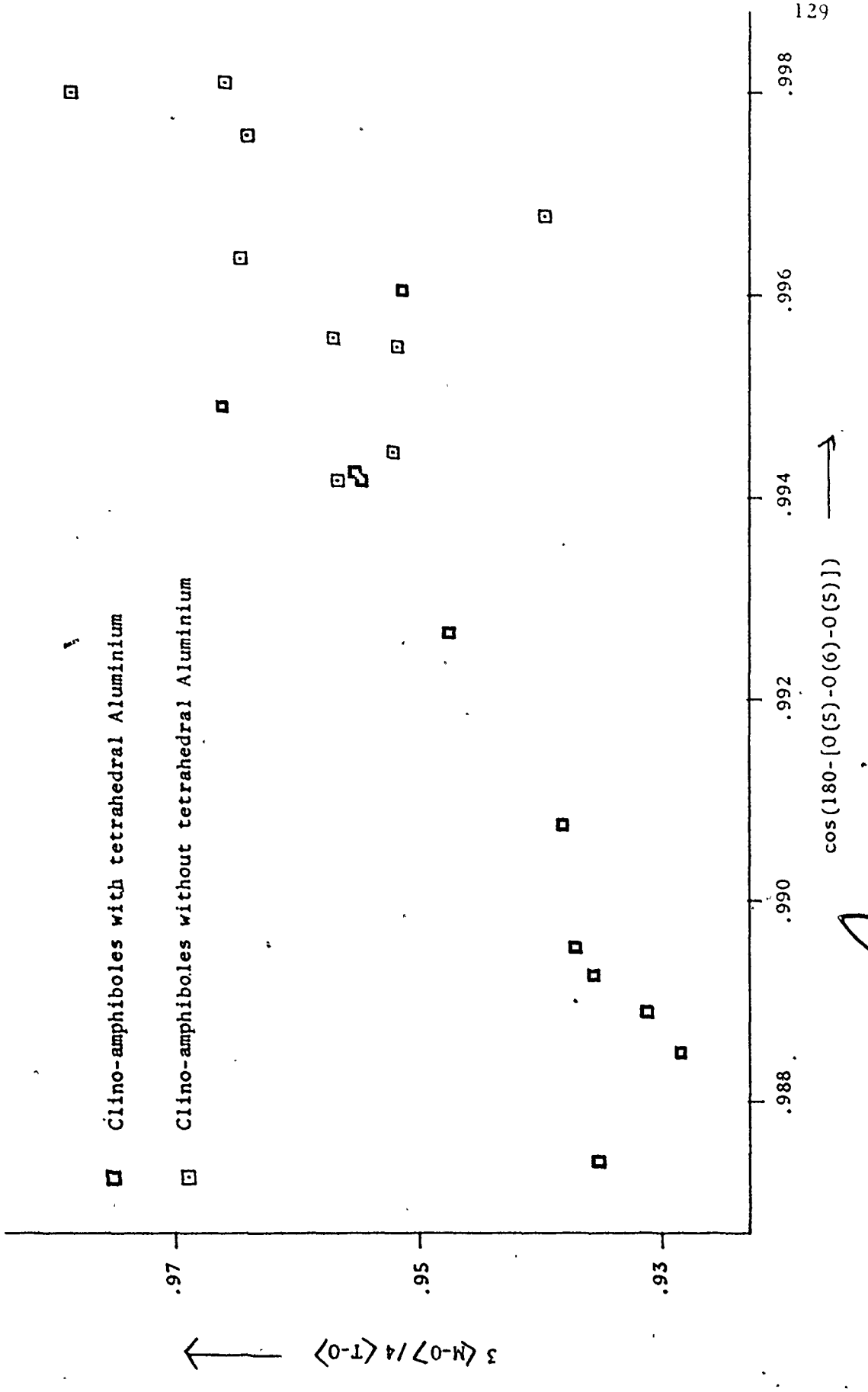

Figure 4.2 3 ⟨M-O⟩ /4 ⟨T-O⟩ versus cos (180-[O(5)-O(6)-O(5)])

as indicated by Robinson (1971) and Hawthorne & Grundy (Min. Mag., in press); the trend for the aluminous amphiboles is very well developed in figure 4.2 although the O(5)-O(6)-O(5) angle is not inversely proportional to Al^{TET} as indicated by Robinson (1971) but inversely proportional to $\langle T\text{-}O \rangle$ $\{\equiv$ Const. + m. $Al^{TET}\}$ and directly proportional to $\langle M\text{-}O \rangle$. The trend for the Si-amphiboles is less well-defined; as there is no variation in tetrahedral chemistry, the trend is defined by variations in $\langle M\text{-}O \rangle$ much more than in the case of the Al amphiboles. It is apparent that the deviation of glaucophane from the trend must be compensated by another mechanism. The relationship between $\langle T\text{-}O(br) \rangle$ and $\langle T\text{-}O(Br)\text{-}T \rangle$ is linear for the Si amphiboles (see next section) and thus neither compensate in the case of glaucophane although they do compensate for the deviation of the general trend in figure 4.2 from the ideal which has a slope of 1.0 (see equation 4.2). The only other mechanism available is the variation of the length in the linking octahedral edges; figure 4.3 is a histogram of the ratio $\langle O\text{-}O \rangle_{OCT}^{LINKING} / \langle O\text{-}O \rangle_{OCT}$ for the amphiboles of Table 4.2. Two distinct populations are apparent, one for the Si amphiboles and one for the Al amphiboles, the Al amphiboles show a much greater expansion of the linking edges concommitant with their greater tetrahedral size. However, glaucophane lies in the aluminous population rather than the Si population corresponding to its much lower $\langle M\text{-}O \rangle / \langle T\text{-}O \rangle$ ratio. This compensates for the large O(5)-O(6)-O(5)

Figure 4.3 Histogram of the ratio of the linking octahedral edge to the mean octahedral edge

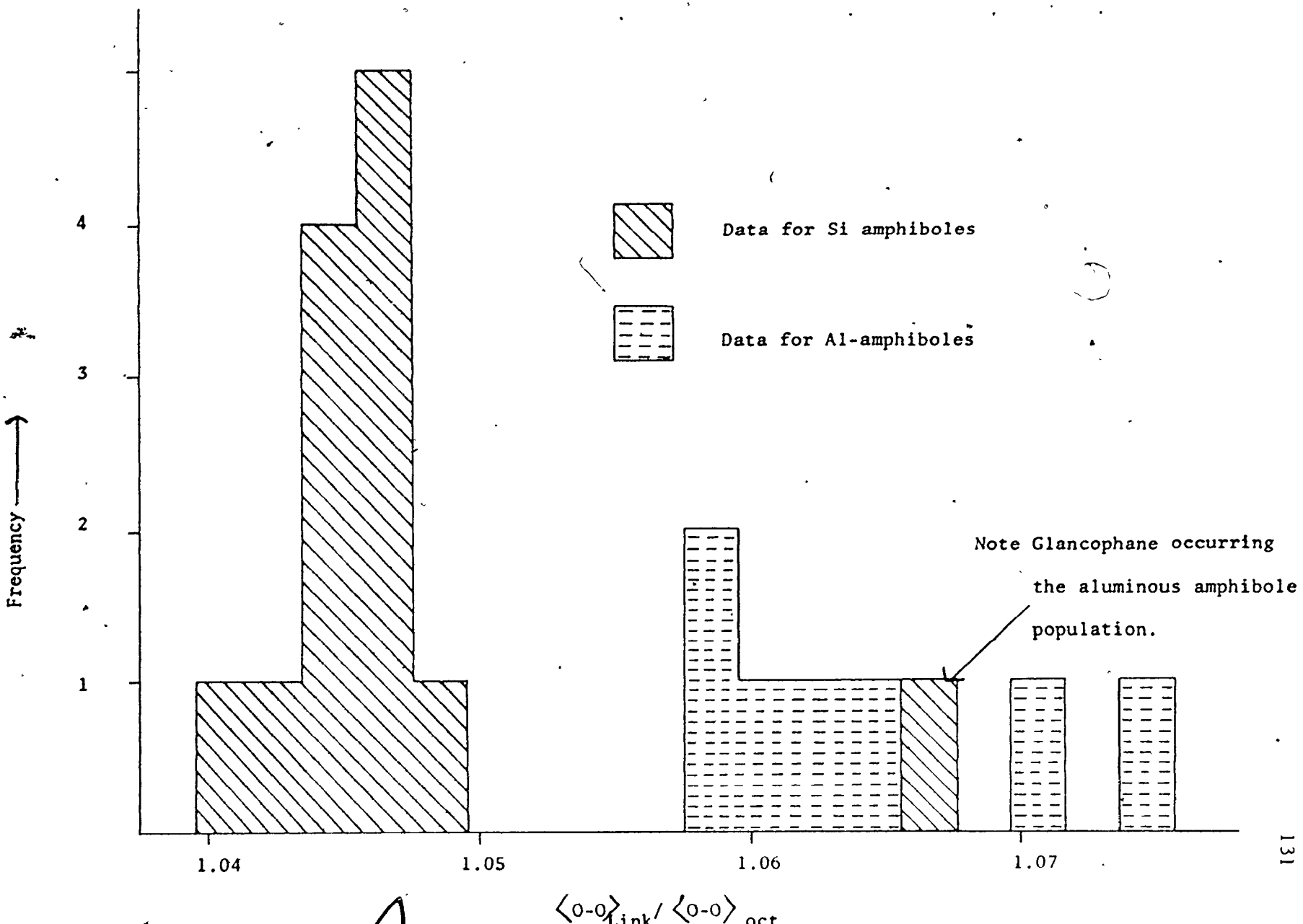

angle and may be seen as a result of the large amount of octahedral Al in glaucophane. It will be shown in a later section that the octahedral layer tends to 'collapse' around M(2) when that site contains a small cation. From figure 4.29b, it may be seen that this would cause a major expansion of the unshared edges in the M(1) and M(3) octahedra, thus compensating for the small linking edge in the M(2) octahedron.

Superimposed on these linkage effects are the bonding requirements of the M(4) site, which has weak bonds to the chain bridging anions O(5) and O(6). M(4) may be occupied by Ca, Fe^{2+}, Mn and Na which have distinctly different ranges of influence (see Figure 4.4). Thus, for glaucophane, M(4) requires much shorter M(4)-O(br) bonds than in tremolite (as Na contributes a much lower bond strength than Ca for an equivalent bond length) to satisfy the O(br) anion charge requirements (see Table 4.10); this condition inhibits ditrigonal rotation in the double chain, accounting for the anomalously large O(5)-O(6)-O(5) angle in glaucophane. It is an elegant feature of the amphibole structure that Na occupancy of M(4) must be accompanied by substitution of trivalent ions such as Al and/or Fe^{3+} to satisfy the charge at O(4), and that the small size of these trivalent cations causes the linking octahedral edges of M(1) and M(3) to expand and offset the effect of the anomalously low ditrigonal chain distortion.

Figure 4.4 Bond-strength versus ionic radius [8] for typical amphibole M(4) cations

Full lines indicate divalent cations

Dashed lines indicate monovalent cations

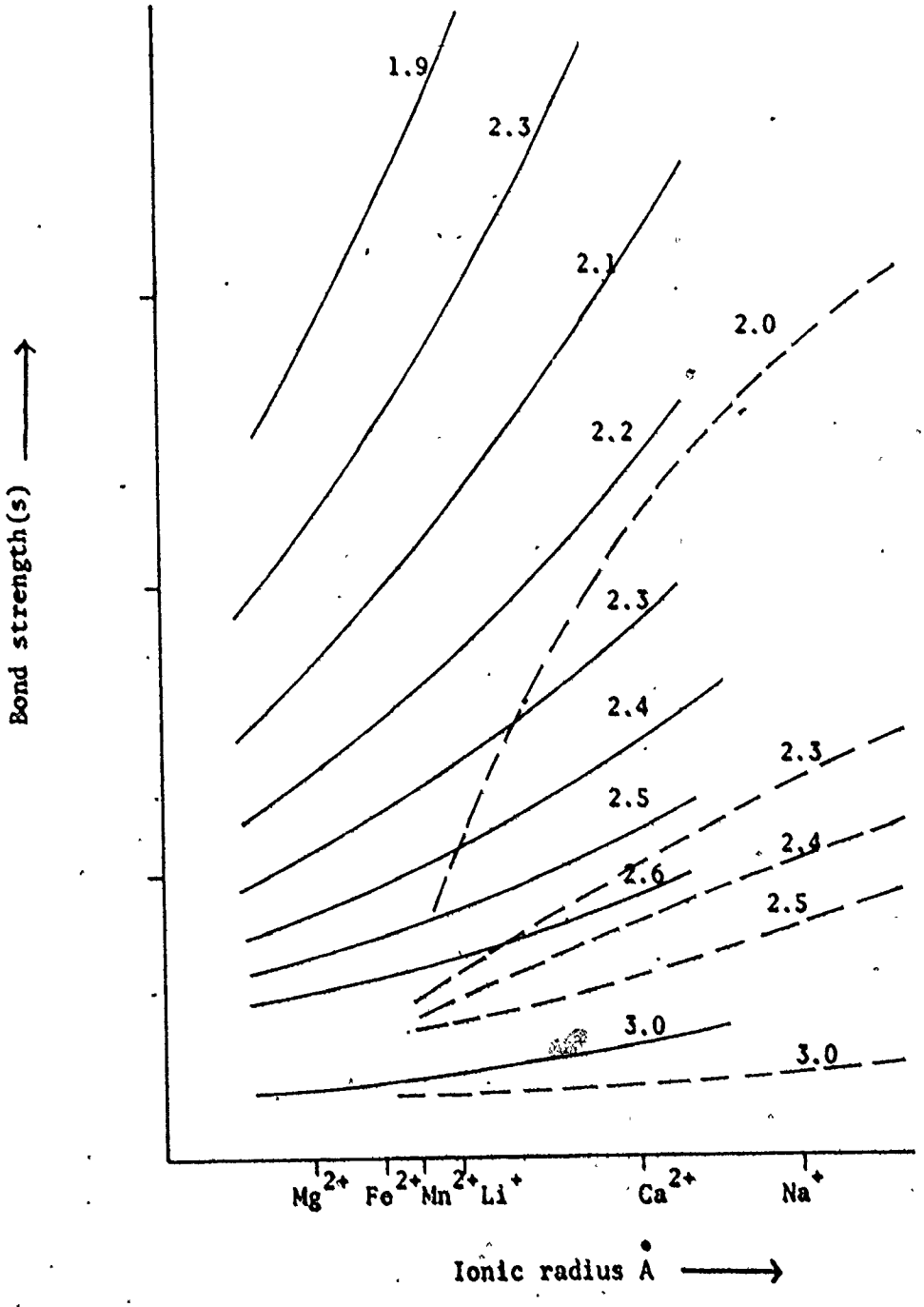

Another prominent linkage effect to some extent controls the distortion of the M(2) site. The O(4)-O(4) edge links along the b crystallographic direction to the T(2) site which links down on to the next octahedral strip; the O(4) anion is formally charge deficient and consequently, has very short bonds to each of the three coordinating cations. Consequently, when the layers stack together, the O(4)-O(4) edge tends to be extended and as the M(2) site becomes smaller, the angular distortion of the O(4)-O(4) edge becomes larger; this is illustrated in Figure 4.5 which shows the variation in O(4)-M(2)-O(4) with $r_{m(2)}$. Ferrotschermakite deviates significantly from the trend because of the low partial occupancy of its A-site which does not keep the 'back-to-back' double chains apart, as occurs in those amphiboles with completely occupied A-sites. The reasons for the deviations in the richterites is not clear. However, this extension of the O(4)-O(4) edge also extends the $O(2^{u})$-$O(4^{d})$ edge which is shared with the M(4) antiprism; in order to keep the mean (O-O) separations in the M(2) octahedron compatible with the ionic radius of its substituent cations, one of the unshared edges is forced to contract. Thus, in the M(2) octahedron, Pauling's rule stating that 'the angle subtended at the cation by a shared edge is less than that subtended by an unshared edge' is violated and the cause may be directly traced to a linkage requirement. The same mechanism also accounts for the large O(2)-T(2)-O(4) angle in the T(2) tetrahedron, which is the other polyhedron involved in this part of the inter-element linkage.

Figure 4.5 The variation in O(4)-M(2)-O(4) with the mean ionic radius of the constituent M(2) cations

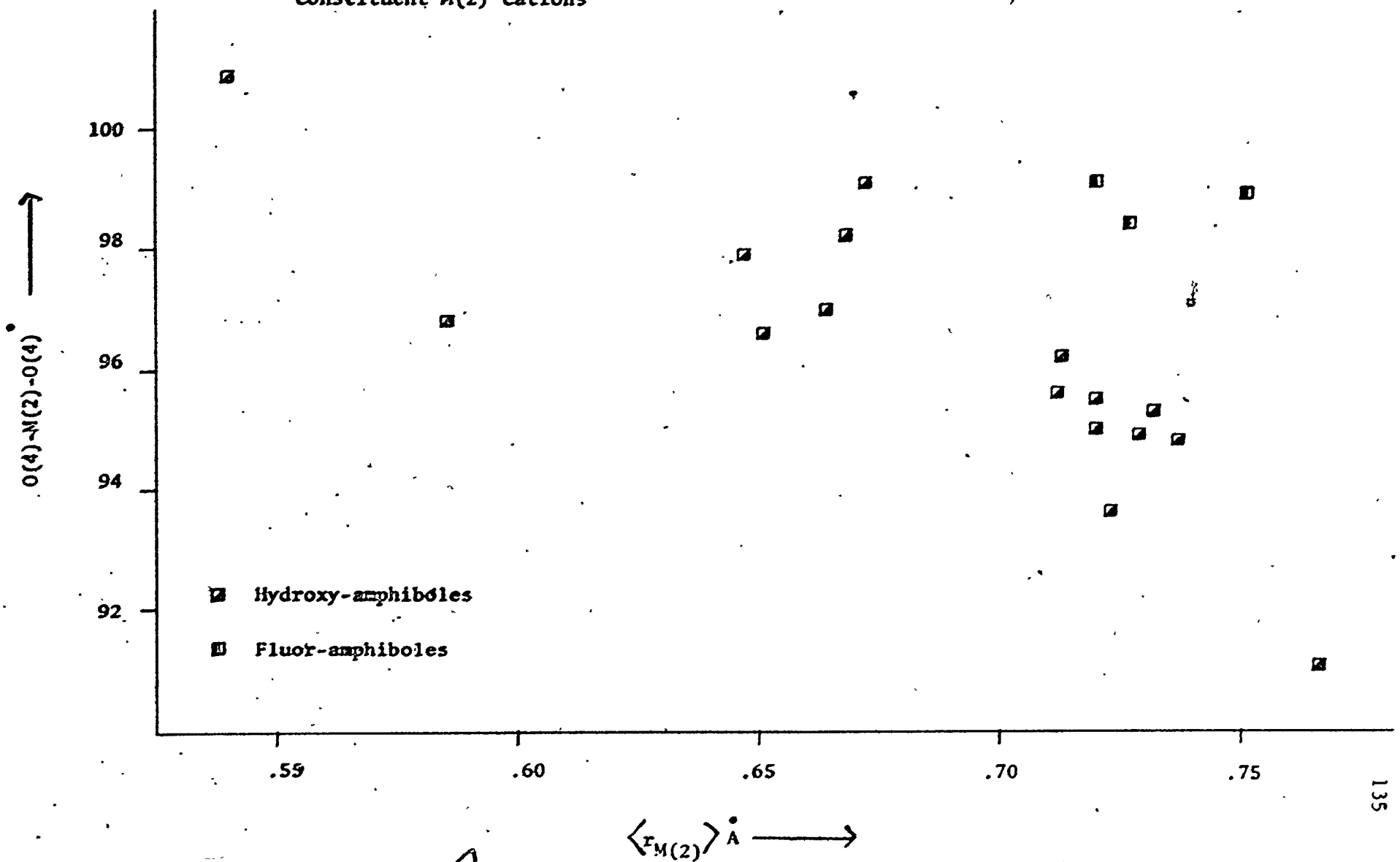

The steric details of the clino-amphiboles will now be examined in an attempt to relate structural changes to various bonding models.

THE Si-O BOND

In the non-aluminous amphiboles, individual Si-O bond lengths range from 1.572 to 1.704Å. There have been several attempts to rationalize these variations in terms of the observed stereochemistry with reference to particular bonding models (Brown & Gibbs, 1969b, 1970; Mitchell, Bloss & Gibbs, 1970, 1971; Baur, 1970, 1971), but these have suffered from a lack of data and consequently do not give sufficient weight to the stereochemical controls inherent in the amphibole structure. Two models for the Si-O bond have been considered:

(i) the covalent, or double bonding model of Pauling (1952) and Cruickshank (1961);

(ii) modifications to the ionic model of Pauling (1929, 1960) as exemplified by Zachariasen (1963) and Baur (1961)

These will be discussed, and bond length and angle variations in the amphibole chain element will be examined in terms of both models. Table 4.2 lists the structures from which the data was taken for this study.

TABLE 4.2: DATA FROM THE FOLLOWING STRUCTURES ARE USED IN THE DISCUSSION OF THE Si-O BOND

1.	Tremolite	Papike, Ross and Clark (1969)
2.	Fluor-tremolite	Cameron (1970)
3.	Synthetic richterite 1	Cameron (1970)
4.	Synthetic richterite 2	Cameron (1970)
5.	Glaucophane	Papike and Clark (1968), Papike et al. (1969)
6.	Cummingtonite	Ghose (1961), Fischer (1966), Mitchell, Bloss and Gibbs (1971)
7.	Grunerite	Finger (1967, 1969)
8.	C-centred Mn-cummingtonite	Papike et al. (1969)

(a) Covalent bonding model

On the basis of the difference between the grand mean observed Si-O distance of ~1.63Å and the sum of the single-bond radii of 1.83Å, Pauling (1939) proposed a double-bond model for tetrahedral Si. This correlates with the large electronegativity difference between these two atoms which suggests (Pauling, ibid.) that the Si-O σ bond has a 50% ionic character. Since the residual charge on Si violated the electroneutrality principle, Pauling suggested that the formation of a double-bond involving the 3d orbitals (in addition to the 3s and 3p orbitals) of silicon would tend to neutralize this excess charge. This idea was extended by Cruickshank (1961), who used simple group theory arguments to show that only two strong d-p-π bonds may be formed (by the e_g orbitals on silicon combining with the $2p\pi$ and $2p\pi'$ orbitals on oxygen) in polymerized tetrahedra of T_d symmetry. Assuming that this argument can be extended to tetrahedra showing slight deviations from T_d symmetry, several predictions can be made concerning the stereochemistry of polymerized SiO_4 tetrahedra (Cruickshank, 1961; Brown, Gibbs & Ribbe, 1969):

(i) Si-O(br) > Si-O(nbr)

(ii) Si-O(br) is a function of Si-O-Si

(iii) O-Si-O angles should decrease in the order O(nbr)-Si-O(nbr) > O(br)-Si-O(nbr) > O(br)-Si-O(br), as forecast by the V.S.E.P.R. theory (Gillespie, 1963).

Subsequent work (Collins, Cruickshank & Breeze, 1972) has shown that this approach is oversimplified and there is evidence of considerable participation of the 3d t_2 silicon orbitals in σ bonds. However, the above conclusions are not invalidated.

A considerable amount of work has recently been done on Extended Huckel Molecular Orbital (E.H.M.O.) calculations in silicates (Gibbs, Hamil, Bartell & Yow, 1972; Louisnathan & Gibbs, 1972a,b,c) and the results tend to substantiate the covalent model. In addition, further stereochemical relationships have come to light. Si-O(br) is not a linear function of Si-O-Si, but an inverse function of cos(Si-O-Si) (Louisnathan & Gibbs, 1972d; c.f. Coulson, 1961). E.H.M.O. calculations on hypothetically distorted tetrahedra show that short Si-O bonds are involved in wide O-Si-O angles; this has been corroborated by calculations and correlations developed for the olivine structures (Louisnathan & Gibbs, 1972a,b).

It is of interest to examine the double-chain element of the non-aluminous amphiboles and compare the observed stereochemistry with the above predictions.

To conform to the structural nomenclature of the amphiboles, Si will be denoted as T. The variation of $\langle$T-O(br)$\rangle$ with $\langle$T-O(br)-T$\rangle$ is shown in figure 4.6a; since the total variation in individual T-O(br)-T angles is only $\sim 10^{\circ}$, the non-linearity of the relationship between the two

In the section on the Si-O bond, the following legend is common to all figures; for convenience, this page may be detached.

- Tremolite - $Ca_2Mg_5Si_8O_{22}(OH)_2$
- Fluor-Tremolite - $Ca_2Mg_5Si_8O_{22}F_2$
- Synthetic Richterite 1 - $Na_2Ca\ Mg_5Si_8O_{22}F_2$
- Synthetic Richterite 2 - $Na_{2.02}Ca_{0.9}Mg_{3.45}Fe_{1.68}Si_8O_{22}F_2$
- Glaucophane - $Na_{1.96}Ca_{0.04}Mg_{2.39}Fe_{0.79}Al_{1.82}Si_8O_{22}(OH)_2$
- Cummingtonite - $Ca_{0.35}Mg_{4.05}Fe_{2.50}Mn_{0.17}Si_8O_{22}(OH)_2$
- Grunerite - $Ca_{0.06}Mg_{0.77}Fe_{4.05}Mn_{0.05}Si_8O_{22}(OH)_2$
- C-Mn Cummingtonite - $Ca_{0.18}Mg_{4.11}Fe_{0.54}Mn_{2.02}Si_8O_{22}(OH)_2$

Figure 4.6a $\langle$T-O(br)$\rangle$ versus $\langle$T-O(br)-T$\rangle$ for the Si clino-amphiboles

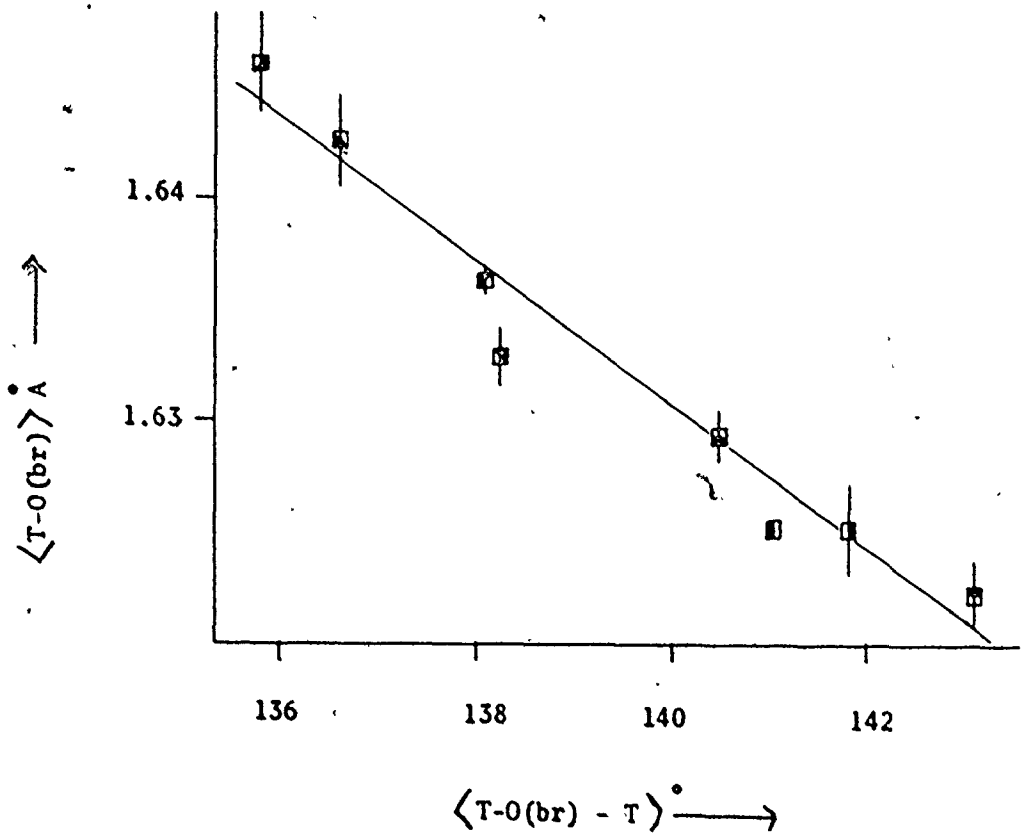

Figure 4.6b $\langle$T-O(br)$\rangle$ versus -1/cos ($\angle$T-O(br)-T$\rangle$) for the Si clino-amphiboles

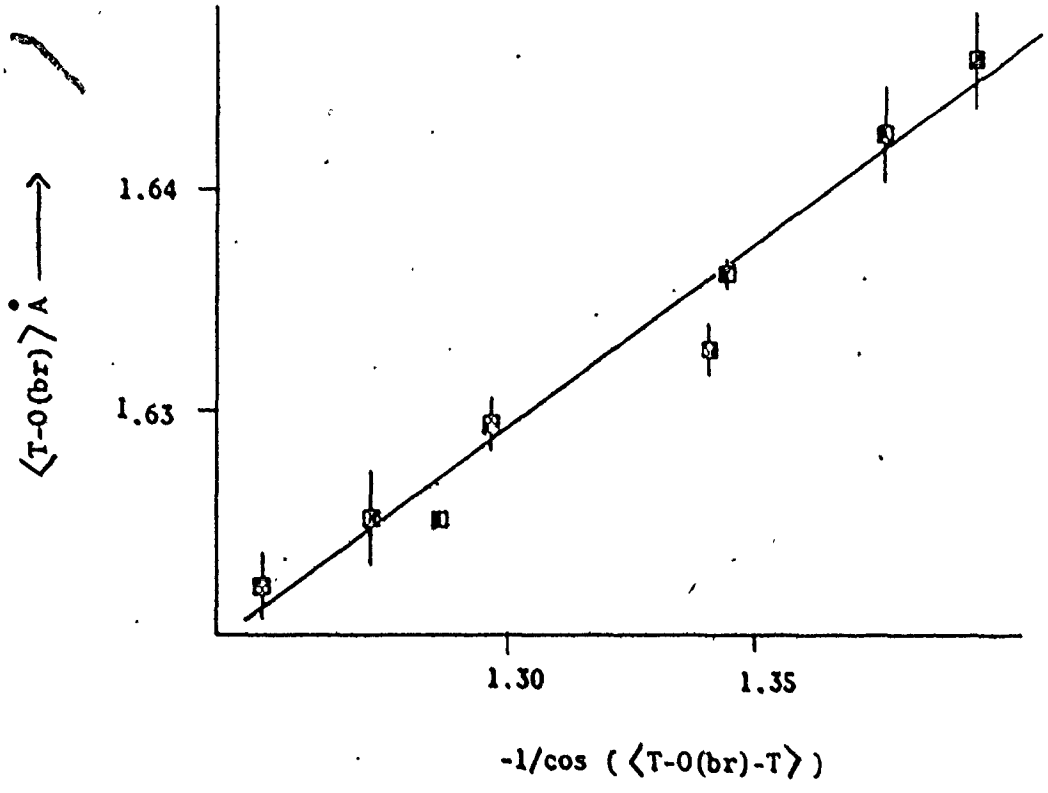

quantities is not apparent. This is illustrated in figure 4.6b where the variation in $\langle$T-O(br)$\rangle$ is shown as a function of $-1/\cos\langle$T-O(br)-T$\rangle$. The results of linear regression analysis for both cases are given in Table 4.3, and confirm the equivalence of the two relationships over this angular range. Thus the variations in the grand $\langle$T-O(br)$\rangle$ distances are compatible with the double-bonding model. A more stringent test of this model is provided by the variation in $\langle$T-O(br)$\rangle$ bond lengths with individual T-O(br)-T angles; these relations are shown in figures 4.7a, 4.8a and 4.9a for the O(5), O(6) and O(7) anions.

These relationships prove to be extremely non-linear with glaucophane and synthetic richterite 1 deviating considerably from linearity. The reason for these deviations becomes apparent on examination of the tetrahedral chain $\longleftrightarrow$ octahedral strip linkage in the a* direction. The geminal anions O(1) and O(2) link to the unshared edges of the M(1), M(2) and M(3) octahedra; the length of these unshared edges is primarily controlled by the mean ionic radius of their constituent cations (and anions) and the amount of distortion due to cation-cation repulsion. Thus in glaucophane, where the M(2) cations are very small, the M(2) site has a very short $O(1^u)$-$O(2^u)$ unshared edge; to retain interelement linkage, the T(1)-O(5)-T(2) angle and/or the T-O(5) distance are 'anomalously' small. This inductive effect of the octahedral strip is shown in figures 4.7b, 4.8b and 4.9b which show the variation in the length of the unshared octahedral

Figure 4.7a $\langle T\text{-}O(5) \rangle$ versus T(1)-O(5)-T(2) for the Si clino-amphiboles

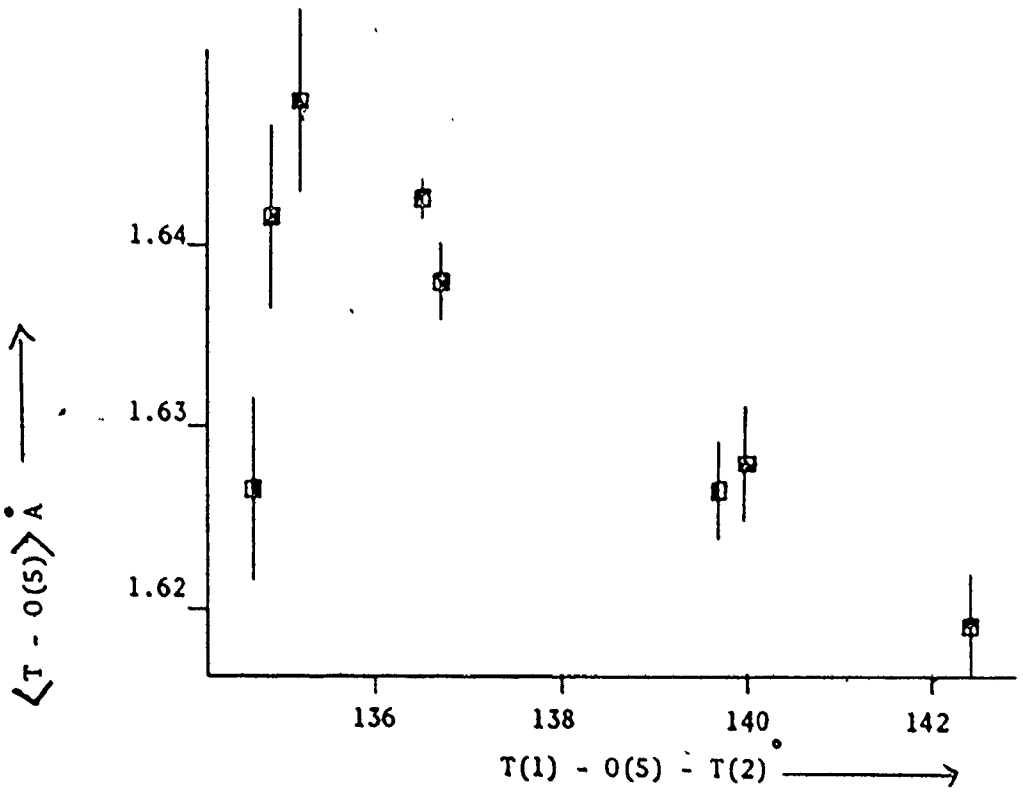

Figure 4.7b $O(1^u) - O(2^u)_{M(2)}$ versus T(1) -O(5) - T(2) for the Si clino-amphiboles

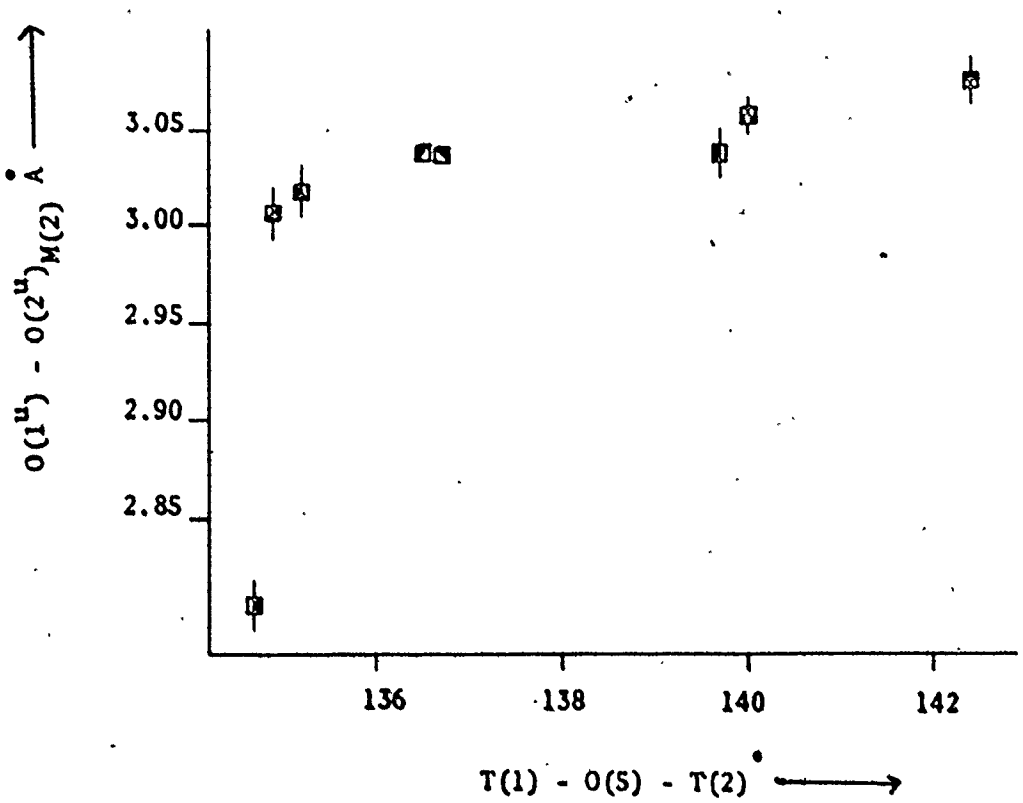

Figure 4.8a $\langle T\text{-}O(6)\rangle$ versus T(1) - O(6) - T(2) for the Si clino-amphiboles 143

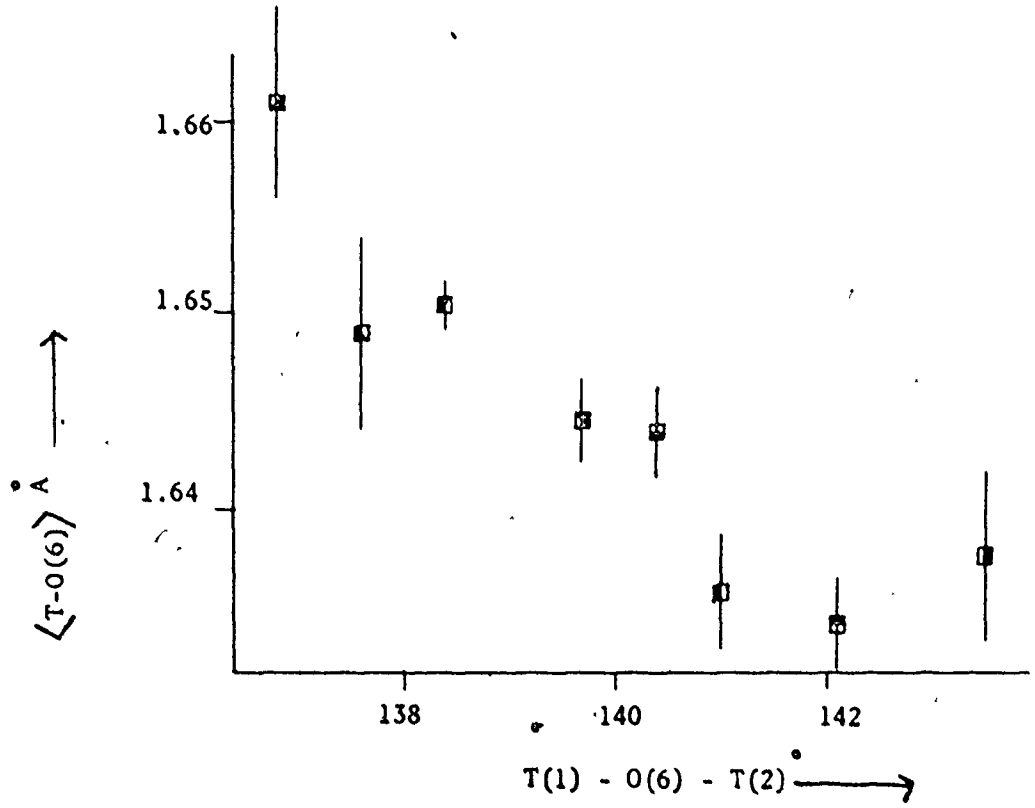

Figure 4.8b $O(1^u) - O(2^u)_{M(1)}$ versus T(1) - O(6) - T(2) for the Si clino-amphiboles

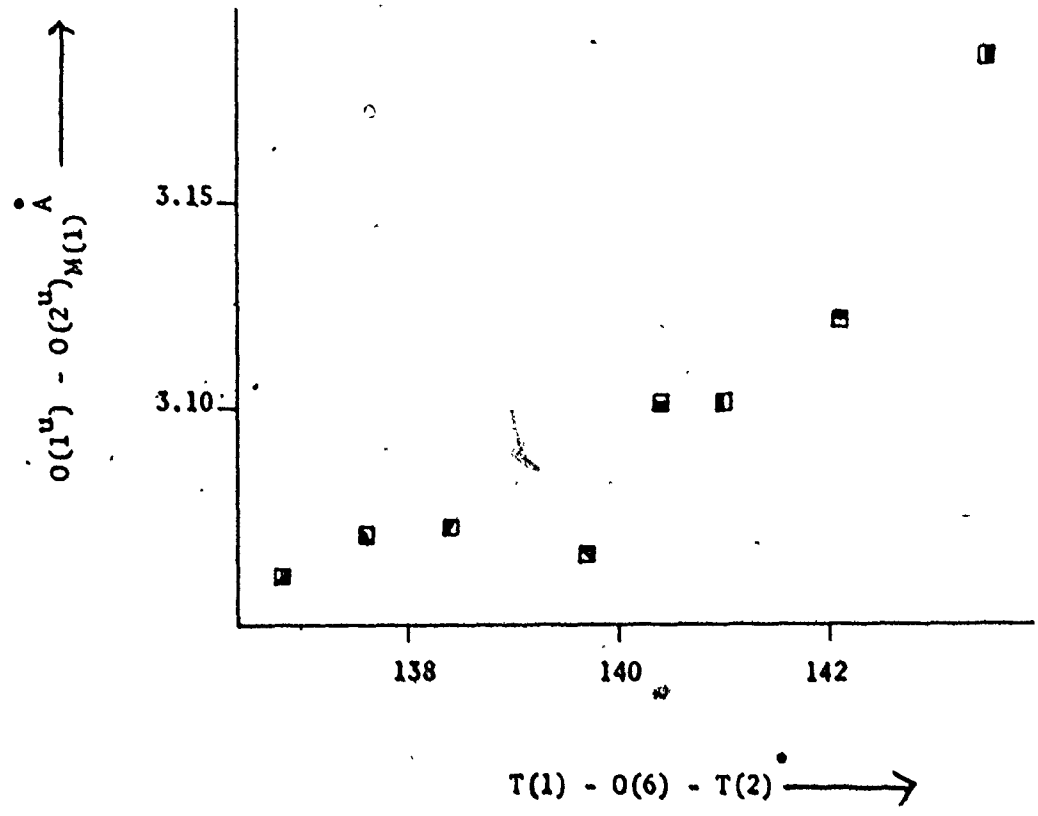

TABLE 4.9a T(1) - O(7) versus T(1) - O(7) - T(1) for the Si clino-amphiboles 144

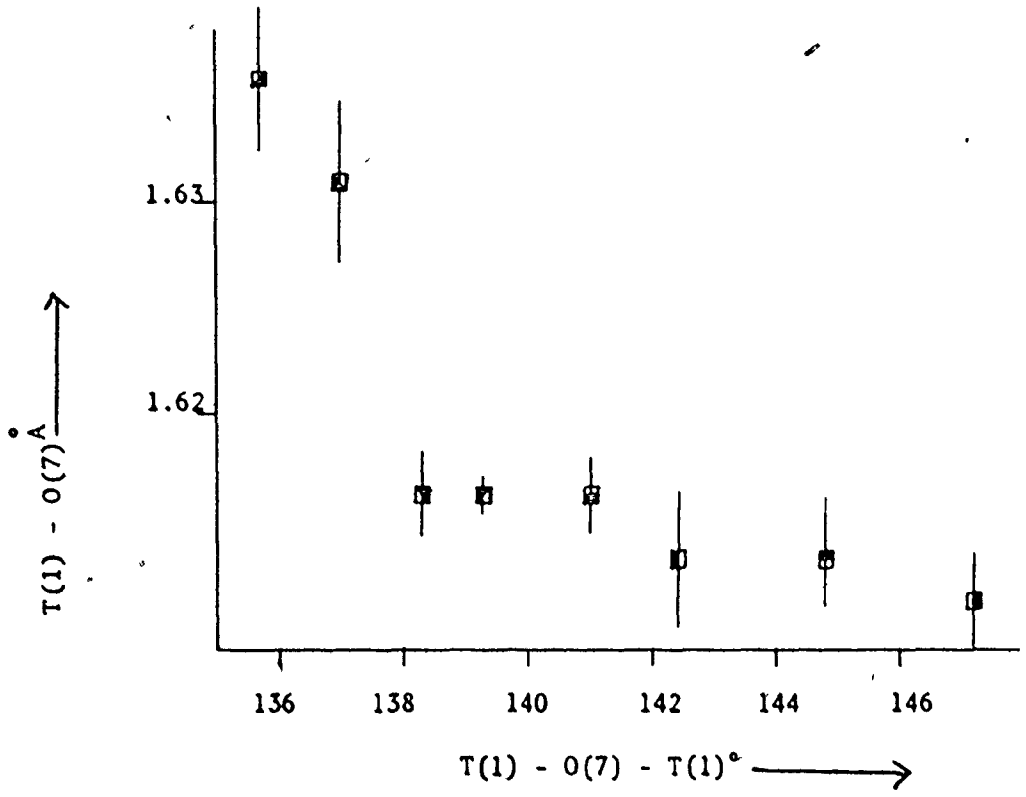

Figure 4.9b $O(1^u) - O(1^u)_{M(3)}$ versus T(1) - O(7) - T(1) for the Si clino-amphiboles

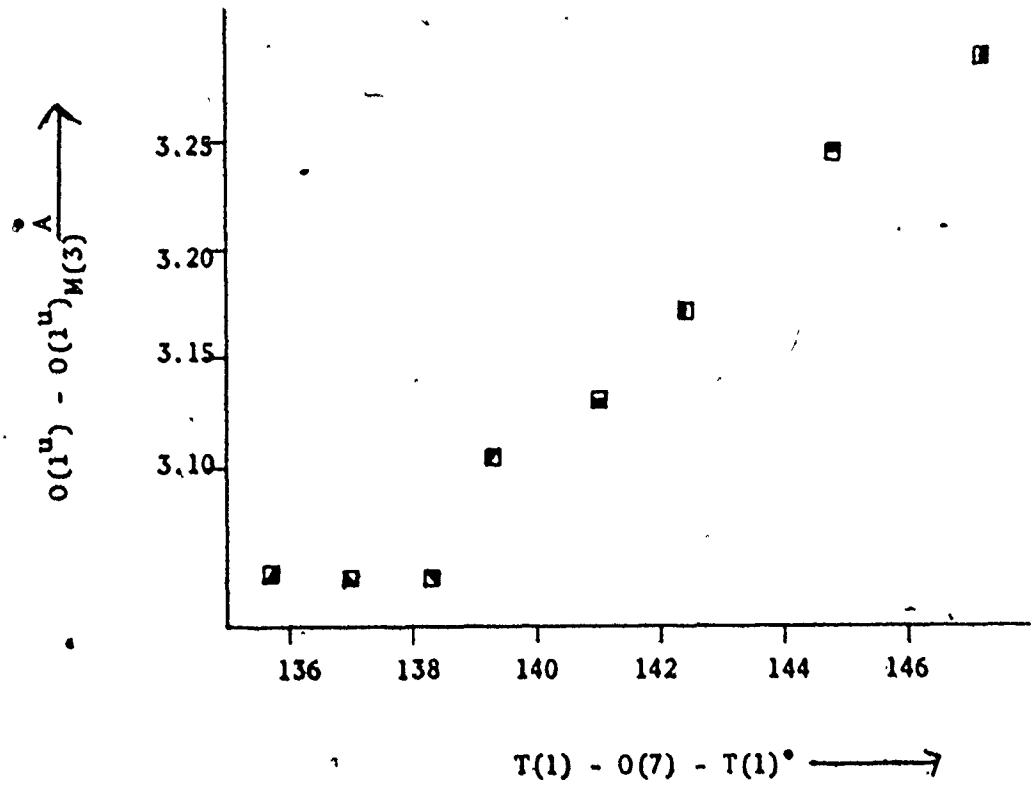

edge opposite O(br) with T-O(br)-T for the O(5), O(6) and O(7) anions. Comparison with figures 4.7a, 4.8a and 4.9a shows that the two effects are antipathetic, and stepwise linear regression (Dixon, 1971) with T-O(br)-T as the dependent variable shows that in each case it is entirely a function of $\langle$T-O(br)$\rangle$ and the length of the corresponding octahedral edge. Stepwise linear regression analysis was repeated with $\langle$T-O(br)$\rangle$ as the dependent variable, and the results of these and the previous analyses appear in Table 4.3. In all cases, correlations are marginally superior when T-O(br)-T is the dependent variable. This is more strikingly demonstrated by repeating the analysis with the data for all bridging anions taken as a single set.

The results are shown in Table 4.3 and suggest that T-O(br)-T is the dependent variable, rather than $\langle$T-O(br)$\rangle$. Many previous authors have implicitly assumed that variations in T-O(br)-T cause variations in $\langle$T-O(br)$\rangle$, the wider T-O(br)-T angles producing increased orbital overlap and a concomitant shortening of the bond. The above results tend to suggest a reciprocal relationship, that short bonds require increased orbital overlap and the T-O(br)-T angles adjusts accordingly. Calculations by Gibbs et al. (1972) tend to negate this alternative mechanism. E.H.M.O. calculations on a $Si_2O_7^{6-}$ group with holosymmetric tetrahedra showed that the Si-O bond overlap population of the bridging bond was a function of the

TABLE 4.3: REGRESSION ANALYSIS RESULTS

The regression equations have the form $y=mx+c$ where y is the dependent variable and x is the independent variable. $\langle R \rangle$ denotes the correlation coefficient, and σ denotes the standard error of estimate. Unless stated, $|t|$ values are calculated for the null hypothesis $H_o: m = 0$.

1. $\langle$T-O(br)$\rangle$ dependent, $\langle$T-O(br)-T$\rangle$ independent

2. $\langle$T-O(br)$\rangle$ dependent, $-1/\cos \langle$T-O(br)-T$\rangle$ independent

3. T(1)-O(5)-T(2) dependent, $\langle$T-O(5)$\rangle$ and $O(1^u)$-$O(2^u)_{M(2)}$ independent

4. T(1)-O(6)-T(2) dependent, $\langle$T-O(6)$\rangle$ and $O(1^u)$-$O(2^u)_{M(1)}$ independent

5. T(1)-O(7)-T(1) dependent, T(1)-O(7) and $O(1^u)$-$O(1^u)_{M(3)}$ independent

6. $\langle$T-O(5)$\rangle$ dependent, T(1)-O(5)-T(2) and $O(1^u)$-$O(2^u)_{M(2)}$ independent

7. $\langle$T-O(6)$\rangle$ dependent, T(1)-O(6)-T(2) and $O(1^u)$-$O(2^u)_{M(1)}$ independent

8. T(1)-O(7) dependent, T(1)-O(7)-T(1) and $O(1^u)$-$O(1^u)_{M(3)}$ independent

9. T-O(br)-T dependent, T-O(br) and $O\text{-}O_{OCT}$ independent, for O(5), O(6) and O(7)

10. $\langle$T-O(br)$\rangle$ dependent, T-O(br)-T and $O\text{-}O_{OCT}$ independent, for O(5), O(6) and O(7)

11. $\langle$T-O(5)$\rangle$ dependent, T(1)-O(5)-T(2) and $\chi_{O(5)}$ independent

12. $\langle$T-O(6)$\rangle$ dependent, T(1)-O(6)-T(2) and $\chi_{O(6)}$ independent

12a. $\langle$T-O(7)$\rangle$ dependent, T(1)-O(7)-T(1) and $\chi_{O(7)}$ independent

Number	Indep. Var.	c	m	⟨R⟩	σ	|t|
1.	⟨T-O(br)-T⟩	2.0926	-0.0033(3)	0.977	0.0020	11.00
2.	-1/cos⟨T-O(br)-T⟩	1.4094	0.169(13)	0.982	0.0018	13.00
3.	(⟨T-O(5)⟩)	432.2	-221.1(20.8)	0.986	0.5	10.63
	($O(1^u)$-$O(2^u)_{M(2)}$		22.1(2.5)			8.84
4.	(⟨T-O(6)⟩)	269.2	-133.4(31.9)	0.979	0.6	4.18
	($O(1^u)$-$O(2^u)_{M(1)}$		29.1(6.8)			4.28
5.	(T(1)-O(7))	195.8	-101.1(27.4)	0.995	0.5	3.69
	($O(1^u)$-$O(1^u)_{M(3)}$		34.6(2.7)			12.81
6.	(T(1)-O(5)-T(2))	1.9401	-0.00433(41)	0.979	0.0025	10.56
	($O(1^u)$-$O(2^u)_{M(2)}$		0.096(14)			6.86
7.	(T(1)-O(6)-T(2))	2.0350	-0.0058(14)	0.939	0.0037	4.14
	($O(1^u)$-$O(2^u)_{M(1)}$		0.137(75)			1.83
8.	(T(1)-O(7)-T(1))	1.9108	-0.0072(20)	0.930	0.0040	3.60
	($O(1^u)$-$O(1^u)_{M(3)}$		0.232(83)			2.80
9.	(⟨T-O(br)⟩)	166.1	-67.2(24.4)	0.900	1.5	2.75
	(O-O_{OCT}		26.9(3.7)			7.27
10.	(T-O(br)-T)	1.9825	-0.0040(14)	0.603	0.012	2.86
	(O-O_{OCT}		0.065(51)			1.27
11.	(T(1)-O(5)-T(2))	2.0056	-0.0029(11)	0.772	0.0076	2.64
	($\chi_{O(5)}$		0.0059(70)			0.84

Number	Indep. Var.	c	m	⟨R⟩	σ	|t|
12.	(T(1)-O(6)-T(2))	2.1875	-0.0038(8)	0.909	0.0044	4.75
	($\chi_{O(6)}$		-0.0036(42)			0.86
12a.	(T(1)-O(7)-T(1))	1.6692	-0.00064(20)	0.990	0.0015	3.20
	($\chi_{O(7)}$		0.0190(21)			9.05

Si-O-Si angle. However, the total variation in n(Si-O) was ~ 0.02 for a variation in Si-O-Si from 130-180°. In the correlations between n(Si-O) and $Si\text{-}O_{OBS}$ presented by Gibbs et al. (1972, figures 8, 9, 10 and 11), deviations of > 0.02 in n(Si-O) occur, and thus it is not clear if the variations in n(Si-O) of this order in the calculations for the $Si_2O_7^{6-}$ group are actually significant in terms of observed bond lengths.

Certainly if T-O(br) for O(5), O(6) and O(7) respectively is partially a function of T-O(br)-T, then the remainder of the variation in T-O(br) is caused by variations in $(O\text{-}O)_{oct}$ unless the variation in T-O(br)-T that controls T-O(br) is that variation in T-O(br)-T not controlled by $(O\text{-}O)_{oct}$. Before any decision is made as to the actual nature of this mechanism, it is circumspect to examine the possibility that T-O(br) is partially a function of T-O(br)-T and the deviations from linearity exhibited by figures 4.7a, 4.8a and 4.9a are caused by an additional dependence of T-O(br) on some other parameter. The most obvious effect is that of non-tetrahedral cations bonded to O(br). In figure 4.9a, the deviation of the two synthetic richterites coincides with the presence of an A-site cation, causing the local environment of the O(7) anion in these two amphiboles to differ considerably from that of the amphiboles corresponding to the linear trend. Similarly the O(5) and O(6) anions bond to a variety of M(4)- and A-site cations, possibly accounting for the deviations from linearity in figures 4.7a and 4.8a. The question now arises as to how to put this factor on a quantitative basis. It has been suggested (Noll, 1963; Pant & Cruickshank, 1967; Brown & Gibbs, 1969b, 1970; Mitchell, Bloss &

Gibbs, 1970, 1971) that Si-O bond lengths are partially a function of the electronegativity (χ) of the non-tetrahedral cations bonded to the tetrahedral group. This quantity was calculated for each of the bridging anions using electronegativity values from Allred (1961), and stepwise linear regression analysis was performed on $\langle$T-O(br)$\rangle$, T-O(br)-T and $\chi_{O(br)}$ with $\langle$T-O(br)$\rangle$ as the dependent variable. The results are presented in Table 4.3 where the $|t|$ -values are calculated for the hypothesis that the slopes are equal to zero. These calculated $|t|$ -values for $\chi_{O(br)}$ do not exceed even the critical value of $t(6,\ 0.90) = 1.94$ and hence the null hypothesis that $\langle$T-O(br)$\rangle$ and $\chi_{O(br)}$ might not be correlated cannot be rejected even at a 90% confidence limit. An exception is the result for the O(7) anion which appears satisfactory; however, this does not constitute an adequate test as the only variation is the presence or absence of Na in the A-site. For the O(5) and O(6) anions where a range of electronegativity values exist, $\chi_{O(br)}$ proves not to be a satisfactory variable. This parallels the situation in the orthosilicates which have lately been examined in detail (Brown, 1970; Brown & Gibbs, in press; Novak & Gibbs, 1971), and suggests either that the effect of electronegativity is more complex than has hitherto been realized (Louisnathan & Gibbs, 1972b) or that the correct variable is not electronegativity but another factor that shows a good correlation with it in some structures.

It has been suggested (Louisnathan & Gibbs, 1972b) that deviations of the kind shown in figures 4.7a, 4.8a and 4.9a are the result of variations in $\langle$O-T-O(br)$\rangle_3$ angles. Figure 4.10 shows the variation in $\langle$T-O(br)$\rangle$ and $\langle$T-O(nbr)$\rangle$ with $\langle\langle$O-T-O(br)$\rangle_3\rangle$ and $\langle\langle$O-T-O(nbr)$\rangle_3\rangle$ respectively. The relationship is approximately linear but significant deviations from linearity do exist for $\langle$T-O(br)$\rangle$; the corresponding relationship for $\langle$T-O(br)-T$\rangle$ (see figure 4.6a) is linear and, in the case of these amphiboles, variations in $\langle$T-O(br)-T$\rangle$ cannot cause the deviations exhibited in the $\langle$T-O(br)$\rangle$-$\langle\langle$O-T-O(br)$\rangle_3\rangle$ relation. As will become evident in the following consideration of O-T-O angles, the inverse relationship also does not apply for the clino-amphiboles. Inspection of figure 4.10 provides an explanation of why the bond lengths in grunerite do not obey the prediction that T-O(br) $>$ T-O(nbr); extremum values of $\langle$O-T-O(br)$\rangle_3$ and $\langle$O-T-O(nbr)$\rangle_3$ are exhibited by grunerite and their influence has caused this prediction to be violated. Theoretical calculations by Louisnathan and Gibbs (1972a, b) and Gibbs et al. (1972) have shown that $\langle$O-T-O$\rangle_3$ is actually correlated with n(Si-O), the bond overlap population calculated by Mulliken population analysis (Mulliken, 1955a, b). The relationship between n(T-O) and T-O differs for bridging and non-bridging bonds (Bartell, Su and Yow, 1970; Gibbs et al., 1972).

Thus, for a similar $\langle$O-T-O$\rangle_3$ angle, $\langle$T-O(br)$\rangle$ will be shorter than $\langle$T-O(nbr)$\rangle$; this is borne out by simple linear regression analysis on the data of figure 4.10 where the regression lines for

FIGURE 4.10 The variation in $\langle T\text{-}O(br)\rangle$ and $\langle T\text{-}O(nbr)\rangle$ with $\langle\langle O\text{-}T\text{-}O(br)\rangle_3\rangle$ and $\langle\langle O\text{-}T\text{-}O(nbr)\rangle_3\rangle$ for the Si clino-amphiboles

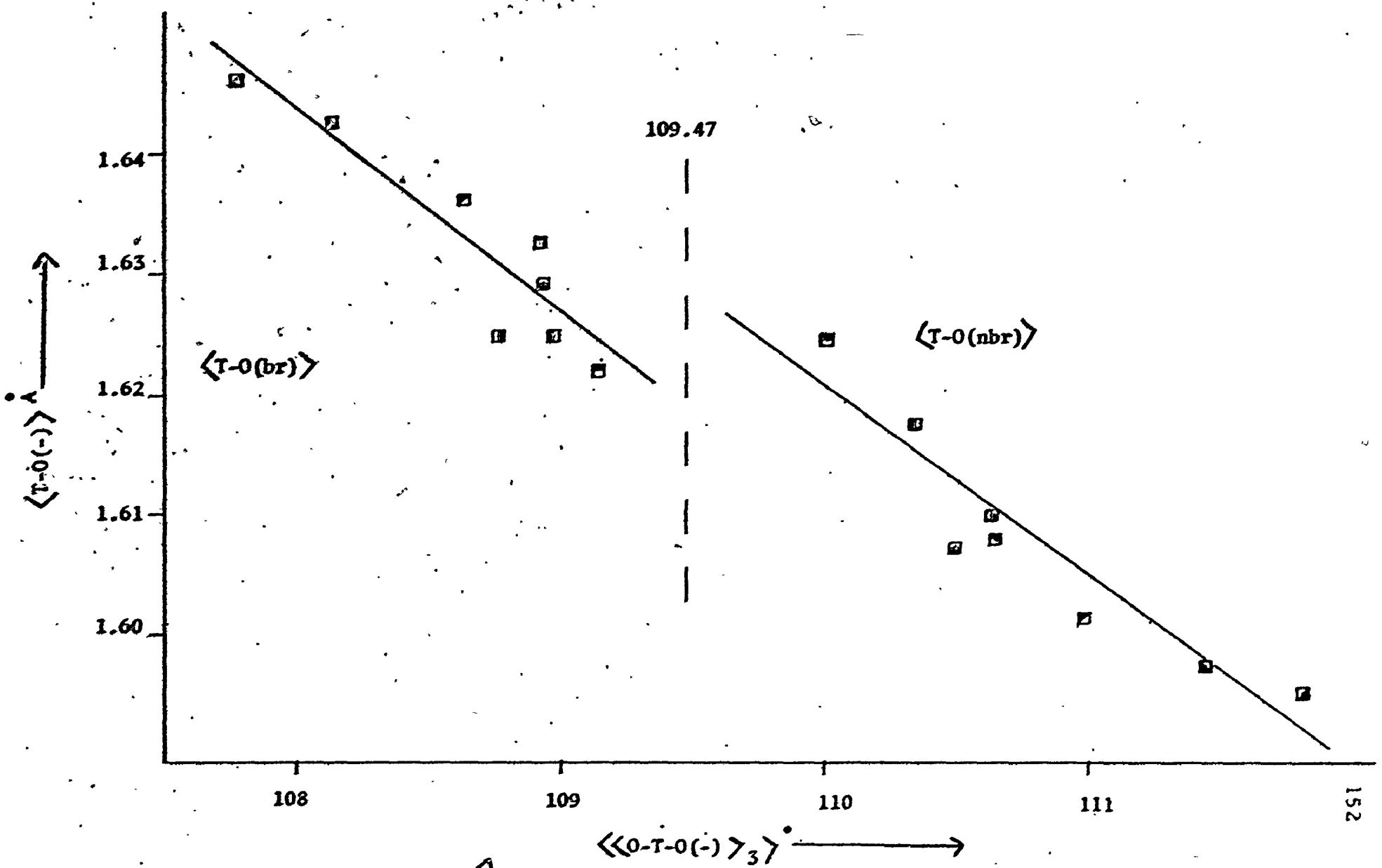

bridging and non-bridging bonds are shown; numerical results for the regression analyses are given in Table 4.4. Variations in $\langle O\text{-}T\text{-}O \rangle_3$ angles appear to be intimately related to changes in T-O bond length, a fact that warrants further consideration. Figures 4.11a and b show the variation in $\langle T\text{-}O(br) \rangle$ bond lengths with $\langle\langle O\text{-}T\text{-}O(br) \rangle_3 \rangle$ for the O(5) and O(6) anions. Discussion of $\langle T\text{-}O(7) \rangle$ will be deferred until later as it shows the variation in a single bond length since T-O(7) is crystallographically unique. For the O(5) and O(6) anions, a linear relationship is displayed and the results of simple linear regression analysis are given in Table 4.4. Significant deviations appear to exist; in figure 4.11a both synthetic richterite 1 and glaucophane deviate from linearity. These two also deviate from a linear $\langle T\text{-}O(5) \rangle$ - $\langle T\text{-}O(5)\text{-}T \rangle$ relationship (see figure 4.7a); however, for both minerals the discrepancy is sympathetic, $\langle T\text{-}O(5) \rangle$ being 'anomalously' short in both cases. Thus neither of these relationships can be invoked to account for non-linearity in the other, and the 'short' bonds lengths of synthetic richterite 1 and glaucophane must be caused by some other factor. Conversely, the difference between the linear parts of the $\langle T\text{-}O(br) \rangle$ -T-O(br)-T curves for O(5) and O(6) can be explained by the difference between the $\langle O\text{-}T\text{-}O(5) \rangle_3$ and $\langle O\text{-}T\text{-}O(6) \rangle_3$ angles, and <u>vice versa</u>. Inclusion of the length of the linking unshared octahedral edge also accounts for the small deviations exhibited by figures 4.11a,b. Stepwise linear regression for

Figure 4.11a $\langle$T-O(5)$\rangle$ versus $\langle\langle$O-T-O(5)$\rangle_3\rangle$ for the Si clino-amphiboles

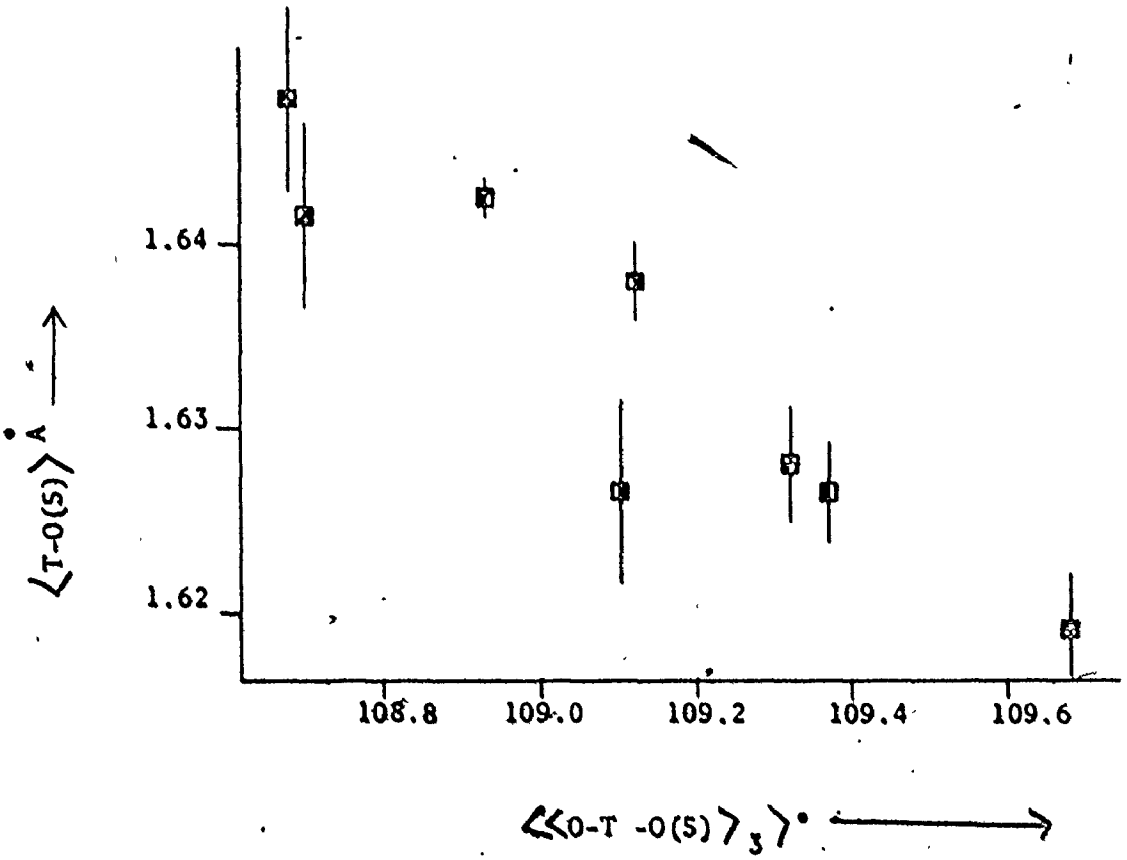

Table 4.11b $\langle$T-O(6)$\rangle$ versus $\langle\langle$O-T-O(6)$\rangle_3\rangle$ for the Si clino-amphiboles

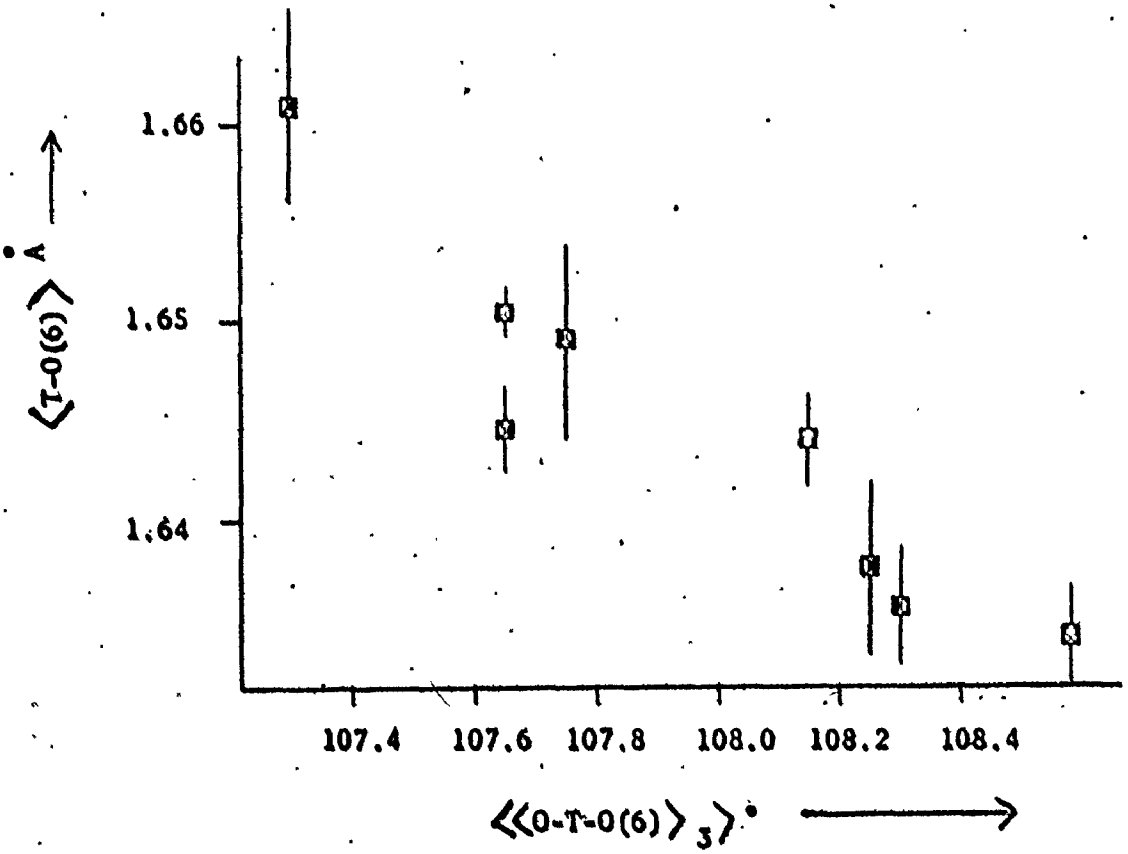

TABLE 4.4: STEPWISE LINEAR REGRESSION ANALYSIS

Legend as for Table 4.3.

1. $\langle$T-O(br)$\rangle$ dependent, $\langle\langle$O-T-O(br)$\rangle_3\rangle$ independent
2. $\langle$T-O(nbr)$\rangle$ dependent, $\langle\langle$O-T-O(nbr)$\rangle_3\rangle$ independent
3. $\langle$T-O(5)$\rangle$ dependent, $\langle\langle$O-T-O(5)$\rangle_3\rangle$ independent
4. $\langle$T-O(6)$\rangle$ dependent, $\langle\langle$O-T-O(6)$\rangle_3\rangle$ independent
5. $\langle$T-O(br)$\rangle$ dependent, $\langle\langle$O-T-O(br)$\rangle_3\rangle$, T-O(br)-T and $(O\text{-}O)_{OCT}$ for O(5) and O(6), independent
6. $\langle$T-O(br)$\rangle$ dependent, $\langle\langle$O-T-O(br)$\rangle_3\rangle$, T-O(br)-T and $(O\text{-}O)_{OCT}$ for O(5), O(6) and O(7), independent
7. T-O(br) dependent, $\langle$O-T-O(br)$\rangle_3$ and $\langle$O-O(br)$\rangle_3$ independent
8. T-O(br) dependent, $\langle$O-T-O(br)$\rangle_3$, $\langle$O-O(br)$\rangle_3$, T-O(br)-T and $(O\text{-}O)_{OCT}$ independent
9. T-O(nbr) dependent, $\langle$O-T-O(nbr)$\rangle_3$ and $\langle$O-O(nbr)$\rangle_3$ independent
10. T-O(nbr) dependent, $\langle$O-T-O(nbr)$\rangle_3$, $\langle$O-O(nbr)$\rangle_3$, $\langle\langle$O-T-O(br)$\rangle_3\rangle$ and $\langle\langle$O-O(br)$\rangle_3\rangle$ independent
11. T-O(nbr) dependent, $\langle$O-T-O(nbr)$\rangle_3$, $\langle$O-O(nbr)$\rangle_3$ and $\langle$T-O(br)-T$\rangle_T$ independent

Number	Indep. Var.	c	m	⟨R⟩	σ	|t|
1.	$\langle\langle$ O-T-O(br)$\rangle_3\rangle$	3.4973	-0.0172(30)	0.921	0.0037	5.73
2.	$\langle\langle$ O-T-O(nbr)$\rangle_3\rangle$	3.3720	-0.0159(24)	0.938	0.0037	6.63
3.	$\langle\langle$ O-T-O(5)$\rangle_3\rangle$	4.5887	-0.0271(47)	0.919	0.0043	5.77
4.	$\langle\langle$ O-T-O(6)$\rangle_3\rangle$	3.7663	-0.0197(30)	0.937	0.0034	6.57
	$(\langle\langle$ O-T-O(5, 6)$\rangle_3\rangle$		-0.00989(94)			10.52
5.	) T-O(5, 6)-T	2.8986	-0.00309(34)	0.983	0.0022	9.09
	$(O^u\text{-}O^u)_{M(1,2)}$		0.079(13)			6.08
	$(\langle\langle$ O-T-O(5, 6, 7)$\rangle_3\rangle$		-0.0118(25)			4.72
6.	) T-O(5, 6, 7)-T	3.1471	-0.0015(11)	0.837	0.0082	1.36
	$(O^u\text{-}O^u)_{M(1,2,3)}$		-0.006(39)			0.15
	$(\langle$ O-T-O(br)$\rangle_3$		-0.02013(64)			31.45
7.	)	1.2215		0.982	0.0035	
	$(\langle$O-O(br)$\rangle_3$		0.983(49)			20.06
	$(\langle$O-T-O(br)$\rangle_3$		-0.01975(68)			29.04
	$(\langle$O-O(br)$\rangle_3$		0.949(50)			18.98
8.	)	1.3277		0.984	0.0034	
	(T-O(br)-T		-0.00037(34)			1.09
	$(O\text{-}O)_{OCT}$		-0.0014(116)			0.12

Number	Indep. Var.	c	m	⟨R⟩	σ	|t|
	$\langle$O-T-O(nbr)$\rangle_3$		-0.0262(39)			6.72
9.		0.6029		0.872	0.0093	
	$\langle$O-O(nbr)$\rangle_3$		1.47(18)			8.17
	$\langle$O-T-O(nbr)$\rangle_3$		-0.0275(14)			19.64
	$\langle$O-O(nbr)$\rangle_3$		1.682(56)			30.04
10.		1.2039		0.991	0.0026	
	$\langle\langle$O-T-O(br)$\rangle_3\rangle_T$		0.0081(11)			7.36
	$\langle\langle$O-O(br)$\rangle_3\rangle_T$		-0.723(88)			8.22
	$\langle$O-T-O(nbr)$\rangle_3$		-0.0120(32)			3.75
11.	$\langle$O-O(nbr)$\rangle_3$	-0.9905	1.21(11)	0.960	0.0054	11.00
	$\langle$T-O(br)-T$\rangle_T$	0.00495(77)				6.43

T-O(br)-T, $\langle$O-T-O(br)$\rangle_3$, $\langle$T-O(br)$\rangle$ and $(O\text{-}O)_{OCT}$ with $\langle$T-O(br)$\rangle$ as the dependent variable for the combined set of O(5) and O(6) data was performed and the results are given in Table 4.4. The result appears satisfactory with a $|t|$-test indicating that all variables contribute significantly. However, inclusion of the data for O(7) in the analysis decreases the significance of the fit and $|t|$-test indicates that only $\langle$O-T-O(br)$\rangle_3$ is a significant variable (see Table 4.4.).

Because of the obvious importance of the relationship between $\langle$O-T-O$\rangle_3$ and T-O, this relationship was examined in more detail. The variation of each crystallographically unique T-O bond with $\langle$O-T-O$\rangle_3$ was, in general, extremely irregular, and this could not be attributed to electronegativity variations in non-tetrahedral cations. It is therefore pertinent to examine the reasons for an $\langle$O-T-O$\rangle_3$ dependence of T-O bond lengths. This has been rationalized (Louisnathan & Gibbs, 1972a) in terms of the non-equivalent hybridization characteristics of the Si atom; their analysis considered a tetrahedral group of C_{3v} symmetry and thus the orbitals formed a basis set for the irreducible representation of this point group (Cotton, 1963).

Since a great deal of the success of E.H.M.O. predictions are attributable to orbital symmetry considerations (Allen, 1970, 1972), it is not clear whether the results of this analysis can be extended by analogy to other point groups, especially as the tetrahedral groups under considera-

tion have minimum symmetry (C_1). However, making the assumption that it can, the relation may be seen to be due to increased σ - (and π -) overlap with increasing $\langle O\text{-}T\text{-}O \rangle_3$. In the calculations performed by Gibbs' group, no account was taken of the non-bonded interactions between anions; these have been shown to be important in the variation of P-O and S-O bonds (Bartell, Su and Yow, 1970). Thus, it is feasible that some of the variation in T-O bond lengths are due to variation in the non-bonded interactions of the anions involved in the $\langle O\text{-}T\text{-}O \rangle_3$ angles. It has been shown by many investigators that n(T-O) is a linear function of T-O; if a similar assumption is made concerning the (O-O) non-bonded interactions, $\langle O\text{-}O \rangle_3$ may be taken as a measure of this interaction and thus may affect T-O. The basic assumption has been made that any inductive effect of non-tetrahedral cations will be reflected in the electronic structure of the TO_4 oxy-anion, and thus the variations in T-O may be rationalized solely in terms of variations in tetrahedral stereochemistry.

Consequently, a stepwise linear analysis was performed for $\langle O\text{-}T\text{-}O \rangle_3$, $\langle O\text{-}O \rangle_3$, and T-O with the latter as the dependent variable. To adequately account for the observed bond lengths, a single relationship is necessary; if different relationships are necessary for each bond, the observed stereochemistry is not adequately explained. One possible exception is the division of T-O bonds into two sets, bridging

and non-bridging, since MO calculations appear to indicate very basic differences between the two groups. Consequently, the amphibole data was divided into two groups, bridging and non-bridging bonds, and the stepwise regression analysis results are given in Table 4.4. Consider first the results for the bridging bonds; variations in $\langle O\text{-}T\text{-}O(br)\rangle_3$ and $\langle O\text{-}O(br)\rangle_3$ appear to account quite adequately for variations in T-O(br). The analysis was repeated with the addition of two more independent variables; T-O(br)-T and $(O\text{-}O)_{OCT}$; these results are given in Table 4.4. No significant improvement was apparent and both additional variables do not contribute significantly to the variation of T-O(br). This might tend to corroborate a previous suggestion that T-O(br) tends to control T-O(br)-T rather than vice versa. Table 4.5 compares the values calculated for T-O(br) from the regression equation

$$T\text{-}O(br) = 1.222 - 0.02013(64)\langle O\text{-}T\text{-}O(br)\rangle_3 + 0.983(49)\langle O\text{-}O(br)\rangle_3$$

with the observed values, and figure 4.12a shows a similar graphical comparison. In general, the deviations do not exceed 1 standard deviation, and the regression equation appears to be adequate.

The results for the non-bridging bonds are not as encouraging although a $|t|$-test indicates that both variables contribute significantly to the variation in T-O(nbr). From the discussions of Cruickshank (1961)

TABLE 4.5: COMPARISON OF OBSERVED AND CALCULATED T-O DISTANCES IN SI-CLINO-AMPHIBOLES

	T(1)-O(1)		T(1)-O(5)		T(1)-O(6)		T(1)-O(7)	
	OBS.	CALC.	OBS.	CALC.	OBS.	CALC.	OBS.	CALC.
Trem	1.602(2)	1.604	1.632(2)	1.629	1.629(2)	1.629	1.616(1)	1.619
Flor	1.614(3)	1.615	1.628(3)	1.625	1.630(4)	1.629	1.616(2)	1.609
SR1	1.582(6)	1.581	1.625(6)	1.623	1.641(7)	1.647	1.636(3)	1.636
SR2	1.594(6)	1.595	1.636(7)	1.630	1.624(7)	1.625	1.631(4)	1.633
Glauc	1.618(6)	1.615	1.616(7)	1.612	1.621(6)	1.616	1.611(3)	1.612
Cumm	1.619	1.618	1.614	1.614	1.628	1.624	1.613	1.615
Grun	1.637(4)	1.641	1.627(5)	1.630	1.630(4)	1.630	1.613(2)	1.624
C-Mn	1.610(3)	1.610	1.622(4)	1.622	1.633(3)	1.627	1.616(2)	1.617

	T(2)-O(2)		T(2)-O(4)		T(2)-O(5)		T(2)-O(6)	
	OBS.	CALC.	OBS.	CALC.	OBS.	CALC.	OBS.	CALC.
Trem	1.616(2)	1.614	1.586(2)	1.585	1.653(2)	1.653	1.672(2)	1.671
Flor	1.623(3)	1.618	1.587(3)	1.584	1.648(4)	1.644	1.659(3)	1.659
SR1	1.625(6)	1.626	1.578(5)	1.583	1.658(7)	1.659	1.681(6)	1.681
SR2	1.626(7)	1.625	1.572(7)	1.573	1.660(8)	1.657	1.674(7)	1.672
Glauc	1.618(6)	1.614	1.594(6)	1.593	1.637(7)	1.638	1.654(7)	1.652
Cumm	1.625	1.627	1.609	1.611	1.639	1.639	1.643	1.648
Grun	1.633(4)	1.632	1.604(4)	1.604	1.611(5)	1.615	1.638(5)	1.637
C-Mn	1.618(3)	1.615	1.594(3)	1.592	1.634(3)	1.633	1.655(4)	1.651

Figure 4.12a Graphical comparison of the observed and calculated T-O(br) bond lengths of the Si clino-amphiboles.

The $T\text{-}O(br)_{calc}$ were calculated from the following regression equation...

$$T\text{-}O(br) = 1.222 - 0.02013(64)\ \langle O\text{-}T\text{-}O(br)\rangle_3 + 0.983(49)\ \langle O\text{-}O(br)\rangle_3$$

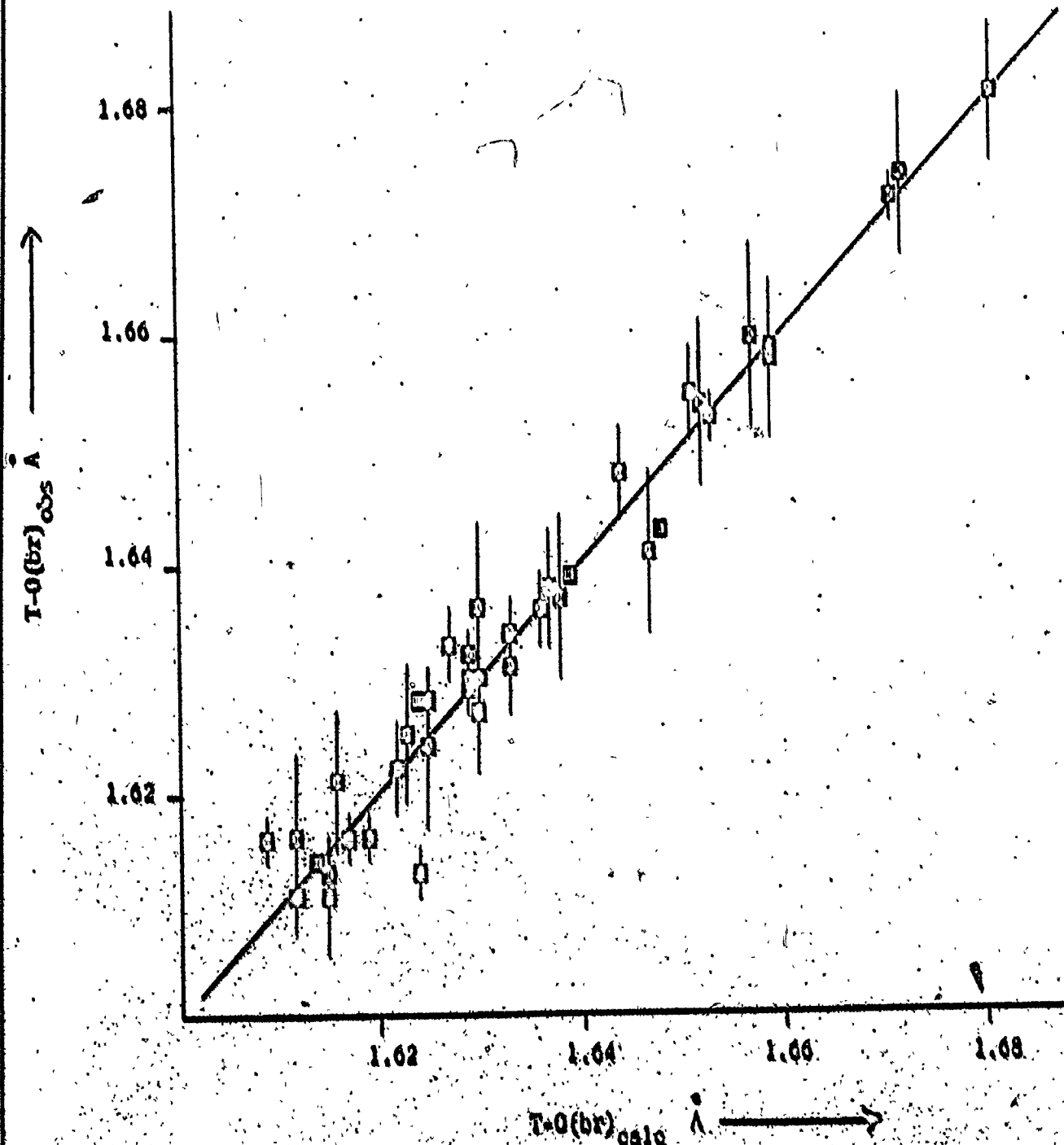

and Mitchell et al. (1971), it appears that an internal constraint on the variation of bond lengths is operative. If it is assumed that the mean bond order of an SiO_4 group is fairly constant at 1.5, lengthening of some bonds will be accompanied by shortening of other bonds. If the T-O(br) bond lengths are controlled solely by the variations in $\langle O\text{-}T\text{-}O(br)\rangle_3$ and $\langle O\text{-}O(br)\rangle_3$, the mean bond order requirement could act as a constraint on the variation in T-O(nbr). Since T-O(br) is a function of $\langle O\text{-}T\text{-}O(br)\rangle_3$ and $\langle O\text{-}O(br)\rangle_3$, the mean of these parameters for each tetrahedron will represent a constraint on the variation of T-O(nbr) in that tetrahedron. Consequently, the analysis was repeated for T-O(nbr) with the variables $\langle\langle O\text{-}T\text{-}O(br)\rangle_3\rangle_T$ and $\langle\langle O\text{-}O(br)\rangle_3\rangle_T$ included. The results are given in Table 4.4; all independent variables are significant and account adequately for the variation in T-O(nbr). Table 4.5 compares the values calculated for T-O(nbr) from the regression equation

$$T\text{-}O(nbr) = 1.204 - 0.0275(14)\langle O\text{-}T\text{-}O(nbr)\rangle_3 + 1.682(56)\langle O\text{-}O(nbr)\rangle_3$$
$$+ 0.0081(11)\langle\langle O\text{-}T\text{-}O(br)\rangle_3\rangle_T - 0.723(88)\langle\langle O\text{-}O(br)\rangle_3\rangle_T$$

with the observed values, and figure 4.12b show a similar graphical comparison. In general, the deviations do not exceed 1 standard deviation, and the regression equation appears to be adequate.

Figure 4.12b Graphical comparison of the observed and calculated T-O(nbr) bond lengths of the Si clino-amphiboles.

The T-O(nbr) were calculated from the following regression equation ...

$$T\text{-}O(nbr) = 1.204 - 0.0275(14)\langle O\text{-}T\text{-}O(nbr)\rangle_3 + 1.682(56)\langle O\text{-}O(br)\rangle_3 + 0.0081(11)\langle\langle O\text{-}T\text{-}O(br)\rangle_3\rangle_T - 0.723(88)\langle\langle O\text{-}O(br)\rangle_3\rangle_T$$

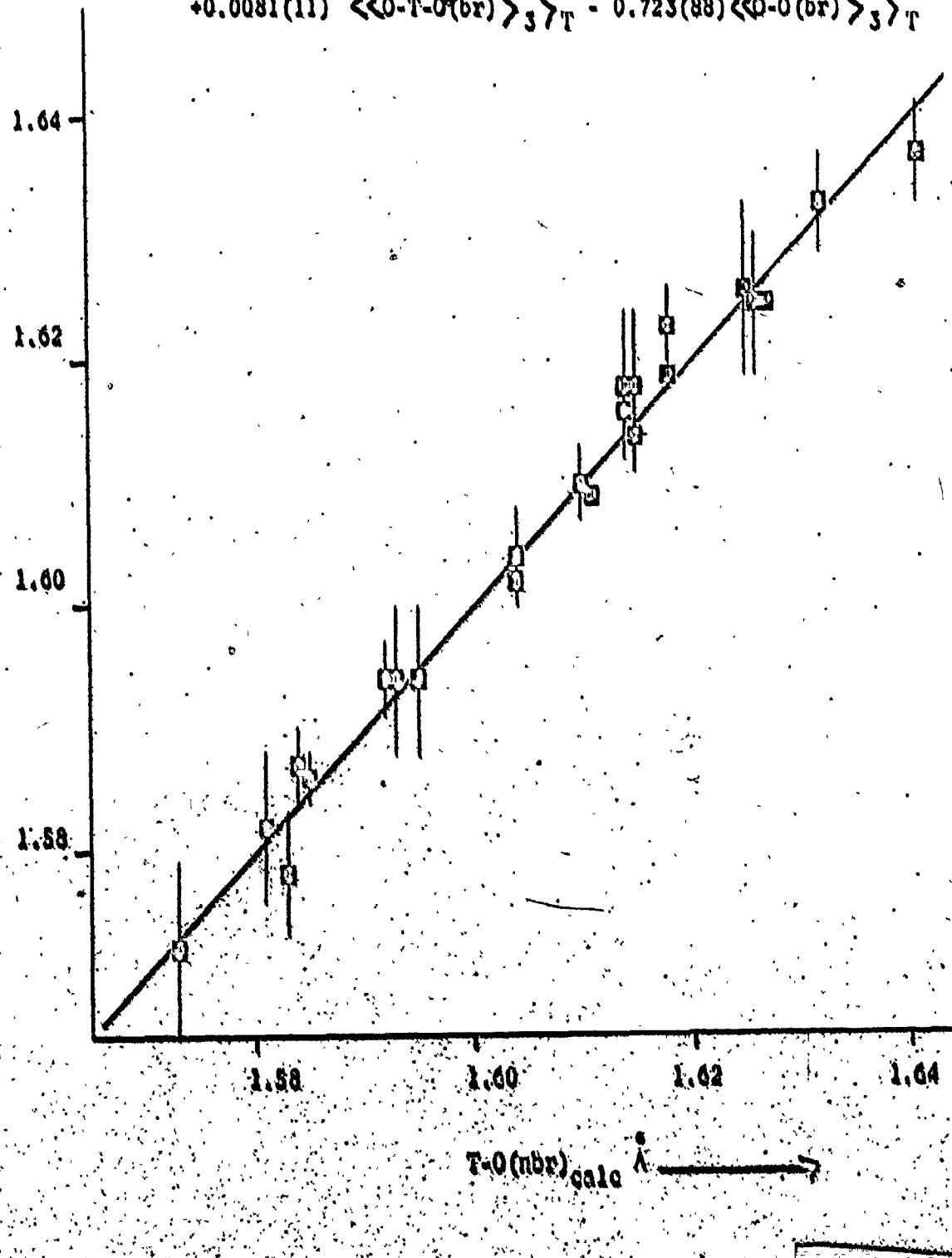

Correlations between T-O(nbr), $\langle$T-O(br)-T$\rangle_T$ and $\bar{\chi}_{O(nbr)}$ were presented by Mitchell et al. (1971). The data set used was smaller than that used in the present study; five structures were considered, one of which contained significant amounts of Al in the T(1) site. In addition, the value used for $\langle$T-O(br)-T$\rangle_{T(1)}$ for glaucophane was in error by 1 degree (compare figure 2c, Mitchell et al., 1971 with Table 6, Papike et al. (1969)), which constitutes 20% of the total variation in $\langle$T-O(br)-T$\rangle_{T(1)}$. Thus, the regression equation presented for T(1)-O(1) is incorrect, and correlation is decreased by inclusion of the correct value. In addition, the regression coefficients for each equation are quite different, indicating that this correlation does not account well for the observed stereochemistry. However, some correlation is apparent and the reason for this becomes apparent upon consideration of some of the previous results. T-O(br)-T is partially correlated with $\langle$T-O(br)$\rangle$ and it is the variation in $\langle$T-O(br)$\rangle_T$ that operates the mean bond order constraint on the variation of T-O(nbr). It may be shown that $\langle$T-O(br)-T$\rangle_T$ is not as adequate a measure of this constraint as $\langle\langle$O-T-O(br)$\rangle_3\rangle_T$ and $\langle\langle$O-O(br)$\rangle_3\rangle_T$ by performing a stepwise regression on $\langle$O-T-O(nbr)$\rangle_3$, $\langle$O-O(nbr)$\rangle_3$, T-O(nbr) and $\langle$T-O(br)-T$\rangle_T$ with T-O(nbr) as the dependent variable. The results of this analysis are given in Table 4.4 and comparison of the results with those of the previous analysis indicates that $\langle$T-O(br)-T$\rangle_T$ is inferior to $\langle\langle$O-T-O(br)$\rangle_3\rangle_T$ and $\langle\langle$O-O(br)$\rangle_3\rangle_T$ as a measure of bond order constraint on T-O(nbr).

The variation in individual T-O distances in amphiboles appear to be susceptible to rationalisation in terms of a simple M.O. model. Thus it could be profitable to examine this model a little further to see if any other relationships are apparent. An equation relating bond length to bond order was deduced by Robinson (1963) and applied to Si-O, P-O and S-O bonds by Gillespie & Robinson (1963, 1964). The equation for Si-O bonds is as follows:

$$T\text{-}O = 1.83 - 0.32/(1+0.60[(2-n)/(n-1)])$$

where n is the bond order. The form of this equation is shown in figure 4.14 and resembles a similar curve developed for C-C bonds by Coulson & Dingle (1968). Since the second derivative of this curve is positive, an increase in some bond lengths must be accompanied by a decrease of lesser magnitude in the remaining bonds in order that the mean bond order remains constant at ~1.5. Consequently, the mean bond length will be a function of the bond length distortion (see Appendix 4). The dependence of T-O bond lengths on ⟨O-T-O⟩ angles, distances, etc. indicates that an involved function could be derived to calculate the ⟨T-O⟩ distances by summing the relevant regression equations over all the bonds in a tetrahedron.

This procedure is rather involved and a simpler relationship would be desirable. The regression analyses suggest that ⟨O-O⟩ distance

Figure 4.14 The variations in bond order with bond length for the Si-O bond, calculated [using the method of Robinson (1963)] from the equation.

$$Si\text{-}O = 1.83 - 0.32/[1 + 0.6([2-n]/[n-1])]$$

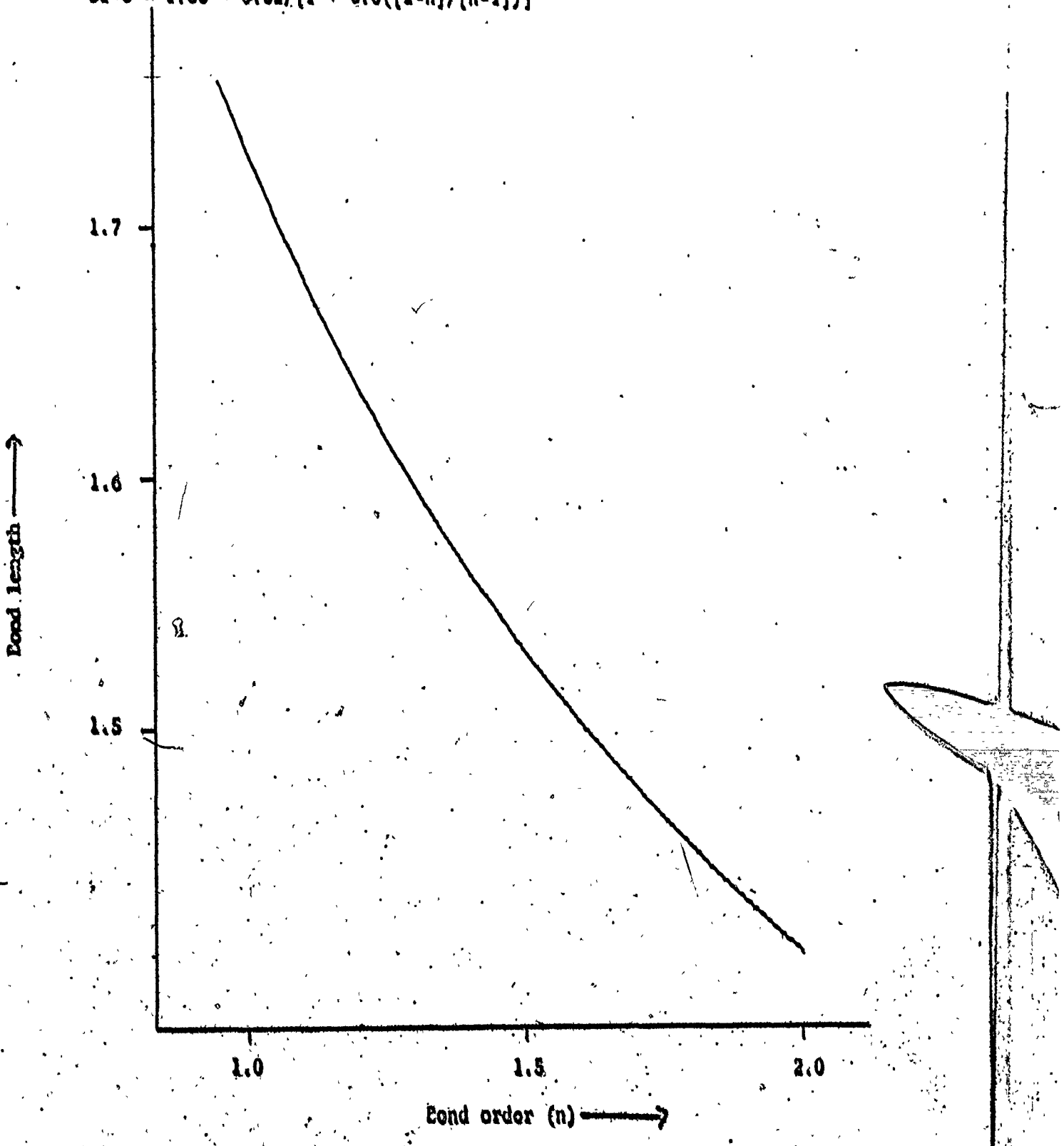

may be an important parameter and figure 4.15 indicates that this is so. The slope of the regression line $\approx 2\sqrt{2/3}$, corresponding to the general result for numerous structures examined in this fashion by Drits (1970). The dependence of T-O distances on O-T-O angles suggests that the $\langle$T-O$\rangle$ distances might also be correlated with angular distortion. A good angular distortion parameter was introduced by Robinson, Gibbs & Ribbe (1971); this was defined as the variance† of the O-T-O angles (or mean square bond angle strain) and the dependence of T-O bond lengths on O-T-O angles outlined previously suggests the reason for its widespread success. Figures 4.16a,b show the variation of $\langle$T(1)-O$\rangle$ and $\langle$T(2)-O$\rangle$ respectively with the angle variance. A reasonable correlation is developed for the T(2) tetrahedron, but not for the T(1) tetrahedron. Similarly, the correlation between $\langle$T(2)-O$\rangle$ and $\langle$T-O(br)-T$\rangle_{T(2)}$ is fairly well developed, but for the T(1) site, it is very weak (figures 4.17a,b). The linearity of these relations is a function of the inter-parameter (independent) correlation since together they are adequate to forecast the mean distances; the above result indicates a much higher inter-correlation for the T(2) tetrahedron as compared with the T(1) tetrahedron.

If the regression equations developed for the Si-amphiboles

† Angular distortion = $\sum_{i=1}^{6} ([O\text{-}T\text{-}O]_i - 109.47)^2/5$

Figure 4.15 The variation in $\langle T\text{-}O \rangle$ bond length with $\langle O\text{-}O \rangle$ edge length for the Si clino-amphiboles

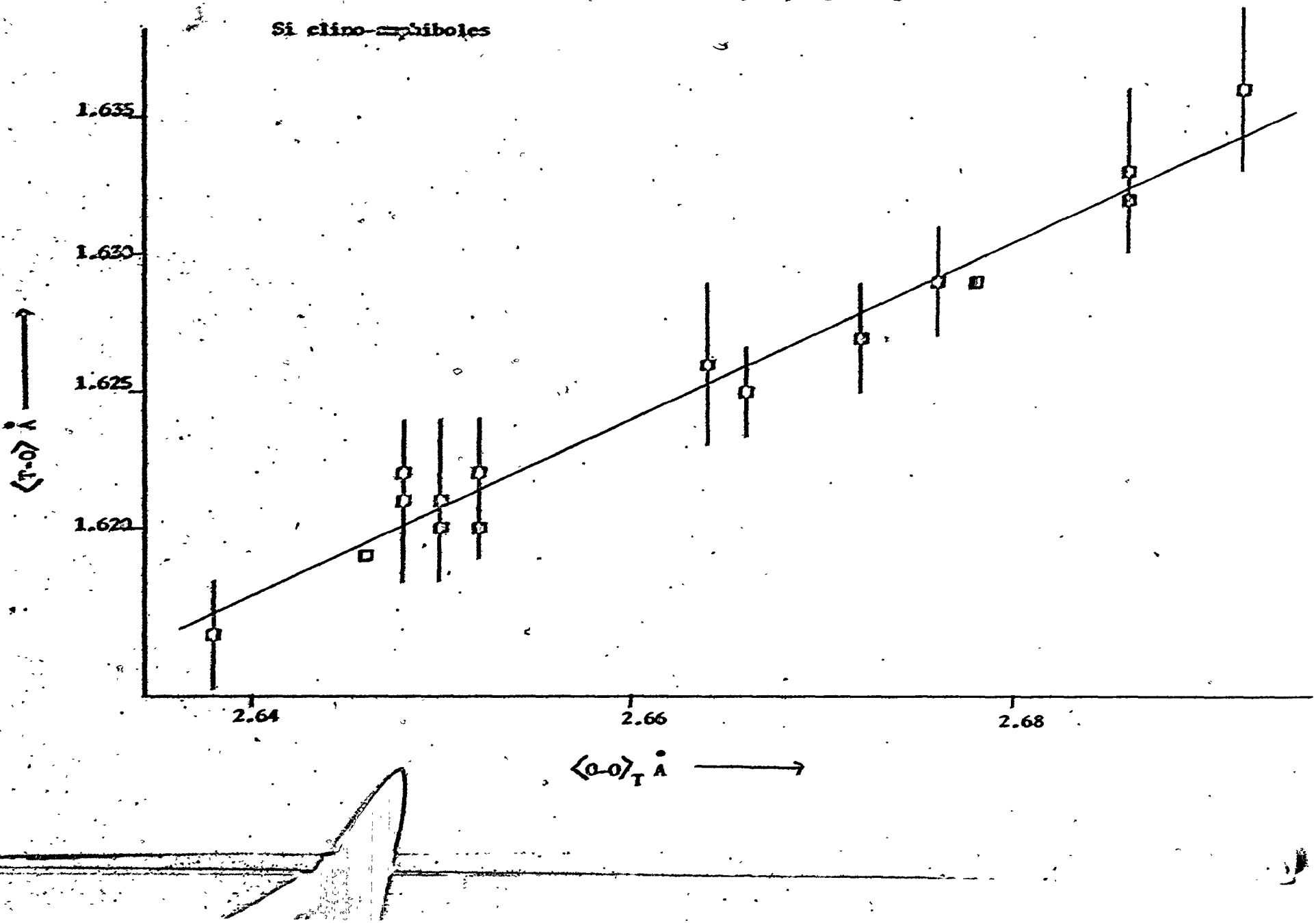

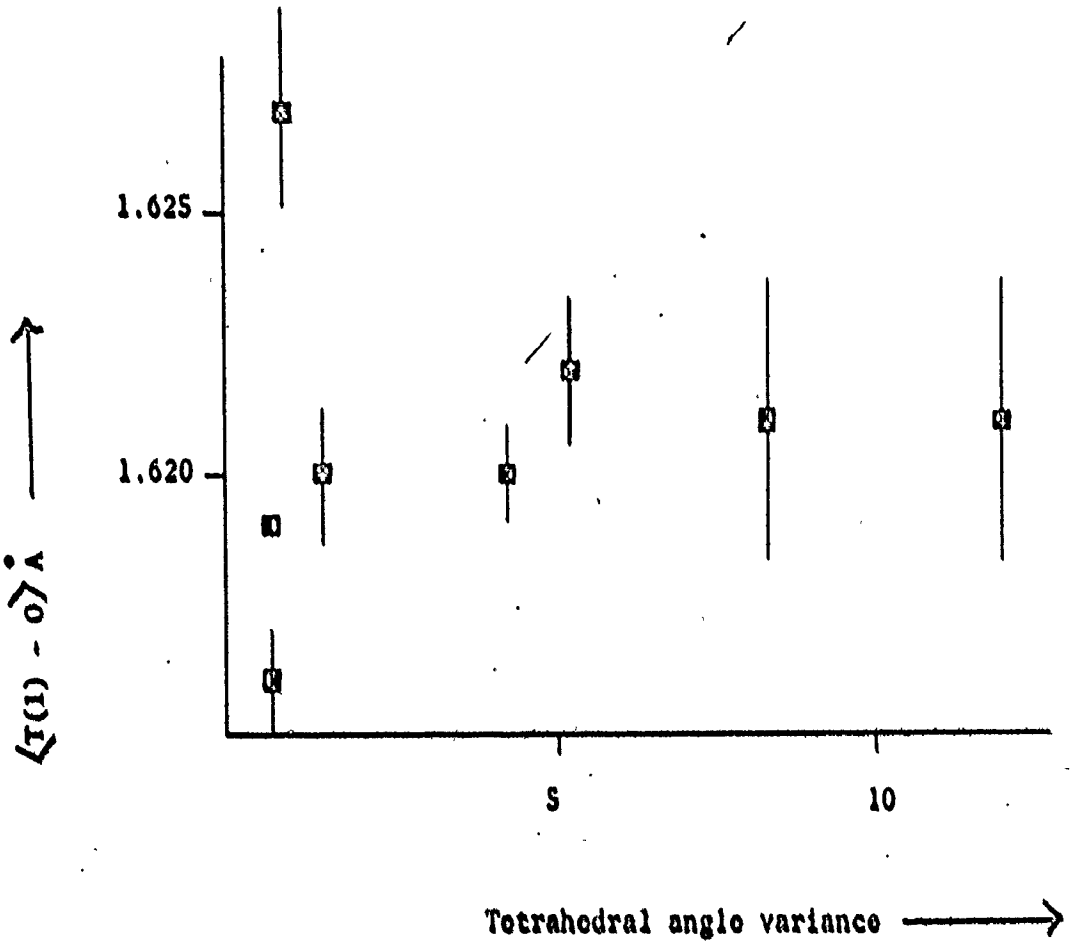

Figure 4.16b ⟨T(2)-O⟩ versus tetrahedral angle variance for the Si clino-amphiboles

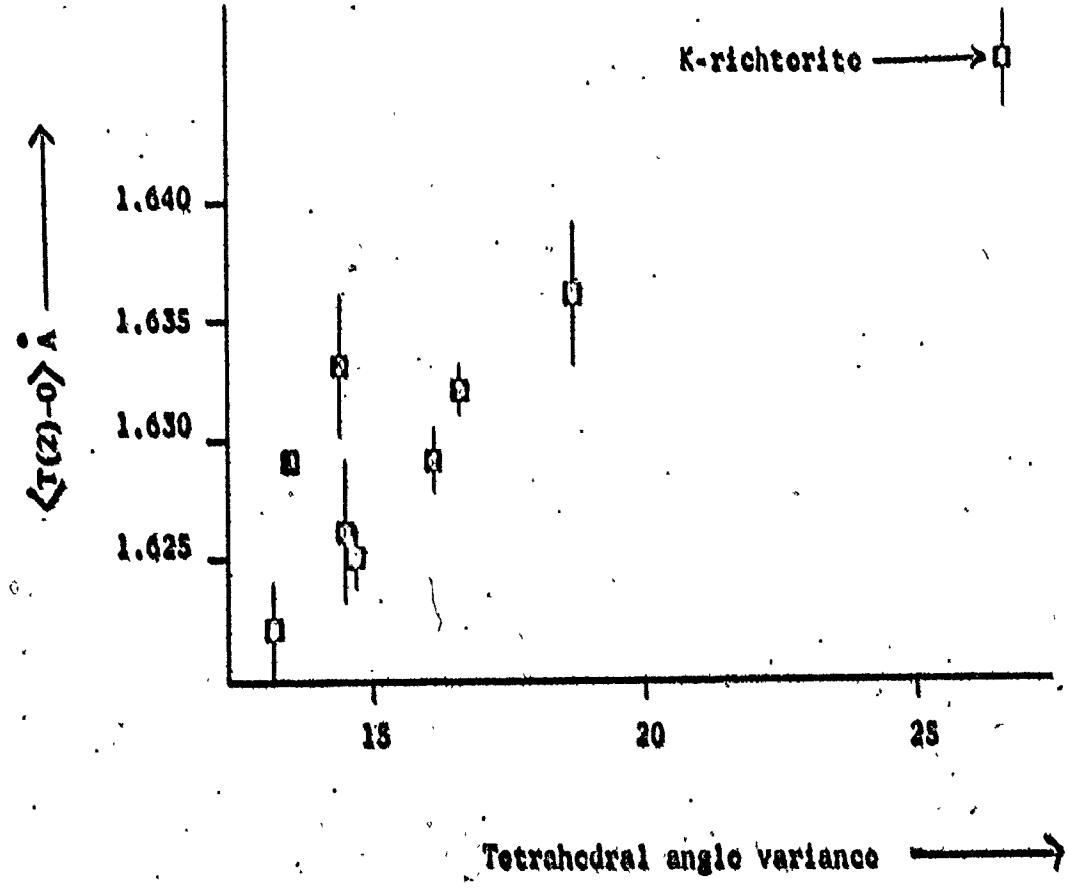

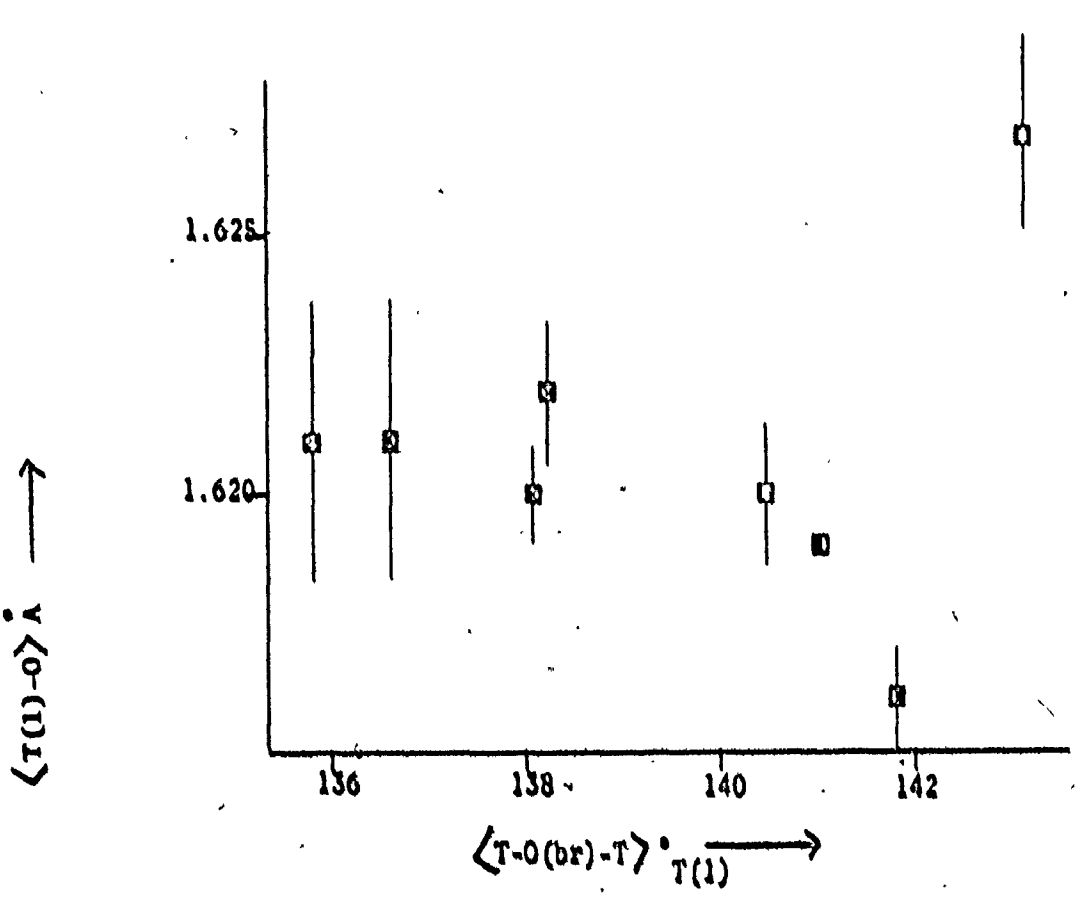

Figure 4.17b T(2)-O versus T-O(br) - T T(2) for the Si clino-amphiboles

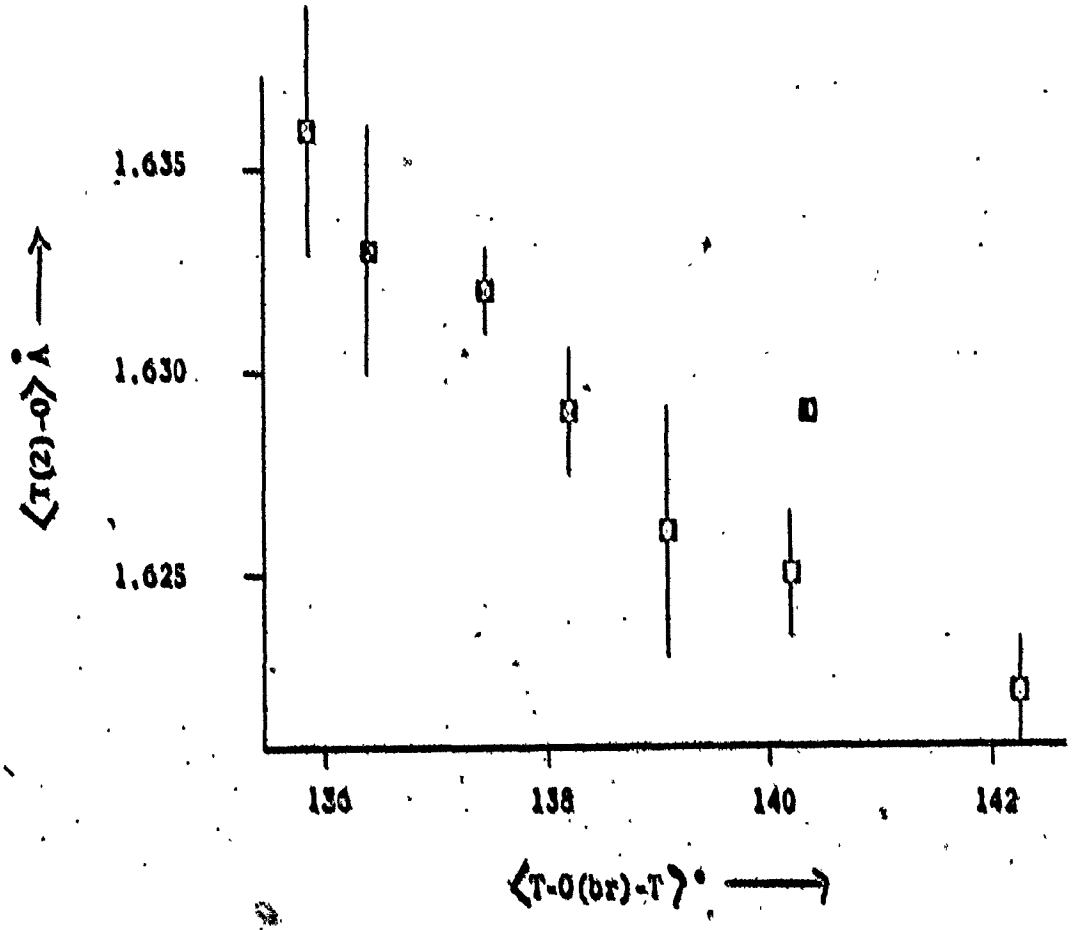

are an adequate description of bonding in the 'covalent' model, they should be successful in forecasting individual bond lengths in other structures containing polymerized Si-tetrahedra. Figure 4.18a shows the observed and calculated Si-O distances for a series of ordered C2/c pyroxenes; the agreement is good. However, the pyroxene and amphibole structures are fairly similar and it is possible that the regression equations contain implicit steric effects that are inherent in both structures. A more stringent test is provided by the R.E. pyrosilicates (Smolin & Shepelev, 1970) which bear no relation to the pyroxene and amphibole structures, and also exhibit a wide range of structure type themselves. Figure 4.18b shows the observed and calculated Si-O distances for this group; again, the agreement is reasonable and suggests that the regression equations developed here may be of wider applicability.

Although no exact geometrical constraint on bond length variation is imposed by the regression equations developed here, the possibility arises that an approximate constraint is imposed that suffices to define the T-O length within the limits of accuracy of measurement. This may be tested by developing similar relationships for other tetrahedral cations of the third row of the periodic table, since the variation in formal charge from Al^{3+} to S^{6+} should change the significance of the bonding and non-bonding interactions; thus similar regression analyses should give markedly

Figure 4.18a Comparison of the observed and calculated T-O distances for ordered clino-pyroxenes

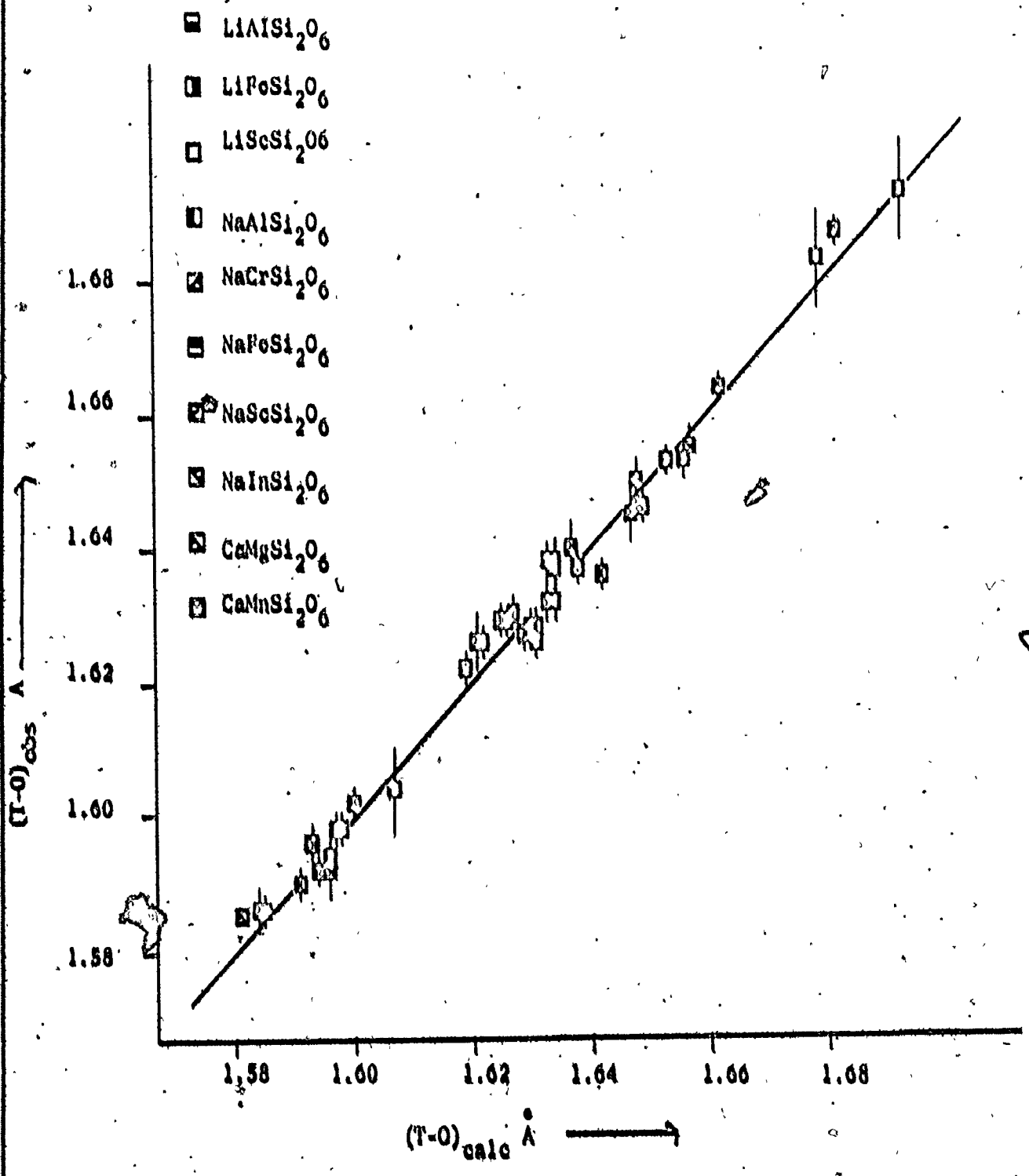

Figure 4.18b Comparison of the observed and calculated T-O distances for rare earth pyrosilicates

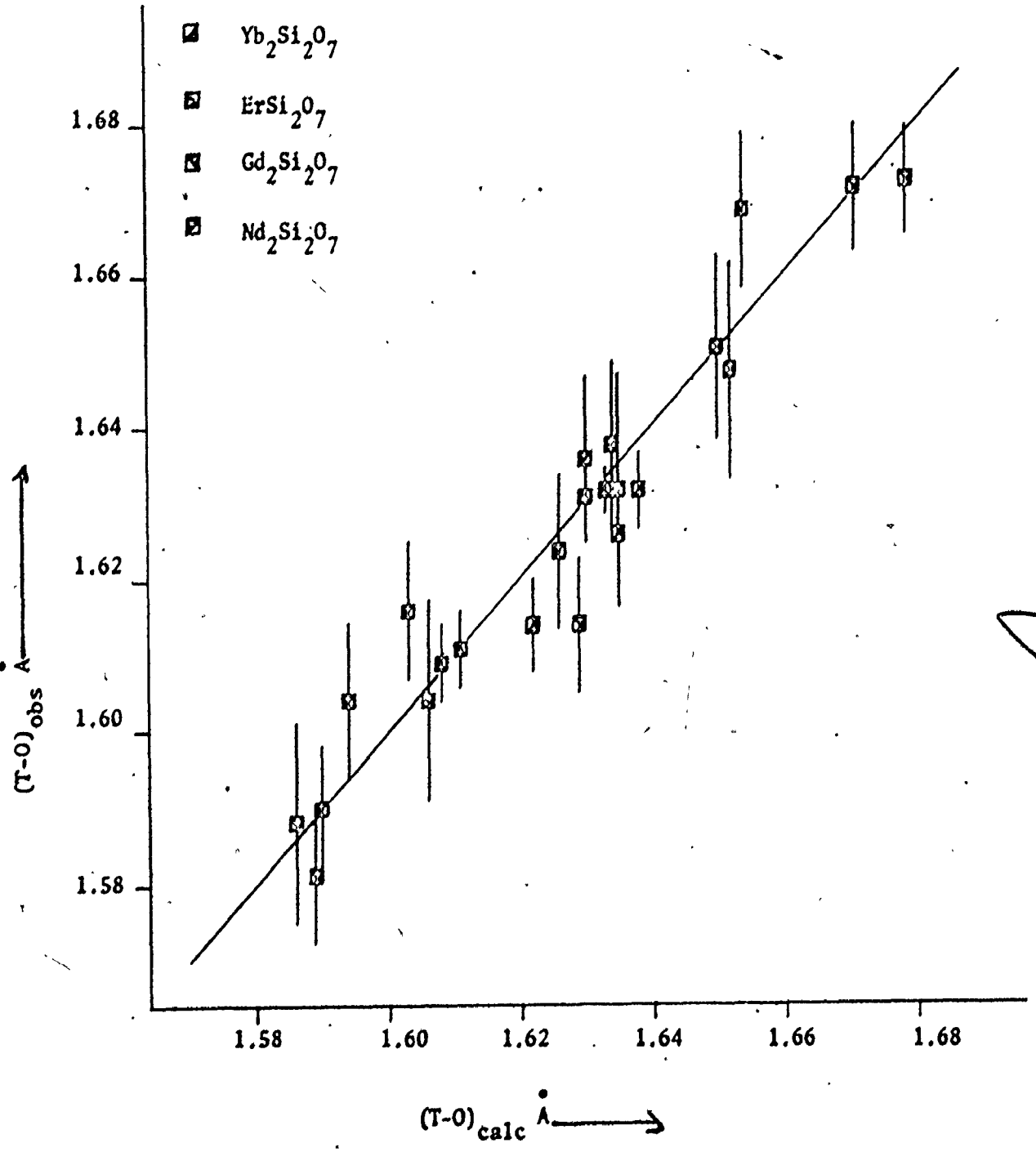

different slopes for the various parameters if these relationships result from bonding effects whereas the slopes will be identical if this is a spurious geometrical effect. This is at present being investigated.

(b) Ionic bonding Model

The utility of electrostatic interaction in the understanding of the chemical bond has long been recognized (Bent, 1968). Together with the hard sphere model of atoms developed by Barlow (Bent, ibid.), it eventually led to the theory of the ionic bond. With the advent of x-rays, the hard sphere model was extended by Bragg (1924, 1926) who also developed the concept of ionic radius (Bragg & West, 1927). Subsequently, sets of ionic radii were developed by Goldschmidt (1929) and Pauling (1929); in addition, Pauling extended previous work and produced a set of empirical rules (Pauling, 1960) to predict stable configurations in complex ionic crystals and to rationalize observed distortions in terms of ion-ion interactions. These rules have been tested extensively in minerals and synthetic inorganic oxides, and have been found to be quite successful. Of particular interest is Pauling's second rule:

"In a stable ionic structure, the valence of each anion, with the sign changed is equal to the sum of the strengths of the electrostatic bonds to it from the adjacent cations."

where the electrostatic bond strength (s) is defined as the formal valence of the cation divided by its coordination number. This has been interpreted as a condition that tends to minimise the potential energy of the resulting configuration (Louisnathan & Gibbs, 1972a). Although this is formally correct, the resulting equation given by Louisnathan & Gibbs is rather misleading. Bragg (1930) has rationalized this rule in terms of lines of force, and similarly the discussions of Zachariasen (1930) and Brown & Shannon (1973) indicate that electrostatic bond strengths are an analogue of crystal forces rather than crystal energies.

Deviations of up to 40% from Pauling's second rule are encountered in mineral structures (Baur, 1970) and many investigators have noted that these deviations are accompanied by antipathetic variations in cation-anion distances (Zachariasen, 1954, 1963; Evans, 1960 Baur, 1961, 1970, 1971). Several schemes that relate bond lengths to bond strengths have recently been developed. The first comprehensive treatment was due to Baur (1961, 1970, 1971); this relates bond length (R) to the sum of the average bond strengths (P) around an anion using a linear relationship of the form

$$R = a + bP$$

where a and b are empirical constants derived from a least-squares procedure using data from a large number of structures. Although this model has had considerable success, it contains several approximations that are of questionable validity. Primarily, it assumes a linear relation between bond length and bond strength; inspection of the commonly used forms of interatomic potentials (Tosi, 1964) indicates that this is incorrect. In addition, in the derivation of the empirical relations, no allowance is made for the different types of isovalent cations coordinated to the anion of the bond being considered, or of its relative bond length. Thus, in the deviation of a and b for a particular cation, the effects of all other cations in the structures are averaged and this will give rise to discrepancies in the scheme. This is highlighted by structures which obey Pauling's second rule exactly; according to this scheme, there should be no variations in bond length within a coordination polyhedron, a feature that is certainly not observed in structures of this type.

Another relationship has been derived by Donnay (Donnay, 1970; Donnay & Allman, 1970; Donnay & Donnay, 1972) who postulated a relationship between bond strength (s) and bond length (R) of the form

$$s = s_o \left(\frac{\bar{R}}{R}\right)^n \qquad R < \bar{R}$$

$$s = s_o\left(\frac{R_{max}-R}{R_{max}-\bar{R}}\right)^n \qquad R_{max} > R > \bar{R}$$

$$n = \frac{\bar{R}}{R_{max}-\bar{R}}$$

where s_o = ideal Pauling bond strength

R_{max} = maximum possible bond length calculated from the ionic radii tables of Shannon and Prewitt (1969, 1970).

The calculation of R_{max} in this procedure is not satisfactory as in some structures (especially the amphiboles, Bauer, 1971; Hawthorne & Grundy, 1972b) some very peculiar coordination schemes result which are not compatible with the argument of Bragg (1930) or the normal concept of coordination. In addition, the scheme relates to differences in two measured quantities $\bar{R}$ and R, and errors in bond lengths need not necessarily be apparent with this scheme. For example, Table 4.6a is a bond strength table calculated for α-quartz using the values:

$$\bar{R} = 1.609, \quad R_1 = 1.603 \text{ and } R_2 = 1.616\text{Å}$$

from Zachariasen and Plettinger (1965). The atom notation used is that of Smith and Alexander (1963).

TABLE 4.6a: BOND STRENGTH TABLE FOR α-QUARTZ USING THE METHOD OF DONNAY & ALLMAN (1970).

Bond lengths were taken from Zachariasen and Plettinger (1965).

	Si	Si'	Σ	Δ
O	1.012x2 ↓	0.987x2 ↓	1.999	0.001
O'	0.987x2 ↓	1.012x2 ↓	1.999	0.001
Σ	3.998	3.998		
Δ	0.002	0.002		

TABLE 4.6b:

As for Table 4.15a but using bond lengths in text.

	Si	Si'	Σ	Δ
O	1.006x2 ↓	0.993x2 ↓	1.999	0.001
O'	0.993x2 ↓	1.006x2 ↓	1.999	0.001
Σ	3.998	3.998		
Δ	0.002	0.002		

A satisfactory result is still obtained (Table 4.6b) if 0.5A is subtracted from the above values and the following ones are used:

$$\bar{R} = 1.109,\ R_1 = 1.103 \text{ and } R_2 = 1.116\text{Å}$$

Because of this, the scheme must be considered as inferior to those of Baur and Brown & Shannon (1973), although it is adequate to fulfil its original purpose of distinguishing between O^{2-}, OH and H_2O in crystal structures.

A third method has been derived by Brown and Shannon (1973) which relates bond strength to bond length using curves of the form

$$s = s_o\left(\frac{R}{R_o}\right)^{-N}$$

where s_o is the ideal Pauling bond strength and R_o and N are parameters derived from least-squares fitting to a large number of refined structures. This curve is similar in form to the previous one but only contains one measured quantity and hence is not subject to the same inadequacy. A curve of this form has some theoretical justification as it can be derived from the first derivative of a Born-Landé or Born-Mayer type two-body potential. The correspondence between the Born exponent as calculated by this method and as derived from elasticity measurements (Anderson,

1970) is perhaps the most impressive feature of this treatment. In addition, the relation between bond strength and covalence (Brown & Shannon, 1973, figure V-2-2) indicates a parallelism between the "ionic" (bond strength) and "covalent" (bond order) models that is gradually becoming apparent (Pant & Cruickshank, 1967; Bent, 1968). Perhaps the one drawback to the scheme is that it only considers nearest-neighbour interactions. Cohesive energy calculations using a Born-Mayer type potential (Benson & Dempsey, 1961; Reitz, Seitz & Genberg, 1961; Wackman, Hirthe & Frounfeller, 1967) have indicated that the nearest neighbour approximation is not sufficient for a good energetic description.

That the method is not quite adequate in this respect is shown by the garnet structures in which all the ions are formally charge-balanced and the SiO_4 tetrahedron has S_4 symmetry. The bond strength scheme indicates that all garnet structures should have an Si-O distance of 1.625 Å (uncorrected for anion coordination) or 1.630 Å (corrected for anion coordination) whereas the observed distances vary between 1.628 and 1.645 Å (Novak & Gibbs, 1971). However, attempts to incorporate anion-anion interactions into the Brown-Shannon scheme have, as yet, been unsuccessful (L.D. Brown, pers. communication).

In addition to the concept of bond strength, the ionic model has given rise to the concept of ionic radius which has proved extremely useful in rationalizing structural stability and distortion (Shannon & Prewitt,

1970; Prewitt & Shannon, 1969; Brown, 1970; Novak & Gibbs, 1971). Modern compilations of ionic radii (Shannon & Prewitt, 1969, 1970; Whittaker & Muntus, 1968) which list radii as a function of valence state and coordination number are extremely useful in this respect, and when combined with recent bond strength schemes, provide a powerful tool for the examination of structural detail.

The tetrahedral double-chain of the clino-amphibole structure is of particular interest as it exhibits a wide range of Si-O bond lengths and angles. Since it has been shown that these are susceptible to analysis using simple MO theory, it is of interest to examine how well the observed stereochemistry conforms to the bond strength models, and to observe any parallelism that might occur between the 'covalent' and 'ionic' models.

Before any systematic analysis of Si-O distances can be made, it is necessary to assign the correct anion coordination numbers for the O(5) and O(6) anions; there has been some uncertainty concerning this in recent literature. In his original description of the structure of grunerite, Finger (1967, 1969a) refers to the M(4) site as six-coordinated on the basis of bond lengths. Subsequently, Donnay and Allman (1970) use their bond strength scheme to 'demonstrate' that the M(4) site in grunerite has a one-sided four-fold coordination with no bonding interaction between M(4) and either of the chain-bridging anions O(5) and O(6). Conversely, Brown

& Gibbs (1969, 1970) and Mitchell, Bloss & Gibbs (1970, 1971) implicitly assume that M(4) is eight-coordinated in all non-aluminous clino-amphiboles, and their treatment of Si-O distances was critized by Baur (1971) because of this. The discussion given by Bragg (1930) would indicate that a one-sided coordination is impossible here. In addition, the supposition of a sharp cut-off in the pairwise interaction of ions is incompatible with all forms of inter-ion potential (Tosi, 1964). Baur's scheme may be used to test a structure for the most likely coordination number; Table 4.7a shows the mean deviations between the observed and calculated bond lengths for the tetrahedral sites in the three cummingtonites considered here, calculated by the methods outlined by Baur (1971) for [4]-, [6]- and [8]-fold coordination of the M(4) site. The results are rather ambiguous; for C-Mn cummingtonite, a [6]- or [8]-fold coordination is indicated, the grunerite results indicate a [4]-fold coordination and the cummingtonite results show no preference. Since this result is not very conclusive, it is worth performing a similar analysis with the bond-strength scheme of Brown and Shannon. Table 4.7b shows the bond strength sums around O(5) and O(6) in the three cummingtonites for different coordination numbers of M(4). In all cases, the deviation from the ideal value of 2 are least for [8]-fold coordination of M(4). However, inspection of the complete bond strength tables for the non-aluminous

TABLE 4.7a: MEAN DEVIATIONS FOR THE TETRAHEDRAL BONDS IN THREE CUMMINGTONITES CALCULATED BY THE METHODS OF BAUR (1971).

For Method 1, the $\langle T\text{-}O \rangle$ bond length is calculated (see text);

For Method 2, the observed $\langle T\text{-}O \rangle$ distance is used.

Mean deviations were calculated for the M(4) coordination numbers (C.N.) of [4], [6] and [8].

METHOD	C.N.	$\langle \sigma T(1) \rangle$ Å		$\langle \sigma T(2) \rangle$ Å		$\langle \sigma T \rangle$ Å	
		1	2	1	2	1	2
	[4]	0.005	0.005	0.015	0.012	0.010	0.009
CUMM	[6]	0.007	0.007	0.012	0.010	0.010	0.009
	[8]	0.009	0.009	0.009	0.010	0.009	0.010
	[4]	0.012	0.007	0.007	0.009	0.010	0.008
GRUN	[6]	0.014	0.013	0.012	0.012	0.013	0.013
	[8]	0.009	0.011	0.018	0.018	0.014	0.015
	[4]	0.007	0.007	0.019	0.017	0.013	0.012
C-Mn	[6]	0.006	0.006	0.005	0.004	0.006	0.005
	[8]	0.004	0.005	0.009	0.009	0.007	0.007

TABLE 4.7b: BOND STRENGTH SUMS AROUND O(5) AND O(6) IN IN THREE CUMMINGTONITES CALCULATED BY THE METHODS OF BROWN & SHANNON (1973)

Calculations were performed for M(4) coordination numbers [4], [6] and [8] using both normal and 'coordination correction' curves

		UNCORRECTED		CORRECTED FOR ANION COORD.	
	C.N.	ΣO(5)	ΣO(6)	ΣO(5)	ΣO(6)
	4	1.980	1.894	1.899	1.855
CUMM	6	1.980	2.020	1.899	2.015
	8	2.030	2.020	1.996	2.015
	4	2.034	1.951	1.932	1.862
GRUN	6	2.034	2.038	1.932	2.004
	8	2.066	2.038	2.021	2.004
	4	1.984	1.899	1.890	1.818
C-Mn	6	1.984	2.033	1.890	1.999
	8	2.033	2.033	1.991	1.999

clino-amphiboles (see Table 4.10) shows that the best anion sums occur around O(5) and O(6); comparison of the deviations for [4]- and [6]-fold coordination of M(4) with other anion deviations (where the nature of the coordination is not in question) shows them to be of the same order. Hence it is questionable whether significance can be attached to this result.

Pertinent to this problem are some E. H. M. O. calculations performed on the M(4) site in grunerite (Cameron, 1970); an electronic population analysis of the results showed positive bond overlap populations between M(4) and both O(5) and O(6), indicating an [8]-fold coordination for M(4). This would tend to support the bond strength results above; however, no firm conclusion can be drawn although the evidence tends to indicate bonding interactions between M(4) and the chain-bridging oxygens O(5) and O(6). In view of this result, the cummingtonites will be considered for all alternatives.

The bond length prediction formalism of Baur may be used in three ways, two of which will be used here. The regression equation presented by Baur (1971) may be used to predic t bond leng ths absolutely from a forecast mean, or they may be used in conjunction with the observed mean bond lengths to predict deviations from that mean. Bond lengths calculated by both methods are presented in Table 4.8 together with the observed values, and a graphical comparison of the observed and

TABLE 4.8: COMPARISON OF OBSERVED AND CALCULATED T-O DISTANCES IN Si-AMPHIBOLES BY THE METHODS OF BAUR (1971)

CALC 1 was performed using $\langle T\text{-}O \rangle$ distances calculated from the equation $\langle T\text{-}O \rangle = 1.584 + 0.0127 \langle C.N. \rangle$.
CALC 2 was performed using the observed $\langle T\text{-}O \rangle$ distances.

		TREM	FLOR	SR1	SR2	GLAUC	CUMM	GRUN	C-Mn	$\bar{\Delta}$
	OBS	1.602(2)	1.614(3)	1.582(6)	1.594(6)	1.618(6)	1.619	1.637(4)	1.610(3)	
T(1)-O(1)	CALC 1	1.611	1.611	1.617	1.617	1.616	1.611	1.611	1.611	.013
	CALC 2	1.609	1.611	1.608	1.608	1.610	1.608	1.616	1.609	.011
	OBS	1.632(2)	1.628(3)	1.625(6)	1.636(7)	1.616(7)	1.614	1.627(5)	1.622(4)	
T(1)-O(5)	CALC 1	1.633	1.633	1.639	1.639	1.628	1.633	1.633	1.633	.009
	CALC 2	1.631	1.633	1.630	1.630	1.622	1.630	1.638	1.631	.007
	OBS	1.629(2)	1.630(4)	1.641(7)	1.624(7)	1.621(6)	1.628	1.630(4)	1.633(3)	
T(1)-O(6)	CALC 1	1.633	1.633	1.639	1.639	1.628	1.633	1.633	1.633	.005
	CALC 2	1.631	1.633	1.630	1.630	1.622	1.630	1.638	1.631	.004
	OBS	1.616(1)	1.616(2)	1.636(3)	1.631(4)	1.611(3)	1.613	1.613(2)	1.616(2)	
T(1)-O(7)	CALC 1	1.611	1.611	1.626	1.626	1.616	1.611	1.611	1.611	.005
	CALC 2	1.609	1.611	1.608	1.608	1.610	1.608	1.616	1.609	.010
	OBS	1.620	1.622	1.621	1.621	1.616	1.619	1.627	1.620	
$\langle T(1)\text{-}O \rangle$	CALC 1	1.622	1.622	1.630	1.630	1.622	1.622	1.622	1.622	.005
	CALC 2	1.620	1.622	1.621	1.621	1.616	1.619	1.627	1.620	-

TABLE 4.8: continued

		TREM	FLOR	SR1	SR2	GLAUC	CUMM	GRUN	C-Mn	$\bar{\Delta}$
	OBS	1.616(2)	1.623(3)	1.625(6)	1.626(7)	1.618(6)	1.625	1.633(4)	1.618(3)	
T(2)-O(2)	CALC 1	1.623	1.623	1.630	1.630	1.618	1.623	1.623	1.623	.004
	CALC 2	1.630	1.627	1.636	1.633	1.620	1.627	1.620	1.623	.007
	OBS	1.586(2)	1.587(3)	1.578(5)	1.572(7)	1.594(6)	1.609	1.604(4)	1.594(3)	
T(2)-O(4)	CALC 1	1.585	1.585	1.586	1.586	1.582	1.585	1.585	1.585	.011
	CALC 2	1.592	1.589	1.592	1.589	1.583	1.589	1.582	1.585	.013
	OBS	1.653(2)	1.648(4)	1.658(7)	1.660(8)	1.637(7)	1.639	1.611(5)	1.634(3)	
T(2)-O(5)	CALC 1	1.646	1.646	1.652	1.652	1.643	1.646	1.646	1.646	.010
	CALC 2	1.653	1.650	1.658	1.655	1.644	1.650	1.643	1.646	.009
	OBS	1.672(2)	1.659(3)	1.681(6)	1.674(7)	1.654(7)	1.643	1.638(5)	1.655(4)	
T(2)-O(6)	CALC 1	1.646	1.646	1.652	1.652	1.643	1.646	1.646	1.646	.015
	CALC 2	1.653	1.650	1.658	1.655	1.644	1.650	1.643	1.646	.013
	OBS	1.632	1.629	1.636	1.633	1.626	1.629	1.622	1.625	
$\langle$T(2)-O$\rangle$	CALC 1	1.625	1.625	1.630	1.630	1.625	1.625	1.625	1.625	.00
	CALC 2	1.632	1.629	1.636	1.633	1.626	1.629	1.622	1.625	-
	$\langle\Delta\rangle_1$	0.008	0.004	0.014	0.012	0.007	0.009	0.014	0.007	
	$\langle\Delta\rangle_2$	0.007	0.004	0.015	0.012	0.006	0.009	0.014	0.007	

Figure 4.19 Comparison of the observed and calculated T-O distances in the Si clino-amphiboles.

Calculations were preformed using the second method of Baur (1971)

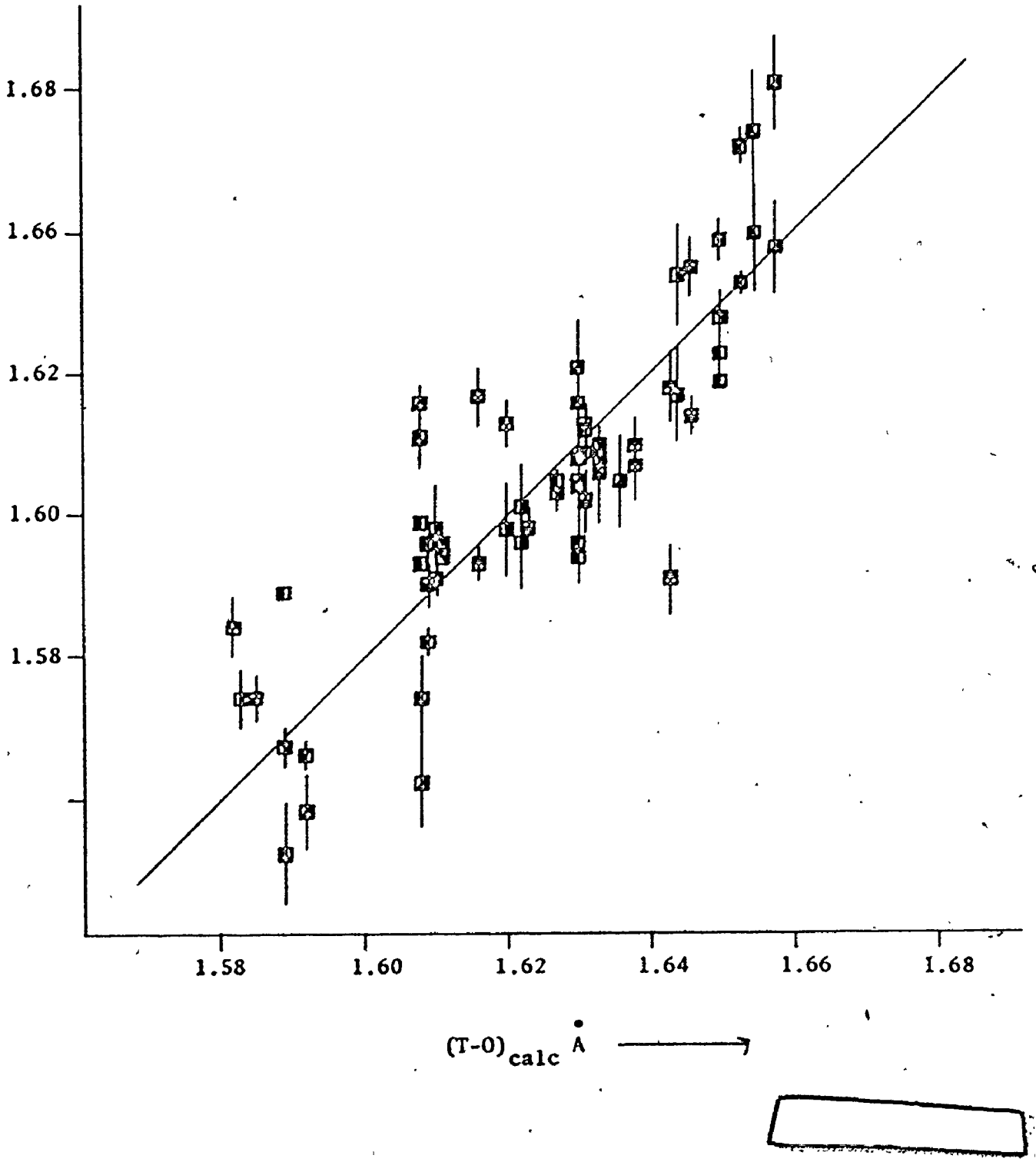

calculated values is given in figure 4.19. The mean bond lengths for method 1 were calculated from the equation

$$T\text{-}O = 1.584 + 0.0127 \langle C.N. \rangle$$

which is derived in Appendix 5. The agreement with the calculated values is much the same for each method with a grand mean deviation of 0.01 Å. The results for the cummingtonites may be improved by considering different coordination numbers for M(4). Table 4.9 shows similar calculations for these species calculated for M(4) coordinations of [4] and [6] respectively. Because of the problem of assigning coordination numbers to M(4) in this species, the absolute significance of the results is uncertain; however, they do illustrate a major drawback to Baur's scheme rather well. Consider the results for T(1)-O(6) and T(2)-O(6); for a [4]-fold M(4) coordination, the P_o value for O(6) is 2.00 and all T(1)-O(6) and T(2)-O(6) distances calculate too low; for a [6]-fold M(4) coordination, the P_o value for O(6) is 2.33 and all T(1)-O(6) and T(2)-O(6) distances calculate too high. A similar consideration of T(1)-O(5) and T(1)-O(6) distances for M(4) coordinations of [6] and [8] shows the same feature. This indicates that the P_o values are actually intermediate between 2.00 and 2.33, and that the scheme cannot allow for weak bonding interactions. Another illustration of this is seen in Table 4.8; when M(4) is [8]-coordinated, the scheme predicts that

TABLE 4.9: BOND LENGTH CALCULATIONS FOR THREE CUMMINGTONITES USING THE METHOD OF BAUR (1971)

Calculations performed for the M(4) coordination numbers [4] and [6] with methods 1 and 2 (see Table 4.7a)

		[4]-COORD			[6]-COORD		
		CUMM	GRUN	C-Mn	CUMM	GRUN	C-Mn
	OBS	1.619	1.637(4)	1.610(3)	1.619	1.637(4)	1.610(3
T(1)-O(1)	CALC 1	1.616	1.616	1.616	1.611	1.611	1.611
	CALC 2	1.619	1.627	1.620	1.611	1.619	1.612
	OBS	1.614	1.627(5)	1.622(4)	1.614	1.627(5)	1.622(4
T(1)-O(5)	CALC 1	1.616	1.616	1.616	1.611	1.611	1.611
	CALC 2	1.619	1.627	1.620	1.611	1.619	1.612
	OBS	1.628	1.630(4)	1.633(3)	1.628	1.630(4)	1.633(3
T(1)-O(6)	CALC 1	1.616	1.616	1.616	1.641	1.641	1.641
	CALC 2	1.619	1.627	1.620	1.641	1.649	1.642
	OBS	1.613	1.613(2)	1.616(2)	1.613	1.613(2)	1.616(2
T(1)-O(7)	CALC 1	1.616	1.616	1.616	1.611	1.611	1.611
	CALC 2	1.619	1.627	1.620	1.611	1.619	1.612
	$\bar{\Delta}$1	0.005	0.012	0.007	0.007	0.014	0.006
	$\bar{\Delta}$2	0.005	0.007	0.007	0.007	0.013	0.006
	OBS	1.625	1.633(4)	1.618(3)	1.625	1.633(4)	1.618(3
T(2)-O(2)	CALC 1	1.634	1.634	1.634	1.622	1.622	1.622
	CALC 2	1.644	1.637	1.640	1.629	1.622	1.625
	OBS	1.609	1.604(4)	1.595(3)	1.609	1.604(4)	1.595(3
T(2)-O(4)	CALC 1	1.604	1.604	1.604	1.592	1.592	1.592
	CALC 2	1.614	1.607	1.610	1.599	1.592	1.595
	OBS	1.639	1.611(5)	1.634(3)	1.639	1.611(5)	1.634(3
T(2)-O(5)	CALC 1	1.619	1.619	1.619	1.622	1.622	1.622
	CALC 2	1.629	1.622	1.625	1.629	1.622	1.625
	OBS	1.643	1.638(5)	1.655(4)	1.643	1.638(5)	1.655(4
T(2)-O(6)	CALC 1	1.619	1.619	1.619	1.653	1.653	1.653
	CALC 2	1.629	1.622	1.625	1.660	1.653	1.656
	$\bar{\Delta}$1	0.015	0.007	0.019	0.012	0.012	0.005
	$\bar{\Delta}$2	0.012	0.009	0.017	0.010	0.012	0.004

$$T(1)\text{-}O(5) = T(1)\text{-}O(6)$$

$$T(2)\text{-}O(5) = T(2)\text{-}O(6)$$

Deviations of up to ten standard deviations in the bond lengths occur in structures where the M(4) coordination is definitely eight (e.g. Tremolite); these occur because the M(4)-O(6) interaction is much stronger than the M(4)-O(5) interaction, and yet no allowance can be made for this. Baur's scheme is expected to work well for structures where the anion polyhedra are fairly regular, and has had spectacular success when these conditons are fulfilled (Baur, 1972). Some of the polyhedra in the amphiboles are highly irregular and failure of this scheme to accurately predict individual bond lengths is not surprising under these circumstances. A theoretical discussion of this point is given by Gopal (1972) and although one of his basic premises is incorrect, the reasoning is unaffected and bears out this particular feature. The overall discrepancy of 0.01 Å between observed and calculated T-O distances indicates that the amphiboles obey an extended electrostatic bond theory quite well and the major discrepancies appear to be related to deficiencies in the particular model used for bond length prediction rather than in the principles of the general model.

Accordingly, it appears that the bond lengths in the double chain element should be more amenable to analysis using the Brown-

Shannon formalism, since the strength of interaction (bond strength) is a function of interatomic distance and weak bonding interactions are recognised. Table 4.10 shows the results of a complete bond strength analysis on all eight clino-amphiboles considered here, both with and without coordination corrections; bond strength parameters for the fluorine anion were supplied by Brown and Wu (pers. communication). Deviations from the ideal anion sums are considerable; mean deviations for each method are given in Table 4.10 and are also expressed as equivalent distances (per bond) for each of the cations in the structure, using the relation

$$\Delta R = -\Delta s \, . \, R_o / S_o . N$$

which may be derived from the bond strength equation.

The much greater errors associated with the lower valence cations reflect the much greater sensitivity of their bond lengths to bond strength values. Certain systematics are apparent in the distribution of deviations from ideality; in general, deviations are positive for the anion sums (with the exception of O(4)) indicating that R_o does not give a good representation of the bond length means in these structures, even when coordination corrections are performed. In addition, the sum of the deviations around the cations is always far greater than the sum of

TABLE 4.10 BOND STRENGTH TABLES FOR THE SI-CHAIN O AMPHIBOLES

HYDROXYTREMOLITE

	M(1)	M(2)	M(3)	M(4)	A	T(1)	T(2)	Σ
O(1)	.361	.307	.356 ×2 ↓			1.066		2.090
	.370	.311	.365 ×2 ↓			1.087		2.133
O(2)	.349	.345		.296			1.025	2.015
	.357	.353		.292			1.019	2.051
O(3)	.345 ×2 →		.368					1.058
	.336 ×2 →		.358					1.030
O(4)		.408		.359			1.116	1.883
		.400		.332			1.076	1.808
O(5)				.125		.981	.926	2.032
				.126		.959	.911	1.996
O(6)				.209		.989	.880	2.078
				.202		.966	.870	2.038
O(7)						1.025 ×2 →		2.050
						.973 ×2 →		1.946
Σ	2.110	2.120	2.160	1.978		4.061	3.947	
	2.126	2.128	2.176	1.904		3.985	3.906	

Without c.c. ⟨Δ⟩ = .063 ∓ ⟨Δ1⟩ = .007 Si ∓ .025 Mg ∓ .033 Ca
With c.c. ⟨Δ⟩ = .072 ∓ ⟨Δ1⟩ = .009 Si ∓ .027 Mg ∓ .041 Ca

FLUOR-TREMOLITE

	M(1)	M(2)	M(3)	M(4)	A	T(1)	T(2)	Σ
O(1)	366	.297	.369			1.031		2.063
	375	.302	.379			1.054		2.110
O(2)	.370	.350		.296			1.025	2.041
	.380	.358		.291			1.030	2.059
O(3)	.282 ×2 →		.311					.875
O(4)		.398		.374			1.116	1.888
		.390		.345			1.073	1.808
O(5)				.129		.992	.916	2.037
				.130		.968	.922	2.020
O(6)				.224		.986	.859	2.069
				.215		.963	.897	2.075
O(7)						1.025		2.050
						.973		1.946
Σ	2.036	2.090	2.098	2.046		4.034	3.916	
	-	2.100	-	1.962		3.958	3.922	

Without c.c. ⟨Δ⟩ = .071 ∓ ⟨Δ1⟩ = .008 Si ∓ .028 Mg ∓ .037 Ca
With c.c. ⟨Δ⟩ = .091 ∓ ⟨Δ1⟩ = .012 Si ∓ .035 Mg ∓ .051 Ca

SYN. RICHTERITE 1

	M(1)	M(2)	M(3)	M(4)	A	T(1)	T(2)	Σ
O(1)	.365	.271	.355 ×2 ↓			1.128		2.119
	.376	.274	.346 ×2 ↓			1.144		2.138
O(2)	.392	.366		.238			1.000	1.996
	.403	.375		.237			1.025	2.040
O(3)	0.256 ×2 →		0.300					.852
O(4)		.412		.282			1.141	1.835
		.403		.266			1.098	1.767
O(5)				.089	.039	1.000	.914	2.076
				.088	.034	1.025	945	2.124
					.035			
					.031			
O(6)				.157	.042	.957	859	2.029
				.152	.014	.998	.893	2.093
					.039			
					.011			
O(7)					.075			
					.052			
					.015	.970 ×2 →		2.082
					.079	.949 ×2 →		2.057
					.048			
					.012			
Σ	2.066	2.098	2.02	1.532	.270	4.055	3.914	
	-	2.104	-	1.486	.255	4.116	3.961	

Without c.c. ⟨Δ⟩ = .089 ∓ ⟨Δ1⟩ = .011 Si ∓ .033 Mg ∓ .046 Ca
With c.c. ⟨Δ⟩ = .111 ∓ ⟨Δ1⟩ = .015 Si ∓ .051 Mg ∓ .062 Ca

SYN. RICHTERITE 2

	M(1)	M(2)	M(3)	M(4)	A	T(1)	T(2)	Σ
O(1)	.361	.273	.367			1.093		2.092
	.366	.277	.373			1.109		2.125
O(2)	.401	.375		.237			0.997	2.010
	.407	.377		.236			1.023	2.043
O(3)	F		F					F .
O(4)		.454		.274			1.161	1.889
		.431		.259			1.115	1.805
O(5)				.086	.042	.970	909	2.041
				.089	.034	998	.940	2.093
					.037			
					.029			
O(6)				.169	.038	1.003	.875	2.099
				.157	.014	1.028	.908	2.135
					.032			
					.010			
O(7)					.068			
					.055			
					.014	.984 ×2 →		2.105
					.060	.961 ×2 →		2.041
					.049			
					.010			
Σ	-	2.204	-	1.532	.265	4.048	3.942	
	-	2.170	-	1.482	.227	4.096	3.986	

Without c.c. ⟨Δ⟩ = .076 ∓ ⟨Δ1⟩ = .010 Si ∓ .030 Mg ∓ .045 Ca
With c.c. ⟨Δ⟩ = .105 ∓ ⟨Δ1⟩ = .014 Si ∓ .047 Mg ∓ .055 Ca

TABLE 4.10: continued

CUMMINGTONITE

	M(1)	M(2)	M(3)	M(4)	A	T(1)	T(2)	Σ
O(1)	.371	.308	.341 ×2			1.017		2.037
	.378	.313	.345 ×2			1.041		2.078
O(2)	.318	.348		.364			1.000	2.030
	.322	.355		.361			1.025	2.063
O(3)	.347 ×2↓		.363					1.057
	.336 ×2↓		.354					1.026
O(4)		.393		.531			1.045	1.969
		.384		.484			1.015	1.883
O(5)				.045		1.031	.962	2.038
				.052		1.002	.942	1.996
O(6)				.107		.992	.952	2.051
				.114		.968	.933	2.015
O(7)						1.034 ×2↓		2.068
						1.005 ×2↓		2.010
Σ	2.072	2.098	2.090	2.094		4.074	3.959	
	2.072	2.104	2.092	2.036		4.016	4.010	

Without c.c. ⟨Δ⟩ = .045 ∓ ⟨Δ1⟩ = .005 Si ∓ .018 Mg ∓ .017 Fe

With c.c. ⟨Δ⟩ = .045 ∓ ⟨Δ1⟩ = .006 Si ∓ .017 Mg ∓ .019 Fe

GLAUCOPHANE

	M(1)	M(2)	M(3)	M(4)	A	T(1)	T(2)	Σ
O(1)	.359	.370	.344 ×2			1.020		2.093
	.364	.385	.348 ×2			1.044		2.141
O(2)	.355	.471		.183			1.020	2.029
	.361	.482		185			1.044	2.072
O(3)	.340 ×2↓		.367					1.047
	.328 ×2↓		.353					1.009
O(4)		.604		.218			1.091	1.913
		.580		.210			1.054	1.844
O(5)				.080		1.025	.967	2.072
				.075		.998	.947	2.020
O(6)				.169		1.011	.923	2.103
				.162		.985	.908	2.055
O(7)						1.040 ×2↓		2.080
						1.010 ×2↓		2.020
Σ	2.108	2.890	2.110	1.300		4.096	4.001	
	2.106	2.894	2.098	1.286		4.037	3.953	

Without c.c. ⟨Δ⟩ = .073 ∓ ⟨Δ1⟩ = .009 Si ∓ .029 Mg ∓ .027 Fe^{2+} ∓ .018 Al ∓ .061Na

With c.c. ⟨Δ⟩ = .068 ∓ ⟨Δ1⟩ = .009 Si ∓ .026 Mg ∓ .028 Fe^{2+} ∓ .018 Al^{VI} ∓ .055Na

GRUNERITE

	M(1)	M(2)	M(3)	M(4)	A	T(1)	T(2)	Σ
O(1)	.394	.319	.361 ×2			.967		2.041
	.391	.322	.361 ×2			.995		2.069
O(2)	.323	.346		.358			.978	2.005
	.325	.348		.357			1.005	2.035
O(3)	.355 ×2↓		.375					1.085
	.339 ×2↓		.356					1.034
O(4)		.397		.531			1.060	1.988
		.376		.486			1.028	1.890
O(5)				.032		.994	1.040	2.066
				.040		.971	1.010	2.021
O(6)				.087		.986	.965	2.038
				.096		.963	.945	2.004
O(7)						1.034 ×2↓		2.068
						1.005 ×2↓		2.010
Σ	2.144	2.124	2.194	2.016		3.981	4.043	
	2.110	2.092	2.156	1.958		3.934	3.988	

Without c.c. ⟨Δ⟩ = .045 ∓ ⟨Δ1⟩ = .005 Si ∓ .018 Mg ∓ .017 Fe

With c.c. ⟨Δ⟩ = .040 ∓ ⟨Δ1⟩ = .005 Si ∓ .015 Mg ∓ .017 Fe

C-Mn CUMMINGTONITE

	M(1)	M(2)	M(3)	M(4)	A	T(1)	T(2)	Σ
O(1)	.375	.303	.349 ×2			1.043		2.070
	.382	.307	.356 ×2			1.065		2.110
O(2)	.329	.346		.330			1.020	2.025
	.334	.352		.334			1.044	2.064
O(3)	.356 ×2↓		.372					1.084
	.344 ×2↓		.361					1.049
O(4)		.410		.421			1.091	1.922
		.397		.401			1.054	1.852
O(5)				.050		1.008	.978	2.033
				.054		.983	.954	1.991
O(6)				.134		.978	.921	2.033
				.137		.956	.906	1.999
O(7)						1.025 ×2↓		2.050
						.998 ×2↓		1.996
Σ	2.120	2.118	2.140	1.870		4.054	4.007	
	2.120	2.112	2.146	1.852		4.002	3.958	

Without c.c. ⟨Δ⟩ = .053 ∓ ⟨Δ1⟩ = .006 Si ∓ .021 Mg ∓ .020 Fe ∓ .020 Mn

With c.c. ⟨Δ⟩ = .055 ∓ ⟨Δ1⟩ = .007 Si ∓ .021 Mg ∓ .023 Fe ∓ .022 Mn

the deviations around the anions which indicates (according to Pauling's original theory) that the model is not electrostatically neutral. The difference in sensitivity between high and low valence cations indicates that a small increase in the 'equivalent bond length error' of the former (e.g. Si) would produce a large decrease in the 'equivalent bond length error' of the latter. Thus the overall bond length errors probably fall within the range of 0.01-0.02Å and are comparable with those obtained using the Baur method.

The observed bond length variations in these structures appear to conform reasonably well to a modified electrostatic model. Consequently, it is of interest to examine certain features of the Brown-Shannon scheme that allow analysis of the SiO_4 groups which parallel arguments based on a covalent model. Assuming that the bond strength sums around the cations are equal to their formal valences, the positive second derivative of the bond-length—bond-strength curves indicates that the mean bond length is a function of the amount of bond length distortion. It is shown in Appendix 4 that the correct form of this distortion, δ, is given by

$$\delta = \frac{1}{n} \sum_{i=1}^{n} (R_i - \bar{R})^2$$

Figures 4.20a,b show the variation of $\langle T(1)\text{-}O \rangle$ and $\langle T(2)\text{-}O \rangle$ with δ; in general, T(2) is more distorted and also shows a much greater range of distortion than T(1). The fluor-richterites are the one exception to this, and the large T(1) distortion may be correlated with the presence of an A-site cation that causes an increase in the $\langle T(1)\text{-}O(br) \rangle$ distance and a corresponding decrease in T(1)-O(nbr). $\langle T(2)\text{-}O \rangle$ is fairly linear with δ but very little correlation is shown by the T(1) site; the same result was obtained by covalent distortion criteria. The spread of δ in T(1) is not great and (with the exception of grunerite and synthetic richterite 1) the points scatter about the trend developed by the T(2) site. The deviations from this relationship remain unexplained; possibly grunerite could contain a small amount of Al in the T(1) site although no indication of any Al is given in the chemical analysis (Klein, 1964; Finger, 1967, 1969a).

The relationship between $\langle T\text{-}O(br)\text{-}T \rangle_T$, $\langle T\text{-}O(br) \rangle_T$ and $\langle T\text{-}O \rangle_T$ demonstrated in the previous section combines with the above relationships and suggests that $\langle T\text{-}O(br)\text{-}T \rangle$ might be related to δ, the bond strength distortion parameter. Figures 4.21a,b show this relationship for both tetrahedra; a regular relationship is apparent for T(1) and T(2). This was to be expected for the T(2) site, but not necessarily for the T(1) site since the 'correlating variable' $\langle T(1)\text{-}O \rangle$ did not show

Figure 4.20a $\langle T(1)\text{-}O \rangle$ versus tetrahedral distortion ($\Sigma\delta 1^2$) for the Si clino-amphiboles.

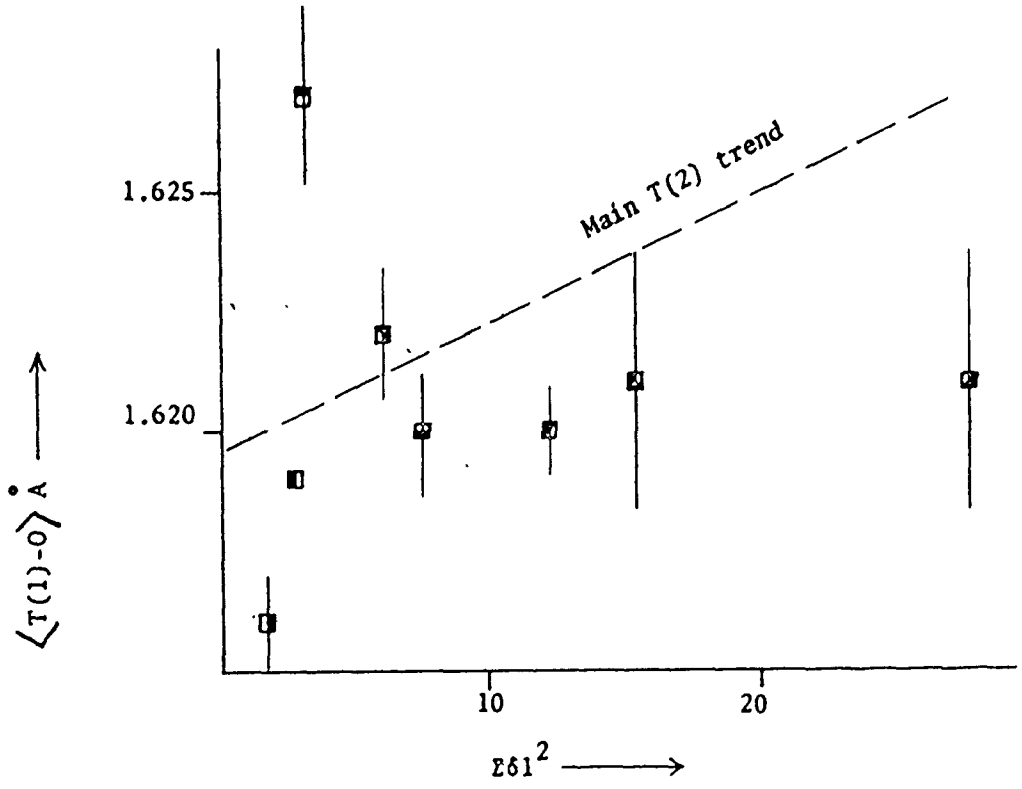

Figure 4.20b $\langle T(2)\text{-}O \rangle$ versus tetrahedral distortion ($\Sigma\delta 1^2$) for the Si clino-amphiboles

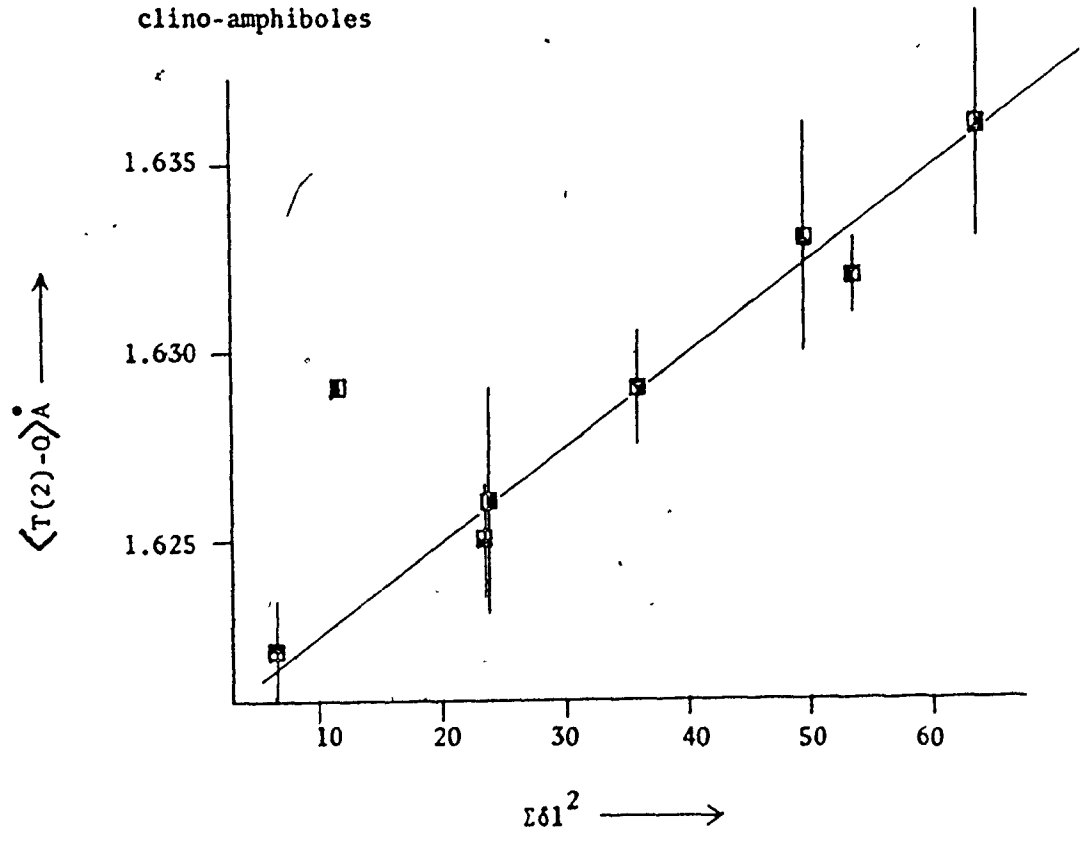

Figure 4.21a $\langle T\text{-}O(br)\text{-}T \rangle_{T(1)}$ versus $\Sigma\delta l^2$ for the Si clino-amphiboles

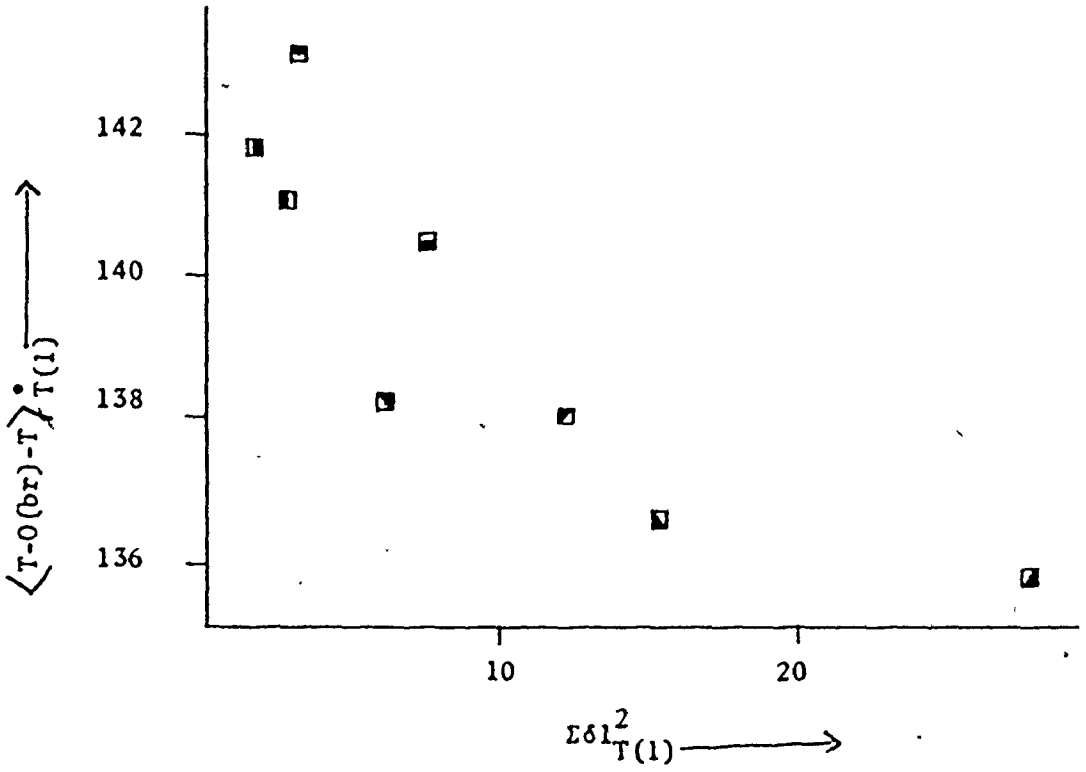

Figure 4.21b $\langle T\text{-}O(br)\text{-}T \rangle_{T(2)}$ versus $\Sigma\delta l^2$ for the Si clino-amphiboles

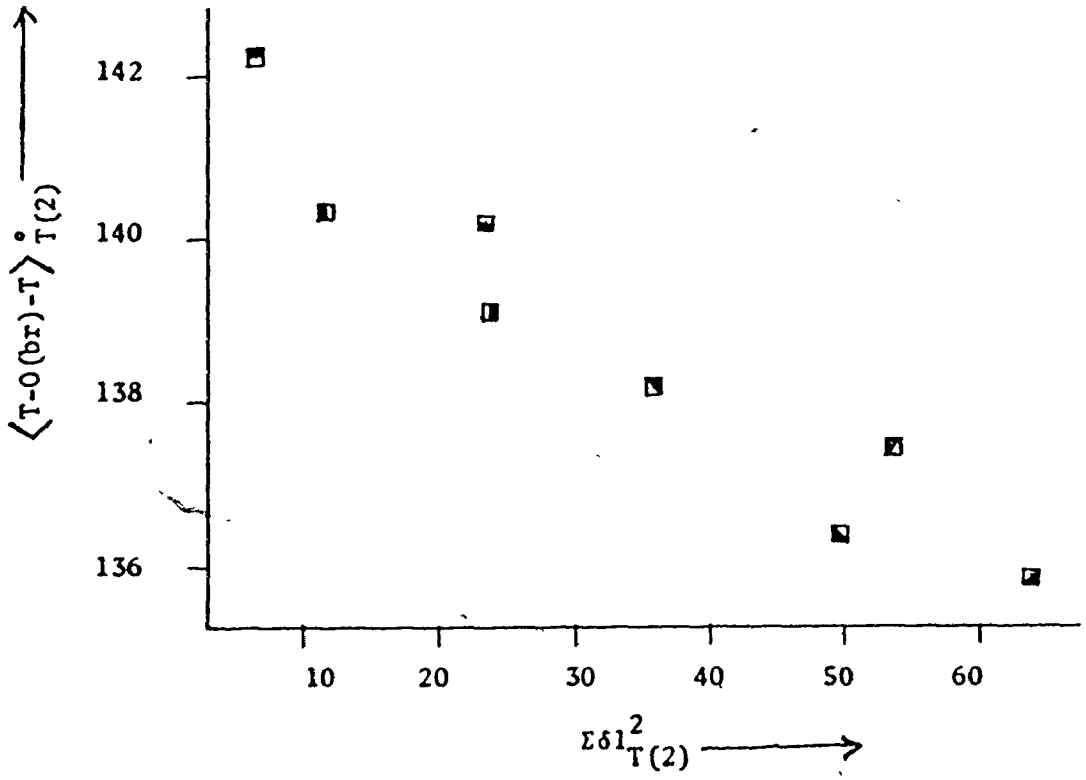

a good correlation in either case. One rather interesting feature is exhibited by both diagrams and that is the gradual decrease in distortion with increasing $\langle$T-O(br)-T$\rangle$. In a statistical study of silicate structures, the grand $\langle$T-O(br)-T$\rangle$ angle was found to be $\sim 140^{\circ}$ (Liebau, 1951) which corresponds approximately to the minimum tetrahedral distortion in both tetrahedral sites in the amphiboles. The ideal T-O(br)-T angle in an ideal double chain of undistorted tetrahedra is 141° corresponding to Liebau's mean value and the minimum tetrahedral distortion. In a previous section dealing with ideal amphibole structures, it was shown that the minimum distortions from ideality ($\langle$T-O(br)-T$\rangle = 141^{\circ}$, tetrahedra of T_d symmetry) would occur for a non-aluminous amphibole with Fe^{2+} octahedra; this accords well with the fact that grunerite is the least distorted with reference to these criteria. This would tend to substantiate the view that interelement linkage plays an important part in controlling the distortions of the major structural elements.

Ionic and Covalent Bonding

Because of ill usage, these terms have tended to become 'dirty words' in mineralogical literature. Thus, proponents of the ionic model have indicated that charges on an ion correspond to their formal valence state, while supporters of the covalent theory argue that these charges are grossly overestimated as can be shown by M.O. calculations.

This rather misses the essential point that these two terms refer to models, not the actual situation that prevails in the solid. Each model is based on a self-consistent set of propositions; there is no basis for criticizing one set of propositions from the standpoint of the other since, as abstractions, they have no common ground. Any comparison of the different models must follow a much more utilitarian path; are the theories useful, can they rationalize the observed facts, and ultimately, can they forecast correctly? If both theories are useful, especially with reference to different facets of chemical behaviour, there is no reason to reject one of them in favour of the other.

The ionic theory was first proposed to reationalize the structural chemistry of inorganic crystals while the M.O. theory was developed to aid in the interpretation of spectral transitions. Later work indicated that they both may be used to 'explain' more detailed stereochemical variation, and it is here that much of the controversy has arisen as to which is the 'correct' bonding theory. Recent work has shown that the ionic model may be extended to homopolar compounds (Bent, 1968) while the covalent model may be extended to very heteropolar compounds (O'Nions & Smith, 1971; Louisnathan & Gibbs, op. cit.). That both models may be used to rationalize the same features does not invalidate either of them; indeed, in this context they may not be mutually incompatible (Pant, 1968). In a recent paper, Brown and Shannon (1973) show

that mean bond strength is related to covalence as calculated by the method of Pauling (op. cit.) and suggest that this relationship may extend to individual bonds. With reference to this suggestion, figure 4.22 shows the variation in E.H.M.O. bond overlap population (Cameron, 1970) with bond strength for hydroxy- and fluor-tremolite. The correlation is quite marked and tends to substantiate their prediction.

Thus the parallel nature of both ionic and covalent models is quite marked and it appears that either is adequate to rationalize observed structural detail. However, neither model may be discarded; the ionic theory cannot serve as a basis for spectral interpretation nor can the covalent theory be used to construct feasible structural models to aid the solution of crystal structures.

ALUMINIUM AND THE TETRAHEDRAL SITES

The Al content of the tetrahedral sites in clinoamphiboles varies between 0.0 and 2.73 atoms per formula unit. This will be distributed over the two crystallographically distinct tetrahedra in the double chain element. Because the scattering factors of Al and Si are very similar, least-squares refinement of site-populations depends on the relative differences in fall-off of scattering power with $\sin\theta/\lambda$. Because the relevant normal equations of the design matrix are sub-

Figure 4.22 E.H.M.O. bond overlap population versus bond strength for the Si-O bonds in hydroxy - and fluor-tremolite.

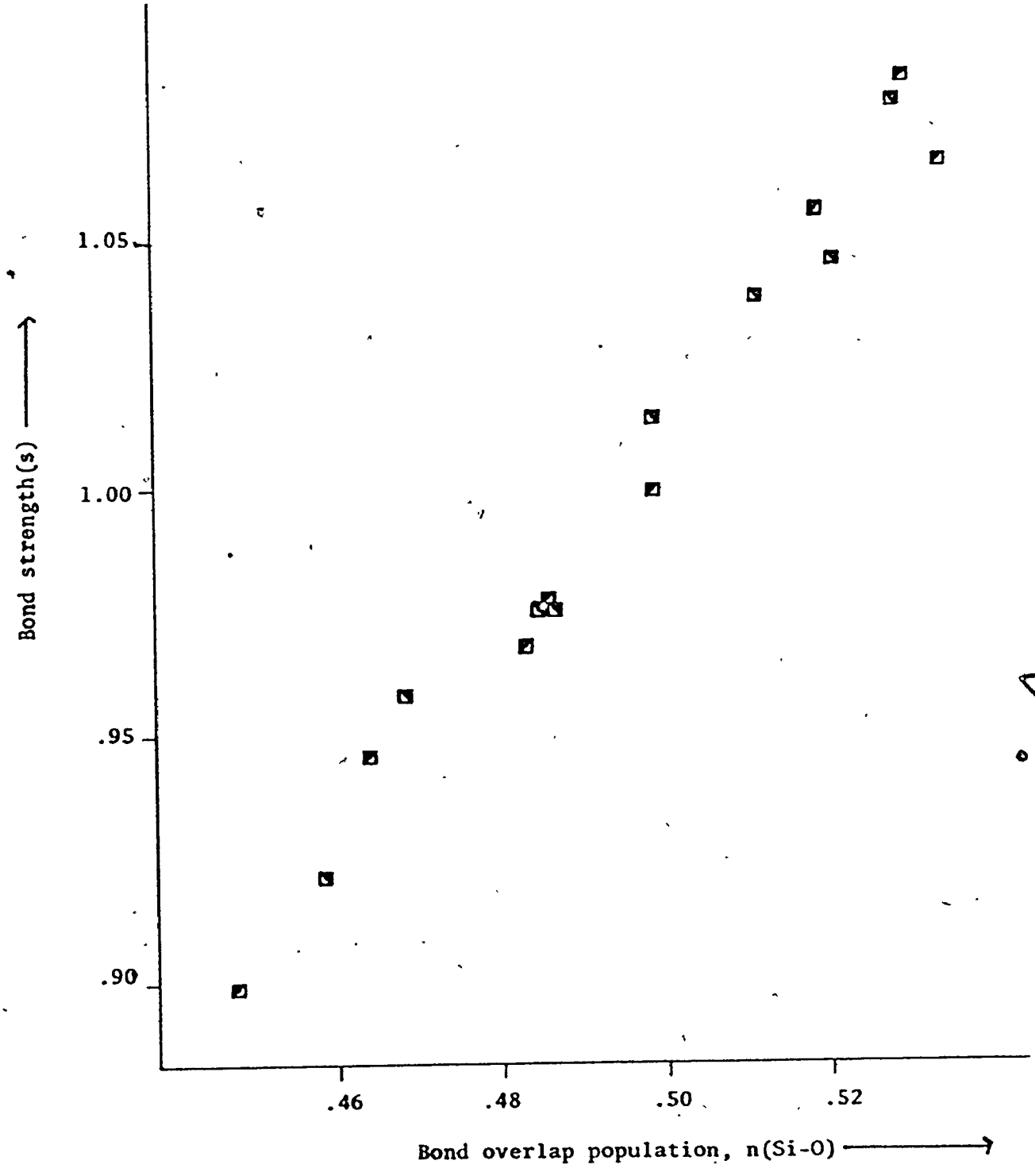

parallel (see Chapter III), correlation in this procedure is extreme and thus the resulting site-populations have an extremely large error. Since the tetrahedral Al site-populations are of considerable interest both from a charge-balance and an inter-element linkage viewpoint, it would be of interest to confirm the refined site-populations and to assign site-populations for those structures where they were not refined. Table 4.11a lists the structures from which the data was taken for this section.

Three methods for assigning tetrahedral Al site-occupancies were described by Papike, et al. (1969) and application to the structure of ferrotschermakite (Hawthorne & Grundy, 1973) indicated that their method 2 was superior to the others. Curves have also been derived by Robinson (1971) relating $\langle T(1)\text{-}O \rangle$ and $\langle T(2)\text{-}O \rangle$ to Al site-occupancy using refined Al occupancies; however, several pyroxenes were included for the T(2) site regression as the spread of $Al_{T(2)}$ values was so low in the small set of data available at that time. The structures of Al-hastingsite and oxykaersutite refined in this study considerably extend the range of Al occupancies and warrant a new treatment.

Figure 4.23a shows the variation in $\langle T\text{-}O \rangle$ with total tetrahedral Al; with the exception of Kakanui hornblende, the trend is perfectly linear. A simple linear regression analysis was performed and the results

TABLE 4.11a: DATA FROM THE FOLLOWING STRUCTURES ARE USED IN THE DISCUSSION OF THE (Si, Al) TETRAHEDRA

1.	Tremolite	Papike, Ross & Clark (1969)
2.	Actinolite	Mitchell (1970), Mitchell, Bloss & Gibbs (1971)
3.	Pargasite	Robinson (1971)
4.	Tri-Pargasite	Robinson (1971)
5.	Ferrotschermakite	Hawthorne & Grundy (1973), this study
6.	Ferrohastingsite	This study
7.	Oxy-kaersutite	Hawthorne & Grundy (in press), this study
8.	Alumino-hastingsite	This study
9.	X-ray Tremolite	This study
10.	Neutron Tremolite	This study

Figure 4.23a $\langle T\text{-}O \rangle$ versus total tetrahedral Al for the clino-amphiboles of Table 4.11a

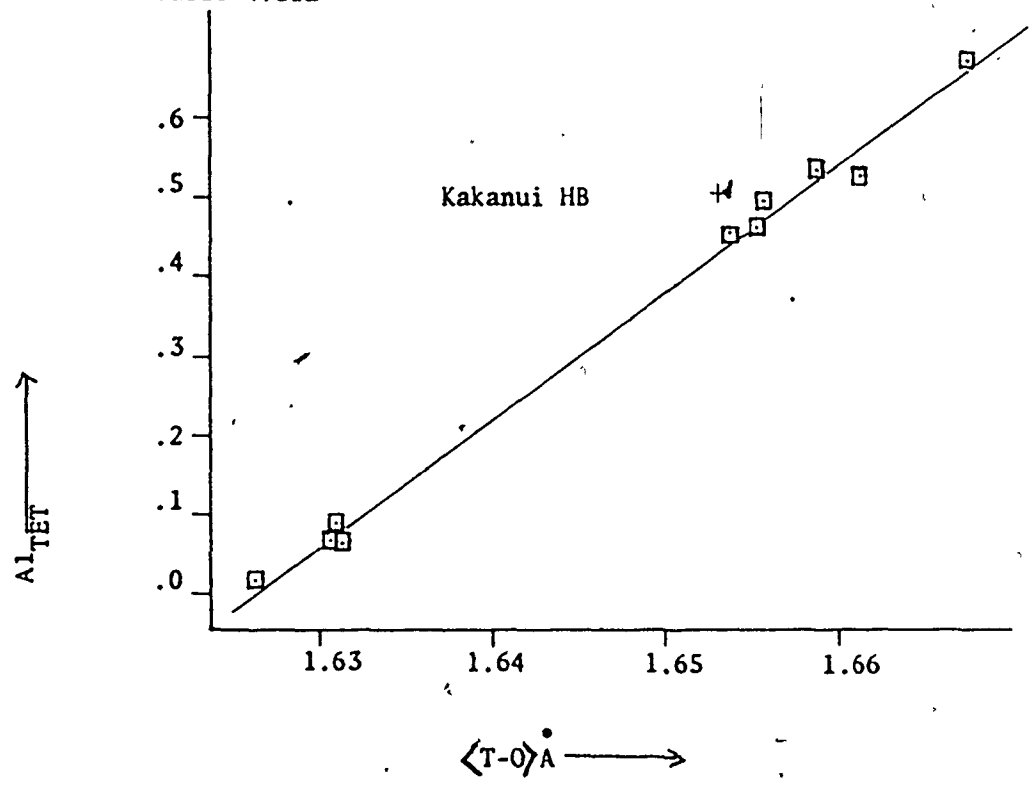

Table 4.23b Mean tetrahedral edge length versus tetrahedral Al occupancy

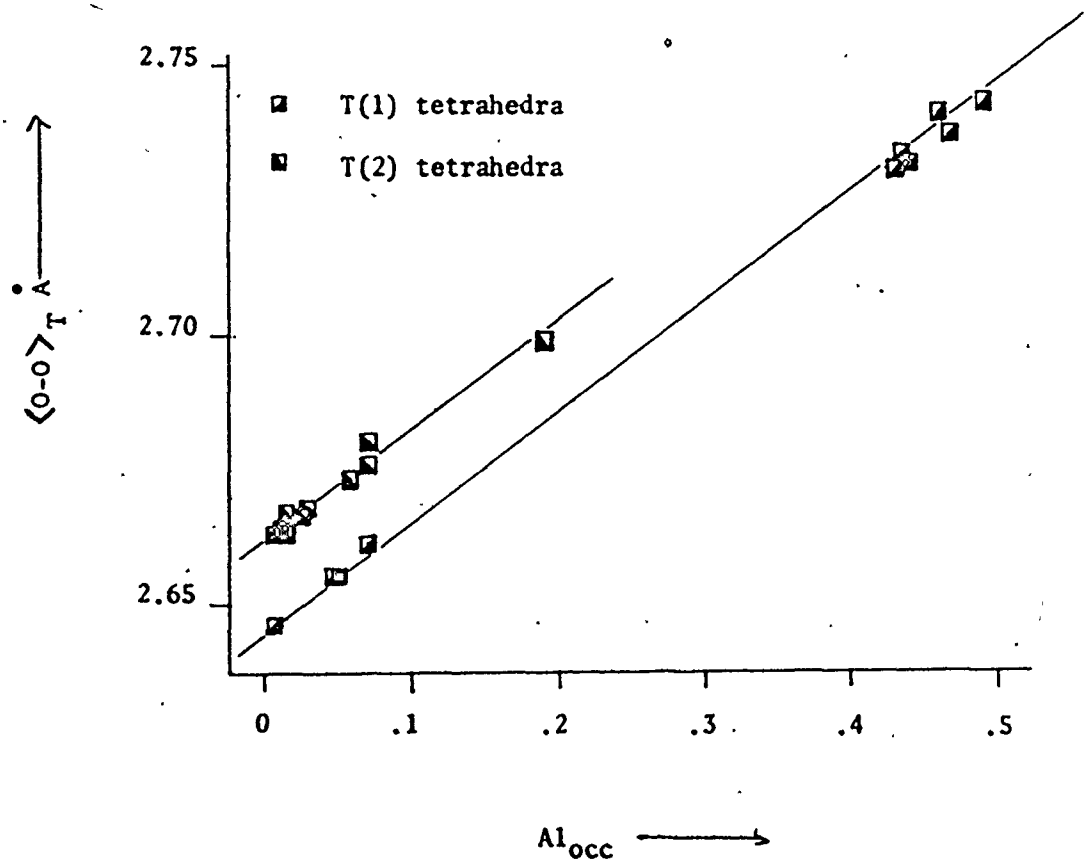

are given in Table 4.11b; Kakanui hornblende was omitted from this regression. This result substantiates the extremely unusual analysis of the Al-hastingsite (Leake, 1968; Appleyard, 1973) and will provide a check on future refined amphiboles for the validity of the chemical analysis with respect to tetrahedral Al.

In the study by Robinson (1971), the slopes for the Al-occupancy-mean bond length curves for T(1) and T(2) were identical. Using this result together with the mean bond lengths for tremolite (Papike et al., 1969) which exhibits similar tetrahedral distortions to the aluminous amphiboles, predictive occupancy curves may be derived. A linear regression was performed between ($\langle T(1)\text{-}O\rangle + \langle T(2)\text{-}O\rangle$) and Al^{TOT}_{TET} with the latter as the dependent variable; the resultant equation may be considered as the sum of two independent equations for T(1) and T(2) occupancy. This gives the slopes of the individual regression lines, and the sum of the two intercepts; this sum may be broken down by considering that the intercept on the distance axis is given by the individual mean bond lengths in tremolite. Using the values of $\langle T(1)\text{-}O\rangle = 1.620$Å and $\langle T(2)\text{-}O\rangle = 1.632$Å for tremolite, the sum of the forecast intercepts agrees with the sum obtained by the regression. The resulting equations are given below:

$$Al_{T(1)} = -12.911 + 7.97 \langle T(1)\text{-}O\rangle$$

$$Al_{T(2)} = -13.007 + 7.97 \langle T(2)\text{-}O\rangle$$

TABLE 4.11b: REGRESSION ANALYSIS RESULTS FOR CLINO-AMPHIBOLES WITH TETRAHEDRAL ALUMINIUM.

Legend as for Table 4.1.

1. Al^{IV}_{TOT} dependent, $\langle T\text{-}O \rangle$ independent

2. Al^{IV}_{TOT} dependent, $\{\langle T(1)\text{-}O \rangle + \langle T(2)\text{-}O \rangle\}$ independent

3. $Al_{T(1)}$ dependent, $\langle T(1)\text{-}O \rangle$ independent

4. $Al_{T(2)}$ dependent, $\langle T(2)\text{-}O \rangle$ independent

5. T-O(br) dependent, $\langle O\text{-}T\text{-}O(br) \rangle_3$ and $\langle O\text{-}O(br) \rangle_3$ independent

6. T-O(br) dependent, $\langle O\text{-}T\text{-}O(br) \rangle_3$, $\langle O\text{-}O(br) \rangle_3$ and $Al_{T(-)}$ independent

7. T-O(br) dependent, $\langle O\text{-}T\text{-}O(br) \rangle_3$, $\langle O\text{-}O(br) \rangle_3$, $Al_{T(-)}$ and T-O(br)-T independent

8. T-O(nbr) dependent, $\langle O\text{-}T\text{-}O(nbr) \rangle_3$, $\langle O\text{-}O(nbr) \rangle_3$ and $\langle\langle O\text{-}O(br) \rangle_3 \rangle$ independent

Number	Indep. Var.	c	m	⟨R⟩	σ	|t|
1.	⟨T-O⟩	-25.943	15.96(40)	0.997	0.019	39.46
2.	{⟨T(1)-O + T(2)-O⟩}	-25.914	7.97(20)	0.997	0.019	39.20
3.	⟨T(1)-O⟩	-12.966	8.00(12)	0.999	0.01	66.66
4.	⟨T(2)-O⟩	-12.938	7.93(47)	0.986	0.01	16.94
5.	(⟨O-T-O(br)⟩$_3$		-0.0182(10)			18.20
	(	2.0637		0.961	0.0061	
	(⟨O-O(br)⟩$_3$		0.587(26)			22.58
6.	(⟨O-T-O(br)⟩$_3$		-0.02067(94)			21.99
	(⟨O-O(br)⟩$_3$	1.3297	0.965(73)	0.977	0.0048	13.22
	($Al_{T(-)}$		-0.069(13)			5.31
7.	(⟨O-T-O(br)⟩$_3$		-0.02055(97)			21.19
	(⟨O-O(br)⟩$_3$		0.947(79)			11.99
	(	1.3913		0.977	0.0049	
	($Al_{T(-)}$		-0.066(13)			5.08
	(T-O(br)-T		-0.00020(34)			0.59
8.	(⟨O-T-O(nbr)⟩$_3$		-0.0180(17)			10.59
	(⟨O-O(nbr)⟩$_3$	1.9690	1.288(64)	0.995	0.0032	20.13
	(⟨⟨O-O(nbr)⟩$_3$⟩		-0.679(78)			8.71

These are only preliminary equations but they may be used to predict occupancies in the amphiboles of Table 4.11a. However, when these occupancies are calculated, the total Al deviates slightly from that of the chemical analysis. A total Al constraint may be applied in deriving these occupancies and this may be done in the following manner

if y and y' are the actual values of the tetrahedral Al occupancies, and $\hat{y}$ and $\hat{y}'$ are the respective values calculated from the initial equations, an equally good fit for both sets of points to both equations is subject to the condition that the sums of the squares of the differences for each equation are equal. Thus

$$(y-\hat{y})^2 = (y'-\hat{y}')^2$$

Since the total amount of tetrahedral Al is known for any one crystal, the following equation constitutes a necessary constraint.

$$y+y' = c$$

where c is a constant. Substituting this equation into the previous equation gives

$$2y(c-\hat{y}-\hat{y}') = c^2 - \hat{y}^2+\hat{y}'^2 - 2c\hat{y}'$$

This may be simplified to give y as a function of $\hat{y}$, $\hat{y}'$ and c, all of which are known; thus

$$y = (c+\hat{y}-\hat{y}')/2$$

y' may be calculated from the above constraint equation.

Table 4.12a shows the calculated Al occupancies for all the refined amphiboles used in this study and figures 4.24a&b show the variation in Al occupancy with $\langle T\text{-}O \rangle$ for each tetrahedron. Linear regression analysis of the data with $\langle T(1)\text{-}O \rangle$ and $\langle T(2)\text{-}O \rangle$ as the dependent variables was performed and the results are given in Table 4.11b. These equations may be used for predicting tetrahedral Al occupancies in future work and are internally self-consistent within the limits of the statistics quoted in Table 4.11b.

In the discussions on the Si-O bond, it was shown that the mean bond length in any tetrahedron is strongly dependent on the degree of distortion as described by the parameter δ. In the derivation of the above equations to predict Al site-occupancies, the effect of δ was ignored. This to some extent is justified as the amphiboles considered exhibit a restricted range of δ values (see Table 4.14) as compared to the non-aluminous amphiboles (Table 4.14). The T(2) tetrahedra are more distorted than the T(1) tetrahedra in general, partially accounting for the larger intercept in the predictive equation for T(2). Thus, these equations are only valid for amphiboles exhibiting a similar range of tetrahedral distortions. This is demonstrated by the richterite structures where no Al occurs, but the mean T-O distances would indicate tetrahedral Al if the large tetrahedral distortions are not taken into account.

Figure 4.24a $\langle T(1)\text{-}O \rangle$ versus calculated $Al_{T(1)}$ occupancy

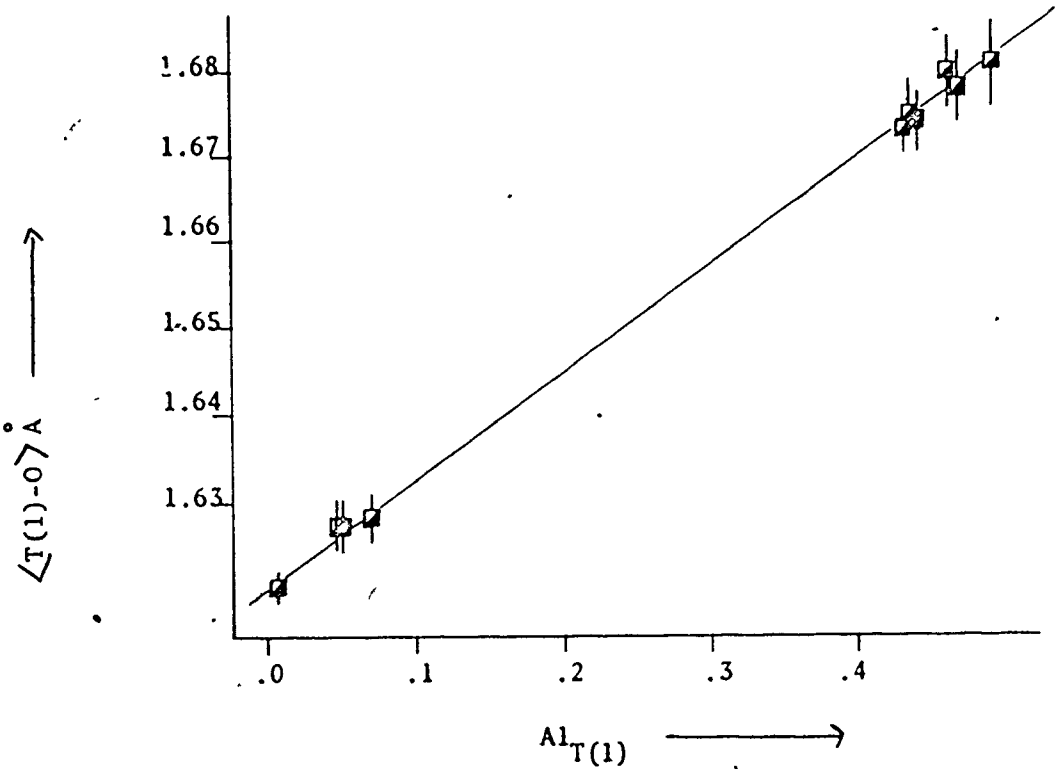

Figure 4.24b T(2)-O versus calculated $Al_{T(2)}$ occupancy

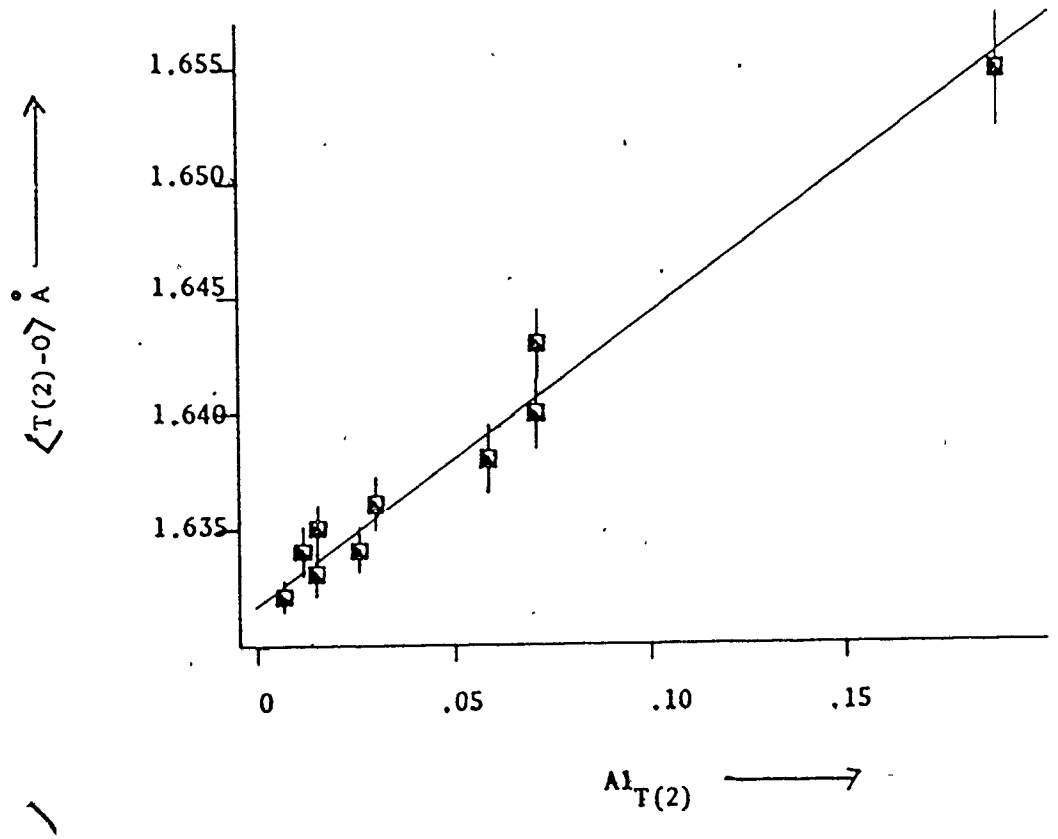

TABLE 4.12a: FORECAST TETRAHEDRAL Al OCCUPANCIES FOR THE TETRAHEDRA IN THE ALUMINOUS CLINO-AMPHIBOLES

	$Al_{T(1)}$ forecast	$Al_{T(1)}$ refined	$Al_{T(2)}$ forecast	$Al_{T(2)}$ refined
Trem	0.007	-	0.006	-
Trex	0.051	0.06(4)	0.011	0.00(4)
Tren	0.047	0.06(1)	0.015	0.00(1)
Parg	0.437	0.38(-)	0.030	0.09(-)
Ti-Parg	0.470	0.46(-)	0.071	0.08(-)
Fetsch	0.442	0.46(3)	0.059	0.04(3)
Fehast	0.432	0.42(4)	0.025	0.04(4)
Oxy	0.462	0.47(4)	0.071	0.06(4)
Alhast	0.493	0.49(11)	0.190	0.19(11)
Act	0.071	0.08(-)	0.014	0.00(-)

TABLE 4.14: TETRAHEDRAL DISTORTIONS (δ) IN CLINO-AMPHIBOLES

Aluminous			Non-aluminous		
	$\delta T(1)$	$\delta T(2)$		$\delta T(1)$	$\delta T(2)$
Tremolite*	0.47	5.11	Tremolite	0.54	4.14
Tremolite^N	0.59	4.98	Fluor-tremolite	0.19	2.88
Actinolite	0.37	4.61	Syn. Richterite 1	2.06	5.60
Pargasite	0.59	1.42	Syn. Richterite 2	1.01	5.79
Ti-Pargasite	0.63	1.74	Glaucophane	0.05	1.88
Ferrotschermakite	0.63	0.61	Cummingtonite	0.14	0.67
Ferrohastingsite	0.25	1.61	Grunerite	0.29	0.78
Oxy-kaersutite	0.29	1.16	C-Mn Cummingtonite	0.28	1.89
Al-hastingsite	0.31	0.63			

An analysis of bonding in the tetrahedra of clino-amphiboles has already been presented for the Si-O bond, and thus to avoid repetition, the results obtained will be applied to the Si-Al tetrahedra.

Initially, a stepwise regression analysis was performed for T-O(br), $\langle O\text{-}T\text{-}O(br)\rangle_3$ and $\langle O\text{-}O(br)\rangle_3$ with T-O(br) as the dependent variable; the results are given in Table 4.11b. Comparison of the values of T-O(br) calculated from the regression equation

$$T\text{-}O(br)=2.0356-0.0181(11)\langle O\text{-}T\text{-}O(br)\rangle_3+0.592(27)\langle O\text{-}O(br)\rangle$$

with the observed values (see Table 4.15, Calc. 1) showed deviations of up to 3σ. Figure 4.23b shows the variation of $\langle O\text{-}O\rangle_T$ with tetrahedral Al occupancy (from Table 4.12a) for these amphiboles; two linear trends are apparent, corresponding to each unique tetrahedron. This would suggest that the terms $\langle O\text{-}O(br)\rangle_3$ do not completely contain the information concerning the Al occupancy and indicates that the distances will also be a function of Al occupancy. Consequently, the previous analysis was repeated with the addition of Al_{TET} as an independent variable; the results are given in Table 4.11b and considerable improvement is noted. Table 4.15 (CALC 2) compares the values calculated for T-O(br) from the resulting regression equation

TABLE 4.15: OBSERVED AND CALCULATED T-O FOR Al-AMPHIBOLES

		Trem	Act	Parg	TiParg	Fetsch	Fehast	Oxy	Alhast	Trex	Tren
T(1)-O(1)	OBS	1.602(2)	1.618(4)	1.663(3)	1.670(4)	1.668(4)	1.665(3)	1.684(4)	1.675(4)	1.609(3)	1.606(3)
	CALC 1	1.603	1.614	1.666	1.671	1.664	1.664	1.692	1.673	1.610	1.609
T(1)-O(5)	OBS	1.632(2)	1.643(4)	1.693(3)	1.698(4)	1.692(4)	1.683(3)	1.689(4)	1.688(3)	1.634(3)	1.637(3)
	CALC 1	1.631	1.640	1.688	1.691	1.687	1.683	1.680	1.693	1.635	1.636
	CALC 2	1.628	1.638	1.690	1.692	1.685	1.682	1.681	1.690	1.631	1.633
T(1)-O(6)	OBS	1.629(2)	1.632(4)	1.682(3)	1.682(4)	1.679(4)	1.680(3)	1.682(5)	1.692(4)	1.638(4)	1.636(3)
	CALC 1	1.632	1.636	1.684	1.684	1.680	1.674	1.679	1.686	1.638	1.637
	CALC 2	1.628	1.632	1.683	1.683	1.677	1.673	1.678	1.689	1.635	1.634
1)-O(7)	OBS	1.616(1)	1.621(2)	1.663(2)	1.663(2)	1.656(2)	1.665(1)	1.665(2)	1.669(2)	1.627(2)	1.628(2)
	CALC 1	1.622	1.626	1.672	1.673	1.657	1.671	1.677	1.675	1.631	1.633
	CALC 2	1.618	1.623	1.671	1.669	1.658	1.668	1.676	1.674	1.627	1.629
2)-O(2)	OBS	1.616(2)	1.614(3)	1.631(2)	1.640(4)	1.640(4)	1.630(3)	1.644(4)	1.660(4)	1.611(3)	1.617(3)
	CALC	1.616	1.612	1.633	1.641	1.635	1.628	1.645	1.660	1.612	1.617
2)-O(4)	OBS	1.585(2)	1.587(4)	1.608(2)	1.608(4)	1.620(4)	1.603(3)	1.615(4)	1.630(4)	1.585(3)	1.586(2)
	CALC	1.588	1.585	1.610	1.611	1.614	1.603	1.619	1.633	1.589	1.590
2)-O(5)	OBS	1.653(2)	1.651(4)	1.642(3)	1.643(5)	1.636(4)	1.647(3)	1.651(5)	1.661(4)	1.663(3)	1.657(3)
	CALC 1	1.643	1.639	1.642	1.645	1.635	1.641	1.650	1.659	1.648	1.647
	CALC 2	1.652	1.648	1.646	1.649	1.640	1.647	1.656	1.665	1.657	1.656
2)-O(6)	OBS	1.672(2)	1.679(4)	1.662(3)	1.669(4)	1.656(4)	1.658(3)	1.663(4)	1.668(3)	1.675(3)	1.681(3)
	CALC 1	1.668	1.669	1.666	1.670	1.661	1.662	1.671	1.677	1.671	1.676
	CALC 2	1.671	1.673	1.666	1.671	1.661	1.662	1.671	1.676	1.673	1.680

$$T\text{-}O(br)=1.2671-0.02068(92)\langle O\text{-}T\text{-}O(br)\rangle_3+0.989(70)\langle O\text{-}O(br)\rangle_3-$$
$$0.072(12)Al_{T(-)}$$

with the observed values and figure 4.25a shows a similar graphical comparison; in general, deviations do not appreciably exceed 1σ. The role of T-O(br)-T angles has been stressed by many other investigators, and in view of the minor role it has played in these discussions, its effect on the Si, Al-O(br) distances was tested by adding T-O(br)-T as another independent variable in a repeat of the previous analysis. The results are given in Table 4.11b and the $|t|$ static indicates that T-O(br)-T (the last variable to be added to the regression) is not significant.

For the non-bridging bonds, a stepwise regression analysis was performed on T-O(nbr), $\langle O\text{-}T\text{-}O(nbr)\rangle_3$, $\langle O\text{-}O(nbr)\rangle_3$, $Al_{T(-)}$ $\langle\langle O\text{-}T\text{-}O(br)\rangle_3\rangle$ and $\langle\langle O\text{-}O(br)\rangle_3\rangle$ with T-O(nbr) as the dependent variable. This indicated that only the variables $\langle O\text{-}T\text{-}O(nbr)\rangle$, $\langle O\text{-}O(nbr)\rangle$ and $\langle\langle O\text{-}O(br)\rangle_3\rangle$ contributed significantly to T-O(nbr) variations, the other variables being virtually redundant. The results of the regression at this stage are given in Table 4.11b; table 4.15 compares the values of T-O(nbr) calculated from the regression equation

$$T\text{-}O(nbr)=1.8991-0.0174(17)\langle O\text{-}T\text{-}O(nbr)\rangle_3+1.268(64)\langle O\text{-}O(nbr)\rangle_3-$$
$$0.659(78)\langle\langle O\text{-}O(br)\rangle_3\rangle$$

Figure 4.25a Comparison of the observed and calculated T-O(br) distances for the (Si, Al) clino-amphiboles

The T-O(br) distances were calculated from the following regression equation...

$$T\text{-}O(br) = 1.267 - 0.02068(92)\langle O\text{-}T\text{-}O(br)\rangle_3 + 0.989(70)\langle O\text{-}O(br)\rangle_3 - 0.072(12)\ Al_{T(-)}$$

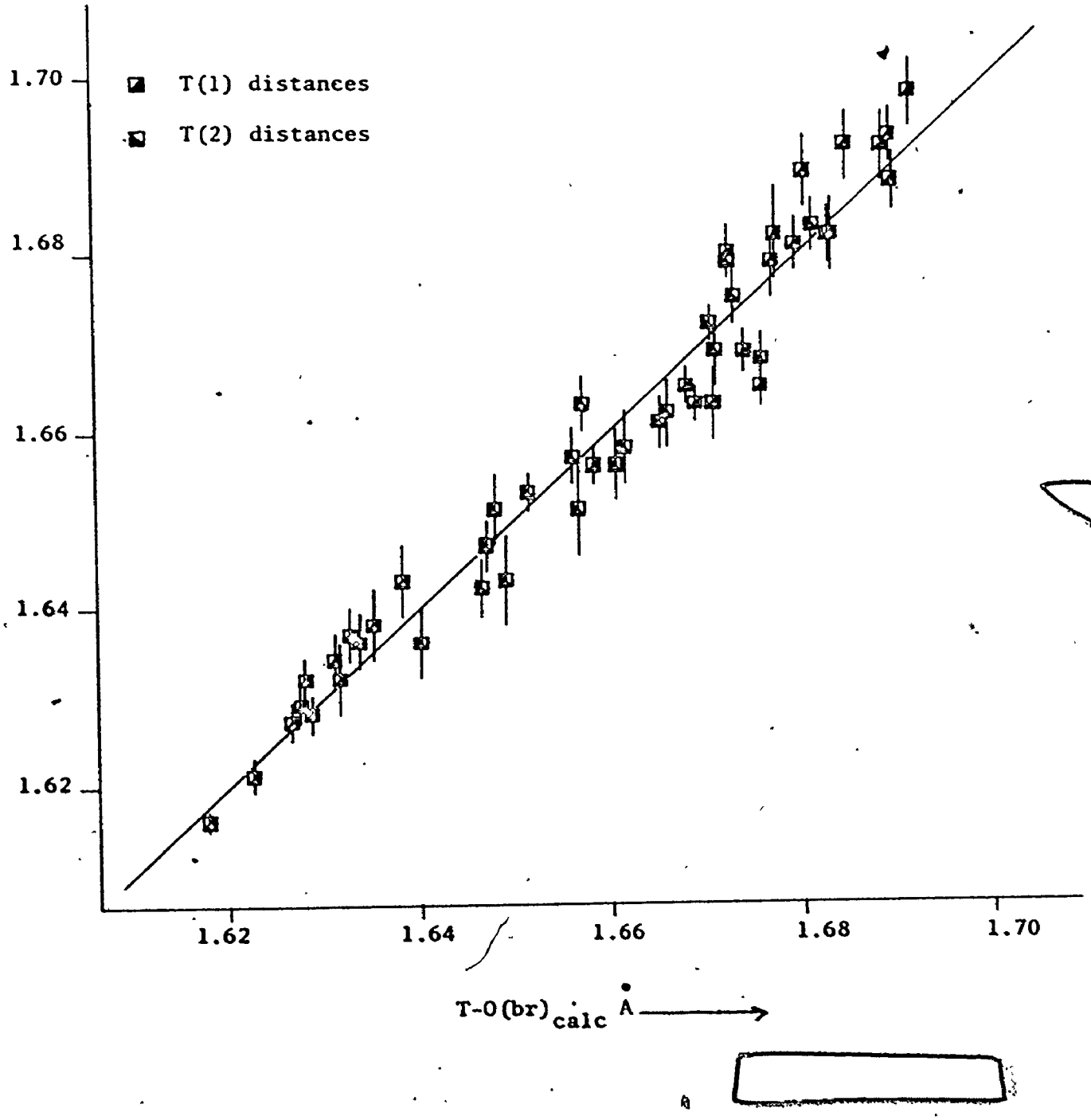

Figure 4.25b Comparison of the observed and calculated T-O(nbr) distances for the (Si, Al) clino-amphiboles.

The T-O(nbr) distances were calculated from the following regression equation...

$$T\text{-}O(nbr) = 1.899 - 0.174(17)\langle O\text{-}T\text{-}O(nbr)\rangle_3 + 1.268(64)\langle O\text{-}O(nbr)\rangle_3 - 0.659(78)\,\langle\langle O\text{-}O(br)\rangle_3\rangle$$

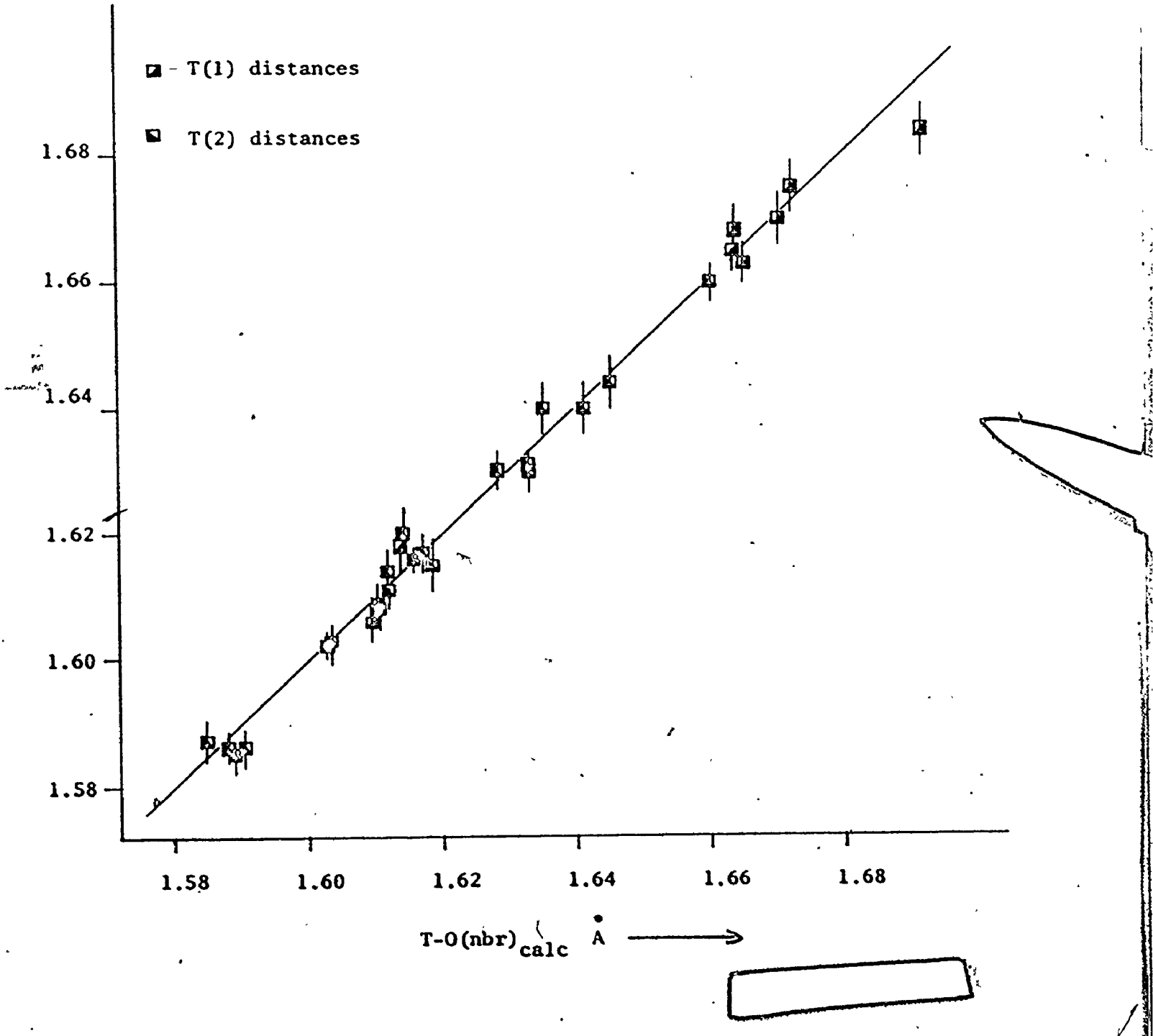

with the observed values and figure 4.25b gives a similar graphical comparison.

THE OCTAHEDRAL SITES

The octahedral strip is the most rigid element in the clino-amphibole structure and is thus of great importance in controlling atomic configurations. The wide range of possible anion and cation substitutions gives rise to considerable variation in octahedral stereochemistry, much of which may be related to the ionic radius of the constituent chemical species.

It is most convenient to consider the three octahedral sites separately as the ligancy and local environment differ in each case. Figures 4.26a,b and c show the variation in mean bond length with ionic radius of the constituent cations for M(1), M(2) and M(3); the results of simple linear regression analysis are given in Table 4.16. Agreement for a linear model is excellent for M(2) but considerable scatter occurs for the M(1) and M(3) sites. This results from the difference in ligancy at each site; M(2) is coordinated by six oxygens and the constancy of the coordination results in good agreement with a simple linear model. Conversely, M(1) and M(3) are coordinated by four oxygens and two additional ligands which may be OH^-, F^-, Cl^- or O^{2-}; some of the scatter in figures 4.26a and c may be correlated with the ionic radius of the anion

Figure 4.26a $\langle M(1)\text{-}O \rangle$ versus $\langle r_{M(1)} \rangle$

The full line indicates the regression line; the dashed line indicates the ideal relationship.

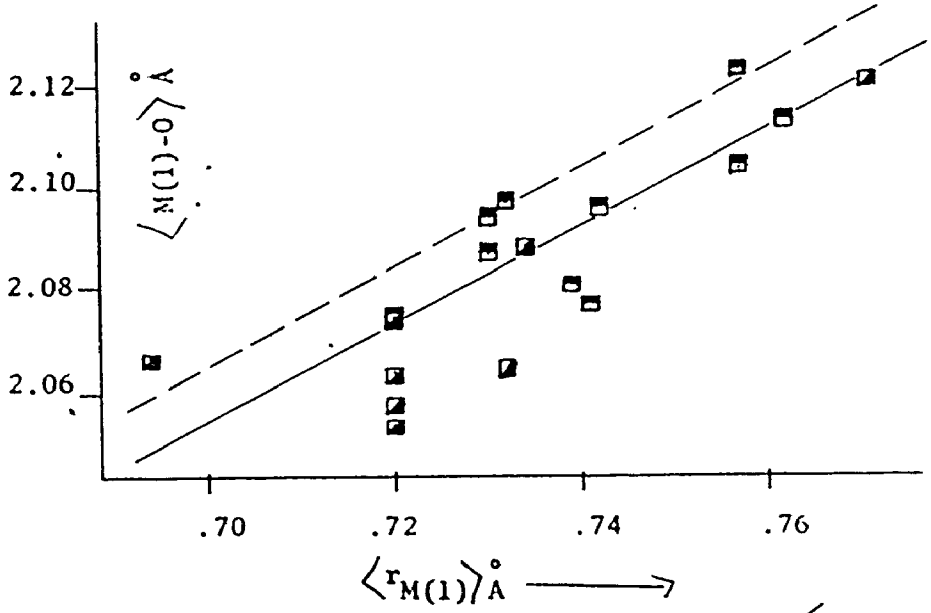

Figure 4.26b $\langle M(2)\text{-}O \rangle$ versus $\langle r_{M(2)} \rangle$

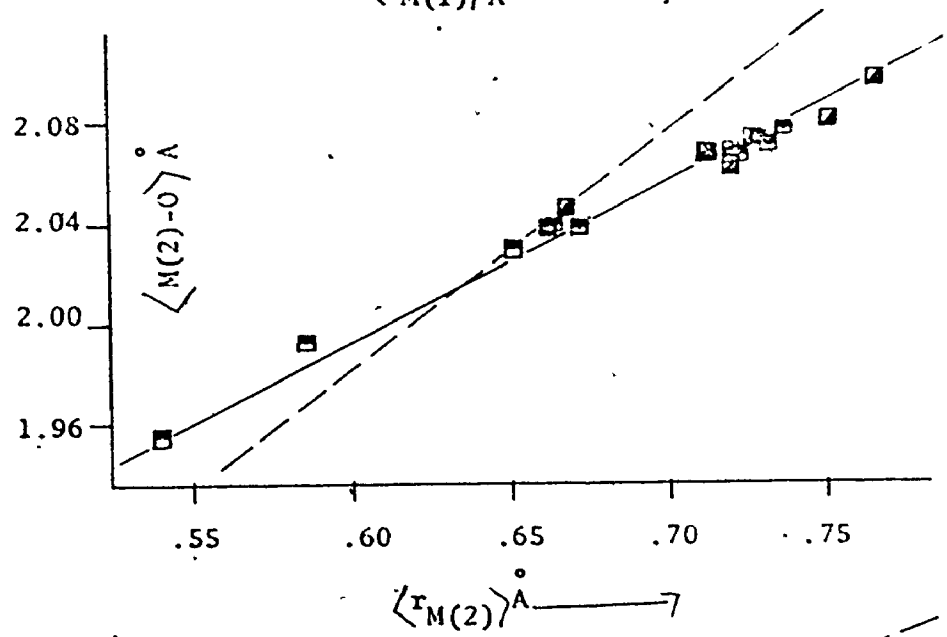

Figure 4.26c $\langle M(3)\text{-}O \rangle$ versus $\langle r_{M(3)} \rangle$

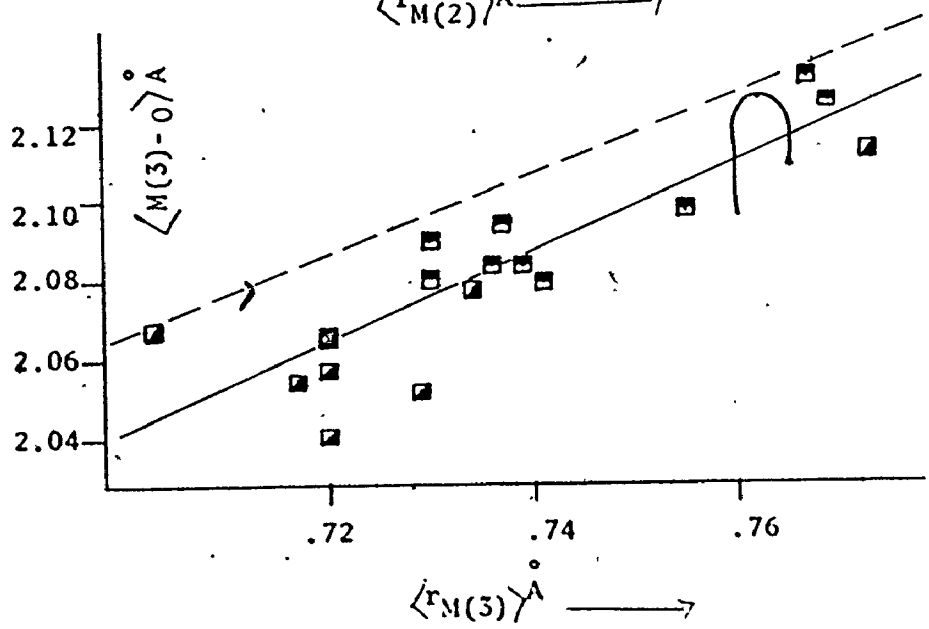

TABLE 4.16: LINEAR REGRESSION RESULTS. LEGEND AS FOR TABLE 4.3

1. $\langle M(1)\text{-}O \rangle$ dependent, $\lceil_{M(1)}$ independent
2. $\langle M(2)\text{-}O \rangle$ dependent, $\lceil_{M(2)}$ independent
3. $\langle M(3)\text{-}O \rangle$ dependent, $\lceil_{M(3)}$ independent
4. $\langle M(1)\text{-}O \rangle_{CORR}$ dependent, $\lceil_{M(1)}$ independent
5. $\langle M(3)\text{-}O \rangle_{CORR}$ dependent, $\lceil_{M(3)}$ independent
6. $\langle M(1)\text{-}O \rangle$ dependent, $\lceil_{M(1)}$ and $\lceil_{O(3)}$ independent
7. $\langle M(3)\text{-}O \rangle$ dependent, $\lceil_{M(3)}$ and $\lceil_{O(3)}$ independent

Number	Indep. Var.	c	m	$\langle R \rangle$	σ	|t|
1.	$\lceil_{M(1)}$	1.3926	0.94(15)	0.836	0.012	6.27
2.	$\lceil_{M(2)}$	1.5572	0.733(22)	0.992	0.0054	32.78
3.	$\lceil_{M(3)}$	1.2501	1.13(15)	0.876	0.012	7.50
4.	$\lceil_{M(1)}$	1.4069	0.93(11)	0.903	0.0084	8.64
5.	$\lceil_{M(3)}$	1.2801	1.09(11)	0.927	0.0087	9.81
6.	$\lceil_{M(1)}$	0.6626	0.90(10)	0.934	0.0078	9.01
	$\lceil_{O(3)}$		0.57(12)			4.73
7.	$\lceil_{M(3)}$	0.4578	1.045(9)	0.960	0.0073	11.50
	$\lceil_{O(3)}$		0.64(11)			5.65

occupying the O(3) position. This is illustrated by figures 4.27a,b which show the variation in $\langle M(1)\text{-}O \rangle$ and $\langle M(3)\text{-}O \rangle$ with O(3) anion radius for $r_{M(1)} = r_{M(3)} = 0.72$Å. When the appropriate cation radii are modified to account for this factor, agreement with a linear model is greatly improved (see Table 4.16); similarly, including $r_{O(3)}$ as an independent variable in a stepwise linear regression analysis indicates that it contributes significantly to variations in $\langle M(1)\text{-}O \rangle$ and $\langle M(3)\text{-}O \rangle$ (see Table 4.16). In many cases, the anion content of the O(3) position is not known and assumed to be hydroxyl; small amounts of fluorine or chlorine would significantly affect M(1) and M(3) sites. In additon, it appears from this study that monovalent anion deficiencies at O(3) are encountered in non-oxidized amphiboles. In the refinement of tremolite, the position of the hydrogen atom was located accurately using neutrons, and the chemically analysed water content was used to give the partial occupancy of the hydrogen position. The very well-behaved thermal vibrations of the partial hydrogen atom indicate that the chemical analysis was most probably correct. The total amount of fluorine and chlorine from the chemical analysis was insufficient to fill the remainder of the O(3) position not occupied by hydroxyl, indicating that some O^{2-} is present in this site. Similar hydroxyl deficiencies in other amphiboles or small amounts of fluorine could possibly account for some of the remaining scatter in the corrected radii and stepwise regression analyses.

Figure 4.27a $\langle M(1)\text{-}O \rangle$ versus $\langle r_{O(3)} \rangle$ for those clino-amphiboles with $\langle r_{M(1)} \rangle$ = 0.72 Å

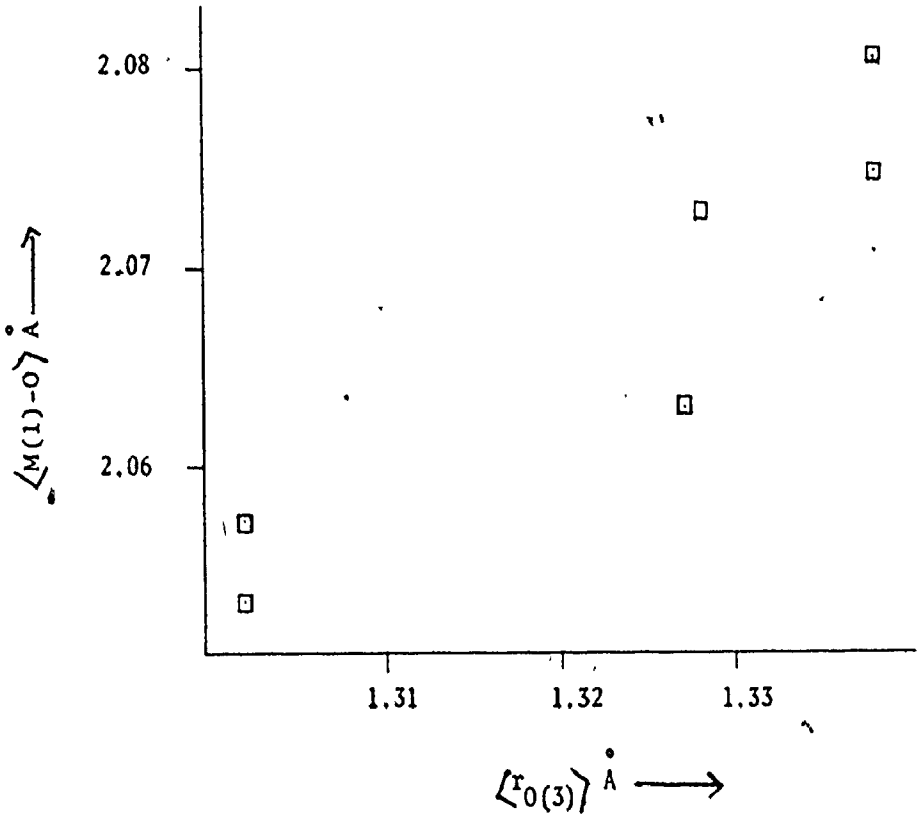

Figure 4.27b $\langle M(3) - O \rangle$ versus $\langle r_{O(3)} \rangle$ for the clino-amphiboles with $\langle r_{M(3)} \rangle$ = 0.72 Å

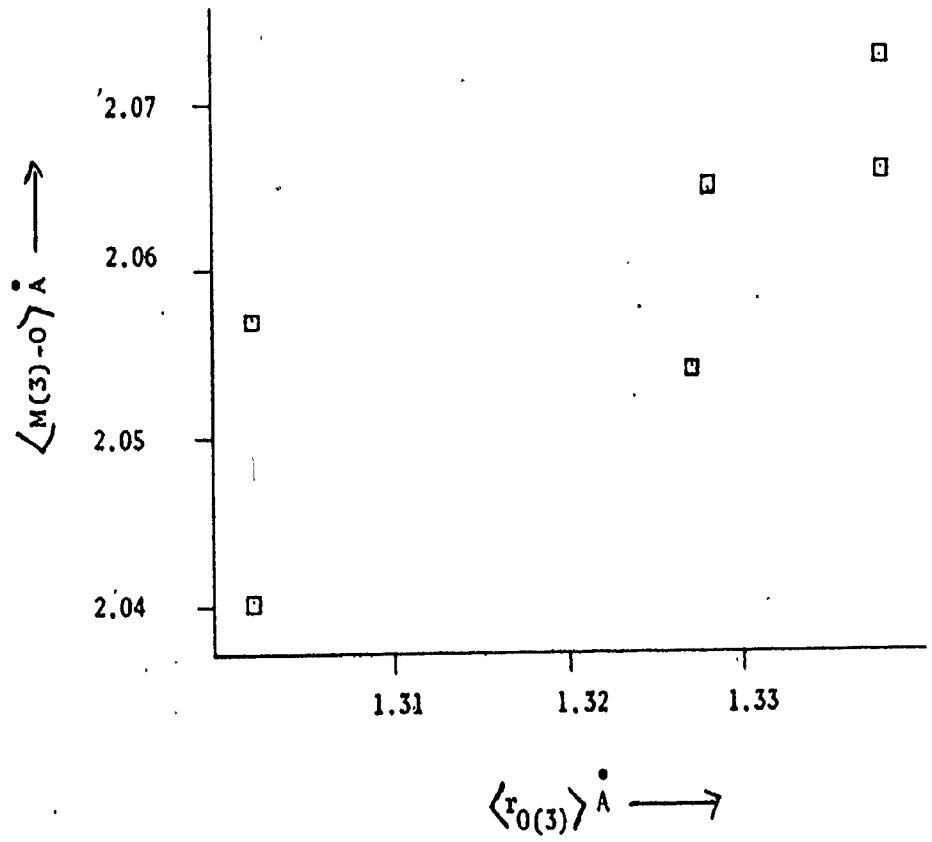

The variations in distortion of the octahedral sites as a function of site-chemistry are of great interest as they are undoubtedly a major factor in determining site-occupancies and compositional stability ranges. Table 4.17 lists the two distortional parameters δ and σ (angle variance) for all the refined clinoamphiboles considered in this study. As the cation type varies in the octahedral sites, the parameter δ was normalized by dividing it by the mean bond length for that site. Immediately apparent on comparing analogous parameters is the disparity between the two distortional indices. According to the σ parameter, the relative degree of distortion is in general represented by $M(3) > M(1) > M(2)$ whereas the δ parameter indicates that the sequence is $M(2) > M(1) > M(3)$. This lack of concurrence is at first surprising since both parameters have much to commend them.

The significance of δ is shown in Appendix 4 and it has been shown to apply (in a slightly different form) to a wide range of structures (Brown & Shannon, 1973; Shannon & Calvo, in press). The success of σ as a distortional parameter has been shown by Robinson (1971) and Robinson et al. (1971) using another distortional index $\langle\lambda\rangle$ (quadratic elongation) although this author was unable to reproduce his calculated values of $\langle\lambda\rangle$ for the amphiboles reported by Robinson (1971). The following considerations appear to indicate that σ is controlled by cation size considerations. The angular distortions of the M(1) and M(3) octahedra appear to be linked to the occupancy of the M(2) site. Figure 4.28a,b shows the variation in σ

TABLE 4.17: OCTAHEDRAL DISTORTION PARAMETERS FOR THE CLINO-AMPHIBOLES

σ = octahedral angle variance

δ_1 = octahedral bond length distortion (without coordination correction)

δ_2 = octahedral bond length distortion (with coordination correction)

	M(1)			M(2)			M(3)		
	σ	δ_1	δ_2	σ	δ_1	δ_2	σ	δ_1	δ_2
Trem	32.6	0.15	1.45	21.0	5.52	3.69	40.0	0.14	0.38
Trex	33.5	0.35	2.20	22.4	5.79	3.89	40.6	0.04	0.49
Tren	34.4	0.42	2.36	24.2	6.41	4.45	41.0	0.01	0.63
Flor	43.0	0.70	3.17	21.1	5.76	4.07	43.9	0.03	0.53
Actin	30.5	0.30	1.54	20.8	6.70	4.54	42.8	0.04	0.54
Parg	46.3	1.56	3.09	22.3	5.98	3.81	69.4	0.19	1.76
Ti Parg	43.1	3.50	2.50	24.3	6.13	3.94	69.2	0.14	1.47
Kak	42.9	4.96	3.53	26.4	5.60	3.56	68.5	0.21	0.29
Fetsch	52.5	4.00	5.22	18.0	5.00	3.02	97.2	0.48	0.10
Fehast	42.1	2.39	3.11	26.3	8.26	5.69	76.2	0.13	0.35
Oxy	43.9	14.29	11.82	28.6	7.06	4.73	65.9	0.44	0.06
Alhast	59.9	3.59	4.57	22.0	6.87	4.48	101.8	0.08	0.35
K-rich	39.5	0.43	2.29	37.8	13.04	10.19	43.6	0.61	0.02
SR1	39.5	2.17	5.62	30.3	12.54	10.30	39.7	0.03	0.56
SR2	40.3	2.30	5.56	34.3	16.11	13.30	36.5	0.12	0.32
Glauc	63.7	0.21	1.82	32.1	15.77	12.44	77.9	0.50	0.10
Cumm	32.5	1.57	2.15	28.6	3.92	2.50	46.3	0.50	0.10
Grun	33.0	2.29	3.39	39.6	2.79	1.56	55.8	0.02	0.32
C-Mn	31.0	1.08	1.65	23.0	5.90	4.04	38.8	0.51	0.10
Zn	30.2	1.37	2.03	23.7	6.34	4.46	39.5	0.39	0.15

Figure 2.28a Variation of M(1) angle variance (σ) with the mean ionic radius of the M(2) cations for the clino-amphiboles

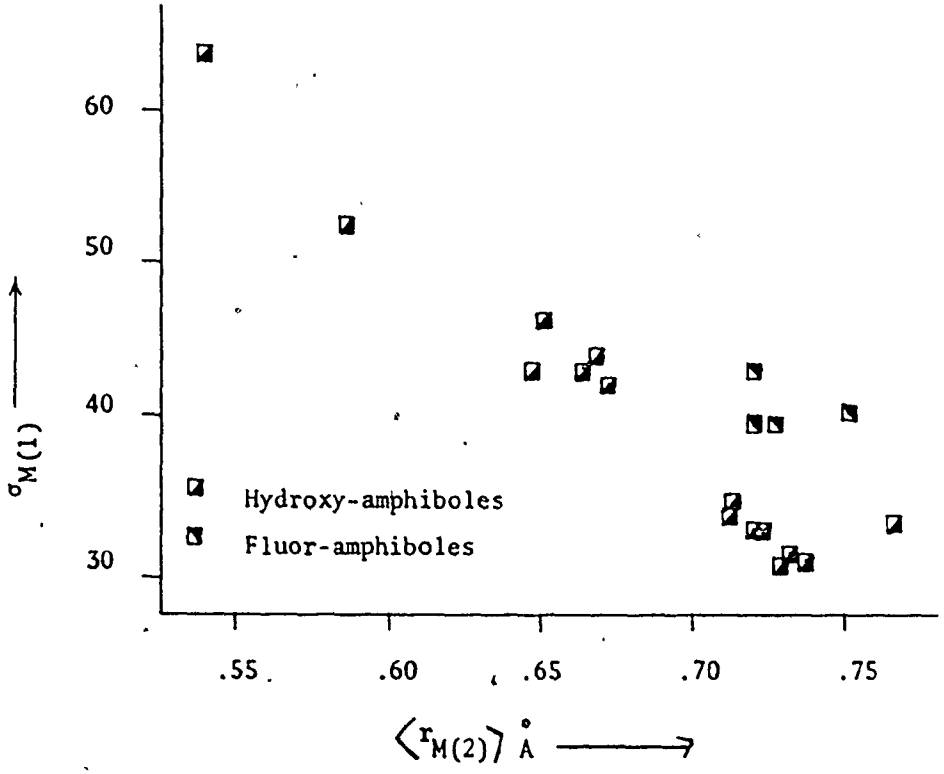

Figure 4.28b Variation of M(3) angle variance (σ) with the mean ionic radius of the M(2) cations for the clino-amphiboles

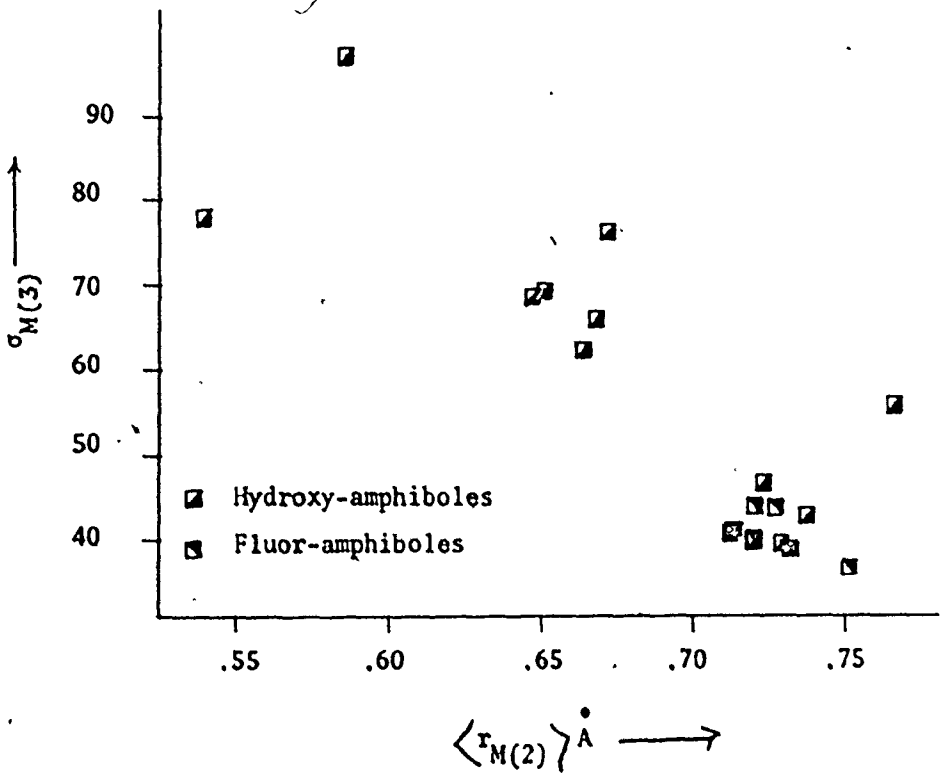

for M(1) and M(3) with the ionic radius of the cations occupying the M(2) site, while figure 4.29b shows the local configuration of the octahedral sites around M(2).

From a purely geometrical viewpoint, identical octahedra may pack together in this way without any distortion; however, a decrease in size of the M(2) octahedron will introduce considerable additional distortion in M(1) and M(3) if the inter-octahedral linkages are to be maintained. Since the range of sizes of the M(2) cations extends to much smaller values than M(1) and M(3), a negative correlation between the parameters is expected, and that is what is observed. The angular nature of this effect is well illustrated by its effect on the O(2)-O(2) edge of the M(1) octahedron; figure 4.29a shows the variation in shear strain for this edge with $r_{M(2)}$, where the shear strain is defined as the angular deviation of the edge from its ideal in a regular close-packed anion framework; inspection of figure 4.29b shows that this will have a considerable effect on several O-M(1)-O angles. Similar arguments indicate corresponding effects on other parts of the M(1) and M(3) octahedra. This distortion imposed by simple linkage requirements is of great potential importance as a control on the ordering of cations between the M(1) and M(3) sites; this will be considered in the next chapter.

Inspection of Tables 3.9 and 3.10 shows that, in general, edges shared between polyhedra are shorter and subtend smaller angles

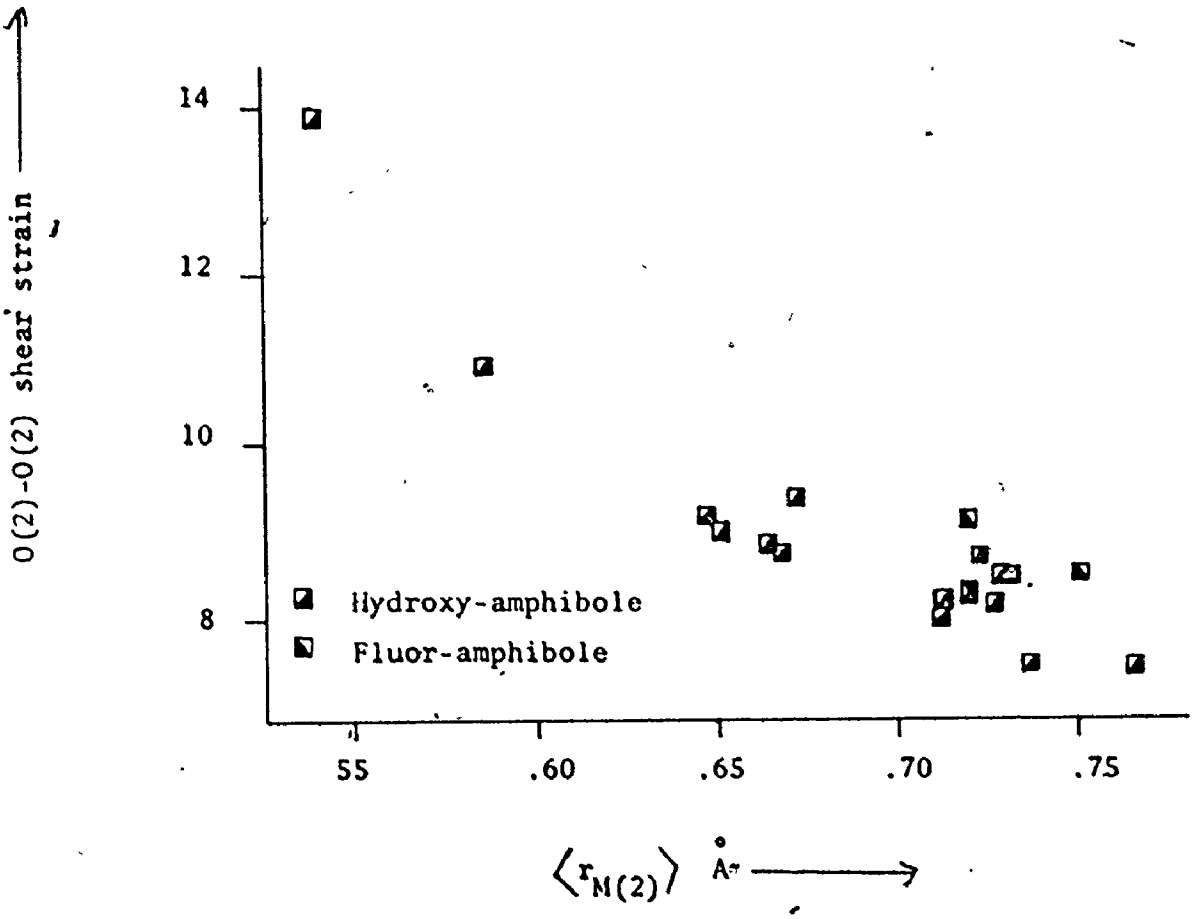

Figure 4.29b The local configuration around the M(2) site, projected on to the b-c plane.

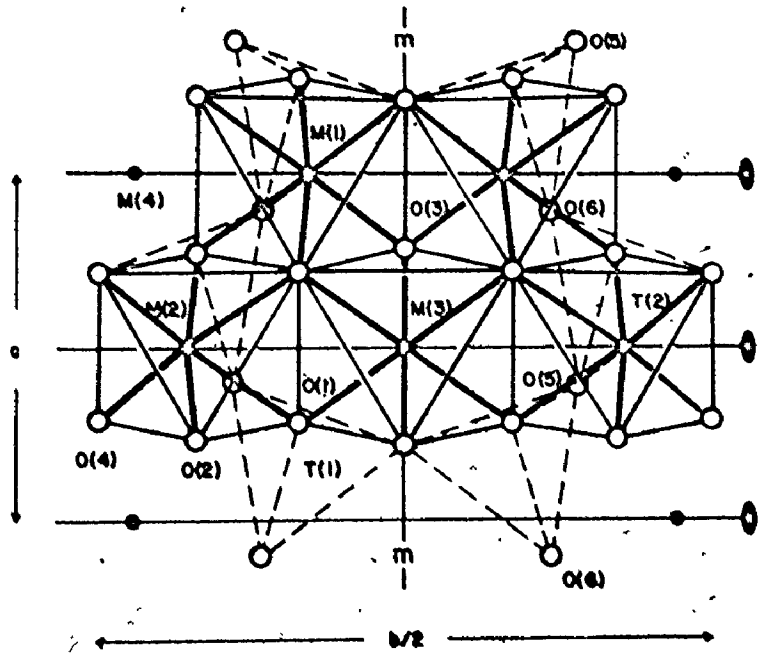

at the cation than unshared edges. This is compatible with the hypothesis that cation-cation repulsive interactions are much stronger than anion-anion repulsive interactions (Pauling, 1960) and suggests that cation-cation repulsion plays an important role in determining octahedral distortions in the amphiboles. There has been little or no work done on quantitative effects of cation-cation interactions, and it is necessary to develop some index representing its effect.

The fact that the interaction is manifest on polyhedron edge lengths and angles suggests that the ratio of unshared to shared elements may be a representative index. Figure 4.30 shows the variation in this ratio for O-M-O angles with that for O-O distances for all three M sites. The linearity is not geometrically implicit in these parameters and both are geometrically independent of cation size; thus, either could serve as an index and the angular ratio was arbitrarily chosen and designed ϵ.

Simple algebraic arguments show that ϵ is formally independent of σ (angular variance) and any relation between them is thus of crystallochemical origin. Figures 4.31a, b, and c show the variation in σ with ϵ for M(1), M(2) and M(3). A fairly good linear correlation occurs for M(1) and M(3) but the variation for M(2) is essentially random. This may be related to the local environment of each octahedron. The M(1) and M(3) sites are completely bounded in the b-c plane by shared edges and thus experience cation-cation repulsion from all sides; hence, the

Figure 4.30. Variation in E(O-M-O) with E(O-O) for the octahedral sites in clino-amphiboles

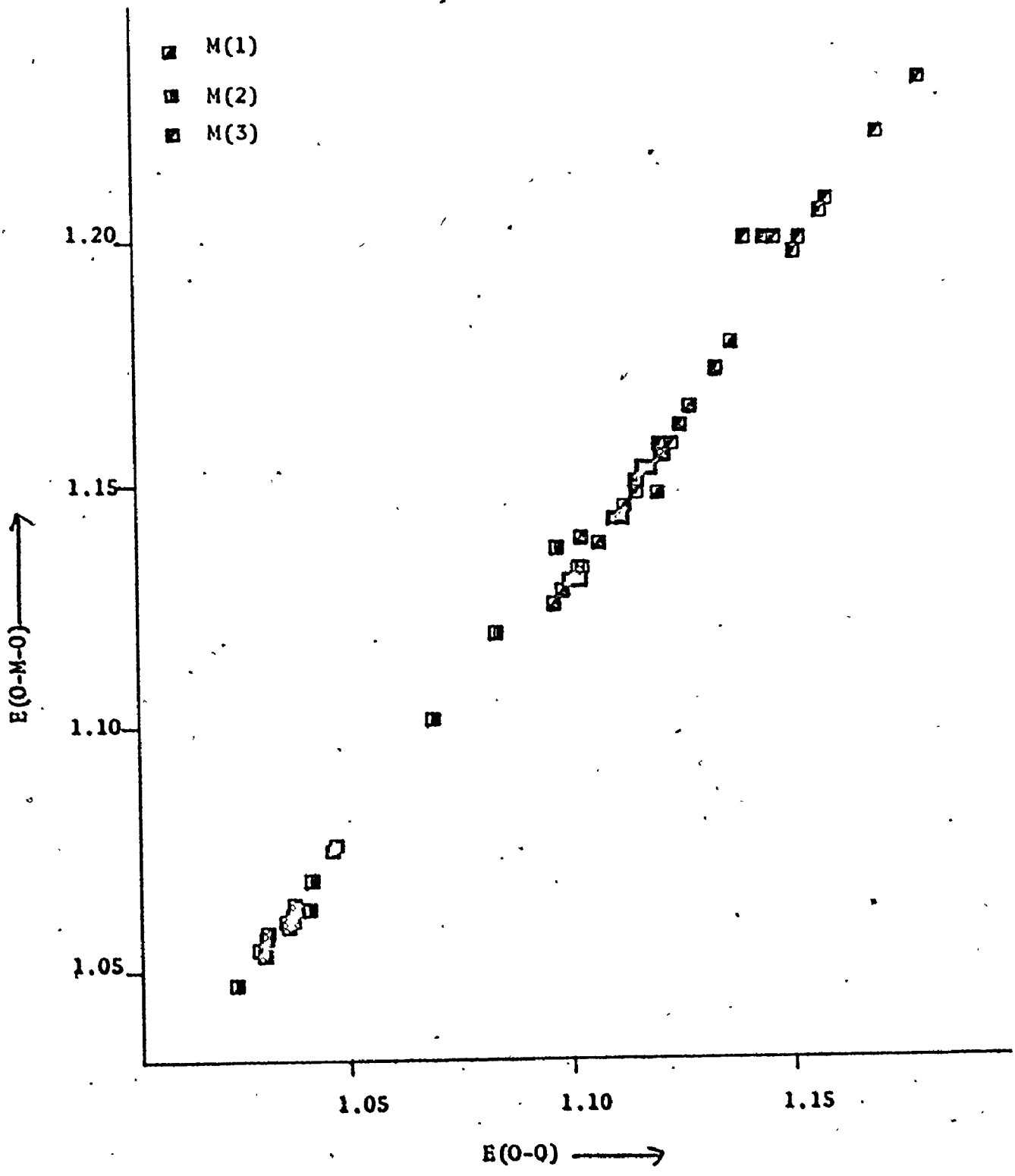

Figure 4.31a Variation in σ (angle variance) with E(O-M-O) for the M(1) site.

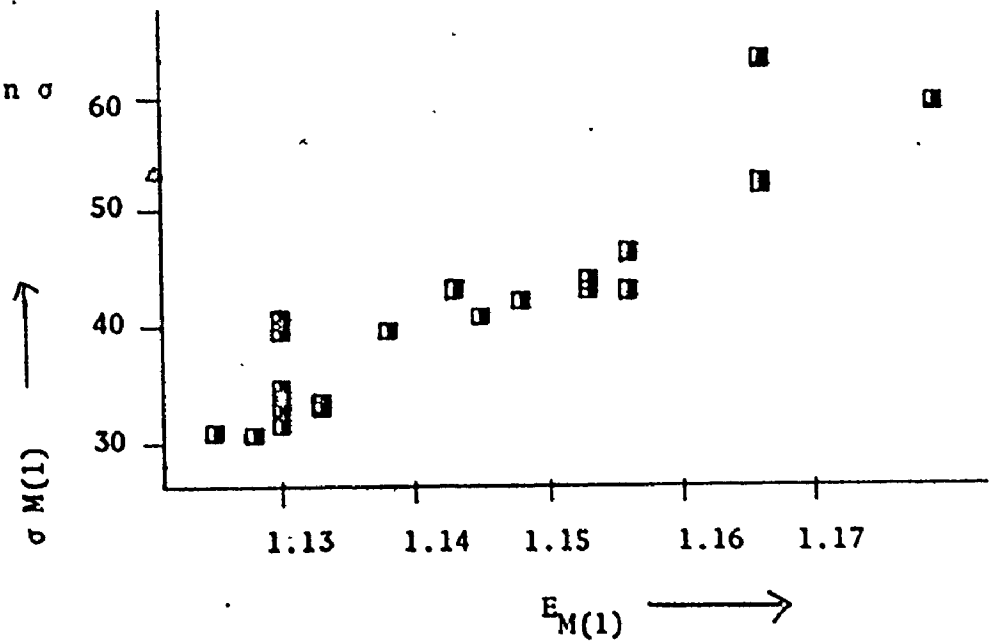

Figure 4.31b Variation in σ (angle variance) with E(O-M-O) for the M(2) site.

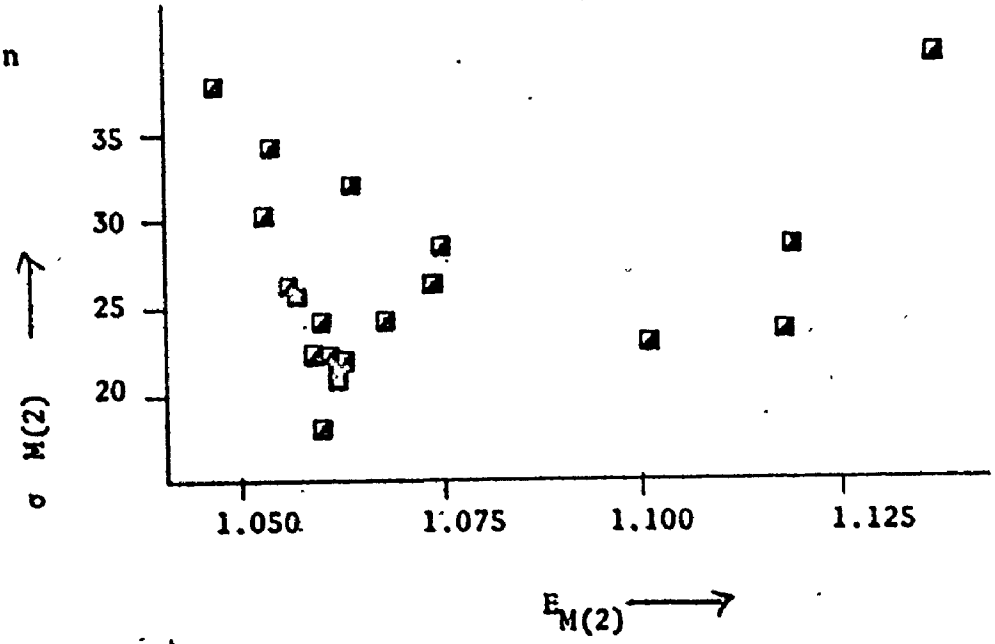

Figure 4.31c Variation in σ (angle variance) with E(O-M-O) for the M(3) site.

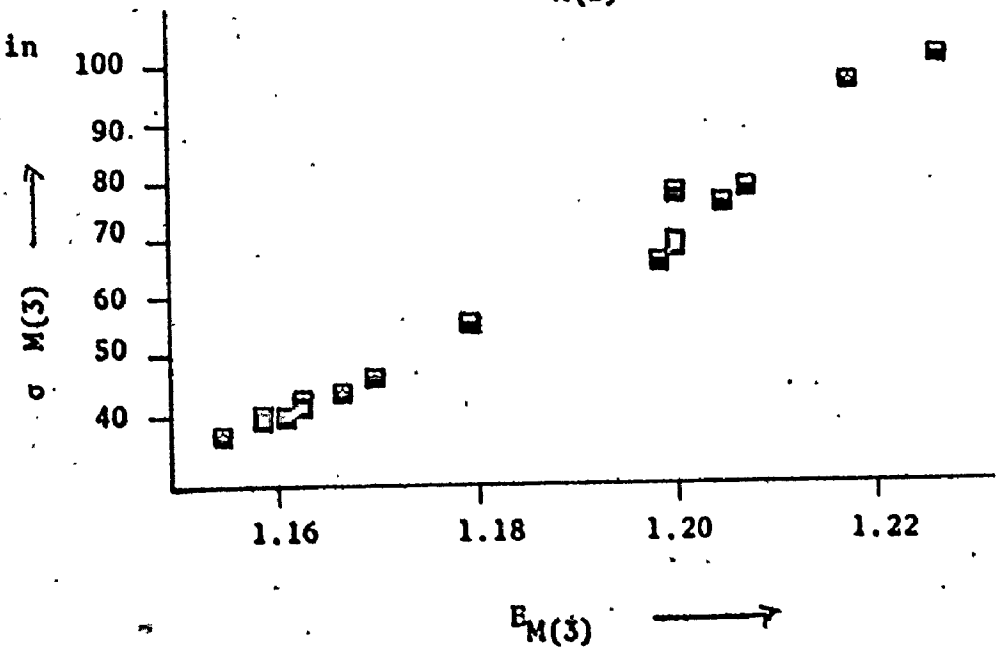

shape of the polyhedron will be controlled by the possible amount of relaxation caused by cation-cation repulsive forces which surround it. Conversely, the M(2) site has one unshared edge in the b-c plane and the M(2) cation can recoil (away from the other octahedral cations) in this direction. This, combined with the previous size arguments coupling $\sigma_{M(1)}$ and $\sigma_{M(3)}$ with $\Gamma_{M(2)}$ suggest that the anion framework of M(2) does not need to relax in order to decrease cation-cation repulsion and its distortion is imposed by those distortions of the bounding octahedra and the ionic radius of its constituent cations.

The parameter ϵ is not sufficient to describe individual cation-cation repulsion relaxations and their effect on specific bond lengths and angles. Although Pauling's third rule refers to polyhedral edges and angles, it makes no predictions concerning the distortion of bond lengths. However, if the mean bond lengths involved in shared elements are increased and the mean bond lengths involved in unshared elements are decreased, this will lower the cation-cation repulsive interaction and consequently help to stabilize the structure. This situation is illustrated by the corundum structures where all the anions are formally charge balanced and cation-cation repulsions across shared faces and edges distorts the octahedron to produce two crystallographically unique M-O bonds.

The structural parameters which would appear to relate most to the degree of bond length relaxation due to cation-cation interactions are the M-M (metal-metal) approaches. In a simple hard-sphere model, these will also be a function of ionic radius; thus it is necessary to remove this dependancy before the additional information contained in these parameters becomes apparent. Below is shown a simplistic model of the undistorted configuration, where M represents a cation and A represents an anion: in the figure

$$AM = r_M + r_A$$

$$MM = \sqrt{2}\,(r_M + r_A)$$

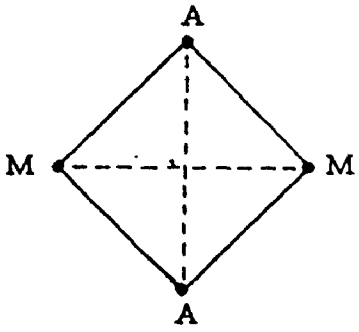

The difference between the observed metal-metal approach and $\sqrt{2}\,(r_{CATION} + r_{ANION})$ represents the amount of cation-cation relaxation due to their repulsive interaction. This parameter, designated τ is listed for all the crystallographically unique M-M distances in all amphiboles in Table 4.18. Figures 4.32a, b, c, d, e and f show the variation in $\langle$O-M-O$\rangle$ angle subtended by the shared edge with τ across the shared edge; in general, the relationships are very encouraging. For the M(1)-M(1) interaction, two good correlations are developed.

TABLE 4.18: CATION-CATION REPULSION PARAMETER, γ FOR THE CRYSTALLOGRAPHICALLY UNIQUE M-M DISTANCES IN THE CLINO-AMPHIBOLES

	M1-M1	M1-M2	M1-M3	M1-M4	M2-M3	M2-M4	MEAN
Tremolite	.25850	.11900	.13830	.17310	.22000	-.03100	.13612
Tremolitex	.28770	.12660	.15330	.18320	.22860	-.00930	.15023
Tremoliten	.28970	.12790	.15430	.17920	.23290	-.01400	.15003
Flor-Tremol	.32750	.10000	.15370	.14510	.20100	-.03500	.13246
Actinolite	.26720	.11080	.11540	.15790	.24620	-.03710	.13215
Pargasite	.33100	.13480	.16310	.17020	.23580	.04170	.16565
Ti-Pargasite	.19570	.15990	.12040	.21470	.23890	.02630	.15601
Kakanut HB	.16290	.18810	.10560	.21040	.26910	.02410	.15977
Ferrotscherm	.30320	.20760	.12790	.17340	.32050	.10820	.19804
Ferrohastite	.27420	.17620	.12590	.17180	.29530	.02430	.16920
Oxy-Kaersut	.04940	.25110	.11620	.33650	.27380	.04070	.18964
K-Richterite	.29810	.13700	.15920	.14600	.26320	-.07210	.14225
Syn Rich 1	.35850	.11000	.17070	.08100	.23700	-.08820	.12541
Syn Rich 2	.35050	.09960	.16290	.07220	.24270	-.12040	.11495
Glaucophane	.29640	.24420	.14120	.02180	.35420	.01700	.16847
Cummingtonite	.23840	.14280	.13810	-.00420	.23980	-.06640	.10351
Grunerite	.25870	.12040	.11340	-.02270	.26200	-.09230	.09275
C-Mn-Cumm	.20940	.12690	.12760	.04860	.22440	-.04050	.10758
Zn-Cumm	.23060	.14010	.13350	.02040	.23130	-.06870	.10398

Figure 4.32a Variation in O(3)-M(1)-O(3) with $\tau_{M(1)-M(1)}$

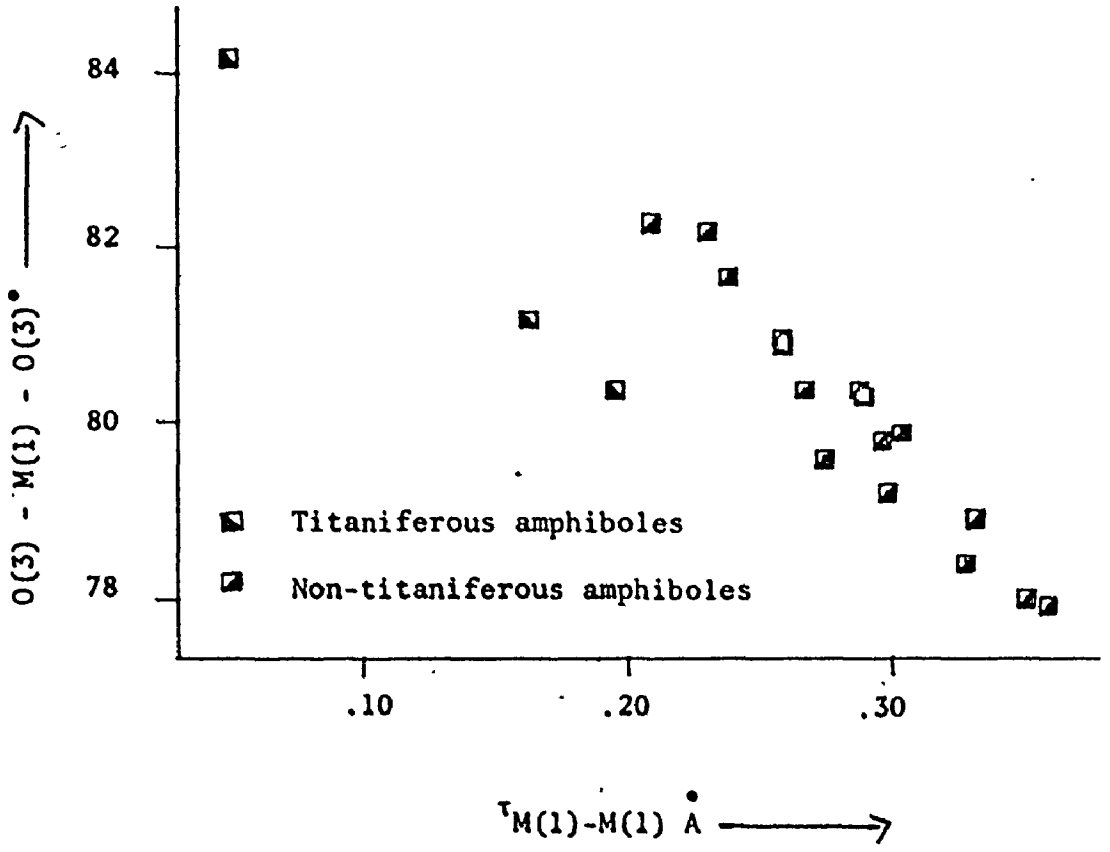

Figure 4.32b Variation in $\langle O(1^u) - M - O(2^d) \rangle$ with $\tau_{M(1)-M(2)}$

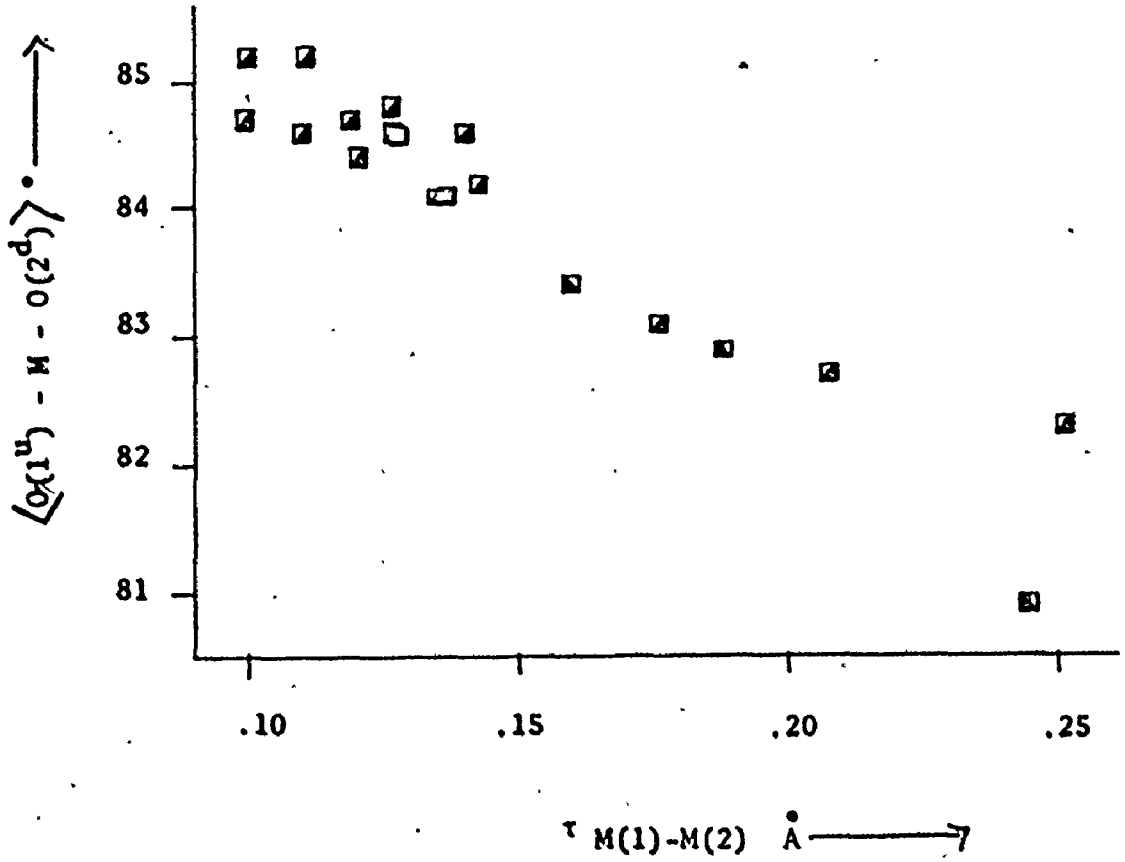

Figure 4.32c Variation in $\langle O(1^u) - M - O(3^d) \rangle$ with $\tau_{M(1)-M(3)}$

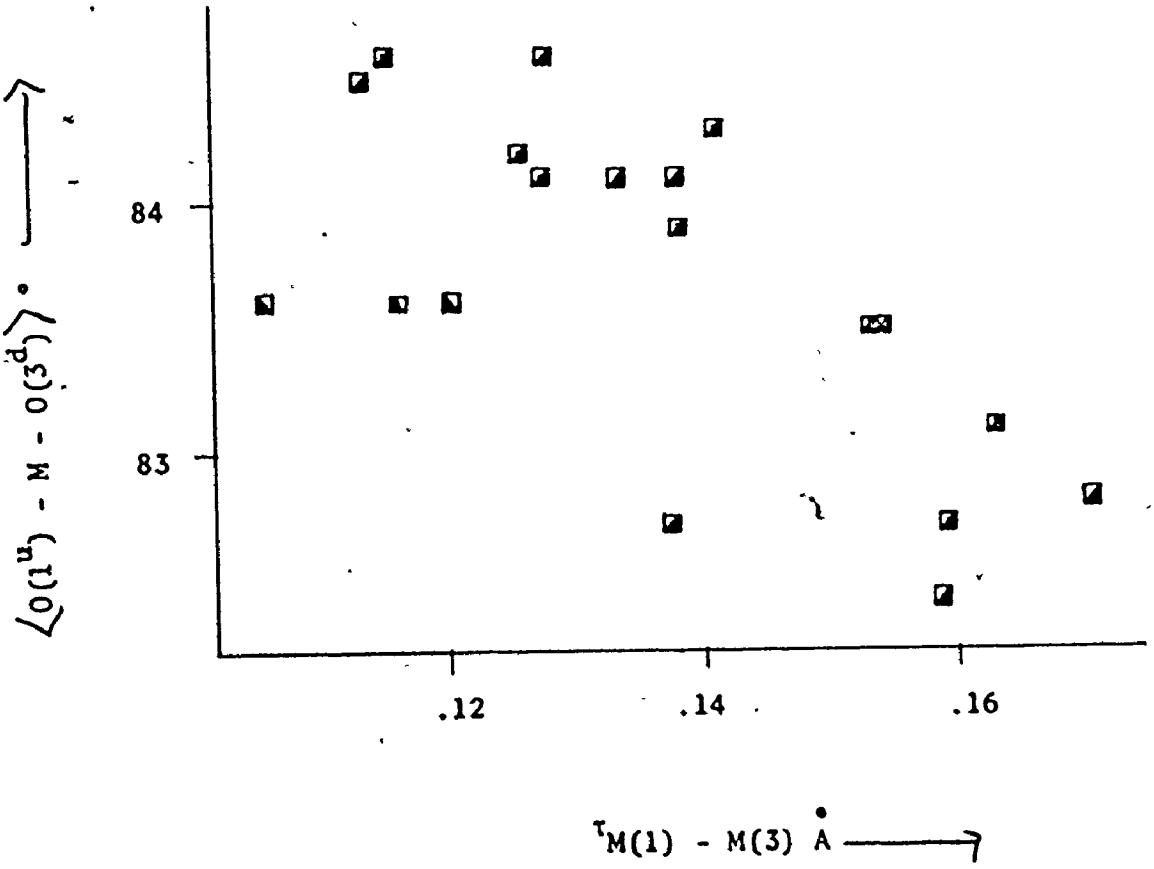

Figure 4.32d Variation in $\langle O(2) - M - O(2) \rangle$ with $\tau_{M(1) - M(4)}$

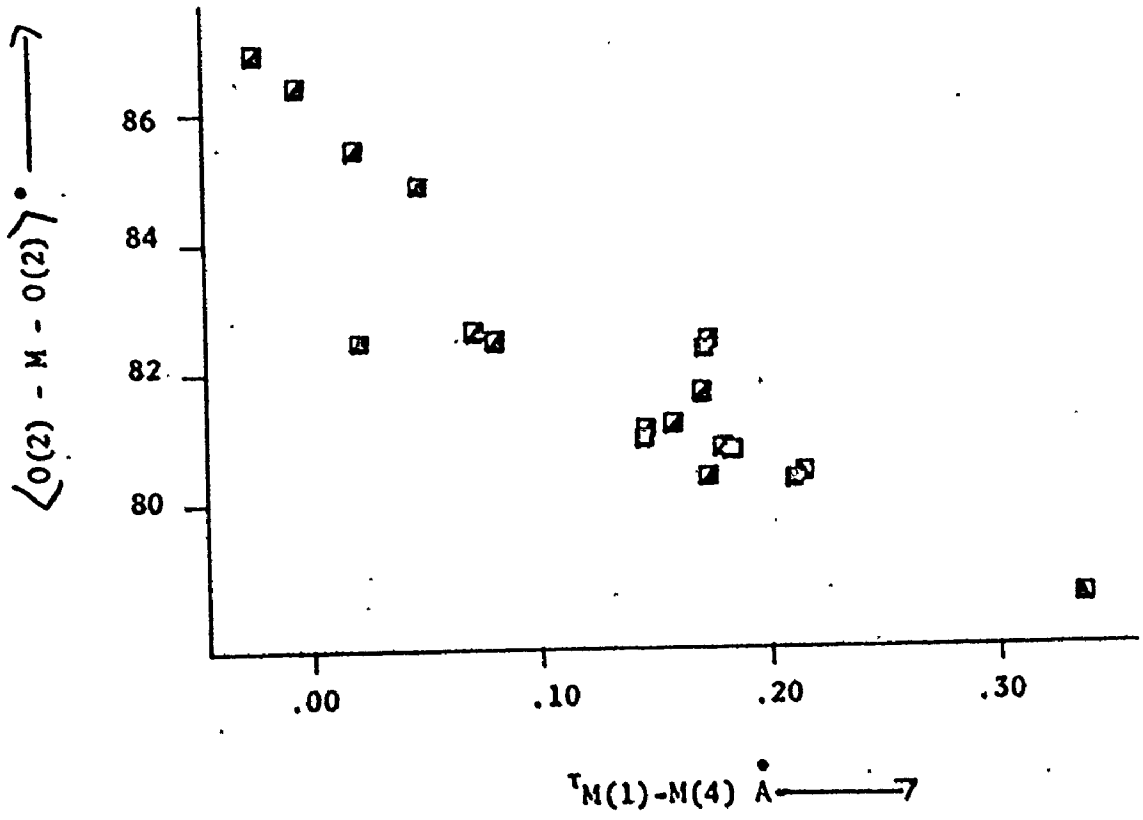

Figure 4.32e $\langle O(1^u) - M - O(1^d) \rangle$ versus $\tau_{M(2) - M(3)}$

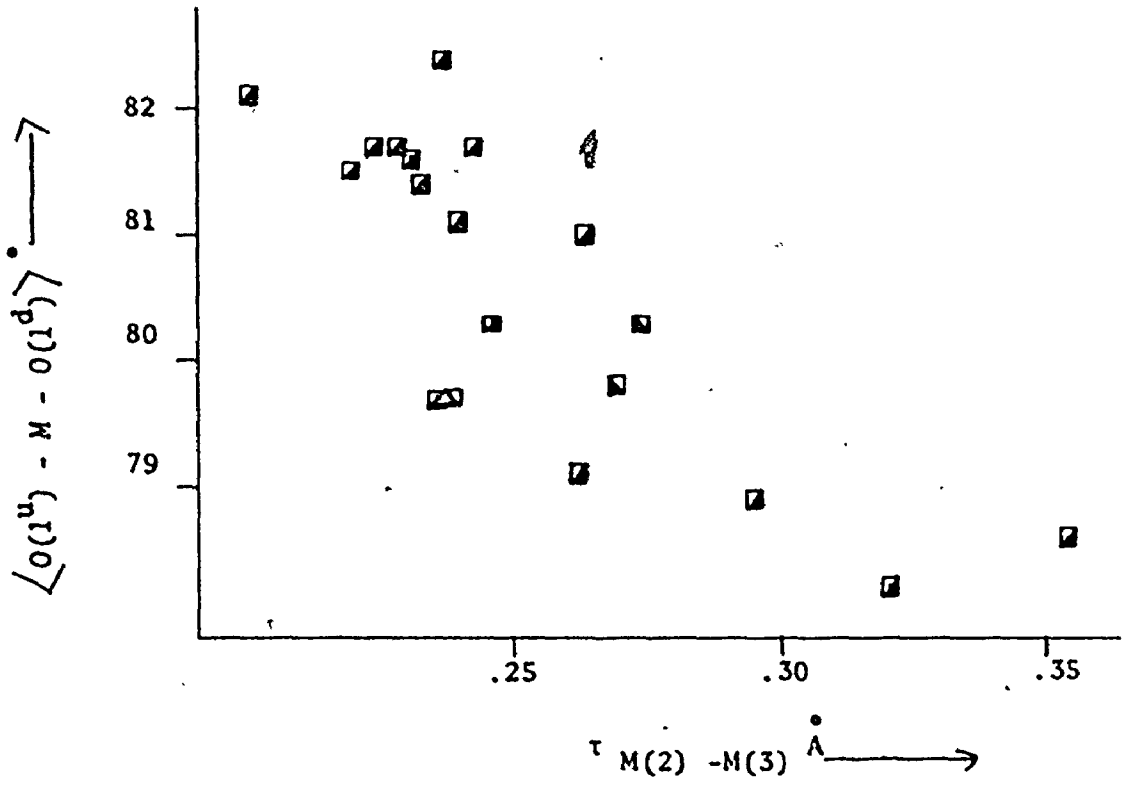

Figure 4.35f $O(2^u) - M - O(4^d)$ versus $\tau_{M(2) - M(4)}$

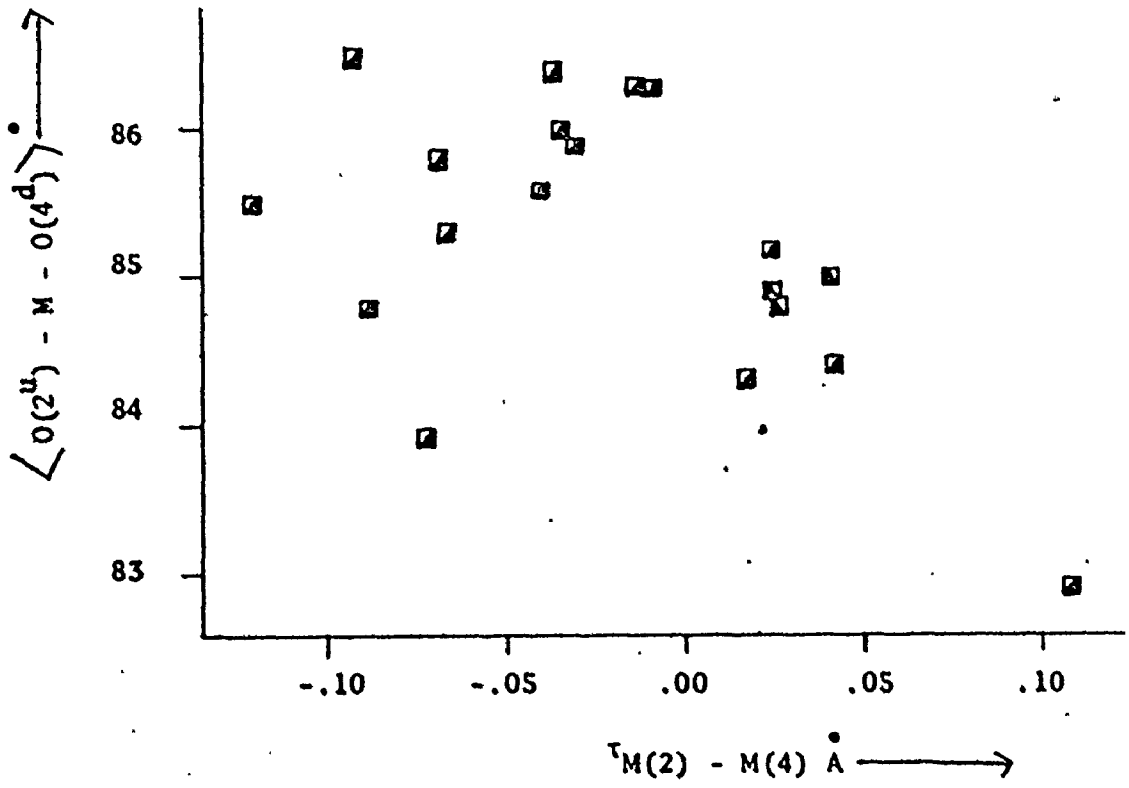

A rather speculative reason may be given for the existence of two trends; the three amphiboles constituting the lower trend are distinguished from the others by the presence of considerable Ti in octahedral coordination. This would indicate that attractive metal-metal interactions could occur (see Hawthorne & Grundy, in press) which would tend to offset the repulsive effect of other next-nearest neighbour interactions. For the M(1)-M(4) interaction, a fairly good linear relationship is developed; some deviation does occur and this is to be expected since the O(2) anion is not formally charge-balanced and bond strength requirements will also influence the distortion.

Figure 4.33a and b show the variation in O(2)-M(1)-O(2) and O(2)-M(4)-O(2) with $\tau_{M(4)-M(4)}$; there is a linear relationship between O(2)-M(1)-O(2) and τ for the calcic and sodic amphiboles but not for the ferromagnesian amphiboles. Conversely, for the O(2)-M(4)-O(2) angle a good linear relationship is developed for the ferromagnesian amphiboles but not for the calcic and sodic amphiboles. These results may be rationalized by considering the form of the bond strength curves for Fe^{2+}, Mn^{2+} and Ca^{2+} and Na^{+}. Since O(2) is formally charge deficient, one or more of the M-O(2) bonds must be short.

The sphere of influence of Fe^{2+} and Mn^{2+} is much smaller than that of Ca^{2+} and Na^{+} (see figure 4.4) and consequently, the major part of the formal charge deficiency must be compensated by a short

Figure 4.33a Variation in O(2) - M(1) - O(2) with $\tau_{M(1)-M(4)}$

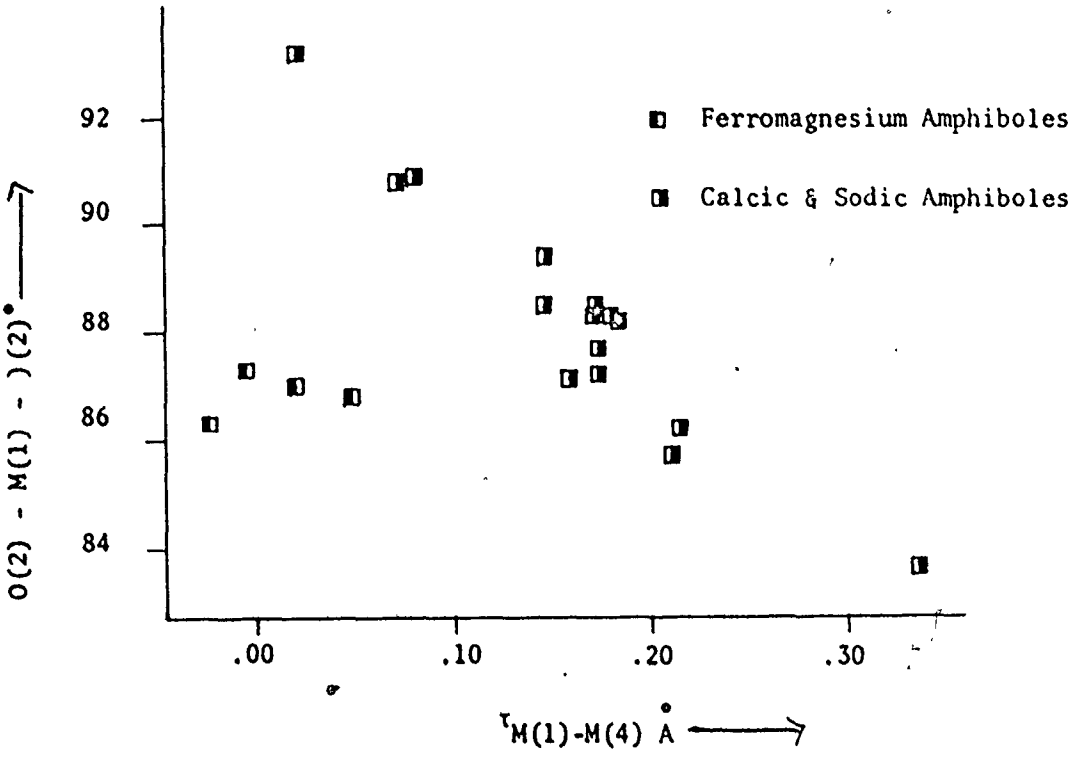

Figure 4.33b Variation in O(2) - M(4) - O(2) with $\tau_{M(1)-M(4)}$

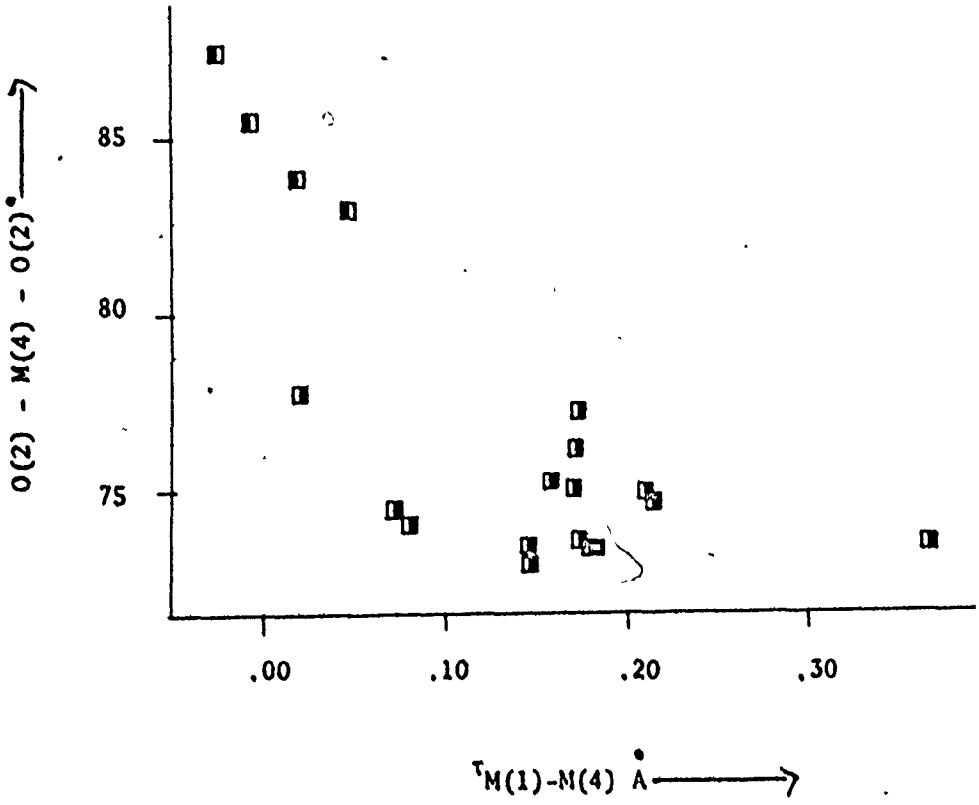

M(1)-O(2) bond in the ferromagnesian amphiboles as the M(4) cation also has to bond to the chain bridging oxygens. Thus, relaxation across the O(2)-O(2) edge in the ferromagnesian amphibole M(1) octahedron is constrained whereas in the calcic and sodic amphiboles, the constraint operates in the M(4) antiprism.

Reasonably good correlations are developed for $\tau_{M(1)-M(2)}$ and $\tau_{M(1)-M(3)}$ and, as with $\tau_{M(1)-M(1)}$ the Ti amphiboles appear to be a distinct population. The parameter τ appears to be an adequate index for rationalizing some of the angular distortions that occur in the octahedral layer. However, it is important to emphasize that these cation-cation relaxations are subject to charge-balance and inter-element linkage constraints.

Examination of Table 4.18 shows that the greatest cation-cation relaxations occur across the $O(1^u)$-$O(1^d)$ and O(3)-O(3) edges, the two shared edges in the structure that have formally charge-balanced anions. The one notable exception to this is oxy-kaersutite where the relaxation across O(3)-O(3) is extremely small, concordant with the fact that the O(3) anion in this dehydroxylated amphibole is not formally charge balanced. The importance of symmetry is very evident here; the large relaxations also occur along the two-fold axes where the cation may recoil away from the shared edge without any necessary expansion of the cell dimensions. Any effect of cation-cation repulsion on bond

lengths would thus be most apparent on those bonds with a strong component in the b direction; this is shown by figure 4.34a which shows the variation in $(\bar{R}-R)/\bar{R}$ for each M(1)-O bond with the controlling cation-cation relaxation parameter γ. The M(1)-O(1) and M(1)-O(2) bonds show a small range of γ and little or no dependence as forecast, while a well-developed linear relationship is exhibited by M(1)-O(3); the data for M(1)-O(3) is plotted separately in figure 4.34b to emphasize the relationship.

Although at first sight, a similar relationship might be expected for the M(2) site, this does not occur. The cation-cation relaxation between M(2) and M(3) is large but has no apparent relation to the bond length distortions. The anions coordinating M(2) have a large formal charge imbalance and the bond length distortions are dominated by this factor. Since this site is one of large structural compliance, its constituent cation radius varies much more than other sites and this is accompanied by a large variation in the mean cation-cation relaxation for this site.

Figure 4.35 shows the variation in $\langle\gamma\rangle$ with the ionic radius of the constituent cation for the M(2) site; a fairly good negative correlation is developed. Examination of Table 4.16 indicates that the slope for the $\langle M(2)\text{-}O\rangle - \langle r_{M(2)}\rangle$ correlation is anomalously small as it should equal

Figure 4.34a Variation in $(\bar{R}-R)/R$ with τ for the M(1)-O bonds in the clino-amphiboles

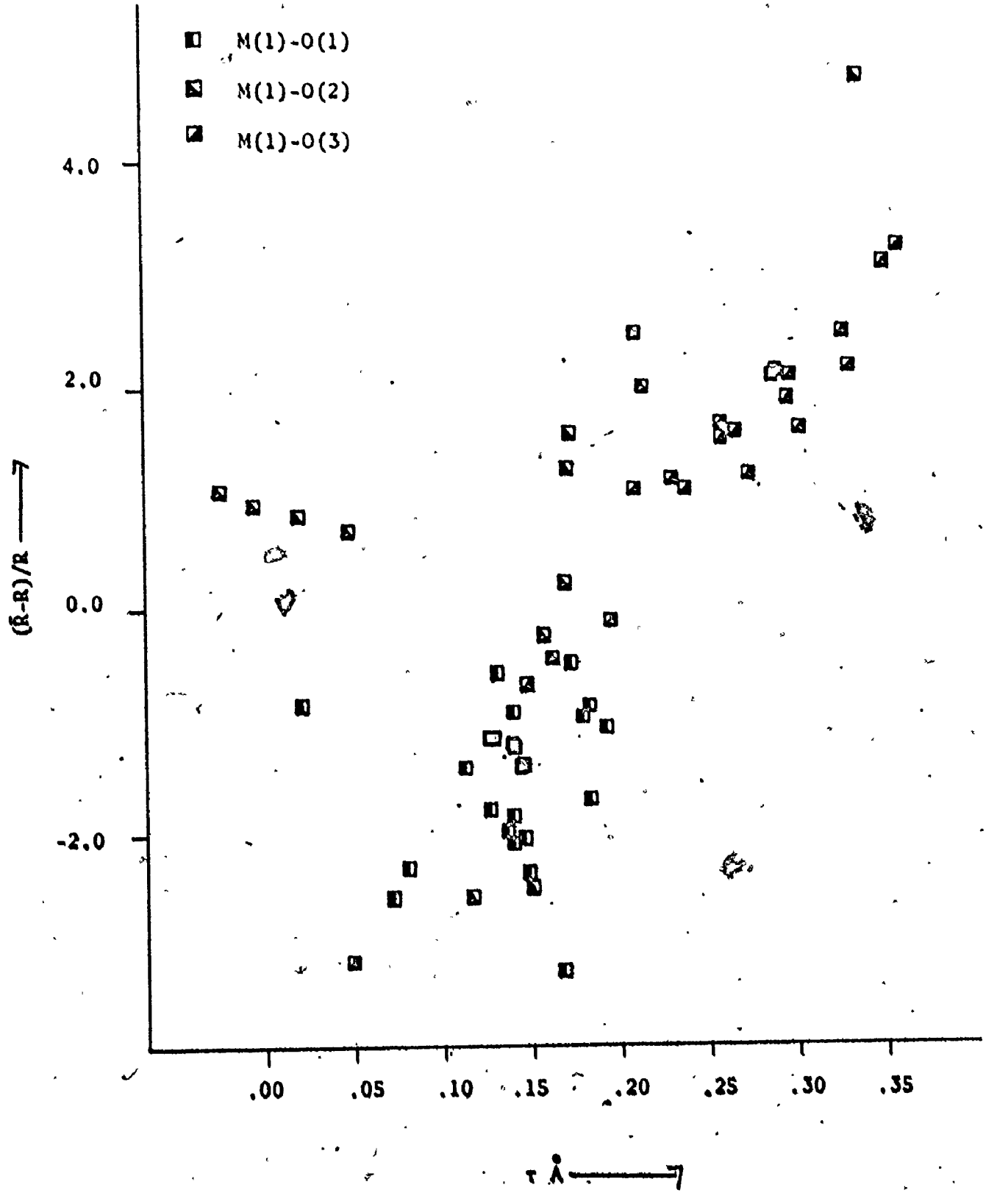

Figure 4.34b. Variation in $\Delta R/R$ for M(1) - O(3) with $\tau_{M(1)-M(1)}$

N.B. Bond lengths have been corrected to O^{IV} coordination

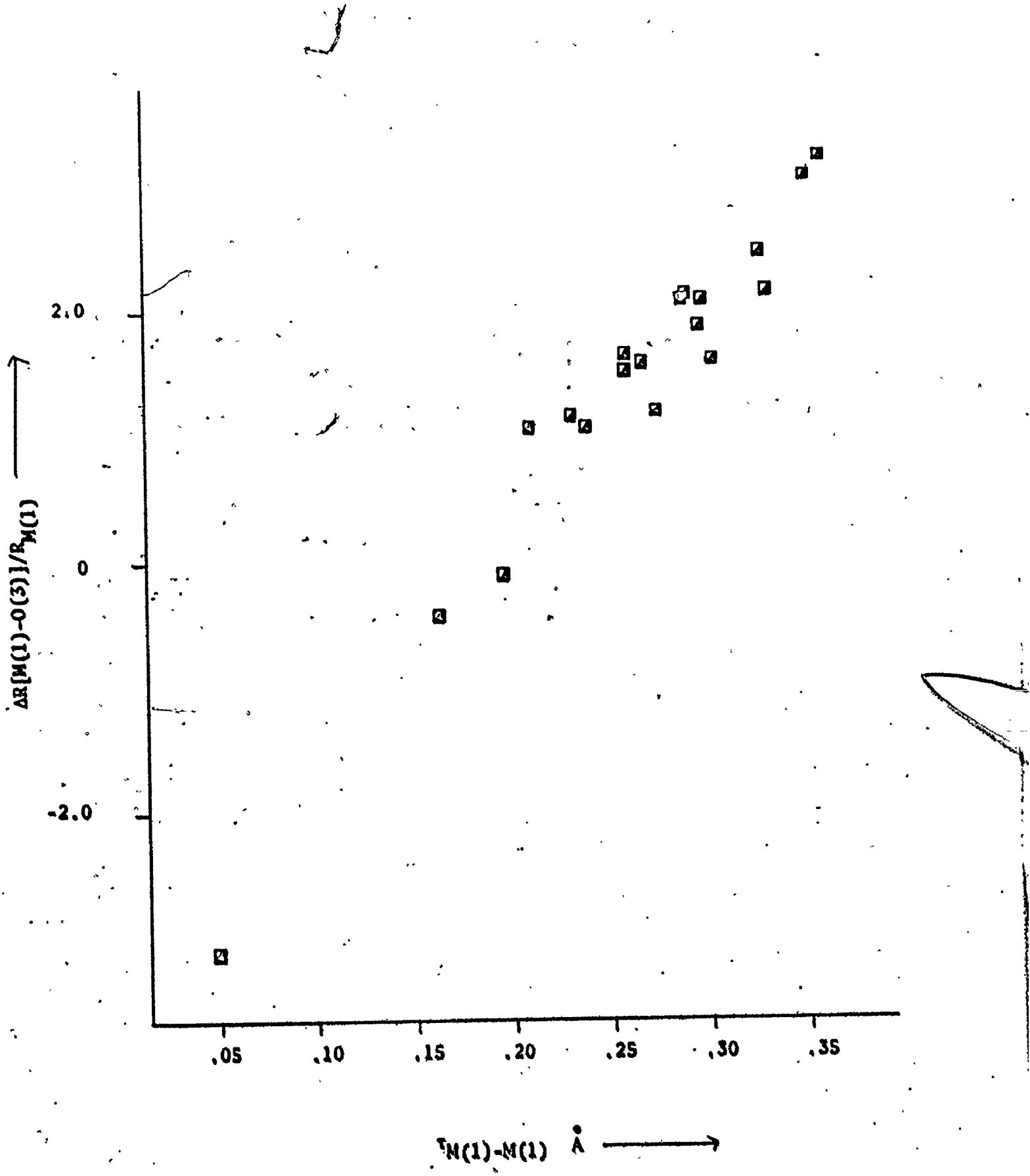

Figure 4.35 $\langle r_{M(2)-M(-)} \rangle$ versus $\langle r_{M(2)} \rangle$

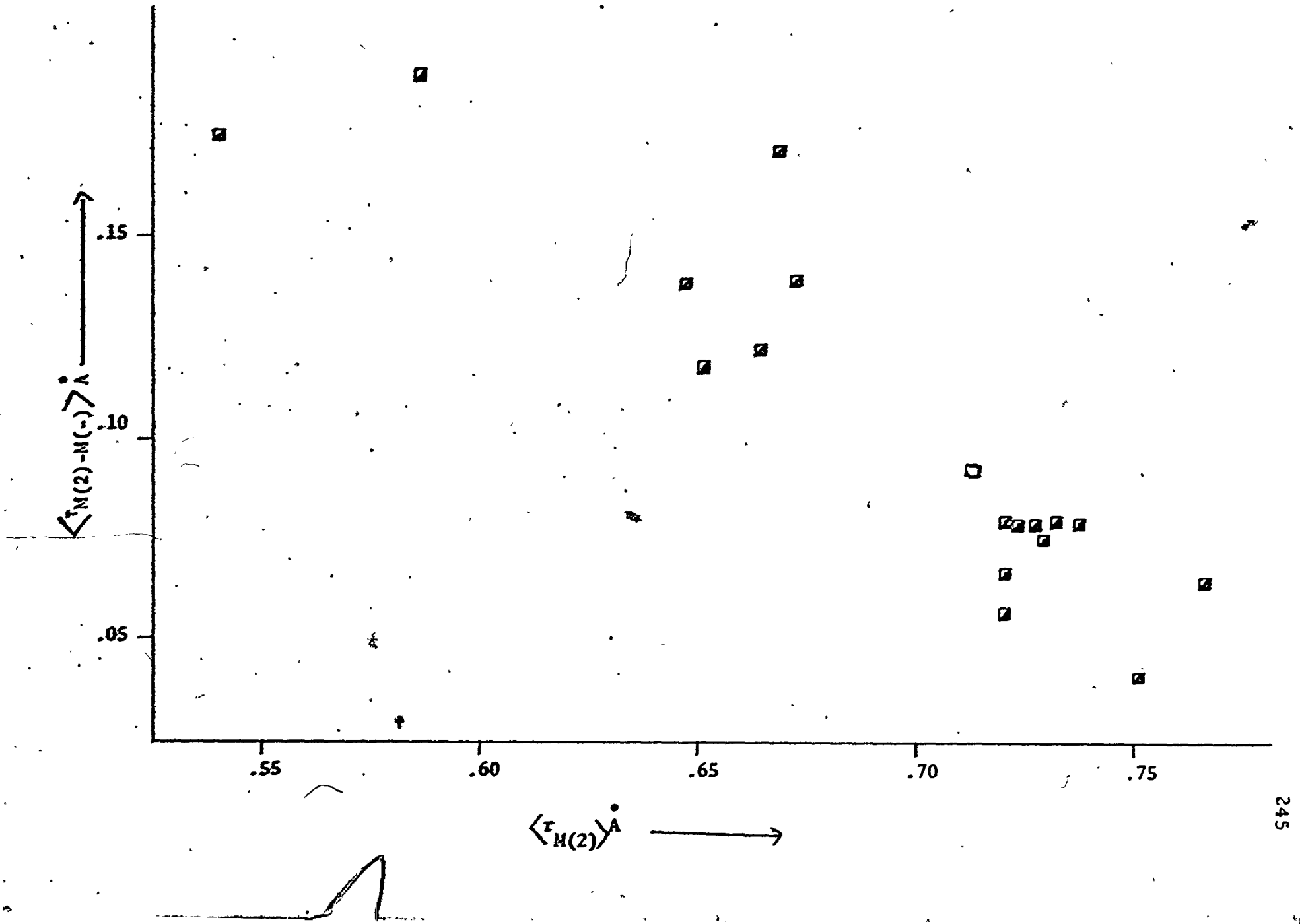

1 for a simple hard sphere model. This variation in cation-cation repulsion relaxation would apparently account for this anomalously shallow slope, an example of the 'high-order effects' postulated by Shannon and Prewitt (1969). It suggests that the site is "held open" for small cations and "held closed" for larger cations.

The cation-cation repulsion effect has a great effect on bond angle distortions in the M4 sites of the clinoamphiboles. In addition, some control on the bond lengths is exercised although this is subject to the constraints of electroneutrality and structural linkage.

Cation-anion electronegativity differences predict a much more ionic character for the octahedral element of these structures than for the tetrahedral element, and it would seem to be of considerable interest to examine the octahedral sites with the various bond-strength models outlined previously. Complete calculations for all the refined amphiboles were performed using the methods of Baur (1970) and Brown and Shannon (1973). However, the results were not encouraging and a detailed discussion is not justified. However, certain systematics were evident in the results that are germain to the application of this type of approach, and these will be briefly considered:

(a) Baur's Scheme

(i) The magnitude of the deviations between the observed and calculated bond lengths appears to be a function of the cation valence; this is reflected in the correlation coefficients given by Baur (1970, Table 1).

(ii) The scheme does not work well for very distorted polyhedra (e.g. M(2) site) and can forecast bond-length variations in the wrong direction.

(b) Brown & Shannon's Scheme

(i) Bond strength deviations from ideality are similar for all cations indicating that the observed bond lengths are less in accord with the theory for the lower valence cations (see Table 4, 10).

(ii) Bond strength sums around the lower valence cations (M^{2+}, M^{+}) are systematically high, indicating that some factor is affecting the mean bond length that is not adequately considered in this approach.

The parallel nature of these factors for both formalisms suggests that the basic concept of nearest-neighbour cation-anion interaction is not quite adequate as a description of bonding in structures; this implies that any further developments in this line should consider next nearest neighbour interactions. Indeed, the anion coordination

corrections in the Brown-Shannon scheme constitute a consideration of next-nearest interactions. Similarly, the consideration of anion-anion interactions in the Baur scheme (Baur, 1972) has produced impressive results.

THE A-SITE

The A-site cations can be positionally disordered into two crystallographically unique sites, the A(m) and A(2) sites; these do not correspond to the C2/m symmetry of these amphiboles unless a statistical occupancy occurs. The reason for this disorder is not apparent from this study. It is presumably connected with the charge-balance requirements of the bridging anions in the chain although no good correlation with cation species or tetrahedral Al occupancy is apparent. In a previous section it was shown that the steric requirements of inter-element linkage have a considerable effect on the stereochemistry of the double-chain element; this in turn could influence the A-site occupancies. It is probable that all of these factors contribute to the A-site disordering, and thus a much larger data set than is now available would be necessary to give any quantitative explanation.

The fact that complete site-populations cannot be derived by the x-ray method hinders the explanation of this disordering. The only method by which reliable site-populations could be derived is by a combined x-ray and neutron diffraction study.

SUMMARY

1. The amphibole structure is built up of two elements, the tetrahedral double chain and the octahedral strip. The size of the constituent cations affects the misfit of the ideal elements, and consequently the linkage requirements impose controls on the stereochemistry of the structure.

2. The variation in the tetrahedral bond distances for the Si-amphiboles may be rationalized by both 'covalent' and 'ionic' models. With the assumption that any inductive effect of non-tetrahedral cations will be reflected in the electronic structure of the TO_4^{n-} oxy-anion and thus the variation in T-O distances may be rationalized solely in terms of variations in tetrahedral stereochemistry, regression equations have been developed which adequately account for the observed Si-O bond length variations. Conversely, the essentially 'ionic' or bond strength models of Baur (1970, 1971) and Brown & Shannon (1973) adequately account for the observed bond lengths. This would tend to indicate a strong parallelism between the 'ionic' and 'covalent' models.

3. The mean T-O distance appears to be a linear function of the tetrahedral Al content for the clino-amphiboles, and site-occupancy curves have been derived for the tetrahedral sites. In addition, regression equations have been developed which appear to adequately account for the observed T-O distances in Al-amphiboles.

4. Mean M-O distances are a linear function of ionic radius of the constituent cations, provided the coordinating anions remain constant. Also the variation in bond angles and bond lengths may be rationalized on a semi-quantitative basis as the result of cation-cation repulsions across shared polyhedral edges.

CHAPTER V

SOME GEOLOGICAL IMPLICATIONS

CATION ORDERING IN CRYSTALS

Numerous criteria have been used to rationalize observed cation ordering patterns in mineral structures. However, none of these has proved to be completely satisfactory and their deficiencies have often been compounded by misuse. In order to avoid this confusion, a preliminary discussion of each of them is warranted.

Ionic Size

The concept of ionic size is given in an earlier section. A reversal of the ideas leading to this concept will obviously give some indication of the ordering patterns in crystals. For example, in Leucophanite, $Ca,NaBeSi_3O_6F$ (Cannillo, Giuseppetti & Tazoli, 1967) the difference in ionic radius indicates that the Ca^{2+} and Be^{2+} will be ordered into the [8]- and [4]-coordinated sites respectively.

This criterion is of use only in extreme cases such as the previous example where distinct variations in cation coordination occur; for cations of a similar size substituting into similar sites, this method appears to lose its effectiveness. For example, the M(2)-O distance in Tremolite (Papike et al., 1969) is the largest of the octahedral site mean bond lengths; however, the M(2) site in Actinolite (Mitchell, Bloss and Gibbs, 1970, 1971) is depleted in Fe^{2+} with respect to the M(1) and M(3) sites. Yet numerous examples exist where ordering patterns of Mg-Fe^{2+} have been 'rationalized' on this basis; of course, this criterion will forecast the corrected distribution in many cases since the number of possible arrangements is low (often 2). The misuse of this idea is to be distinguished from the reciprocal relation often used by crystallographers (and shown for the amphiboles in this study) that the size (mean bond length) of a site is a function of the ionic radius of its constituent cations.

Charge Balance

According to Pauling's second rule, all atoms in a crystal should be approximately charge balanced; this has been discussed in detail in a previous section, and although deviations do occur, they tend to be offset by variations in bond lengths. The requirement that the anions be charge balanced imposes certain restrictions on ordering for polyvalent cation substitutions in crystals. This is well illustrated by some of the

amphibole structures: if Tremolite ($Ca_2Mg_5Si_8O_{22}(OH)_2$) is taken as a 'parent' structure, Glaucophane ($Na_2Mg_3Al_2Si_8O_{22}(OH)_2$) is formed by substitution of $2Na^+$ for $2Ca^{2+}$ and $2Al^{3+}$ for $2Mg^{2+}$.

In tremolite, the M(4) cation forms two strong bonds with the O(2) and O(4) anions (see figure 1.1) and consequently, when Ca^{2+} is replaced by Na^+ at M(4), the O(2) and O(4) anions receive half the bond strength from the M(4) cation. The M(2) site is the only octahedral site coordinated by both O(2) and O(4) and consequently, Al^{3+} would be expected to be ordered into M(2) in order to maintain charge balance at O(2) and O(4). This result is confirmed by the crystal structure refinement of Glaucophane (Papike & Clarke, 1968). Restrictions of this type are quite common in minerals and appear to exercise a considerable influence upon cation ordering patterns.

Polarization

Strongly polarizing cations usually form covalent bonds and thus will tend to be ordered into those sites where the coordinating anions are formally strongly underbonded. The concept of electronegativity could also be used in the same argument (although see discussion by Fajans, 1967 and Jørgenson, 1966, 1967).

Crystal Field Stabilization Energy

The basic principles of crystal field theory are well-known and require no discussion; for details, see Griffith, 1961; Ballhausen, 1962; Hutchings, 1964.

In a crystal where Fe^{2+} occurs in more than one site, the energy of the one spin-paired 3d-orbital at each site relative to the mean orbital energy at that site is taken to indicate the site-preference if all other energy contributions are ignored. Using this approach, McClure (1957) and Dunitz & Orgel (1957) were able to rationalize the structures of transition-metal spinels from optical spectra measurements. Numerous other applications of this principle (for a review, see Burns, 1970) have had partial success, and qualitative rules have been developed (e.g. Burns, 1968a, b) to predict Fe^{2+} site-preferences based on mean bond length and site-distortion parameters.

Relative C.F.S.E.'s have been estimated from optical absorption spectra of silicates. However, this is subject to error since the interpretation of these spectra is not simple and many erroneous transition assignments have been made in the past [e.g. Orthopyroxene-Bancroft & Burns (1967); Runciman, Sengupta & Marshall (1973); Olivine-Burns (1970); Runciman, Sengupta & Gourley (1973)]. An attempt was made in the present study to calculate C.F.S.E.'s using a first-order perturbation method incorporating the crystal field and the d-orbital

wave-equations in the form of spherical harmonics (Griffith, 1961); using the free-ion values of $\langle r^2 \rangle$ and $\langle r^4 \rangle$ from Freeman & Watson (1965), the agreement (for trial calculations on simple silicates) with optical spectra was poor and the calculations were abandoned. Subsequently, a semi-empirical method of calculation of C.F.S.E.'s was published by Wood & Strens (1972) where the agreement with optical spectra is excellent. If more extensive tests prove this method to be adequate, it may form the basis for a more successful application of crystal field theory to cation ordering.

Site Potentials

A site-potential is defined as the energy required to separate a particular ion from its equilibrium position in the structure to an infinite distance. The total site-potential consists of the electrostatic site-energy, the repulsive energy, the van der Waals energy and various multipole interactions. Few calculations have, as yet, been performed on silicates and those have been fairly simple. All calculations have ignored the van der Waals and polarization energies, and repulsive energies have only involved nearest neighbours, whereas more sophisticated calculations (Reitz, Seitz and Genberg, 1961; Benson and Dempsey, 1961; Wackman, Hertha and Frounfelder, 1967) show that repulsive interactions

between other neighbours are also of importance. In addition, for a disordered structure, the actual configuration surrounding a particular cation is not known from crystal structure refinement as only the mean structure is determined; this difference between the actual and mean environments has been shown to be of importance in energy calculations (Das, 1960).

Notwithstanding these drawbacks, preliminary calculations (Raymond, 1971; Whittaker, 1971; Ohashi & Burnham, 1972) have had some success, although the question does arise as to how meaningful this is. The most extensive and systematic calculations are those of Whittaker (1971) which were performed on amphiboles. The calculated site-potentials involved only the electrostatic (Madelung) energy component, with the assumption that the repulsive potential would be fairly constant in all cases. This is most probably an invalid assumption since $|\partial E_{REP}/\partial R| > |\partial E_{MAD}/\partial R|$ for most, if not all simple intermolecular interactions (Kittel, 1966; Tosi, 1964). This could account for the marked discrepancies between some of the site-preferences forecast by Whittaker (1971) and some of those observed in this study (see Table 5.1). Because the site-preference energies involve small differences between large numbers, more detailed calculations are needed before much confidence may be placed in the results.

TABLE 5.1: A COMPARISON OF THE SITE-PREFERENCES (IN AMPHIBOLES) FORECAST BY WHITTAKER (1971) AND THOSE OBSERVED FROM SITE-POPULATION REFINEMENT OF SINGLE-CRYSTAL X-RAY DATA

Predicted	Observed
Richterite, $Na_2Ca[M]_5Si_8O_{22}(OH)_2$	
$[Na]^A$ $[Na, Ca]^{M(4)}$	$[Na]^A$ $[Na, Ca]^{M(4)}$
Lithium Richterite, $LiNaMg_6Si_8O_{22}F_2$	
$[Na]^A$ $[Mg]^{M(4),M(1),M(2)}[Li]^{M(3)}$	Proto-amphibole, $\sim Li_{1.2}Mg_{6.44}Si_8O_{22}F_2$ has: $[Li]^A$ $[Li]^{M(4)}$ $[Mg]^{M(1),M(2),M(3)}$
Oxy-Amphibole	
$[M^{3+}, M^{4+}]^{M(1)}$	Not applicable; most oxy-amphiboles have oxidised rapidly in the solid state and quenched. Thus, the observed site-populations are those of a normal hydroxy-amphibole.
Hydroxy- & Fluor-amphiboles	
$[M^{3+}]^{M(2)}$	$[M^{3+}]^{M(2)}$
"Hornblende"	
$[Al^{3+}]^{T(2)}$ $[Si^{4+}]^{T(1)}$	$[Al^{3+}]^{T(1)}$ $[Si^{4+}]^{T(2)}$
Tschermakite	
$[Al^{3+}]^{T(2)}$ $[Si^{4+}]^{T(1)}$	$[Al^{3+}]^{T(1)}$ $[Si^{4+}]^{T(2)}$

Quantitative Considerations

In a crystal structure, the stable configuration is determined by the Gibbs free energy (Born & Huang, 1954) which is at a minimum at equilibrium. Thus the expression

$$G = U + PV - TS$$

is a minimum for an observed cation distribution at the temperature and pressure of equilibration. With temperature and pressure constant, variation in cation disorder produces changes in U, V and S. The changes in S (entropy) will mainly be configurational (Strens, 1968) although some vibrational contributions are feasible if the relative vibrational energy levels differ sufficiently in various configurations. Changes in volume are also produced by ordering (Ernst, 1963; Smith, 1968). However, changes in internal energy probably contribute most to changes in G, and are usually invoked to rationalise cation ordering.

Internal energy changes associated with ordering may be divided into two types, structure energy changes and C.F.S.E. changes. It should be noted that the total structure energy and not the site-potential is the determining factor in site-occupancy changes if only the internal (structure) energy is considered. Thus, many factors are involved in the Gibbs free energy changes that accompany ordering, and failure of any

method that does not incorporate all of the above energy terms is to be expected in many cases.

Empirical Considerations: Cation ordering in Amphiboles

(i) The M-sites

The distribution of a cation species over various non-equivalent sites in a structure will be affected by the other cation species present. This has been considered implicitly by most workers but has been only invoked in the most obvious cases. For example, the Fe^{2+} site-preference M(4)>M(1), M(2), M(3) is observed in the non-manganiferous cummingtonites; the presence of Ca^{2+} in the tremolites alters the Fe^{2+} site-preference to M(1), M(2), M(3)>M(4), even though the M(4) is still the largest and most distorted site. In exaggerated cases such as this, the difficulty is overcome by considering the minerals as two different series. A similar but less pronounced effect occurs in the cummingtonite structures; as indicated above, Mg-Fe^{2+} cummingtonites exhibit the site-preference M(4)>M(1), M(2), M(3). When Mn^{2+} is present, it tends to substitute into the M(4) site. The two Mn-cummingtonites for which data are available (Bancroft, Burns & Maddock, 1967†, and this study) show the Fe^{2+} site-preference of M(2)>M(4)>M(1), M(3).

† there is a misprint in Table 4, page 1021 of this reference; the quoted Fe^{2+} occupancy of M(2) in the unit formula should read 0.57 NOT 0.07.

In these obvious cases, the presence of cations other than Mg and Fe^{2+} has a marked effect on the Fe^{2+} ordering patterns. This suggests that the presence of cations other than Mg and Fe^{2+} could also have an effect on the Fe^{2+} site-populations, albeit a more subtle one than the examples given above. In the previous chapter, it was shown that the angular distortional parameters of the M(1) and M(3) sites are a function of the mean ionic radius of the cations occupying the M(2) site. These distortional parameters will have a strong effect on the site-preference energies of the cations occupying the M(1) and M(3) sites. Thus it is feasible that the M(2) cations affect the degree of ordering between the M(1) and M(3) sites. Figure 5.1 shows the variation on

$$K_D \left(= \frac{X_{Fe}^{M(1)} \ (1 - X_{Fe}^{M(3)})}{(1-X_{Fe}^{M(1)}) \ X_{Fe}^{M(3)}} \right)$$

with the mean ionic radius of the M(2) cations for the amphiboles considered in this study. A fairly good correlation is developed, and linear regression analysis gave a correlation coefficient of 0.89, indicating an 80% dependency of the ordering parameter on the M(2) cations.

Several authors (Burns & Prentice, 1968; Bancroft & Burns, 1969) have attempted to qualitatively relate the degree of $Mg\text{-}Fe^{2+}$ disorder in clino-amphiboles to the temperature of crystallization. As

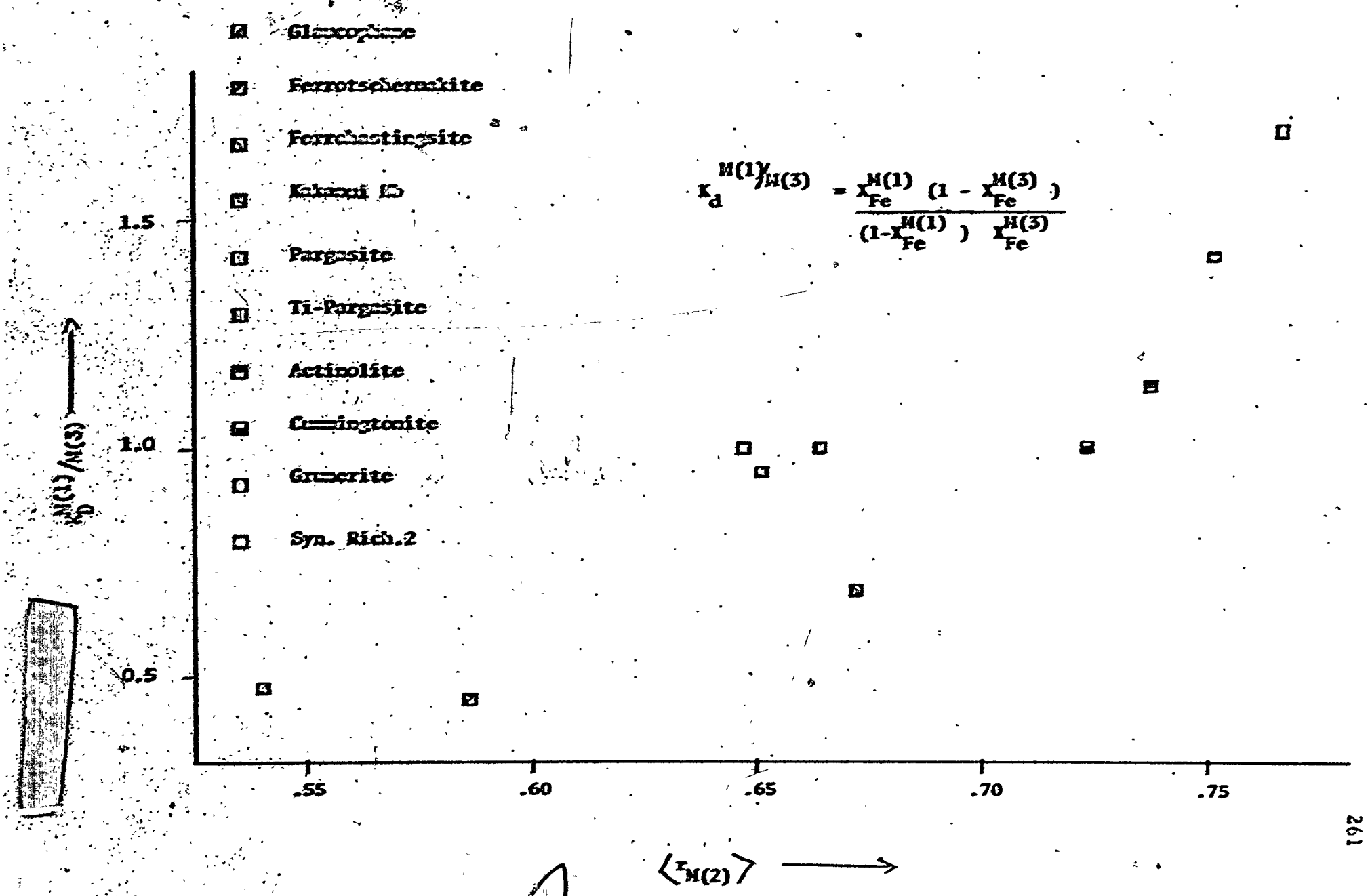
Glaucophane
Ferrotschermakite
Ferrohastingsite
Kaersutite
Pargasite
Ti-Pargasite
Actinolite
Cummingtonite
Grunerite
Syn. Rich.2
1.5
1.0
0.5
.55
.60
.65
.70
.75
$K_d^{M(1)/M(3)}$
$\langle r_{M(2)} \rangle$
$K_d^{M(1)/M(3)} = \frac{X_{Fe}^{M(1)} (1 - X_{Fe}^{M(3)})}{(1 - X_{Fe}^{M(1)}) X_{Fe}^{M(3)}}$

indicated above, much of the observed disordering is apparently a steric effect due to bulk compositional variation. The higher valence cations tend to substitute into the M(2) site, and the species and amounts of these cations is a function of several factors. A correlation between octahedral Al and rock composition has been noted by several workers (Tilley, 1937; Bloxam & Allen, 1960; Leake, 1965); highly aluminous amphiboles occur in highly aluminous rocks. In addition, it has also been suggested that the amount of octahedral Al is partially a function of pressure (Leake, 1965, page 312) although this effect is not yet well-characterized and is possibly of less importance than rock composition. The Fe^{3+} content is presumably a function of oxygen fugacity at the time of crystallization. A recent study of synthetic magnesiohastingsite (Semet, 1973) showed that the Fe^{2+}/Fe^{3+} ratio in this amphibole was a function of the oxygen fugacity of synthesis. Finally, the amount of Ti in an amphibole is partially a function of the temperature of crystallization (Compton, 1958; Leake, 1965). Thus the chemistry of the M(2) site is a complex function of many factors, the most dominant of which is probably bulk rock composition (since bulk composition will also tend to control the total amount of Fe in the amphibole). Hence any attempt to relate the degree of ordering in amphiboles to conditions of equilibration must take into account these bulk compositional effects.

(ii) The T-sites

In general, the tetrahedral sites in the amphiboles are occupied only by Si^{4+} and Al^{3+} in significant amounts. Analysis of the mean bond lengths indicates the Al^{3+} site-preference $T(1) \gg T(2)$ in all clino-amphiboles so far examined. This distribution does not agree with several schemes of Al^{3+} site-preference prediction developed recently. Whittaker (1971) predicts the Al^{3+} site-preference $T(2) > T(1)$ for "common hornblende" $[Ca_2Mg_4Al\,Si_7Al\,O_{22}(OH)_2]$ and tschermakite $[Ca_2Mg_3Al_2Si_6Al_2O_{22}(OH)_2]$*; this is not compatible with the results for ferrotschermakite, and the consistent results on a fairly wide range of amphiboles suggests that the site-preference $T(2) > T(1)$ is unlikely.

Brown & Gibbs (1970) propose that Si^{4+} will prefer those sites involved in the widest $\langle T\text{-}O(br)\text{-}T \rangle$ angles, and Al^{3+} [+B, Be & Mg] will prefer those sites involved in the smallest $\langle T\text{-}O(br)\text{-}T \rangle$ angles; this rule was proposed for framework silicates and, as they state, does not appear to work well for chain silicates; the much larger data set available in the present study confirms this contention. Gibbs (1969) suggested that the Al^{3+} distribution in amphiboles will be controlled by charge-balance considerations; this appears to be borne out both by the observed distributions and by the structural discussions given in an earlier chapter.

---

* The formula given by Whittaker (1971, page 995, line 13) for tschermakite-$Ca_2Mg_3Al_2Si_7Al\,O_{22}(OH)_2$-is in error.

The O(4) anion is formally under-bonded, suggesting that the substitution of Al^{3+} for Si^{4+} in the T(2) site is not favoured by local charge-balance criteria. However, where the total amount of tetrahedral Al significantly exceeds 2 atoms/formula unit (as in Alumino-hastingsite), significant amounts of Al enter the T(2) site. This is in agreement with the Al-avoidance rule (Loewenstein, 1954) which states that Al-O(br)-Al linkages will not occur in silicates. This rule was rationalized by Goldsmith and Laves (1955) as being due to local charge-balance requirements, and this explanation holds well for the amphiboles where the O(7) anion is coordinated only to two T(1) tetrahedra.

THERMAL STABILITY OF CLINO-AMPHIBOLES

It is apparent from discussions in the previous chapter that linkage requirements play an important role in controlling structural distortions in the clino-amphiboles. These linkage requirements will also control the thermal stability limits which will be affected by the relative thermal expansions of the octahedral strip and the tetrahedral layer.

It has been shown that in an 'ideal' amphibole structure, the $\langle$T-O(br)-T$\rangle$ angle is $\sim 141^{\circ}$, correlating with the mean T-O(br)-T angle found by Liebau (1951) in a survey of silicate structures. The fact that the minimum tetrahedral distortions are observed for this

value of ⟨T-O(br)-T⟩(see Figure 5.2) suggests that this may be a minimum energy configuration. With this assumption, certain generalizations may be made as to the effect of temperature on the clino-amphibole structure. If the amphiboles are assumed to crystallize in this minimum energy configuration, it is apparent that $\langle\langle$ T-O(br)-T$\rangle_{T(-)}\rangle$ must decrease with falling temperature to produce the observed values. Thus the thermal expansion of the octahedra must be greater than that of the tetrahedra; this has been confirmed for cummingtonite (Brown et al., 1972; Sueno et al., 1972). Thus while at room temperature, the interelement linkage involves the fitting together of an octahedral strip with an oversized tetrahedral double chain, the upper thermal stability is probably controlled by the fitting together of an octahedral strip with an undersized tetrahedral double chain. If this is so, the value of $\langle\langle$ T-O(br)-T$\rangle_{T(-)}\rangle$ and/or $\langle \Sigma\, \delta l^2_{T(-)}\rangle$ may reflect the amount of contraction due to cooling, and hence give an indication of the upper thermal stability limits and typical crystallization or equilibration temperature. Below is given a comparison of the $\langle\langle$ T-O(br)-T$\rangle_{T(-)}\rangle$ angle and $\langle \Sigma\, \delta l^2_{T(-)}\rangle$ with the upper thermal stability at 1 kb.:

Figure 5.2 Variation in $\langle\langle T\text{-}O(br)\text{-}T\rangle_{T(-)}\rangle$ with $\langle\Sigma\delta\ell^2_{T(-)}\rangle$

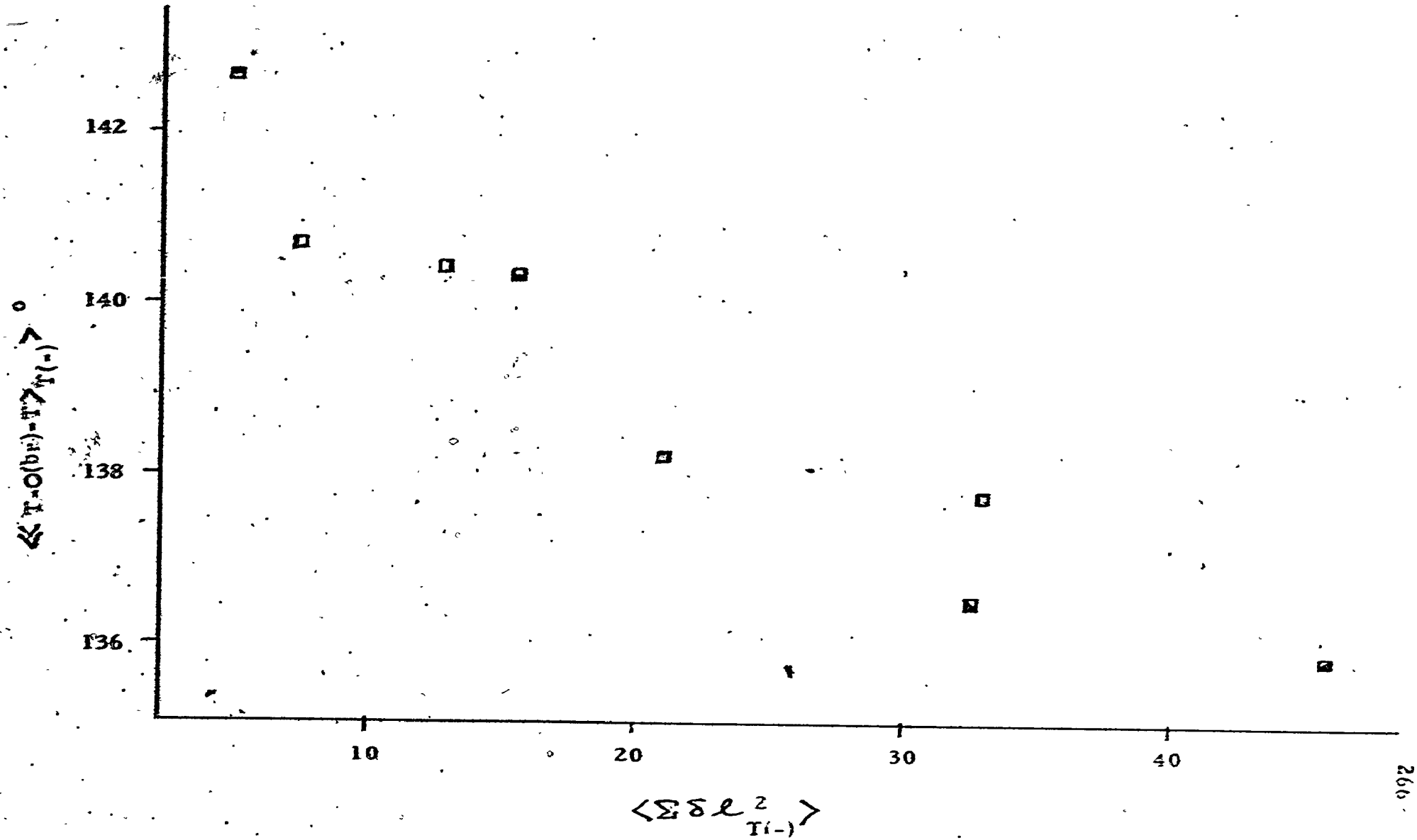

	$\ll$T-O(br)-T$\rangle_{T(-)}$	$\langle\Sigma\delta\ell^2\rangle_{T(-)}$	Analogue*	T°C. (1 k
S.R.1	135.83	45.76	$[Na_2Ca\,Mg_5Si_8O_{22}(OH)_2]$	1031
S.R.2	136.5	32.53	$\{[Na_2Ca\,Mg_5Si_8O_{22}(OH)_2]$	1031
			$[Na_2Ca\,Fe_5Si_8O_{22}(OH)_2]\}$	811
Trem	137.76	32.92	$Ca_2Mg_5Si_8O_{22}(OH)_2$	865
Glauc	140.45	12.85	$\{Na_2Mg_3Al_2Si_8O_{22}(OH)_2$	868
			$Na_2Fe_3Al_2Si_8O_{22}(OH)_2\}$	358

The stability data were taken from Boyd (1959), Hoffmann (1972) and Charles (1972). In addition, petrographic relationships (e.g. Bonnichsen, 1969) indicate that grunerite is often of late-stage, low temperature paragenesis as would be expected from figure 5.2.

However, consideration of the other amphiboles in figure 5.2 indicates that other factors are involved. The fluor-tremolite of Cameron (1970) was synthesised at a temperature of 1150°C. which is about the maximum thermal stability of fluor-tremolite (Troll & Gilbert, 1972). The synthetic richterites S.R.1 and S.R.2 were synthesised at 1170-1000°C. and 1050-880°C. (Cameron & Gibbs, 1971) indicating that the maximum

---

* Large curly brackets denote that the structural data comes from an amphibole intermediate to those indicated; the square brackets denote that the stability limits are for a hydroxy analogue of a fluor-amphibole.

thermal stability of these fluorine amphiboles is at least as high as that of their hydroxyl analogues. The additional stabilizing effect of fluorine (which is not recognised in figure 5.2) is its effect on the dimensions of the octahedral strip (Cameron, 1970) which are reduced. Comparison of the octahedra in fluor- and hydroxy-tremolite shows that the anion sheets defining the upper and low bounds of the strip are much more sheared in fluor-tremolite producing a lengthening of the unshared edges relative to those of tremolite:

	$\epsilon(O\text{-}O)_{M(1)}$	$\epsilon(O\text{-}O)_{M(2)}$	$\epsilon(O\text{-}O)_{M(3)}$
Hydroxy-tremolite	1.101	1.039	1.116
Fluor-tremolite	1.112	1.041	1.121

This will offset the need for smaller T-O(br)-T angles to maintain interelement linkage (since the double chain cannot rotate very much because the bonding requirements of the M(4) cation (Ca^{2+}) is the same in both structures). As temperature increases, the smaller fluor-tremolite octahedra have a larger range of thermal expansion while maintaining inter-element linkage, and consequently will exhibit a higher thermal stability. The same arguments presumably may be applied to the fluor-richterites which most probably have a higher thermal stability than their hydroxyl analogues for the same reason.

The above relations are reflected in the paragenesis of these amphibole types. Richterites are typically found in potassic lavas (Pridor, 1939; Carmichael, 1967), late-stage alkaline intrusives (Larson, 1942), ultramafic nodules in kimberlites (Erlank & Finger, 1970), and even as a primary phase in kimberlites (Aoki, Fodor, Keil & Dowty, 1972), all high temperature environments. Tremolite (sensu stricto) typically occurs in calc-silicate skarns and marbles (e.g. Engel & Engel, 1953, 1958, 1960 and 1962) and marks the onset of 'higher temperatures' (Bowen, 1940). Glaucophanes are typically a high-pressure, low temperature mineral occurring in the glaucophane schist (or 'blue schist') facies (e.g. Ernst & Seki, 1967; Coleman & Lee, 1963), where estimated temperatures of formation are between 200-300°C. (Ernst & Seki, 1967), although this is probably a little low for the glaucophane of Papike & Clark (1968) in figure 5.2. Grunerites are typically found in metamorphosed iron-formations and is generally interpreted as a very late-stage retrograde mineral (Bonnichsen, 1969). Thus the paragenesis of these amphiboles correlates very well with that indicated by an analysis of their crystal structure data.

The one exception appears to be cummingtonite which is apparently stable in volcanic rocks (e.g. hypersthene dacite (Buckley & Wilkins, 1971; Klein, 1968) at temperatures estimated at between 700-800°C.

In metamorphic rocks, it typically occurs in amphibolite facies rocks of basic composition (e.g. Robinson & Jaffe, 1969; Stout, 1972) with maximum temperatures of 600-700°C. (Robinson & Jaffe, 1969). However, a mechanism similar to that in the fluor-amphiboles could occur for cummingtonite. The cummingtonite strip dimensions are significantly smaller than those of grunerite, and yet the site-population refinements (Fischer, 1966; Finger, 1967, 1969a) indicate that the M(4) site in both minerals is filled only by Fe^{2+} and Ca. Thus the M(4) bonding requirements are the same, and the linkage requirements are satisfied by a greater shear in the octahedral sheet in cummingtonite. As before, this allows a greater relaxation during thermal expansion and could account for the much higher thermal stability of cummingtonite.

Substitution of Al into the tetrahedral site results in an increase in the dimensions of a straight chain; to accommodate this, the aluminous amphiboles show a much greater di-trigonal rotation (see Figure 4.2) that is complementary to the changing bonding requirements of the M(4) and O(5) and O(6) ions. This allows more thermal expansion of the octahedral strip before it becomes oversized with respect to the tetrahedral chain and accounts for the much greater stability of the aluminous amphiboles with respect to the Si-amphiboles (for a summary of amphibole stability limits, see Ernst, 1968).

This is probably reinforced by the presence of an A-site cation in many amphiboles, which may disorder about the large A-cavity and satisfy the bridging anion bond-strength requirements, allowing the chain to straighten out more easily as the octahedral strip expands. This mechanism is obviously operative in the richterite structures, allowing the chain a lot more freedom than in the lower temperature Si-amphiboles with vacant A-sites.

These few applications appear to indicate that a considerable amount of geological information is resident in the amphibole structure, and further studies (especially at high temperatures) should help in extracting this information for use as a tool in mineralogy and petrology.

REFERENCES

ALEXANDER, L. E. and G.E. SMITH (1964) Single-crystal diffractometry the improvement of accuracy in intensity measurements, Acta Crystallogr. 17: 1195-1201.

ALLEN, L.C. (1970) Why three-dimensional Huckel Theory works and where it breaks down. In O. Sinanoglu and K. B. Wiberg, Eds., Sigma Molecular Orbital Theory, Yale University Press, New Haven, Connecticut: 227-248.

_____ (1972) The shape of molecules. Theoret. Chim. Acta, 24: 117-131.

ALLRED, A. L. (1961) Electronegavity values from thermochemical data. J. Inorg. Nucl. 17: 215-221.

ANDERSON, O. L. (1970) Elastic constants of the central force model for three cubic structures. Pressure Derivatives and Equations of state. J. Geophys. Res. 75: 2719-2740.

_____ and D. L. ANDERSON (1970) The bulk modulus-volume relationship for oxides. J. Geophys. Res. 75: 3494-3500

ANNERSTEN, H., S. DEVANARAYANAN, L. HAGGSTROM, and R. WAPPLING (1971) Mössbauer study of synthetic ferriphlogopite $KMg_3 Fe^{3+} Si_3 O_{10} (OH)_2$. Phys. Stat. Sol. (B): K137-K138.

AOKI, K., R. V. FODOR, K. KEIL and E. DOWTY (1972) Tremolite with high richterite-molecule content in Kimberlite from Buell Park, Arizona. Amer. Mineral. 57: 1889-1893.

APPLEYARD, E.C. (1969) Nepheline Gneisses of the Wolfe Belt, Lyndoch Township, Ontario. 11. Textures and Mineral Paragenesis. Can. J. Earth Sci. 6:689-717.

_____ (1973) Sub-Silicic Hastingsite Amphiboles from Alkaline Gneisses at Wolfe, Eastern Ontario. (Abstr.) Mineral. Ass. Can. Ann. Meet. Programs.

BAILEY, S.W. (1969) Refinement of an Intermediate Microcline Structure. Amer. Mineral. 54:1540-1545.

BALLHAUSEN, C.J. (1962) Introduction to Ligand Field Theory. McGraw-Hill Book Co. Inc., New York.

BANCROFT, G.M. (1970) Quantitative Site-Population in Silicate Minerals by the Mössbauer Effect. Chem. Geol. 5:255-258.

_____ and R.G. BURNS (1967) Interpretation of the Electronic Spectra of Iron in Pyroxenes. Amer. Mineral. 52:127-1287.

_____ and _____ (1969) Mössbauer and Absorption Spectral Study of Alkali Amphiboles. Mineral. Soc. Amer. Spec. Paper 2, 137-148.

_____, _____ and A.G. MADDOCK (1967) Determination of Cation Distribution in the Cummingtonite-Grunerite Series by Mössbauer Spectra. Amer. Mineral. 52:1009-1026.

_____, P.G.L. WILLIAMS and E.J. ESSENE (1969) Mössbauer Spectra of Amphacites. Mineral. Soc. Amer. Spec. Pap. 2, 59-65.

BARTELL, L.S., L.S. SU and H. YOW (1970) Lengths of Phosphorus-Oxygen and Sulphur-Oxygen Bonds. An extended Huckel Molecular Orbital Examination of Cruickshanks D_{π}-P_{π} Picture. Inorg. Chem. 9:1903-1912.

BAUER, W.H. (1961) Verzerrte Koordinationspolyeder in Heteropolaren Kirstallstrukturen und die Elektrostatische Valenzregel Von Pauling. Naturwissenschaften 48:549-550.

_____ (1970) Bond Length Variation and Distorted Coordination Polyhedra in Inorganic Crystals. Trans. Amer. Crystallogr. Ass. 6: 129-155.

_____ (1971) The Prediction of Bond Length Variations in Silicon-Oxygen Bonds. Amer. Mineral. 56:1573-1599.

_____ (1972) Computer-Simulated Crystal Structures of Observed and Hypothetical Mg_2SiO_4 Polymorphs of Low and High Density. Amer. Mineral. 57:709-731.

BEGER, R.M. (1969) The Crystal Structure and Chemical Composition of Pollucite. Z. Kristallogr. 129:280-302.

BENSON, G.C. and E. DEMPSEY (1961) The Cohesive and Surface Energies of Some Crystals Possessing the Fluorite Structure. Proc. R. Soc. 266:344-358.

BENT, H.A. (1968) Tangent-Sphere Models of Molecules. VI. Ion-Packing Models of Covalent Compounds. J. Chem. Ed. 45:768-777.

BLOXHAM, T.W. and J.B. ALLEN (1958) Glaucophane-Schist, Eclogite and Associated Rocks from Knockormal in the Girvan-Ballantrae Complex, South Ayrshire. Trans. Roy. Soc. Edinburgh 64:1-27.

BONNICHSEN, B. (1969) Metamorphic Pyroxenes and Amphiboles in the Biwabik Iron Formation, Dunka River Area, Minnesota. Mineral. Soc. Amer. Spec. Pap. 2, 217-239.

BORN, M. and K. HUANG (1954) The Dynamical Theory of Crystal Lattices. Clarendon Press, Oxford, England.

BOWEN, N.L. (1940) Progressive Metamorphism of Siliceous Limestone and Dolomites. J. Geol. 48:225-274.

BOYD, F.R. (1959) Hydrothermal Investigations of Amphiboles. In Researches in Geochemistry. Ed. P.H. Abelson. John Wiley and Sons, New York, 377-396.

BRAGG, W.H. (1924) X-Rays and Crystal Structure. G. Bell & Sons, London.

BRAGG, W.L. (1926) Interatomic Distances in Crystals. Phil. Mag. 2:258-266.

BRAGG, W.L. (1929) Atomic Arrangements in the Silicates. Trans. Far. Soc. 25:291-314.

_____ and G.F. CLARINGBULL (1965) Crystal Structure of Minerals. G. Bell & Sons, London, England.

BROWN, F.F. and A.M. PRITCHARD (1969) The Mössbauer Spectrum of Iron Orthoclase. Earth Plant. Sci. Lett. 25:259-260.

BROWN, G.E. Jr. (1970) Crystal Chemistry of the Olivines. Ph.D. Thesis, Virginia Polytechnic Institute, University of Virginia.

BROWN, G.E. and G.V. GIBBS (1969a) Refinement of the Crystal Structure of Osumilite. Amer. Mineral. 54:101-116.

_____ and _____ (1969b) Oxygen Coordination and the Si-O Bond. Amer. Mineral. 54:1528-1539.

_____ and _____ (1970) Stereochemistry and Ordering in the Tetrahedral Portion of Silicates. Amer. Mineral. 55:1587-1607.

BROWN, G.E. Jr. and G.V. GIBBS (1973) The Crystal Chemistry of the Olivines. Amer. Mineral. (in press).

BROWN, G.E., G.V. GIBBS and P.H. RIBBE (1969) The Nature and the Variation in length of the Si-O and Al-O Bonds in Framework Silicates. Amer. Mineral. 54:1044-1061.

BROWN, I.D. and R.D. SHANNON (1973) Empirical Bond Strength-Bond Length Curves for Oxides. Acta Crystallog. A29:266-282.

BUCKLEY, A.N. and R.W.T. WILKINS (1971) Mössbauer and Infrared Study of a Volcanic Amphibole. Amer. Mineral. 56:90-100.

BUERGER, M.J. (1960) Crystal Structure Analysis. John Wiley & Sons, N.Y.

BURNHAM, C.W. (1966) Computation of absorption corrections and the Significance of the End Effect. Amer. Mineral. 51:159-167.

BURNHAM, C.W., Y. OHASHI, S.S. HAFNER and D. VIRGO (1971) Cation distribution and Atomic Thermal Vibrations in an Iron-rich Orthopyroxene. Amer. Mineral. 56:850-876.

BURNS, R.G. (1968a) Enrichments of Transition-metal ions in Silicate Crystal Structures. In L.H. Ahrens (ed.) Origin and Distribution of the Elements. Pergamon Press, Oxford.

_____ (1968b) Site Preferences of Transition Metal ions in Silicate Crystal Structures. Chem. Geol. 5:275-283.

_____ (1970) Mineralogical applications of Crystal Field Theory. Cambridge University Press, Cambridge, England.

_____ and F.J. PRENTICE (1968) Distribution of Iron Cations in the Crocidolite Structure. Amer. Mineral. 53:770-776.

_____ and C.J. GREAVES (1971) Correlations of Infrared and Mössbauer Site Populations Measurements of Actinolite. Amer. Mineral. 56:2010-2033.

_____ (1972) Mixed Valences and Site Occupancies in Silicate Minerals from Mössbauer Spectroscopy. Can. J. Spectroscopy 17:51-59.

BUSING, W.R. and H.A. LEVY (1957) High-Speed Computation of the Absorption Correction for Single Crystal Diffraction Measurements. Acta Crystallog. 10:180-182.

CAMERON, M.J. (1970) The Crystal Chemistry of Tremolite and Richterite. A Study of Selected Anion and Cation Substitutions. Ph.D. Thesis, Virginia Polytechnic Institute and State University.

CAMERON, M. and G.V. GIBBS (1971) Refinement of the Crystal Structure of Two Synthetic Fluor-Richterites. Carnegie Inst. Wash. Year Book 70:150-153.

_____, S. SUENO, C.T. PREWITT, and J.J. PAPIKE (1973) High-Temperature Crystal Chemistry of K-Fluor-Richterite (Abstr.) Trans. Amer. Geophys. Union 54:497-498.

CANNILLO, E., G. GIUSEPPETTI and V. TAZZOLI (1967) The Crystal Structure of Leucophanite. Acta Crystallogr. 23:255-259.

CARMICHAEL, I.S.E. (1967) The Mineralogy and Petrology of the Volcanic Rocks from the Leucite Hills, Wyoming. Contrib. Mineral. Petrology 15:24-66.

CERRINI, S. (1971) Tensor Analysis of the Harmonic Vibrations of Atoms in Crystals. Acta Crystallogr. A27:130-133.

CHARLES, R.W. (1972) Phase Equilibria of the Richterite End Members $Na_2CaMg_5Si_8O_{22}(OH)_2$ and $Na_2CaFe_5Si_8O_{22}(OH)_2$. Carnegie Inst. Wash. Year Book 71:506-510.

CLARK, J.R., D.E. APPLEMAN and J.J. PAPIKE (1969) Crystal-Chemical Characterization of Clinopyroxenes based on Eight New Structure Refinements. Mineral. Soc. Amer. Spec. Pap. 2:31-50.

COLEMAN, R.G. and D.E. LEE (1963).Glaucophane-Bearing Metamorphic Rock Types of the Cazadero Area, California. J. Petrology, 4:260-301.

COLLINS, G.A.D., D.W.J. CRUICKSHANK and A. BREEZE (1972) Ab Initio Calculations on the Silicate Ion, Orthosilicic Acid and their $L_{2,3}$ X-Ray Spectra. J. Chem. Soc., Faraday Trans. II, 68:1189-1195.

COLVILLE, A.A. and G.V. GIBBS (1964) Refinement of the Crystal Structure of Riebeckite (Abstr.) Geol. Soc. Amer. Spec. Pap. 82:31.

COMPTON, R.R. (1958) Significance of Amphibole Paragenesis in the Bidwell Bar Region, California. Amer. Mineral. 43:890-907.

COTTON, F.A. (1963) Chemical Applications of Group Theory. Interscience Publishers, New York.

COULSON, C.A. (1961) Valence, 2nd Ed., Oxford University Press, London.

_____ and T.W. DINGLE (1968) The B-O Bond Lengths in Boron-Oxygen Compounds. Acta Crystallogr. B24:153-155.

CROMER, D.T. (1965) Anomalous Dispersion Corrections Computed from Self-Consistent Field Relativistic Dirac-Slater Wave Functions. Acta Crystallogr. 18:17-23.

_____ and J.B. MANN (1968) X-Ray Scattering Factors Computed from numerical Hartree-Fock Wave Functions. Acta. Crystallogr. A24:321-324.

CRUICKSHANK, D.W.J. (1956) The Determination of the Anisotropic Thermal Motion of Atoms in Crystals. Acta Crystallogr. 9:747-753.

_____ (1961) The role of 3d-Orbitals in π-Bonds between (A) Silicon, Phosphorus, Sulpher, or Chlorine and (B) Oxygen or Nitrogen. J. Chem. Soc. 1077:5486-5504.

CZAYA, R. (1971) Refinement of the Structure of γ-Ca_2SiO_4. Acta Crystallogr. B27:848-849.

DAS, T.P. (1960) Theory of Crystalline Fields of Iron-group Ions in Solid Solutions. Phys. Rev. 140:A1957-A1964.

DEER, W.A., R.A. HOWIE and J. ZUSSMAN (1963) Rock-Forming Minerals. Vol. 2, Chain Silicates. Longmans, Green & Co., London.

DIXON, W.J. (1971) BMD Biomedical Computer Programs. University of California Press.

DOLLASE, W.A. (1969) Crystal Structure and Cation Ordering of Piemontite. Amer. Mineral. 54:710-717.

_____ (1969) Least-Squares Refinement of a Plutonic Nepheline. Z. Kristallogr. 132:27-44.

DONNAY, G. (1970) Further use for the Pauling-Bond Concept. Carnegie Inst. Wash. Year Book 68:292-295.

DONNAY, G. and R. ALLMANN (1970) How to Recognize O^{2-}, OH and H_2O in crystal structures determined by X-Rays. Amer. Miner. 55:1003-1015.

_____ and J.D.H. DONNAY (1972) Bond-Valence Summation for Borates (Abstr.) A.C.A. Winter Meet., Florida.

DOWTY, E. (1971) Crystal Chemistry of Titanian and Zirconian Garnet. I. Review and Spectral Studies. Amer. Mineral. 56: 1983-2009.

DOYLE, P.A. and P.S. TURNER (1968) Relativistic Hartee-Fock X-Ray and Electron Scattering Factors. Acta. Crystallogr. A24:390-397.

DRITS, V.A. (1970) The relationship between the average anion-anion distances and anion-cation distances in the simplest crystal structure units. Tetrahedra and Octahedra. Kristallogr. 15:913-917 (Transl. Sov. Physics Crystallogr., 15:795-798).

DUNITZ, J.D. and L.E. ORGEL (1957) Electronic Properties of Transition-Metal Oxides-II. Cation distribution amongst octahedral and tetrahedral sites. J. Phys. Chem. Solids 3:318-323.

ENGEL, A.E.J. and C.E. ENGEL (1960) Progressive Metamorphism and Granitization of the major paragneiss, Northwest Adirondack Mountains, New York. Geol. Soc. Amer. Bull. 71:1-58.

ENGEL, A.E.J. and C.E. ENGEL (1962) Hornblendes Formed during Progressive Metamorphism of Amphibolites, Northwest Adirondack Mountains, New York. Geol. Soc. Amer. Bull. 73:1499-1515.

ERLANK, A.J. and L.W. FINGER (1970) The Occurrence of Potassic Richterite in a Mica Nodule from the Wesselton Kimberlite, South Africa. Carnegie Inst. Wash. Year Book 68: 320-324.

ERNST, W.G. (1963) Polymorphism in Alkali Amphiboles. Amer. Mineral. 48:241-260.

_____ (1968) Amphiboles. Springer-Verlag., New York.

_____ and Y. SEKI (1967) Petrologic Comparison of the Franciscan and Sanbagawa Metamorphic Terranes. Tectonophys. 94:463-478.

_____ and C.M. WAI (1970) Mössbauer, Infrared, X-ray and Optical study of cation ordering and dehydrogenation in natural and heat-treated sodic amphiboles. Amer. Mineral. 55:1226-1258.

EVANS, H.T. (1960) Crystal Structure Refinement and Vanadium Bonding in the Meta-Vanadates KVO_3, NH_4VO_3 and $KVO_3.H_2O$. Z. Kristallogr. 114: 257-277.

FAJANS, K. (1967) Degrees of Polarity and Mutual Polarization of Ions in the Molecules of Alkali Fluorides, SrO and BaO. Structure and Bonding 3:88-105.

FAYE, G.H. and E.H. NICKEL (1970) The Effect of Charge-Transfer Processes on the colour and pleochroism of amphiboles. Can. Mineral. 10:616-635.

FINGER, L.W. (1967) The Crystal Structures and crystal chemistry of Ferromagnesian amphiboles. Ph.D. Thesis, University of Minnesota.

_____ (1969a) The Crystal Structure and cation distribution of a Grunerite. Mineral. Soc. Amer. Spec. Pap. 2, 95-100.

_____ (1969b) Determination of cation distribution by Least-squares refinement of single-crystal X-ray data. Carnegie Inst. Wash. Year Book 67:216-217.

_____ (1970) Refinement of the Crystal Structure of an Anthophyllite. Carnegie Inst. Wash. Year Book 68:283-288.

_____ and T. ZOLTAI (1967) Cation distribution in Grunerite (abstr.). Trans. Amer. Geophys. Union 48:233-234.

FISCHER, K.F. (1966) A further refinement of the crystal structure of Cummingtonite, $(Mg,Fe)_5(Si_8O_{22})(OH)_2$. Amer. Mineral. 51:814-818.

FRAUENFELDER, H. (1962) The Mössbauer Effect. Benjamin, New York.

FREEMAN, A.J. and R.E. WATSON (1965) Hyperfine Interactions in Magnetic Materials. In G.T. Rado and H. Suhl (Eds.), Magnetism. Academic Press, New York, 167-305.

GHOSE, S. (1961) The Crystal Structure of Cummingtonite. Acta Crystallogr. 14:622-627.

_____ and E. HELLNER (1959) The Crystal Structure of Grunerite and Observations on the Mg-Fe Distribution. J. Geol., 67:691-701.

GIBBS, G. V. (1962) The Crystal Structure of Protoamphibole. Ph. D. Thesis, The Pennsylvania State University.

_____ (1964) Crystal Structure of Protoamphibole (Abstr.) Geol. Soc. Amer. Ann. Meet. (Geol. Soc. Amer. Spec. Pap. 82, 71 (1965)).

_____, F. D. BLOSS and H. R. SHELL (1960) Protoamphibole, A new polytype. Amer. Mineral. 45:974-989.

_____ (1969) The Crystal Structure of Protoamphibole. Mineral. Soc. Amer. Spec. Pap. 2:101-110.

_____ and C. T. PREWITT (1968) Amphibole Cation Site Disorder (Abstr.). Int. Mineral. Ass. Pap. Proc. 5th Gen. Meet. Mineralogical Society, London (1958), 334-335.

_____, M. M. HAMIL, S. J. LOUISNATHAN, L. S. BARTELL and H. YOW (1972) Correlation between Si-O Bond Length, Si-O-Si Angle and Bond Overlap Populations calculated using extended huckel molecular orbital theory. Amer. Mineral. 57:1578-1613.

GIBBS, J.W. (1901) The Collected Works of J. Willard Gibbs. Dover Edition.

GILLESPIE, R.J. (1963) The Valence-Shell Electron-pair Repulsion (VSEPR) Theory of Directed Valence. J. Chem. Ed. 40:295-301.

_____ and E.A. Robinson (1963) The Sulphur-Oxygen Bond in Sulphuryl and Thionyl Compounds. Correlation of Stretching frequencies and force constants with bond lengths, bond angles, and bond orders. Can. J. Chem. 41:2074-2085.

_____ and _____ (1964) Characteristic vibrational frequencies of compounds containing Si-O-Si, P-O-P, S-O-S, and Cl-O-Cl bridging groups. Can. J. Chem. 42:2496-2503.

GOLDANSKII, V.I. and R.H. HERBER (1968) Chemical Applications of Mössbauer Spectroscopy. Academic Press, New York.

GOLDSCHMIDT, V.M. (1929) Crystal structure and chemical constitution. Trans. Far. Soc. 25:253-283.

GOLDSMITH, J.R. and F. LAVES (1955) Cation order in anorthite ($CaAl_2Si_2O_8$) as revealed by gallium ahd germanium substitutions. Z. Kristallogr. 106:213-226.

GOPAL, R. (1972) The Crystal Chemistry and bonding in vanadates of divalent metal ions and the crystal structure of Whitlockite. Ph.D. Thesis, McMaster University.

GRIFFITH, J.S. (1961) The theory of transition-metal ions. Cambridge University Press.

HAFNER, S.S. and S. THOSE (1971) Iron and magnesium distribution in Cummingtonites $(Fe,Mg)_5Si_8O_{22}(OH)_2$. Z. Kristallogr. 133: 301-326.

_____ and H.G. HUCKENHOLZ (1971) Mössbauer spectrum of synthetic ferri-diopside. Nature, Phys. Sci. 233:9-11.

HAMILTON, W.C. (1965) Significance tests on crystallographic R-factors. Acta. Crystallogr. 18:502-510.

HAWTHORNE, F.C. (1972) Use of G.E. Single Crystal Diffractometer. McMaster University, Dept. Geol., Tech. Memo. 72-3.

_____ and H.D. GRUNDY (1972) Positional Disorder in the A-Site of Clinoamphiboles. Nature 235:72-73.

_____ and _____ (1973) The Crystal Chemistry of the amphiboles. I. Refinement of the crystal structure of Ferrotschermakite. Mineral. Mag. 39:36-48.

HENRY, N.F.M. and K. LONSDALE (1965) International Tables for X-Ray Crystallography, Vol. 1. The Kynoch Press, Birmingham, England.

HERITSCH, H. and E. KAHLER (1960) Strukturuntersuchung an Zwei Kluftkarinthine Ein Beitrag Zur Karinthinfrage. Tschermaks Mineral. Petrog. Mitt. 7:218-234.

HERITSCH, H. and L. RIECHERT (1960) Strukturuntersuchung an Einer Basaltischen hornblende von Cernosin, CSR. Tschermaks Mineral. Petrog. Mitt. 7:235-245.

_____, G. BERTOLDI and E.M. WALITZI (1960) Strukturuntersuchung in einer Basaltischen Hornblende von Kuruzzenkogel, Sudlich Fehring, Steirmark. Tschermaks Mineral. Petrog. Mitt. 7:210-217.

_____, P. PAULITSCH and E.M. WALITZI (1957) Die Struktur von Karinthin und einer Barroisitschen hornblende. Tschermaks Mineral. Petrog. Mitt. 6:215-225.

HEY, M.H. (1954) A further note on the presentation of chemical analyses of Minerals. Mineral. Mag. 23:481-497.

HOFFMANN, G. (1972) Natural and Synthetic Ferroglaucophane. Contrib. Mineral. Petrology 34:135-149.

HOLMES, A. (1965) Principles of Physical Geology. Thomas Nelson and Sons Ltd., London.

HUTCHINGS, M.T. (1964) Point-charge calculations of energy levels of magnetic ions in crystalline fields. Solid State Physics 16:227-273.

JORGENSEN, C.K. (1966) Electric Polarizability, Innocent Ligands and Spectroscopic oxidation states. Structure abd Bonding 1: 234-248.

JORGENSEN, C.K. (1967) Relations between softness, covalent bonding, ionicity and electric polarizability. Structure and Bonding 3:106-115.

KASPER, J.S. and K. LONSDALE (1959) International Tables for X-Ray Crystallography, Volume 2. The Kynoch Press, Birmingham, England.

KAWAHARA, A. (1963) X-Ray studies on some Alkaline Amphiboles. Mineral. Jour. 4:30-40.

KITAMURA, M. and M. TOKONAMI (1971) The Crystal Structure of Kaersutite. Sci. Reps., Tohoku Univ., Ser. III, 11:125-141.

_____ and N. MORIMOTO (1973) Crystal Structure of Kozulite and Tetrahedral Al in Amphiboles (abstr.). Collected Abstracts, Ninth Gen. Ass. and Int. Con., Kyoto, Japan. Int. Union Crystallogr., S71. Science Council of Japan.

KITTEL, C. (1966) Introduction to Solid State Physics. John Wiley & Sons, New York.

KLEIN, C. (1964) Cummingtonite-Grunerite Series. A Chemical, Optical and X-Ray Study. Amer. Mineral. 49:963-982.

_____ (1966) Mineralogy and Petrology of the Metamorphosed Wabush Iron Formation, Southwestern Labrador. J. Petrology 7:246-305.

_____ (1968) Coexisting Amphiboles. J. Petrology 9:281-330.

KLEIN, C. and J. ITO (1968) Zincian and Manganoan Amphiboles from Franklin, New Jersey. Amer. Mineral. 53:1264-1275.

KOSTER, G.F. (1957) Space Groups and their representations. Academic Press, New York.

LARSEN, E.S. Jr. (1942) Alkalic rocks of Iron Hill, Gunnison County, Colorado U.S. Geol. Surv. Prof. Pap. 197-A, 1-64.

LAW, A.D. (1973) Critical evaluation of statistical best fits to Mössbauer spectra. Amer. Mineral. 58:128-131.

LEAKE, B.E. (1965) The relationship between composition of calciferous amphiboles and grade of metamorphism. In Controls of Metamorphism. Ed. W.S. Pitcher and G. Flinn. Boyd and Oliver, 299-318.

_____ (1968) A catalogue of analyzed calciferous and subcalciferous amphiboles together with their nomenclature and associated minerals. Geol. Soc. Amer. Spec. Pap. 98.

LIEBAU, F. (1961) Untersuchungen uber die Grosse des Si-O-Si Valenzwinkels. Acta. Crystallogr. 14:1103-1109.

LINDEMANN, W. (1964) Beitrag zur Struktur des Anthophyllits (Abstr.). Forts. Mineral. 42:205.

LOEWENSTEIN, W. (1954) The distribution of aluminium in the tetrahedra of silicates and aluminates. Amer. Mineral. 39:92-96.

LOUISNATHAN, S.J. and G.V. GIBBS (1972a) The Effect of Tetrahedral angles on Si-O bond overlap populations for isolated tetrahedra. Amer. Mineral. 57:1614-1642.

_____ and _____ (1972b) Variation in Si-O Distances in Olivines Soda Melilite and Sodium metasilicate as predicted by semi-empirical molecular orbital calculations. Amer. Mineral. 57:1643-1663.

_____ and _____ (1972c) Bond Length variations into oxyanions of the Third Row Elements, T=Al, Si, P, S, and Cl. Mat. Res. Bull. 7:1281-1292.

_____ and _____ (1972d) Aluminium-Silicon distribution in Zunyite. Amer. Mineral. 57:1089-1108.

MacGillavry, C.H. and G.D.RIECK (1962) International Tables for X-Ray Crystallography, Volume 3. The Kynoch Press, Birmingham, England.

McCLURE, D.S. (1957) The distribution of transition metal cations in spinels. J. Phys. Chem. Solids 3:311-317.

MEGAW, H.D. (1968) A simple theory of the off-centre displacement of cations in octahedral environments. Acta. Crystallogr., B24: 149-153.

MITCHELL, J.T. (1970) The Crystal Structure refinement of Actinolite. M.S. Thesis, Virginia Polytechnic Institute, University of Virginia.

_____, F.D. BLOSS and G.V. GIBBS (1970) The Variation of Tetrahedral bond lengths and angles in Clinoamphibole. Abstr. Programs, Geol. Soc. Amer. Ann. Meet. Milwaukee, Wisc. 2:626.

_____, _____ and _____ (1971) Examination of the Actinolite structure and four other C2/m amphiboles in terms of double bonding. Z. Kristallogr. 133:273-300.

MIZOGUCHI, T. and M.J. TANAKA (1963) The Nuclear Quadrupole interaction of Fe in Spinel Type Oxides. J. Phys. Soc. Japan, 18:1301-1312.

MULLIKEN, R.S. (1955a) Electronic Population analysis on LCAO-MO Molecular Wave Functions. I. J. Chem. Phys. 23:1833-1841.

_____ (1955b) Electronic Population Analysis on LCAO-MO molecular wave functions. II. Overlap Populations, Bond Orders, and Covalent Bond Energies. J. Chem. Phys. 23:1841-1846.

NEUTRON DIFFRACTION COMMISSION (1969) Coherent Neutron-Scattering Amplitudes. Acta. Crystallogr. A25:391-392.

NICHOLSON, W.J. and G. BURNS (1964) Quadrupole Coupling Constant eq Q/h of Fe^{3+} in Several Rare-Earth Iron Garnets. Phy. Rev. 133A:1568-1607.

NOLL, W. (1963) The Silicate Bond from the standpoint of Electronic Theory. Ang. Chem. (Int. Ed.) 2:73-80.

NOVAK, G.A. and G.V. GIBBS (1971) The Crystal Chemistry of the Silicate Garnets. Amer. Mineral. 56:791-825.

OHASHI, Y. and C.W. BURNHAM (1972) Electrostatic and Repulsive Energies of the M1 and M2 cation sites in Pyroxenes. J. Geophys. Res. 77:5761-5766.

O'NIONS, R.K. and D.G. SMITH (1971) Investigations of the $L_{II, III}$ X-Ray Emission Spectra of Fe by Electron Microprobe, Part 2. The Fe $L_{II, III}$ Spectra of Fe and Fe-Ti Oxides. Amer. Mineral. 56:1452-1463.

PANT, A.K. and D.W.J. CRUICKSHANK (1967) A reconsideration of the structure of Datolite, $CaBSiO_3(OH)$. Z. Kristallogr. 125: 286-298.

PAPIKE, J.J. and J.R. CLARK (1967) Crystal-Chemical role of Potassium and Aluminium in a hornblende ~~of proposed~~ mantle origin (Abstr.). Geol. Soc. Amer. Prog. 1967 Ann. Meet., New Orleans (Geol. Soc. Amer. Spec. Pap. 115:171 (1968)).

_____ and _____ (1968) The Crystal Structure and Cation distribution of Glaucophane. Amer. Mineral. 53:1156-1173.

PAPIKE, J.J., M. ROSS and J.R. CLARKE (1968) Crystal-Chemical and Petrologic significance of the $P2_1/m$ Amphibole analogue of Pigeonite (Abstr.). Trans. Amer. Geophys. Union 49:340-341.

_____, _____ and _____ (1969) Crystal-Chemical characterization of Clinoamphiboles based on five new structure refinements. Mineral. Soc. Amer. Spec. Pap. 2:117-136.

_____ and M. ROSS (1970) Gédrites. Crystal Structures and Intracrystalline cation distributions. Amer. Mineral. 55:1945-1972.

PAULING, L. (1929) The Principles determining the structure of complex ionic crystals. J. Amer. Chem. Soc. 51:1010-1026.

_____ (1939) The nature of the Chemical Bond, 1st Ed. Cornell University Press, Ithaca, New York.

_____ (1952) Interatomic distances and bond character in the oxygen acids and related substances. J. Phys. Chem. 56:361-365.

_____ (1960) The nature of the Chemical Bond, 3rd Ed. Cornell University Press, Ithaca, New York.

PERRY, K. Jr. (1967) An application of linear algebra to petrologic problems. Part 1. Mineral Classification. Geochim. et Cosmochim. Acta. 31:1043-1073.

_____ (1968a) Representation of mineral analyses in 11-Dimensional Space. Part 1. Feldspars, Lithos 1:201-218.

_____ (1968b) Representation of mineral analyses in 11-Dimensional Space. Part 2. Amphiboles. Lithos 1:307-321.

PETERSE, W.J.A.M. and J.H. PALM (1966) The Anisotropic temperature factor of atoms in special positions. Acta Crystallogr. 20: 147-150.

PHILLIPS, R. (1966) Amphibole Compositional Space. Mineral Mag. 35: 945-952.

_____ and W. LAYTON (1964) The calciferous and alkali amphiboles. Mineral. Mag. 33:1097-1109.

POLLAK, H., M. De COSTER and S. AMELINCKX (1962) Mössbauer Effect in Biotite. Phys. Stat. Sol. 2:1653-1659.

PREWITT, C.T. (1963) Crystal structures of two synthetic amphiboles (Abstr.) Geol. Soc. Amer. Pro. 1963 Ann. Meet. (Geol. Soc. Amer. Spec. Pap. 76:132-133 (1964)).

_____ and R.D. SHANNON (1969) Use of Radii as an aid to understanding the crystal chemistry of high pressure phases. Trans. Amer. Crystallogr. Ass. 5:51-60.

_____, J.J. PAPIKE and M. ROSS (1970) Cummingtonite. A Reversible, non-quenchable transition from $P2_1/m$ to C2/m symmetry. Earth Planet. Sci. Lett. 8:448-450.

PRIDER, R.T. (1939) Some minerals from the Leucite-rich rocks of the West Kimberly Area, Western Australia. Mineral. Mag. 25: 373-387.

RAYMOND, M. (1971) Madelung Constants for several silicates. Carnegie Inst. Wash. Year Book 70:225-227.

REITZ, J.R., R.N. SEITZ and R.W. GENBERG (1961) Closed-Shell Ion-Ion interactions in calcium fluoride. J. Phys. Chem. Solids 19:73-78.

RIBBE, P.H. and G.V. GIBBS (1971) Crystal structures of the Humite Minerals. 111. Mg/Fe ordering in Humite and its relation to other ferromagnesian silicates. Amer. Mineral. 56: 1155-1173.

RINGWOOD, A.E. (1969) Phase transformations and the constitution of the Mantle. Publication No. 680, Department of Geophysics and Geochemistry, Australian National University, Canberra A.C.T.

ROBINSON, E.A. (1963) Characteristic vibrational frequencies of oxygen compounds of Silicon, Phosphorous, and Chlorine. Correlation of stretching frequencies and force constants with bond lengths and bond orders. Can. J. Chem. 41:3021-3033.

ROBINSON, K. (1971) The crystal structures of Zircon, Clinohumite and the hornblendes. A determination of polyhedral distortion and order-disorder. Ph.D. Thesis, Virginia Polytechnic Institute and State University.

ROBINSON, K., G.V. GIBBS and P.H. RIBBE (1969) A refinement of the crystal structure of Pargasite (Abstract). Amer. Mineral. 55:307.

_____, _____ and _____ (1971) Quadratic Elongation. A quantitative measure of distortion in coordination polyhedra. Science 172: 567-570.

_____, _____ and _____ (1973) The crystal structures of the Humite Minerals. Clinohumite and Titanoclinohumite. Amer. Mineral. 58:43-49.

ROBINSON, P. and H.W. JAFFE (1969) Chemographic exploration of Amphibole Assemblages from Central Massachusetts and Southwestern New Hampshire. Mineral. Soc. Amer. Spec. Pap. 2:251-274.

_____, M. ROSS and H.W. JAFFE (1971) Composition of the Anthophyllite-Gedrite Series, Comparisons of Gedrite-hornblende, and the Anthophyllite-Gedrite solvus. Amer. Mineral. 56:1005-1041.

ROLLET, J.S. (1965) Computing Methods in Crystallography. Pergamon Press, Oxford.

RUNCIMAN, W.A., D. SENGUPTA, and M. MARSHALL (1973) The Polarized spectra of iron in silicates. 1. Enstatite. Amer. Mineral. 58:444-451.

RUNCIMAN, W.A., D. SENGUPTA, and J.T. GOURLEY (1973) The Polarized spectra of iron in silicates. 2. Olivine. Amer. Mineral. 58:451-456.

SAMMIS, C.G. (1970) The pressure dependence of the elastic constants of cubic crystals in the NaCl and Spinel structures from a lattice model. Geophys. J.R. Astr. Soc. 19:285-297.

SEMET, M.P. (1973) A crystal-chemical study of synthetic magnesio-hastingsite. Amer. Mineral. 58:480-494.

SHANNON, R.D. (1970) Effects of covalency on average interatomic distances in Germanates. Chem. Comm., 821-822.

_____ and C.T. PREWITT (1969) Effective ionic radii in oxides and fluorides. Acta Crystallogr. B25:925-946.

_____ and _____ (1970a) Revised values of effective ionic radii. Acta Crystallogr. B26:1046-1048.

_____ and _____ (1970b) Effective ionic radii and crystal chemistry. J. Inorg. Nucl. Chem. 32:1427-1441.

_____ and C. CALVO (1973a) Refinement of the crystal structure of synthetic Chervetite, $Pb_2V_2O_7$. Can. J. Chem. 51:70-76.

_____ and _____ (1973b) Refinement of the crystal structure of low temperature Li_3VO_4 and analysis of mean bond lengths in Phosphates, Arsenates and Vanadates. (To be published.)

SINGH, S.K. and M. BONARDI (1972) Mössbauer Resonance of Arfvedsonite and Aegirine-Augite from the Joan Lake Agpaitic Complex, Labrador. Lithos 5:217-225.

SMITH, G.S. and L.E. ALEXANDER (1963) Refinement of the Atomic parameters of α-Quartz. Acta Crystallogr. 16:462-471.

SMITH, J.V. (1968) Cell dimensions and other physical properties should depend on local rather than distant order (Abstr.) Geol. Soc. Amer. Meet., Mexico City, 284.

SMOLIN, Y.I. and Y.F. SHEPELEV (1970) The crystal structures of the rare earth pyrosilicates. Acta Crystallogr. B26:484-492.

STOUT, J.H. (1972) Phase Petrology and Mineral Chemistry of coexisting amphiboles from Telemark, Norway. J. Petrology 13:99-145.

STRENS, R.G.J. (1967) Symmetry-Entropy-Volume relationships in polymorphism. Mineral. Mag. 36:565-577.

SUENO, S., J.J. PAPIKE, C.T. PREWITT and G.E. BROWN (1972) Crystal structure of high Cummingtonite. J. Geophys. Res. 77:5767-5777.

_____, M. CAMERON, J.J. PAPIKE, and C.T. PREWITT (1972) High-temperature crystal chemistry of pyroxenes and amphiboles (Abstr.). Collected Abstracts, Ninth Gen. Ass. and Int. Con., Kyoto, Japan, Int. Union Crystallogr. S69, Science Council of Japan.

SUNDIUS, N. (1946) The classification of the hornblendes and the solid solution relations in the Amphibole Group. Arsbok Sver. Geol. Unders. 40:1-36.

TEMPLETON, D.H. (1956) Systematic absences corresponding to false symmetry. Acta Crystallogr. 9:199-206.

THOMPSON, J.B. (1970) Geometrical possibilities for amphibole structures. Model Biopyriboles. (Abstr.) Amer. Mineral. 55:292-293.

TILLEY, C.E. (1937) The paragenesis of Kyanite Amphibolites. Mineral. Mag. 24:555-568.

TOKONAMI, M. (1965) Atomic Scattering Factors for O^{2-}. Acta. Crystallogr. A10:486.

TOSI, M.P. (1964) Cohesion of ionic solids in the born model. Sol. State Phys. 16:1-120.

TROLL, G. and M.C. GILBERT (1972) Fluorine-Hydroxyl substitution in Tremolite. Amer. Mineral. 57:1386-1403.

VIRGO, D. (1972) ^{57}Fe Mössbauer Analyses of Fe^{3+} clinopyroxenes. Carnegie Inst. Wash. Year Book 71, 534-538.

WACKMAN, P.H., W.M. HIRTHE and R.E. FROUNFELKER (1967) The cohesive energy of TiO_2(Rutile). J. Phys. Chem. Solids 28:1525-1531.

WARREN, B.E. (1929) The structure of Tremolite, $H_2Ca_2Mg_5(Si_8O_{24})$. Z. Kristallogr. 72:42-57.

WARREN, B.E. (1930) The crystal structure and chemical composition of the Monoclinic Amphiboles. Z. Kristallogr. 72:493-517.

WERTHEIM, G.K. (1964) Mössbauer Effect. Principles and Applications. Academic Press, New York.

WHITTAKER, E.J.W. (1949) The structure of Bolivian Crocidolite. Acta. Crystallogr. 2:312-317.

_____ (1968) Classification of the amphiboles. International Mineralogical Ass., Proceedings of the Fifth Gen. Meet., 1966, 232-242. Mineralogical Society, London.

_____ (1969) The structure of the Orthorhombic Amphibole Holmquistite. Acta. Crystallogr. B25:394-397.

_____ (1971) Madelung Energies and site preferences in amphiboles. I. Amer. Mineral. 56:980-996.

_____ and R. MUNTUS (1968) Ionic radii for use in geochemistry. Geochim. Cosmochim. Acta 2:155-169.

WINCHELL, A.N. and H. WINCHELL (1951) Elements of optical mineralogy. Pt. 2. Description of Minerals. John Wiley & Sons, New York.

WOOD, B.J. and R.G.J. STRENS (1972) Calculation of crystal field splittings in distorted coordination polyhedra. Spectra and Thermodynamic properties of minerals. Mineral. Mag. 38:909-917.

ZACHARIASEN, W. H. (1945) Theory of X-ray Diffraction in crystals. John Wiley & Sons, New York.

_____ (1954) Crystal chemical studies of the 5F-Series of Elements XXIII. On the crystal chemistry of Uranyl compounds and of related compounds of transuranic elements. Acta Crystallogr. 7:795-807.

_____ (1963) The crystal structure of cubic metaboric acid. Acta. Crystallogr. 16:380-384.

_____ and H. A. PLETTINGER (1965) Extinction in Quartz. Acta. Crystallogr. 18:710-714.

ZUSSMAN, J. (1955) The crystal structure of Actinolite. Acta. Crystallogr. 8:301-308.

_____ (1959) A Re-examination of the structure of Tremolite. Acta. Crystallogr. 12:309-312.

APPENDIX I

X-Ray Scattering

An atom contains electrons distributed over a finite volume; due to the spatial separation of the electrons, phase differences exist between x-rays scattered from different parts of the atom. Hence, the total scattering by an atom is dependent upon its internal electron distribution (Zachariasen, 1945). If $U(r)dr$ is the number of electrons lying between r and r + dr from the centre, the atom will scatter at any particular 2θ angle as though it was equivalent to f electrons (Kaspar & Lonsdale, 1967) where

$$f = \int_0^\infty \frac{U(r)\sin(4\pi r \sin\theta/\lambda)}{4\pi r \sin\theta/\lambda}\, dr$$

and λ is the radiation wavelength. The function $U(r)$ is given by

$$U(r) = r^2 \rho(r)$$

where $\rho(r)$ is the total charge density at a distance r from the centre. Values for $\rho(r)$ are derived from wave-function calculations (e.g. Doyle & Turner, 1968). Values of f are generally expressed as the analytic function

$$f = \sum_{i=1}^{4} a_i \exp(-b_i \sin^2\theta/\lambda^2) + c$$

where a_i, b_i and c are parameters determined by curve-fitting procedures.

The unit cell of a crystal contains atoms in various positions and the scattered waves from the different atoms will have phase differences with respect to each other. The amplitude, F_{hkl} of the resultant wave is given by the following equation (Buerger, 1960)

$$F_{hkl} = \sum_j f_j \exp 2\pi i(hx_j+ky_j+lz_j)$$

where f_j is the scattering factor of the j^{th} atom. In general, F_{hkl} is a complex quantity; however, for centric space groups, F_{hkl} is real and the above equation reduces to

$$F_{hkl} = \sum_j f_j \cos 2\pi (hx_j+ky_j+lz_j)$$

In theory, this expression may be further reduced for space groups other than $P\bar{1}$ because of the symmetry properties of the group (Buerger, 1960; Henry & Lonsdale, 1965). In practice, it is far more convenient to use the generalized form given above and generate the full structure factor by operating on the asymmetric unit with the symmetry operators to generate the full cell.

Atoms in a crystal vibrate, and thus in general any two atoms that are ideally related by a lattice translation are not actually separated by an integral multiple of the cell dimensions. Hence the scattered waves are not quite in phase and this has the effect of reducing the intensity of the resultant scattered radiation. This effect is incorporated by modifying the scattering factor of each atom by the function

$$\exp(-\beta_j \sin^2\theta/\lambda^2)$$

where β_j is known as the (isotropic) temperature factor and is related to the vibrational properties of the atom by the equation

$$\beta_j = 8\pi^2 \overline{U_j^2}$$

where $\overline{U_j^2}$ is the mean square displacement of the j^{th} atom. This function assumes that the vibrational properties of atoms in a crystal are isotropic. Allowance can be made for the fact that vibration is anisotropic by replacing the scalar quantity β_j by a symmetric second rank tensor (Cruickshank, 1956; Cerrini, 1971) of the form

$$\sum_{i=1}^{3} \sum_{j=1}^{3} h_i h_j \beta_{ij}$$

where β_{ij} are the nine contravariant components of the tensor and h_i is the i^{th} index of the set hkl. Symmetry restrictions for this function are tabulated

by Peterse and Palm (1966). For further details of the x-ray method, see Zachariasen (1945), Buerger (1960) and Rollet (1965).

Mössbauer scattering

The Mössbauer effect is the recoil-free emission and absorption of gamma-rays by a specific atomic nucleus. The emission of a gamma ray during a nuclear transition causes a recoil of the emitting atom; this recoil energy dissipates by transfer to the phonon spectrum of the lattice. Since the lattice is quantized, this transfer must occur in integral multiples of the phonon energy, and thus the probability exists that no energy is transferred (Wertheim, 1964). The effective line-width of the zero phonon (recoil-free) process is that of the gamma ray; this is extremely small (Wertheim, 1964; Chapter 4, fig. 1) in relation to the characteristic energies of interaction between the nucleus and its surrounding electrons.

If the zero-phonon gamma ray encounters another nucleus, its energy may be absorbed by raising that nucleus to an excited state, provided the transition energies of the emission and absorption events are equal to within the line-width of the gamma ray. Since this is much smaller than the characteristic interaction energies between nuclei and electrons, a change in environment is sufficient to bring the two nuclei out of resonance. However, the energy of the gamma ray may be modulated by applying a doppler shift to bring the system into resonance. Thus nuclear transition energies may be compared in varying environments.

A change in the s-electron density at the nucleus will result in a shift in the nuclear energy levels. Thus where there is such variation between emitter and absorber, the processes are separated in the energy spectrum by an amount known as the ISOMER SHIFT (I.S.). This quantity is thus a measure of the relative s-electron density at the nucleus and hence may be used to characterize atoms in different environments.

If the nucleus is not spherical or does not have a uniform charge density, a quadrupole moment arises which can interact with the electric field gradient (E.F.G.) at the nucleus to life the degeneracy of the nuclear state. This gives rise to a doublet in the energy spectrum; the separation of the two components is known as the QUADRUPOLE SPLITTING (Q.S.) and is a measure of the E.F.G. at the nucleus. This is a function of the non-spherical distribution of electrons around the nucleus and is thus highly sensitive to the occupancy of the outer shell and the magnitude of the non-spherical crystal field imposed by the structure.

It is of interest in this study to examine the reasons for variations in these two parameters with respect to the ^{57}Fe nucleus. The screening of the 4s-electrons from the nucleus by the 3d-electrons is more efficient for Fe^{2+} than for Fe^{3+}. Consequently, the inner s-orbitals are more expanded in Fe^{2+} which thus shows a larger I.S. than Fe^{3+}; this difference in I.S. enables the oxidation state of the Fe in the structure to

be determined. Covalent bonding will tend to delocalize the 3d-electrons which lowers the shielding of the nucleus, resulting in a smaller I.S. Thus information on bonding characteristics and hence coordination can be obtained. The non-spherical electron distribution gives rise to the Q.S. and therefore, the Q.S. values for Fe^{2+} (d^6) are much greater than those for Fe^{3+} (d^5). In addition, a component of the total E.F.G. at the nucleus is provided by the crystal field; thus the magnitude of the Q.S. gives information on coordination number, site-symmetry and site-distortion.

The most important application of this technique in mineralogy is the derivation of site-populations in known structures. The basic assumption involved in this usage is that the recoil-free fractions of Fe in all sites are the same, and thus the site-population is directly proportional to the peak areas of the doublets involved. Experimental measurements on ordered Fe silicates appear to uphold this assumption, provided the bonding is not significantly different at the sites involved in the ordering (see Zn-cummingtonite, this study). Further details of the Mössbauer method are given in Wertheim, 1964; Frauenfelder, 1962 and Goldanskii & Herber (1968), and a discussion of the use of area ratios to derive site-populations is given by Bancroft (1970).

APPENDIX 2

Observed and Calculated Structure Factors for

Ferrotschermakite

Ferrohastingsite

Oxy-kaersutite

Alumino-hastingsite

Zinc cummingtonite

Tremolite (X-ray)

Tremolite (Neutron)

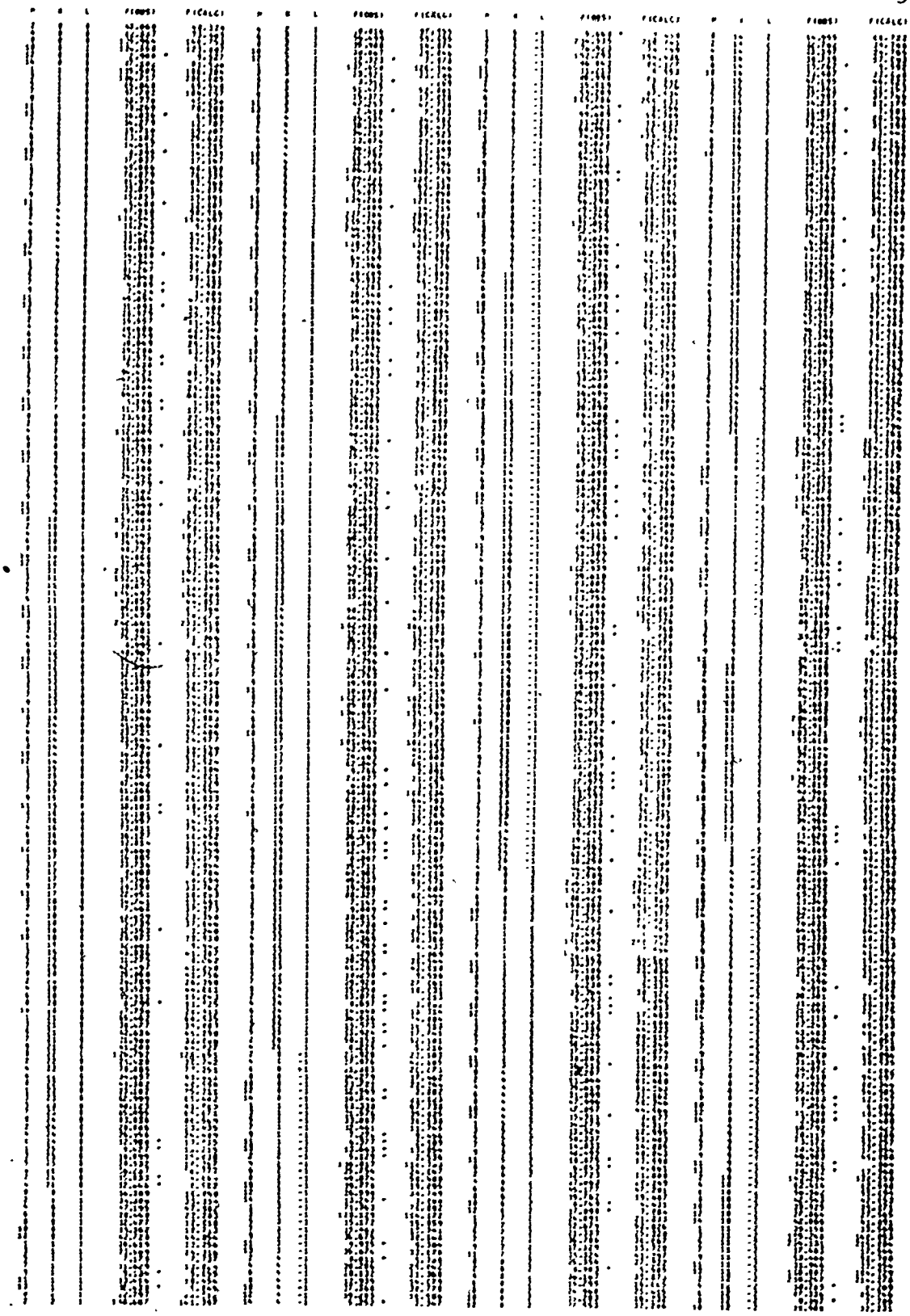

FERROTSCHERMAKITE (continued)

FERROHASTINGSITE

FERROHASTINGSITE (continued)

ALUMINO-HASTINGSITE

ZINC-CUMMINGTONITE (continued)

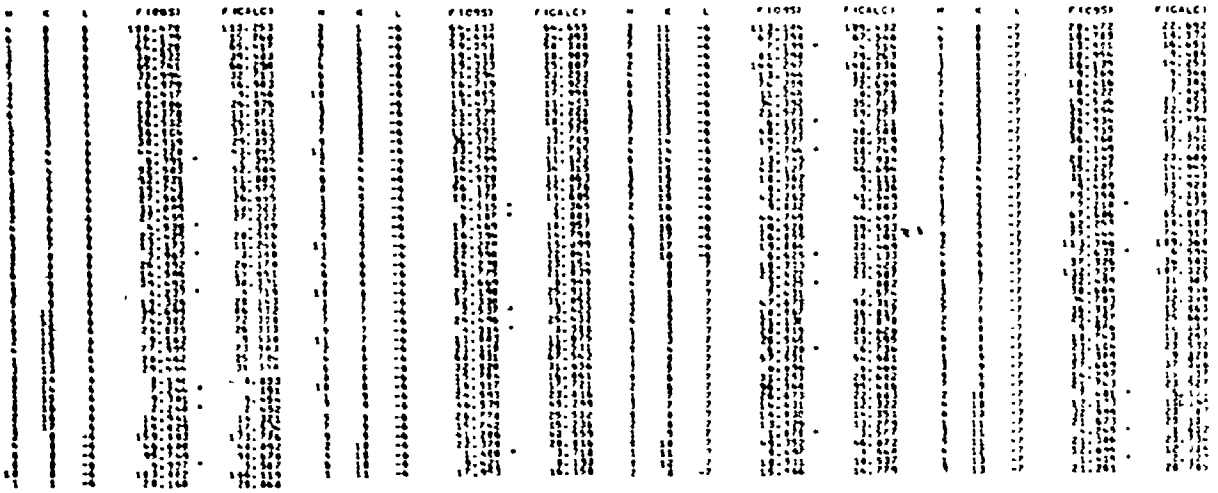

TREMOLITE (X-RAY)

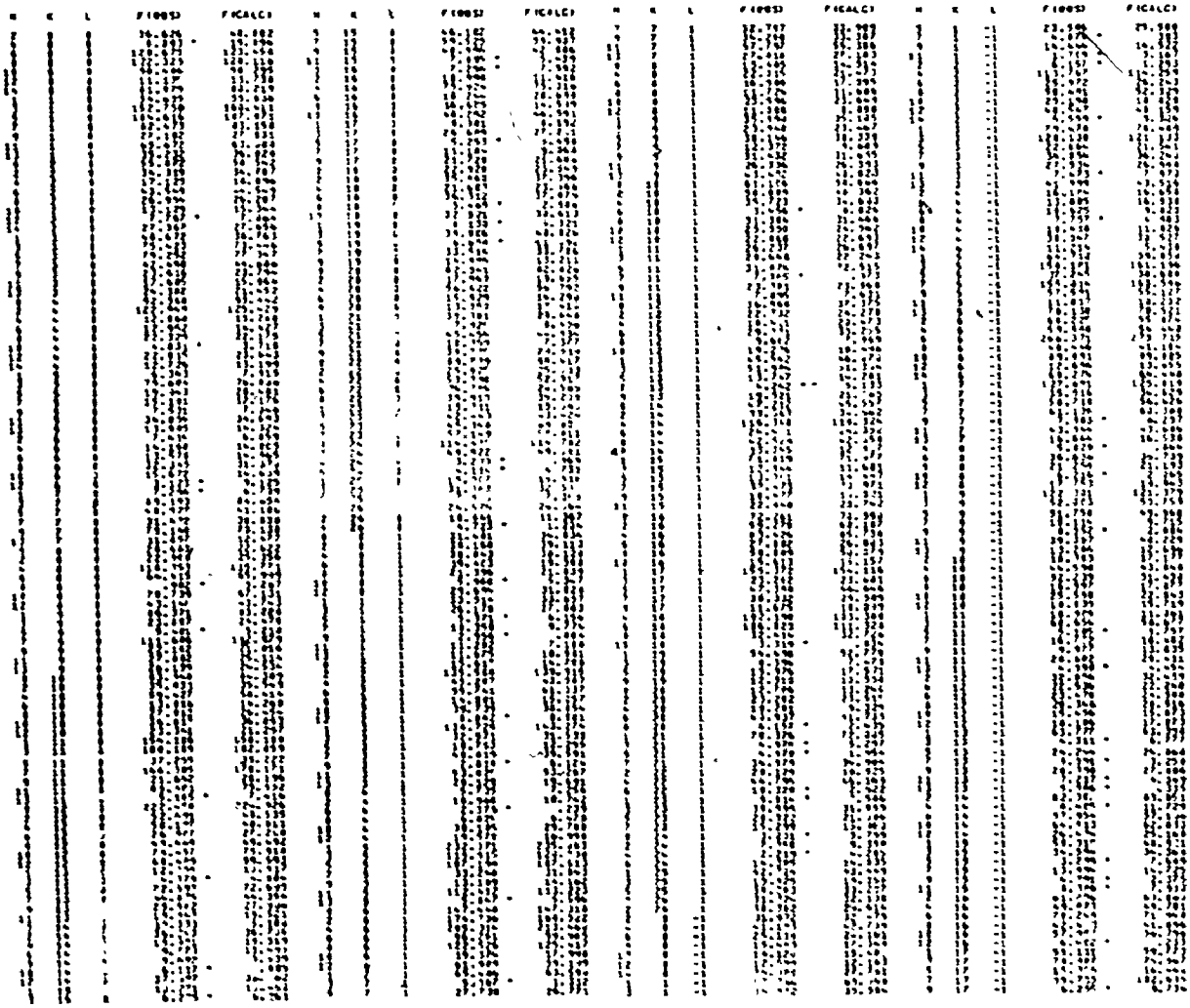

TREMOLITE (X-RAY) (continued)

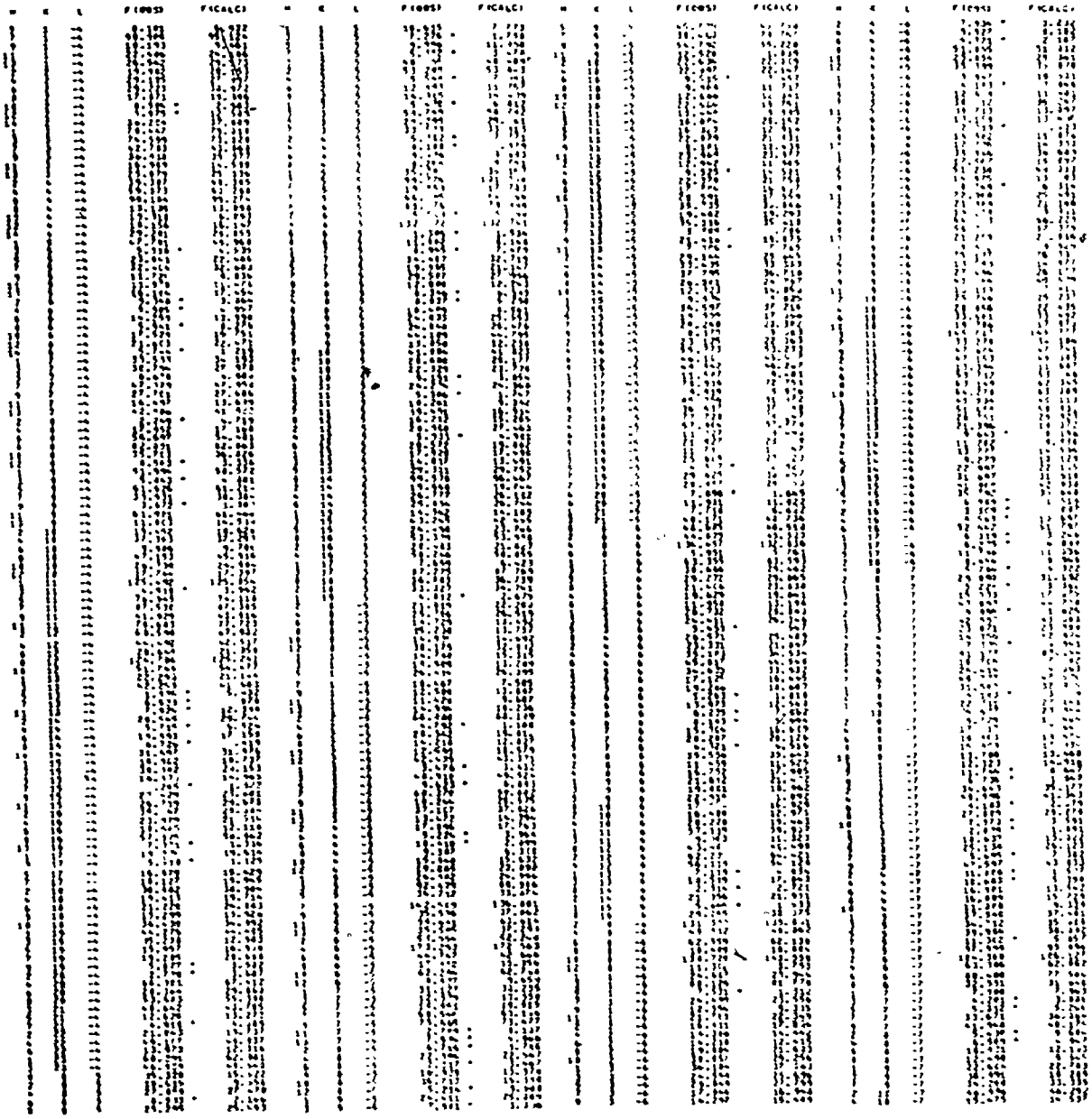

TREMOLITE (NEUTRON)

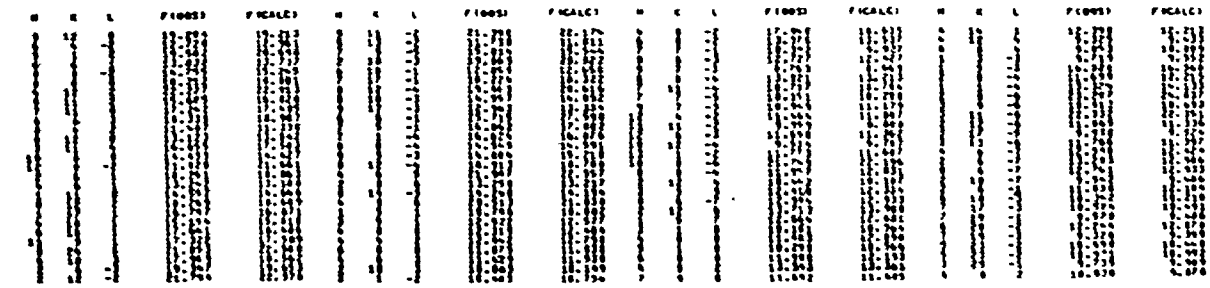

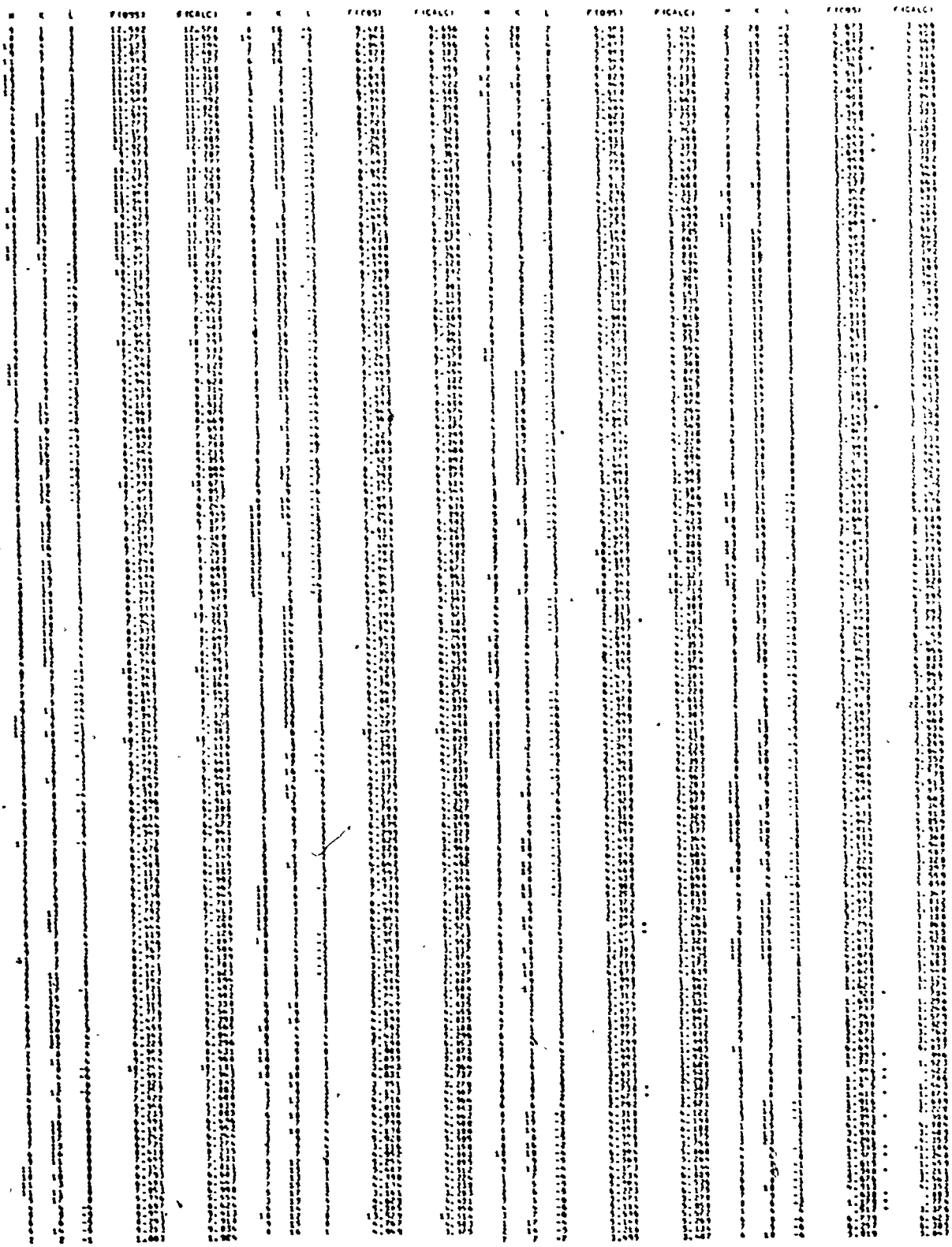

APPENDIX 3

CORRELATION MATRICES FOR SELECTED MOSSBAUER SPECTRA

APPENDIX 3

CORRELATION MATRICES FOR SELECTED MOSSBAUER SPECTRA

Correlation Matrix for Ferrotschermakite

All half-widths constrained to be equal

	1.00											
	1.00											
Sine	-.80	1.00										
	-.82	1.00										
Drift	-.64	.31	1.00									
	-.69	.43	1.00									
Position 1	-.02	-.03	.15	1.0								
	.00	-.02	.16	1.0								
Width 1	-.25	.38	.49	.27	1.00							
	-.28	.44	.48	.40	1.00							
Area 1	-.42	.65	.50	.07	.77	1.00						
	-.21	.32	.42	.59	.70	1.00						
Position 2	-.01	-.01	-.08	-.21	-.30	-.11	1.00					
	.07	-.13	.06	.22	.05	.45	1.00					
Area 2	....	....	....	....	....	....	....	....				
	-.06	.05	.13	-.48	-.05	-.58	-.45	1.00				
Position 3	-.11	.12	.02	.09	-.23	.07	-.02	....	1.00			
	.03	-.13	.06	.04	-.28	-.19	-.26	.29	1.00			
Area 3	....	....	....	....	....	....	....	....	....	....		
	-.41	.65	.23	-.13	.38	.20	-.30	-.08	-.30	1.00		
Position 4	-.15	.18	.18	.08	.14	.29	.07	....	.26	....	1.00	
	-.13	.14	.24	.09	.17	.16	.02	.09	.19	.10	1.00	
Position 5	.10	-.11	-.08	.06	.10	-.02	-.06	....	-.08	....	-.02	1.00
	.12	-.17	-.11	-.34	-.15	-.58	-.38	.56	.08	-.06	-.28	1.00
Position 6	.09	-.17	.09	-.01	-.06	-.07	.02	....	.01	....	.00	.13	1.00
	.12	-.20	-.07	-.41	-.22	-.61	-.31	.66	.26	-.20	.00	.54	1.00

Correlation Matrix for Ferrotschermakite

Doublet half-widths constrained to be equal

	1.00													
	1.00													
Sine	-.82	1.00												
	-.83	1.00												
Drift	-.67	.40	1.00											
	-.70	.49	1.00											
Position 1	.02	-.06	.15	1.00										
	.11	-.17	-.02	1.00										
Width 1	-.21	.30	.48	.34	1.00									
	.04	-.04	-.02	.62	1.00									
Area 1	-.17	.28	.31	.39	.65	1.00								
	.15	-.20	-.23	.60	.87	1.00								
Position 2	.01	.00	-.08	-.11	-.32	.06	1.00							
	.10	-.15	-.17	.21	.34	.60	1.00							
Width 2	-.22	.30	.44	.52	.63	.59	.05	1.00						
	-.29	.40	.54	-.23	-.48	-.75	-.46	1.00						
Area 2	....	....	....	....	....	....	....	....	1.00					
	-.25	.33	.44	-.48	-.71	-.94	-.60	.90	1.00					
Position 3	.14	-.21	-.20	.10	-.11	.17	-.38	-.41	....	1.00				
	.19	-.30	-.23	.36	.39	.48	-.12	-.61	-.52	1.00				
Width 3	-.25	.36	.23	-.14	.01	-.14	.39	.05	....	-.43	1.00			
	-.19	.29	.07	-.09	.05	.09	.42	-.10	-.11	-.26	1.00			
Area 3	....	....	....	....	....	....	....	....	....	....	....	1.00		
	-.32	.50	.02	-.16	.13	.16	.16	-.19	-.21	-.13	.67	1.00		
Position 4	-.12	.13	.16	.10	.13	.27	.05	.09	....	.18	.06	....	1.00	
	-.15	.16	.24	.05	.05	-.01	.00	.11	.09	.06	.10	.09	1.00	
Position 5	.17	-.19	-.17	-.03	.08	-.04	-.11	-.17	....	.13	-.07	....	-.01	1.00
	-.14	.18	.30	-.51	-.69	-.92	-.62	.75	.90	-.44	-.10	-.17	.04	1.00
Position 6	.13	-.22	-.04	-.21	-.12	-.20	-.10	-.42	....	.20	-.01	....	.00	.22	1.00
	-.09	.10	.23	-.56	-.71	-.84	-.56	.56	.80	-.29	-.10	-.20	.04	.81	1.00

Correlation Matrices for Ferrohastingsite (R.T.)

Doublet Half-Widths Equal (continued overleaf)

	1.00										
	1.00										
Sine	-.82	1.00									
	-.82	1.00									
Drift	-.70	.41	1.00								
	-.71	.42	1.00								
P1	-.08	.08	.20	1.00							
	.05	-.12	-.05	1.00							
W1	-.27	.38	.44	.25	1.00						
	-.01	-.04	-.01	.85	1.00						
A1	-.48	.71	.50	.17	.65	1.00					
	.04	-.13	-.12	.85	.94	1.00					
P2	.05	-.06	-.15	-.18	-.53	-.13	1.00				
	.09	-.18	-.16	.79	.74	.84	1.00				
W2	-.27	.38	.40	.56	.55	.60	-.14	1.00			
	-.07	.20	.19	-.63	-.80	-.92	-.68	1.00			
A2	....	....	....	....	....	....	....	....	1.00		
	-.05	.16	.15	-.74	-.90	-.97	-.74	.98	1.00		
P3	.04	-.07	-.11	-.09	-.27	-.15	-.09	-.49	....	1.00	
	.02	-.03	.03	.14	.00	.00	.16	.10	.11	1.00	
W3	-.21	.33	.24	.19	.28	.54	.30	.35	....	-.11	1.00
	-.20	.36	.07	-.14	-.15	-.17	-.03	.21	.18	.04	1.00

Correlation Matrices for Ferrohastingsite (R. T.) continued

A3	....	....	....	....	....	....	....	....	....	....	....	1.00										
	-.20	.53	.06	-.13	-.08	-.12	-.06	.17	.14	-.02	.72	1.00										
P4	-.02	.00	-.03	-.11	-.20	-.08	.12	-.20	....	.02	-.39	....	1.00									
	.03	.01	.08	-.31	-.49	-.56	-.24	.69	.68	.10	-.17	-.02	1.00									
W4	-.19	.26	.24	.27	.21	.39	.03	.33	....	.28	.30	....	-.11	1.00								
	-.13	.06	.14	.37	.53	.58	.26	-.69	-.69	-.10	-.15	-.23	-.74	1.00								
A4	....	....	....	....	....	....	....	....	....	....	....	....	....	....	1.00							
	-.04	-.06	-.02	.45	.66	.75	.39	-.89	-.87	-.28	-.20	-.23	-.80	.89	1.00							
P5	-.10	.12	.11	.05	.07	.18	.04	.07	....	.06	.08	....	.13	.11	....	1.00						
	-.11	.11	.17	.05	.07	.05	.01	-.04	-.05	.00	-.01	.00	.00	.17	.11	1.00						
P6	.13	-.14	-.15	.06	-.01	-.11	-.01	.06	....	-.11	-.03	....	-.04	-.12	....	-.02	1.00					
	.02	-.11	-.06	.29	.47	.54	.19	-.70	-.69	-.40	-.13	-.16	-.74	.75	.86	.08	1.00					
P7	.09	-.09	-.06	-.02	.32	-.01	-.25	-.01	....	-.15	-.04	....	-.06	-.28	....	-.03	.34	1.00				
	-.06	.13	.15	-.84	-.80	-.88	-.92	.70	.77	-.23	.11	.04	.27	-.29	-.41	.00	-.17	1.00				
P8	.15	-.24	-.10	-.32	-.16	-.27	-.01	-.55	....	.26	-.18	....	.10	-.19	....	-.03	.05	.10	1.00			
	-.02	.08	.11	-.88	-.90	-.94	-.85	.78	.87	-.02	.10	.04	.44	-.45	-.59	-.03	-.39	.89	1.00			

P = Position

W = Half-width

A = Area (Intensity)

APPENDIX 4

Using the relation of Brown & Shannon (1973), bond strength (S) may be related to bond length (R) by the following equation:

$$S = S_o \left(\frac{R}{R_o} \right)^{-n} \qquad (1)$$

where S_o is the Pauling bond strength (Pauling, 1929) and R_o is a parameter fitted by least-squares analysis to a large number of experimental data. For a cation polyhedron of p equal bonds (R'), the following equations may be written:

$$S' = S_o \left(\frac{R'}{R_o} \right)^{-n} \qquad (2)$$

$$p\,S' = z = pS_o \left(\frac{R'}{R_o} \right)^{-n} \qquad (3)$$

where z is the formal valence of the cation. Rearranging equation (3) gives

$$R' = \sqrt[n]{pS_o/z}\; R_o \qquad (4)$$

Writing $S = S' + \delta S$ and $R' = R' + \delta R$, equation (1) becomes

$$S' + \delta S = S_o \left(\frac{R' + \delta R}{R_o} \right)^{-n} = S_o \left(\frac{R'}{R_o} \right)^{-n} \left(1 + \frac{\delta R}{R'} \right)^{-n} \qquad (5)$$

Expanding the R.H.S. of equation (5) using the binomial expansion gives

$$S'+\delta S=S_o\left(\frac{R'}{R_o}\right)^{-n}\left[1-n\frac{\delta R}{R'}+\frac{n(n+1)}{2!}\left(\frac{\delta R}{R'}\right)^2+\text{higher order terms}\right] \quad (6)$$

Assuming $\delta R/R'$ is small, the higher order terms may be neglected and equation (6) may be rearranged to give

$$\delta S=S_o\left(\frac{R'}{R_o}\right)^{-n}\left(-n\frac{\delta R}{R'}+\frac{n(n+1)}{2}\frac{\delta R}{R'}\right)^2\Bigg) \quad (7)$$

Summing this equation over all bonds (p) and applying Pauling's electroneutrality rule

$$\frac{1}{S_o}\left(\frac{R'}{Ro}\right)^n\sum_p \delta S = 0 = -n\left(\sum_p\frac{\delta R}{R'}-\frac{n+1}{2}\sum_p\left(\frac{\delta R}{R'}\right)^2\right) \quad (8)$$

Rearranging this equation (8) gives

$$\sum_p\frac{\delta R}{R'}=\frac{n+1}{2}\sum_p\left(\frac{\delta R}{R'}\right) \quad (9)$$

If $\langle R\rangle$ is the mean bond length of the distorted polyhedron

$$\langle R\rangle = \frac{1}{p}\sum_p (R'+\delta R) \quad (10)$$

Rearranging this equation gives

$$\sum_p \frac{\delta R}{R'} = p\left(\frac{\langle R\rangle}{R'} - 1\right) \qquad (11)$$

Substitution of equation (11) and equation (4) into equation (9) gives the following equation which expresses the mean bond length as a linear function of the distortion parameter $\sum_p (\delta R^2)$

$$\langle R\rangle = \sqrt[n]{\frac{p S_o}{z}}\; R_o + \frac{n+1}{2p}\; \sqrt[n]{\frac{z}{p S_o}}\; \frac{1}{R_o}\; \sum_p (\delta R^2) \qquad (12)$$

APPENDIX 5

The variation in ⟨Si-O⟩ bond lengths in structures has been found to be a linear function of the mean coordination number, ⟨C.N.⟩ of the anions of the tetrahedral group (Shannon & Prewitt, 1969; Brown & Gibbs, 1969).

However, in the study by Brown & Gibbs (1969), the grand mean Si-O distance for each structure was related to the overall anion coordination for each structure. Since these changes in ⟨Si-O⟩ are related to local environment, it is more appropriate to consider the variation in individual ⟨Si-O⟩ distances with the mean anion coordination of that tetrahedral group. Linear regression analysis on 134 individual ⟨Si-O⟩ distances from 71 structures gave the relation

$$\langle \text{Si-O} \rangle = 1.584 + 0.0127 \langle \text{C.N.} \rangle$$

with a correlation coefficient of 0.704.